UNIVERSITÀ DEL PIEMONTE ORIENTALE

Department of Translational Medicine

Ph.D. Program in Science & Medical Biotechnology

XXXIII cycle

SSD: MED/50

GRADUATION THESIS

Repurposing of psychotropic drugs for cancer therapy

Ph.D. supervisor

Prof. Daniela Capello

Ph.D. candidate

Annamaria Antona

Academic years 2017-2020

Summary

According to the World Health Organization, cancer incidence and mortality are rapidly growing worldwide. Despite improvements in cancer therapy, overall survival for most cancer types has changed a little in the past decades. Drug repositioning represents a promising approach for discovering new therapeutic strategies for cancer therapy.

Since several epidemiological studies reported lower cancer incidence in individuals receiving long term psychotropic drugs treatment, in this project we investigated 27 psychotropic drugs for their cytotoxic activity in colorectal carcinoma, glioblastoma and breast cancer cell lines. Consistent with the cationic amphiphilic structure of the most cytotoxic compounds, we investigated their effect on mitochondrial and lysosomal compartments. Penfluridol, ebastine, pimozide, fluoxetine, fluspirilene and nefazodone showed significant cytotoxicity, in the low micromolar range, in all cell lines tested. In MCF7 cells these drugs triggered mitochondrial membrane depolarization, increased the acidic vesicular compartments and induced phospholipidosis. Both penfluridol and spiperone induced AMPK activation and autophagy. Neither caspase nor autophagy inhibitors rescued cells from death induced by ebastine, fluoxetine, fluspirilene and nefazodone. Treatment with 3-methyladenine partially rescued cell death induced by pimozide and spiperone, whereas enhanced the cytotoxic activity of penfluridol. Conversely, inhibition of lysosomal cathepsins significantly reduced cell death induced by ebastin, penfluridol, pimozide, spiperone and mildly in fluoxetine treated cells.

Lastly, spiperone cytotoxicity was restricted to colorectal cancer and breast cancer and caused apoptotic cell death in MCF7 cells. Our unpublished data on the characterization of spiperone activity on both adherent and stem-like colorectal cancer cells demonstrated that its cytotoxicity is mainly linked to perturbations of intracellular calcium (Ca^{2+}) homeostasis, which likely result in mitochondrial Ca^{2+} overload and membrane depolarization, cell cycle block in G1 phase, and apoptosis. Spiperone induced a PLC dependent Ca^{2+} release from the endoplasmic reticulum (ER) along with ER stress and unfolded protein response activation, resulting in CHOP upregulation.

In conclusion, the cytotoxicity of psychotropic drugs with cationic amphiphilic structures relied on simultaneous mitochondrial and lysosomal disruption and induction of cell death that does not necessarily require apoptosis. Dual targeting of lysosomes and mitochondria constitutes a new promising therapeutic approach for cancer, particularly those in which the apoptotic machinery is defective. Besides, the newly identified mechanism of action of spiperone in cancer cells could represent a starting point for the development of new therapeutic strategies.

Altogether these data support the clinical development of psychotropic drugs for cancer therapy.

TABLE OF CONTENTS

1. Introduction 3

1.1 Cancer: a major worldwide public health problem 4

1.1.1 Breast cancer 6

1.1.2 Colorectal cancer 8

1.2 Challenges in cancer treatment 10

1.2.1 Drug resistance 10

1.2.2 Cancer stem cells (CSCs) 13

1.3. Cell death pathways for cancer therapy 14

1.3.1 Apoptosis: the main target of anticancer therapies 14

1.3.2 Mitochondrial targeting in cancer treatment 17

1.3.3 Role of autophagy in cancer treatment 19

1.3.3.1 Lysosomes and cancer 22

1.3.4 Endoplasmic reticulum stress induction 24

1.3.5 Intracellular Ca^{2+} dynamics in cancer 27

1.4 Drug repurposing: psychotropic drugs and cancer 30

2. Aim of the study 33

3. Materials and methods 35

3.1 Cell culture 36

3.2 Psychotropic drugs 36

3.3 MTT (Thiazolyl blue tetrazolium bromide) viability assay 37

3.4 Viability rescue assay 37

3.5 Apoptosis assay 38

3.6 Migration assay 38

3.7 Vacuolization assay 38

3.8 Mitochondrial membrane potential analysis 38

3.9 Lysotracker assay 39

3.10 Phospholipidosis assay 39

3.11 Western blotting 39

3.12 Immunofluorescence microscopy analysis 41

3.13 Compounds chemical analysis 41

3.14 Cell cycle analysis 42

3.15 Intracellular Ca^{2+} concentration measurements 42

3.16 RNA extraction and real time PCR 42
3.17 Analysis of XBP1 splicing variants 43
3.18 Extreme limiting dilution assay 43
3.19 Statistical analysis 44

4. Results 45

4.1 Psychotropic drugs show anticancer activity by disrupting mitochondrial and lysosomal function 46

4.1.2 The antitumoral activity of psychotropic drugs transcends the conventional therapeutic classes and tumor type 46
4.1.3 Cytotoxicity of psychotropic drugs is not mediated by biogenic amine receptors 48
4.1.4 Psychotropic drugs affect tumor cell migration 51
4.1.5 Psychotropic drugs with significant antitumoral activity display a cationic amphiphilic structure 53
4.1.6 Psychotropic drugs cause mitochondrial membrane depolarization 54
4.1.7 Psychotropics drugs induce vacuolization and increase acidic compartments 55
4.1.8 Psychotropic drugs alter autophagy flux by affecting mTOR pathway 58
4.1.9 Psychotropic drugs cause lysosomal disruption 60
4.1.10 Psychotropic drugs induce different types of cell death 63

4.2 Effective cytotoxic activity of spiperone on human colorectal cancer cells 65

4.2.1 Spiperone is cytotoxic for CRC cells and impairs the clonogenic potential of CRC-SC 65
4.2.2 Spiperone induces cell cycle arrest resulting in apoptotic cell death 69
4.2.3 Spiperone does not induce lysosomal disruption in CRC cells 72
4.2.4 Spiperone induces endoplasmic reticulum (ER) Ca^{2+} release resulting in a Ca^{2+}- mediated activation of PKC 74
4.2.5 Spiperone-mediated calcium increase in CRC cells is a PLC dependent process 76
4.2.6 Spiperone induces ER stress 78
4.2.7 Spiperone induces mitochondrial damage 80
4.2.8 Intracellular Ca^{2+} chelation and PLC inhibition protects from cell death 83

5. Discussion 84

6. References 91

7. Supplementary material 114

8. Publications 134

1. Introduction

1.1 Cancer: a major worldwide public health problem

In the 21st century, according to the World Health Organization (WHO), cancer incidence and mortality are rapidly growing worldwide. The lifetime cumulative risk of developing cancer is about 10% for both women and men [1]. Moreover, by being the first or second cause of death before age 70 in 91 out of 172 countries, cancer represents one of the major obstacles to the increase of life expectancy [2].

In 2018, GLOBOCAN estimated a total of 18.1 million new cases and 9.6 million cancer deaths all over the world [2]**,** with lung, breast and colorectal cancer as the top three cancers worldwide in term of incidence, whereas the first, the fifth, and the second respectively, in term of mortality [3](**Figure 1**).

An additional emerging challenge in the oncological field is represented by population aging, in fact, it is well established that cancer incidence and mortality increase in elderly with nearly 50% of all new cancer cases each year diagnosed in people over 70 along with a 16-fold increase in mortality rate in this population [4]. Since demographic projection suggests that the major part of the population is expected to live more than 60 years (**Who, 2018**), the age-related increase in tumor incidence, along with the expected rise in the number of elderly people, will trigger an elevated number of elderly oncological patients, highlighting not only the scientific achievements accomplished in term of cancer treatment, but also the need of a constant effort by the scientific community on this major public health problem.

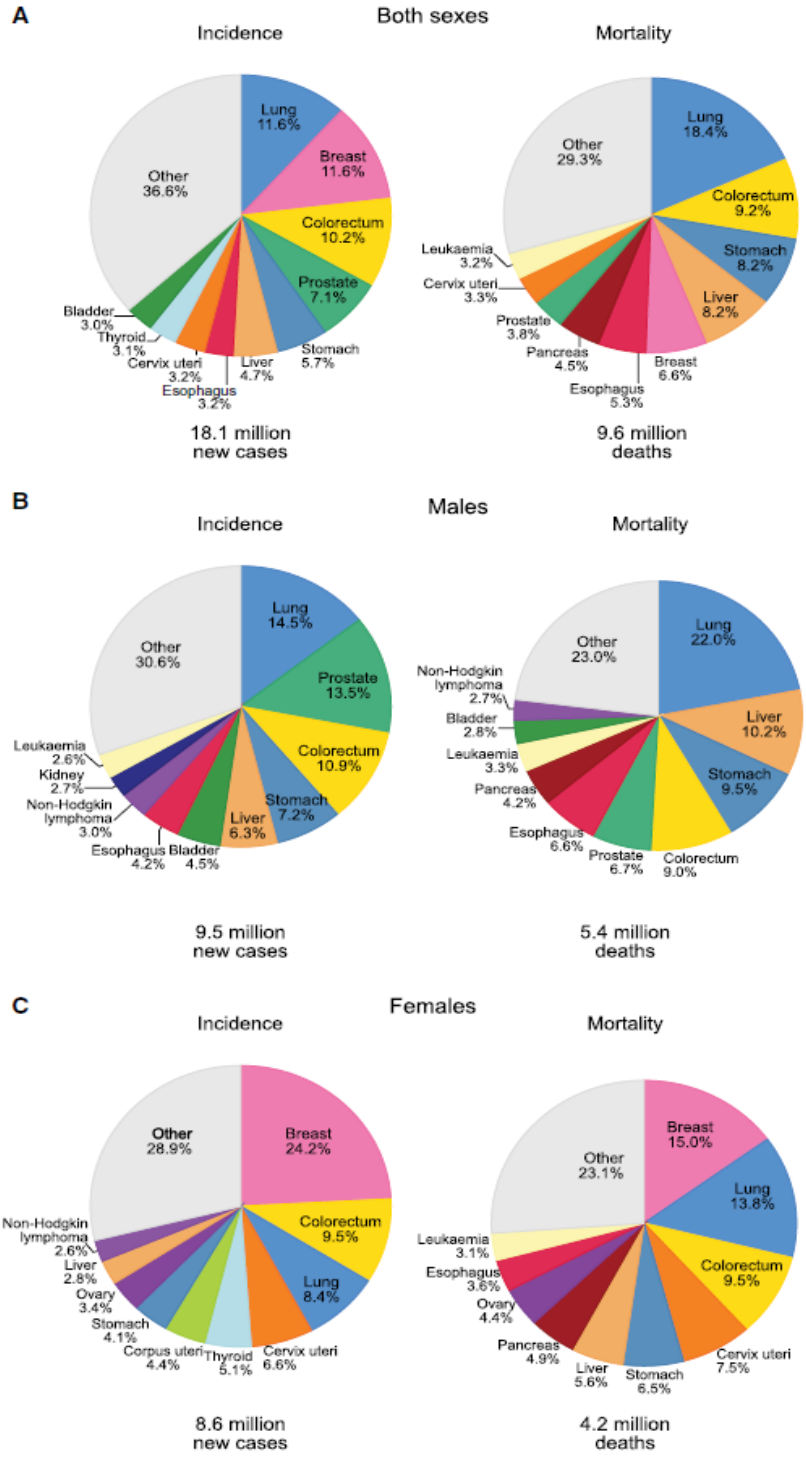

Figure 1 Pie charts presenting the distribution of cases and deaths for the 10 most common cancers in 2018 for (**A**) Both sexes, (**B**) Males, and (**C**) Females. For each sex, the area of the pie chart reflects the proportion of the total number of cases or deaths (*Adapted from Bray et al., 2018*)

1.1.1 Breast cancer

In 2018 GLOBOCAN estimated about 2.1 million newly diagnosed breast cancer cases, which account for almost 1 out of 4 cancer cases among women [2]. However, there is a high variability of the incidence-mortality ratio worldwide: while in low-income countries the overall incidence is lower with a high mortality rate, in developed countries incidence is constantly increasing, although a major improvement in mammographic screening, diagnosis and management is significantly reducing the mortality rate [5].

At present, the identification of successful strategies and interventions to prevent breast cancer is still challenging, although many risks factor associated with the development of this tumor have been identified, such as age, family history (such as the inheritance of BRCA1 and BRCA2 mutations), reproductive factors, estrogen exposure, life style and bad dietary habits [6].

Breast cancer is a heterogeneous complex of diseases, a spectrum of many subtypes with distinct biological and clinical features [7]. The classification system is based on histopathology, histologic grade, stage, and receptor status. Breast cancer is classified into four main histological types: ductal carcinoma in situ (DCIS), infiltrating ductal carcinoma (IDC), lobular carcinoma in situ (LCIS) and invasive lobular carcinoma (ILC). IDC is the most frequent and is characterized by the presence of infiltrating tumor cells in the surrounding stromal tissue [8]. Based on tumor cell differentiation, tumors can be distinguished into low grade - I (differentiated cells), intermediate grade - II (moderately differentiated cells), and high grade - III (poorly differentiated cells). Cases characterized by undifferentiated cells and nuclear heterogeneity are associated with the worst prognosis [9]. The stage of the tumor is determined by the conventional TNM (tumor, node, metastasis) classification, which considers tumor size (T1 to T4), involvement of lymph nodes (N0 to N3) and presence of metastasis (M0 or M1) [10].

According to the receptor status and the proliferative rate (defined by the Ki67 staining), breast cancer could be distinguished in three distinct molecular subtypes: luminal-like, basal-like and epidermal growth factor receptor 2 positive (HER-2+) (**Table 1**).

Luminal-like breast cancers are localized close to the luminal side of the duct and could be further distinguished into two different subtypes: luminal A and luminal B. Luminal A tumors show elevated expression of estrogen (ER) and/or progesterone receptors (PR), while moderate expression of proliferative genes and absence of HER2 is observed [11, 12]. Luminal B tumors are usually characterized by higher aggressiveness because of the greater expression of proliferative genes along with a lower expression of ER. If luminal A tumors are usually sensitive to endocrine therapies, luminal B tumors are less sensitive and usually lead to tumor relapse [13].

The HER-2+ subtype is distinguished by the overexpression or the amplification of the oncogene HER2 along with the absence of PR and ER. For patients diagnosed with HER-2+ subtype, the therapy is usually based on the administration of a monoclonal antibody, such as Trastuzumab, targeting HER2 in combination with chemotherapy. However, despite improvement in therapy, HER-2+ patients usually undergo tumor relapse with a short overall survival rate [14].

Lastly, the basal-like subtype is characterized by a lack of PR and ER expression as well as HER2 overexpression, for this reason, it is called triple-negative breast cancer. This subtype is usually referred to as the most aggressive with a high risk of relapse and poor prognosis. The only therapy for patients with triple-negative breast cancer is chemotherapy [15, 16].

Table 1 **Classification of 4 major subtypes of invasive breast cancer and their corresponding clinical features, current treatment** (*Adapted from Tang et al., 2016*)

Type	Immunohistochemical Characteristics	Clinical Features	Treatment	Resistance
Luminal A	ER^+/PR^+, HER-2−, low Ki-67 (<14%)	~40% of invasive breast cancers; best prognosis among all 4 types	Endocrine therapy; chemotherapy (less responsive than in luminal B type)	Tamoxifen resistance; MDR; de novo or acquired, mostly acquired
Luminal B	ER^+/PR^+, $HER\text{-}2^+$ (or HER-2− with high Ki-67) (>14%)	~20% of invasive breast cancers; higher grade than luminal A; good prognosis although not as good as luminal A	Endocrine therapy (less responsive than in luminal A type); chemotherapy	Tamoxifen resistance; MDR; de novo or acquired, mostly acquired
HER-2	ER−, PR−, $HER\text{-}2^+$	15% ~ 20% of invasive breast cancers; high grade; lymph node positive; better prognosis than triple negative but worse than luminal type	HER-2 targeted therapy; anthracycline-based chemotherapy	Trastuzumab resistance; MDR; de novo or acquired, mostly acquired
Basal-like	ER−, PR−, HER-2−	10% ~15% of invasive breast cancers; *BRCA1* dysfunction; worst prognosis among all 4 types	Platinum-based chemotherapy and PARP inhibitors	MDR; de novo or acquired, mostly acquired

Abbreviations: ER = estrogen receptor; HER-2 = human epidermal growth factor receptor 2; MDR = multidrug resistant; PARP = poly ADP ribose polymerase; PR = progesterone receptor.

The current strategy for breast cancer patients is divided into two subtypes: local treatment and systemic treatments. Local treatment is usually the first choice for early-stage breast cancers, and it consists of breast-conserving surgical resection of the neoplastic lesion along with radiotherapy or mastectomy. This strategy leads to nearly 5 % of the local tumor recurrence rate in 10 years. Also, before tumor rejection, neoadjuvant chemotherapy is usually administrated to downstage the disease and enable breast conservation [17].

After surgical rejection, patients undergo systemic therapy with the purpose to reduce the risk of recurrence and metastasis. The therapy is usually selected according to the disease burden (lymph nodes involved, size of the primary tumor) and disease biology (receptor status and genetic alterations). For patients that display a severe prognosis, chemotherapy, containing both an anthracycline and a taxane is generally recommended. Instead, for HER-2+ breast cancers, targeted therapy including trastuzumab and pertuzumab in combination with chemotherapy reduces by 50% tumor recurrence [18, 19].

Lastly, endocrine therapy is proposed to patients with ER and PR positive disease for 5 or 10 years. It was in fact reported that the administration for five years of adjuvant tamoxifen decreases the risk of tumor relapse by approximately 50% during years 0-4, with a constant risk reduction of more than 30% in years 5-9 [17]. In this context, tamoxifen, a selective ER antagonist, block the ER-estrogen binding, whereas fulvestrant directly interferes with ER synthesis [20, 21].

Although the significant progress in local and systemic treatments, tumor heterogeneity and genomic instability allows the selection of therapy-resistant clones that may cause a relapse. For this reason, it is necessary to identify more effective therapies or synergetic combinations strategies to overcome therapy resistance and recurrence [22].

1.1.2 Colorectal cancer

Colorectal cancer (CRC) is one the most common malignancies with an estimated over 1.8 million newly diagnosed cases about 1 million deaths worldwide each year. In Western countries it ranks, in both sexes, third in terms of incidence but second in terms of mortality. Moreover, temporal profiles and demographic projections suggest that the global burden of CRC is expected to increase by 60% by 2030 [2] (Global Cancer Observatory (GCO)). Aging represents a major risk factor for CRC. Incidence strongly increases after the age of 40; 95% of the patients with a diagnosis of CRC can be accounted for in the range between 45 and 75 years. Approximately 60% of CRC patients are >70 years of age at the time of diagnosis, and 40% are >75 (**https://gco.iarc.fr/**). Other important risk factors are mainly associated with lifestyle and nutrition, including poor dietary habits, smoking and low physical activity [23].

The majority of CRC are sporadic, accounting for about 70% of cases, with no family history or genetic predisposition and are mainly characterized by an acquired mutation in APC, TP53 and SMAD4 [24]. The remaining 30% of cases are represented by familiar CRC, which can be categorized into hereditary diseases (4-7%) arising in the setting of well-defined highly penetrant inherited syndromes, and familiar, non-Mendelian inherited diseases (10-30%). The most common inherited CRC are represented by high-risk susceptibility syndromes related to polyp formation such as Lynch syndrome or Hereditary Non-Polyposis Colorectal Cancer (HNPCC, 4%) which is characterized by MSI, a consequence of a defective DNA mismatch repair (MMR) system, and familial adenomatous polyposis (FAP, 1%), characterized by a mutated copy of the adenomatous polyposis (APC) gene [25].

From a molecular point of view, CRCs can be divided into three main categories associated to distinct phenotypes: microsatellite instability (MSI), chromosomal instability (CIN), and CpG island

methylator phenotype (CIMP) [26]. All CRCs develop slowly and silently until they reach considerable size, resulting in polyps, precancerous lesions characterized by aggregations of cells within intestinal mucosa that protrude into the intestinal lumen [27].

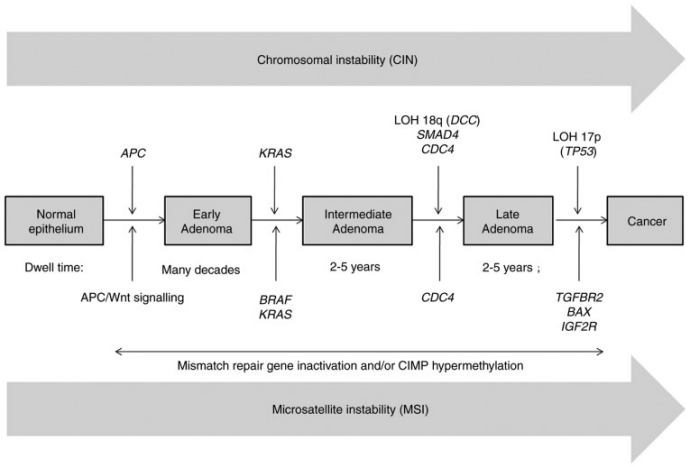

Figure 2 **Representation of different steps of progression in Colorectal cancer** (*Adapted from Niguyen et al. 2018*)

The progression from this benign lesion to invasive CRC is mediated by the sequential acquisition of genetic and epigenetic modifications [26]. The first step is usually represented by the inactivation of APC and suppression of Wnt/β-catenin destruction complex (**Figure 2**). Consequently, β-catenin, which is now accumulated inside the cytoplasm, is translocated into the nucleus where form complexes with the transcription factors TCF/LEF and activates the downstream effectors of Wnt, promoting proliferation, migration, invasion and metastasis [28]. Consequently, oncogenic KRAS mutations can occur and eventually deletion of chromosome18q (LOH18q), SMAD4 mutations and loss of TP53 (LOH17p) in the last stages of tumor progression [29, 30].

Activating mutations of KRAS or BRAF, deletion of chromosome18q (DCC), SMAD4 mutations and loss of TP53 (LOH17p) are typical and frequent mutations acquired during tumor progression. Mutations in KRAS, BRAF and TP53, are specific markers of CIN tumors, representing 85% of cases, and characterized by genomic instability and frequent loss of whole or large portions of chromosomes [31].

Conversely, MSI phenotype constitutes 15-20% of sporadic CRC and more than 95% of HNPPC. These tumors are characterized by DNA MMR genes deficiency that causes replication errors in microsatellites, leading to progressive insertions or deletions and resulting in frameshift mutations of oncogene or onco-suppressor genes such as BAX (38% of cases) and TGFBR2 (79% of cases) [26, 32].

Lastly, CIMP is found in 35% of cases and is represented by an aberrant methylation phenotype in which a variety of tumor suppressor genes are silenced by CpG islands methylation [33].
Despite several improvements, CRC treatment remains a demanding challenge. The 5-year survival rate is approximately 90% in patients diagnosed at an early stage; however, only 39% of tumors are diagnosed at this stage; in fact, around 20% of patients show metastasis already at the time of diagnosis, with the liver being one of the most affected organs [34, 35] and CRC survival declines to 12.5 % when the disease has spread to distant organs [35].
Surgery is the first option for patients with early CRC, while neoadjuvant chemotherapy or radiotherapy remains the main option for patients with advanced CRC [36]. Chemotherapy includes two distinct regimens: FOLFOX, which involves 5-fluorouracil, leucovorin and oxaliplatin and FOLFIRI, which involves 5-fluorouracil, leucovorin and irinotecan [36]. Moreover, two main biologic agents are used as first-line therapy and are represented by cetuximab, a monoclonal antibody that targets the epidermal growth factor receptor (EGFR) and bevacizumab, a monoclonal antibody against the vascular endothelial growth factor (VEGF) [37].

1.2 Challenges in cancer treatment

1.2.1 Drug resistance

Despite the advances in the development of new therapeutic strategies for the management of cancer patients, drug resistance and the subsequent ineffectiveness of drug treatment are responsible for nearly 90% of cancer-related deaths [38]. The factors involved in drug resistance are varied: enhanced drug efflux, survival cues from the microenvironment, epigenetic changes or/and genetic mutations impairing cell death and sustaining cell survival (**Figure 3**) [39]. Drug resistance can be both intrinsic and acquired. Whereas intrinsic drug resistance already exists at the time of the first treatment, acquired drug resistance develops during therapy; however, since acquired drug resistance mechanisms can be entirely different from the pre-existing ones, both these processes can coexist during tumor progression [40].
Intrinsic drug resistance, also defined as innate resistance, is one of the major causes of therapy ineffectiveness and tumor relapse. It is caused by three main mechanisms: i) activation or enhancement of intracellular pathways crucial for the resistance to environmental toxins; ii) pre-existing genetic mutations that, in the majority of cancers, lead to decreased responsiveness of tumor

cells, not only to chemotherapy but also hormone and biological therapies; iii) cancer heterogeneity, in which unresponsive subpopulations, such as cancer stem cells, will be selected upon drug treatment causing tumor relapse [38].

Conversely, acquired drug resistance occurs during cancer treatment and it is mediated by both environmental and genetic factors that facilitate the development of drug-resistant tumor cell clones. Some of the leading causes are represented by the activation of secondary proto-oncogenes, alterations in crucial metabolic pathways, altered expression or selection of mutated drug targets, modifications in the tumor microenvironment (TME) [40].

Among the molecular mechanisms that lead to chemoresistance, drug resistance-associated membrane proteins play a crucial role, in fact, they reduce intracellular drug accumulation by extruding drug molecules out of cells and indirectly affect drug accumulation through physicochemical processes [41]. The ATP-binding cassette (ABC) transporter superfamily is the main group of membrane transporters involved in drug efflux, including 48 genes grouped into 7 subfamilies (ABCA-ABCG) [42]. Among these subfamilies, ABCB1 (MDR1 or P-gp), ABCC1 (MRP1) and ABCG2 (or breast cancer resistance protein) are involved in the acquisition of multidrug resistance (MDR) in many cancer types [38].

ABCB1, one of the most studied ABC transporters, is characterized by a nucleotide-binding domain, that bind and hydrolyze ATP, while the two transmembrane domains generate a passage for the amphipathic and lipid-soluble substrates. ABCB1 has multiple drug binding sites and it can bind and extrude many chemotherapeutic agents such as paclitaxel, doxorubicin, and vinblastine [43–45].

ABCG2 is strongly associated with breast cancer chemoresistance, apart from being reported as a marker of cancer stem cells in some tumors [46, 47]. It leads to the efflux of both positively and negatively charged drugs including not only chemotherapeutic agents but also several, newly identified, target drugs such as several TKIs like imatinib and gefitinib [48].

Another crucial role in chemoresistance is played by the tumor microenvironment (TME), which is characterized by the presence of several cell types including immune and inflammatory cells, and the extracellular matrix (ECM). It was observed that while in normal condition extracellular pH (7.3-7.5) is usually more basic than intracellular pH (6.8-7.2), during tumor progression cancer cells are characterized by the *reversed pH gradient*, that leads to increased intracellular pH and decreased extracellular pH, leading to the impairment of the normal distribution of weak base anticancer drugs through the phenomenon called *ion trapping* [38]. In this context, lansoprazole, an example of a proton pump inhibitor demonstrated a synergistic effect *in vivo* in combination with paclitaxel [49].

Furthermore, TME can also support the enrichment of genetic heterogeneity. Because of the dynamic variation of the intra-tumoral vasculature, fluctuating hypoxia can lead to oxidative stress which

results in genetic instability, accumulation of mutation, and selection of a different clonal subpopulation [38].

From a genetic point of view, the DNA damage repair (DDR) pathway represents an additional crucial component in the response to several targeted therapies and chemotherapy drugs and genes involved in the DDR response are frequently upregulated in cancer [50]. For example, FANCG, FEN1, RAD23B were identified upregulated in 5-FU resistant human CRC cell lines [51]. This response leads to the upregulation of p53 target genes in cancer cells, resulting in DNA damage repair and reduced cell cycle arrest and apoptosis [51, 52].

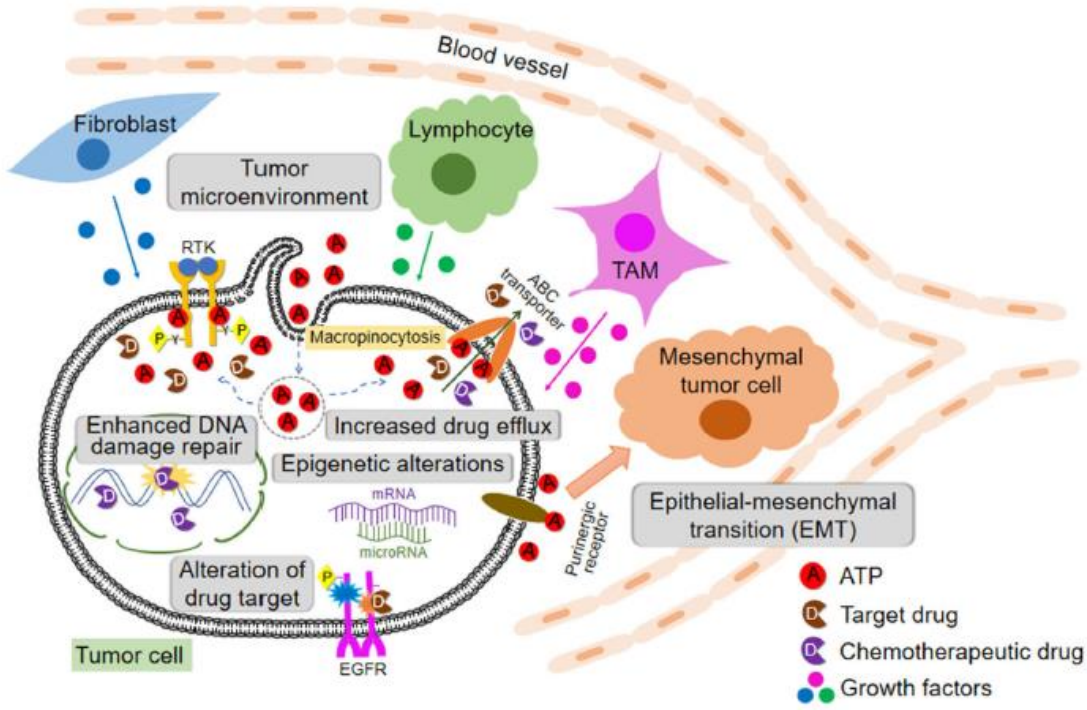

Figure 3 **Representation of cells, protein factors, and mechanisms involved in drug resistance in cancer** (including extracellular ATP-induced resistance. ABC: ATP binding cassette; RTK: receptor tyrosine kinases; EGFR: epidermal growth factor receptor; TAM: tumor-associated macrophage) (*Adapted from Wang et al., 2019*)

Senescence is a stable type of growth arrest, usually (but not only) caused by persistent activation of the DNA damage response (DDR) and other stress conditions that significantly alter cell morphology, gene expression and/or secretory program [53]. Despite the previous belief that chemotherapy-induced senescence was an irreversible state, more recent observations sustain the hypothesis that cancer cells can escape cell cycle arrest. In this scenario, senescence represents a mechanism allowing a long term survival of a subset of cancer cells with stem-like features that can re-enter the cell cycle and contribute to tumor relapse [54, 55]. The eradication of senescent could therefore provide a survival advantage for oncological patients, and recent studies are investigating the efficacy of senolytic agents for cancer therapy [53, 55, 56].

1.2.2 Cancer stem cells (CSCs)

As previously mentioned, heterogeneity is one of the major characteristics of cancer cells and represents one of the main causes of intrinsic drug resistance. In the past few decades, scientists identified a subpopulation of tumors cells with stem-like features that, like normal stem cells, are capable of self-renewal and proliferation. These cells, defined as Cancer Stem Cells (CSCs) now are recognized as the major challenge in cancer therapy for their distinct features, including self-renewal, proficiency to maintain a quiescent state, resistance to anticancer agents, capability to originate new tumor masses and metastases [57–59]. CSCs can undergo both symmetric and asymmetric cell division. Symmetric cell division leads to the production of two identical daughter CSCs and allows self-renewal and expansion of CSCs population; asymmetric cell division results in the production of one daughter CSC (self-renewal) and a daughter progenitor cell able to expand and generate the tumor mass [60].

Several studies reported that CSCs are mainly enriched in late stages of cancer progression and after chemotherapy [61, 62], demonstrating that conventional treatments such as chemo- and radiotherapy, are not effective in targeting CSCs, rather they contribute to induce a stem-like phenotype. Resistant CSCs are then responsible for tumor recurrence (**Figure 4**) [63].

Chemoresistance is primarily linked to CSC ability to remain quiescent in a so-called dormancy state, that is mainly associated with the increased expression of multiple genes, including TGF-β2, p53, RB, cyclin-dependent protein kinase inhibitors (p27, p21, and p57), Notch- pathway-related proteins, along with FoxOs (Forkhead Box O) and NFI (Nuclear Factor 1) transcription factors [64]. Furthermore, recent pieces of evidence show that acquired mechanisms of CSCs chemoresistance are directly associated with their highly effective DNA repair mechanisms and their efficient resistance against reactive oxygen species (ROS) [59].

Another characteristic of CSCs is their capacity to disseminate from their primary site to distant sites where they may seed new metastatic colonies. Many studies demonstrated that compared to epithelial cells, which generally require attachment to extracellular matrix or other cells to survive, therapy-resistant CSCs acquire mesenchymal features that promote metastasis, including higher expression of EMT transcription factors and a progressive increase in stemness markers (CD133, OCT4, SOX2, CD44 and Nanong) [65–67].

Besides, several studies highlighted that CSCs differently respond to anticancer treatment *in vitro* and *in vivo* suggesting the crucial role of the niche environment, which is usually characterized by the presence of different cell types, including fibroblasts, perivascular and vascular cells, and tissue macrophages. However, even if some studies propose a model of CSC-niche interactions mediated by cytokine receptors, adhesion receptors, membrane-bound and soluble cytokine ligands, and

various chemotactic factors, still little is known about how these cells or the niche micro-environment affects CSCs stemness and proliferation [68].

Altogether these shreds of evidence suggest not only the need for a better understanding of CSCs biology and the necessity of novel therapeutic strategies that can prove effective in eradicating not only the bulk of the tumor, but also the tumor latent and chemoresistant subset of CSCs.

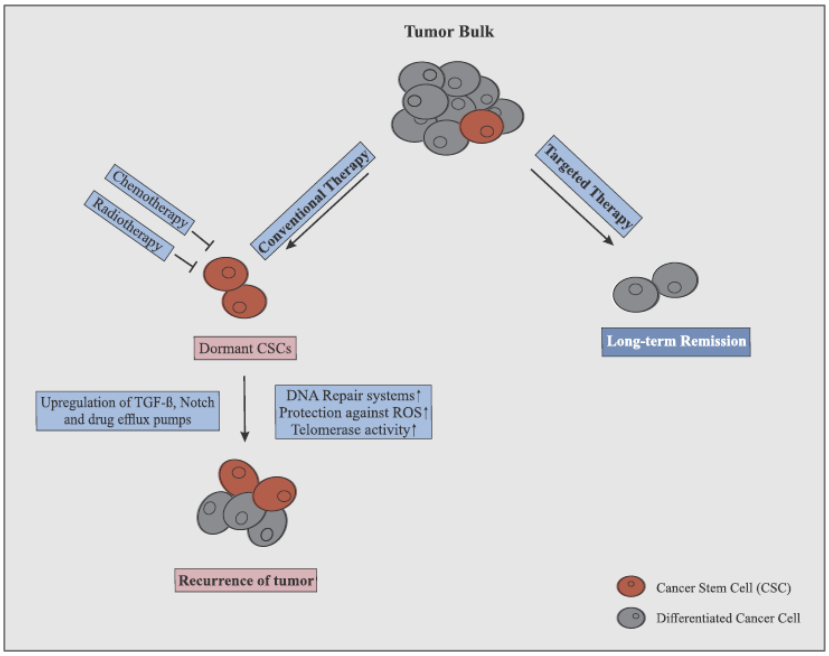

Figure 4 **Effect of conventional and targeted therapy on tumor cells and cancer stem cells (CSCs) during carcinogenesis** (*Adapted from Kuşoğlu et al., 2019*)

1.3. Cell death pathways for cancer therapy

1.3.1 Apoptosis: the main target of anticancer therapies

Apoptosis represents a regulated mechanism of cell death; it occurs physiologically and leads to the removal of unnecessary or damaged cells by maintaining the balance between cell proliferation and cell death [69]. During cancer progression, the impairment of apoptotic control allows tumor cells to survive longer, leading to the accumulation of mutations that can increase their invasiveness, interfere with differentiation, deregulate cell proliferation, and stimulate angiogenesis [70]. For these reasons, in recent years, apoptosis has been considered a crucial process for cancer treatment, and most of the research in drug discovery is focused on the development of therapies inducing apoptosis [69].

The great interest in understanding the apoptotic process headed to a clear comprehension of two distinct molecular signaling pathways involved: the intrinsic or mitochondria-mediated pathway, and the extrinsic, or extracellular triggered pathway (**Figure 5**) [71].

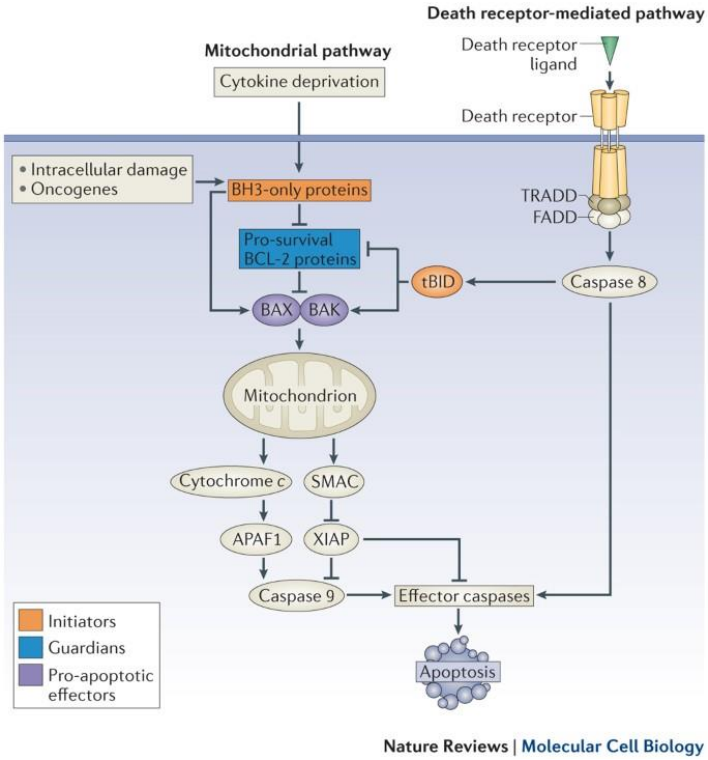

Figure 5 **Schematic representation of both intrinsic (or mitochondrial pathway) and extrinsic (death receptor mediated) apoptotic pathway** (*Adapted from Czabotar et al., 2013*)

Intrinsic apoptosis is activated in response to several cellular perturbations such as ROS, growth factor withdrawal, endoplasmic reticulum (ER) stress, DNA damage, mitotic defects [72]. A crucial event in intrinsic apoptosis is the irreversible outer mitochondrial membrane permeabilization (MOMP) which is regulated by the pro-apoptotic members of the BCL-2 family [73]. In normal conditions, BAK and BAX exist as inactive monomers and, while BAK constitutively resides at the outer mitochondrial membrane (OMM), BAX constantly cycles between the cytosol and the OMM. Upon apoptosis induction, BAX and BAK undergo direct or indirect activation by pro-apoptotic BH3-only proteins BID, BIM, PUMA and NOXA [74]. Activated BAX can form oligomers that pierce the OMM, causing MOMP and the formation of pores. The MOMP is mainly antagonized by the antiapoptotic members of the BCL2 family such as BCL2 itself, BCL2 like 1 (BCL2L1/BCL-XL), BCL2 family apoptosis regulator (MCL1), BCL2 like 2 (BCL2L2/BCL-W), and BCL2 related protein A1 (BCL2A1/BFL-1). This group of proteins mainly resides at the mitochondrial or ER membrane and inhibits proapoptotic proteins by direct binding [73].

MOMP results in the release of apoptogenic factors that usually reside in the mitochondrial intermembrane space including the electron shuttle, cytochrome C and diablo IAP-binding mitochondrial protein (DIABLO/SMAC) [72]. The cytosolic cytochrome C leads to the formation of the apoptosome and activation of the pro-caspase 9 (CASP9), which then leads to the activation of CASP3 and CASP7 [75]. Conversely, when released into the cytosol, SMAC triggers apoptosis by associating with proteins belonging to the family of the inhibitor of apoptosis (IAP) such as the X-linked inhibitor of apoptosis (XIAP) [76].

While intrinsic apoptosis is triggered by intracellular perturbations, extrinsic apoptosis is mediated by two plasma membrane receptors: death receptors and dependence receptors [72]. Death receptors include FAS and TNFR1 that, after binding to their ligands - FAS ligand and TRAIL respectively – induce the cleavage of CASP8. This event triggers the activation of CASP3 and CASP7 mainly in lymphocytes and thymocytes. In other cell types such as cancer cells (in which CASP3/7 activation is controlled by XIAP), CASP8 triggers the truncation of BID (tBID) that translocates to the OMM and acts as BH3-only protein. This event leads to the activation of BAX and BAK-dependent MOMP-driven resulting in regulated cell death controlled by CASP9 [77]. Extrinsic apoptosis can also be mediated by dependence receptors (DR). These receptors lead to cell death when the concentration of their ligands decreases and reaches a limit threshold [72]. Nearly twenty members belong to the DR family, including netrin 1 receptors, neurotrophin receptor neurotrophic receptor tyrosine kinase 3 (NTRK3); and the sonic hedgehog (SHH) receptor patched 1 (PTCH1) [72, 78]. Generally, the absence of ligands leads to a conformational change in DR resulting in increased DR susceptibility to caspases proteolytic cleavage, a crucial step for caspase amplification and apoptosis induction [78]. However, the mechanisms behind extrinsic apoptosis mediated by dependence receptors remain unclear, its clearer comprehension could lead to the identification of a therapeutic strategy that prevents cancer cell proliferation by inducing apoptotic cell death [78, 79].

Nowadays, chemotherapy and radiotherapy represent the backbone of cancer treatment. These traditional strategies trigger apoptosis induction through direct DNA damage and ROS production, however, cancer cells usually acquire mechanisms that lead to apoptosis resistance, in particular by downregulating pro-apoptotic signals and upregulating anti-apoptotic signals [80]. For example, the overexpression of Bcl-2 inhibits cell death and develops cell resistance to DNA damage factors including several chemotherapeutic drugs [81]. Nearly 80% of tumors are triggered by dysfunctional p53 signaling and 50% of cases carry p53 gene inactivation. Aberrant p53 expression leads to the downregulation of Bax/Noxa/Puma expression and upregulates Bcl-2, resulting in impeded cytochrome C release from the mitochondria and apoptotic resistance [80]. Besides, it was reported

that the aberrant upregulation of IAPs abolishes the downstream caspase cascade resulting in improved cancer progression [82].
Thus, alternative cell death pathways capable of killing apoptosis- and therapy-resistant cancer cells, have gained considerable interest among cancer researchers.

1.3.2 Mitochondrial targeting in cancer treatment

The intracellular role of mitochondria is not only related to apoptosis, in fact, mitochondria are also defined as the powerhouse of the cell and their biosynthesis, bioenergetics, and signaling are crucial for cancer progression [83]. During neoplastic progression, cancer cells acquire molecular modifications that cause not only alterations of the mitochondrial apoptotic pathway but also metabolic modifications, such as increased glycolytic metabolism and resistance to hypoxia. These events trigger abnormal lactate secretion along with tumor microenvironment acidification, resulting in a favorable setting for tumor invasion [84].
From a biochemical point of view, the strategies for mitochondrial targeting in cancer treatment are mainly divided into four macro-areas: (1) targeting bioenergetics, (2) targeting the biosynthetic function, (3) targeting the redox capacity, (4) targeting the mitochondrial membrane (MM).
Targeting mitochondrial ATP production has always been considered a non-effective strategy since cancer cells can upregulate glycolysis to produce ATP, bypassing the lack of ATP production from altered mitochondria [83]. On the other hand, it is well-known that during tumorigenesis the bulk of the tumor is characterized by low oxygen and low glucose concentration and that the electron transport chain (ETC) efficiently works at oxygen levels as low as 0.5% [83, 85]. Consequently, even poorly perfused tumors, with low glucose availability, have enough oxygen to generate mitochondrial ATP. Therefore, mitochondrial bioenergetic targeting could be an effective strategy both in poorly perfused tumors, possibly in synergy with therapies targeting glycolysis, such as PI3K signaling pathway inhibitors [86]. In this context, metformin, the widely used antidiabetic drug, is a promising candidate, because of its inhibitory effect on the complex one of ETC [83]; however, its use in advanced tumors therapy is still under investigation [87]. The compound VLX600, an ETC inhibitor, significantly reduced colon cancer cell growth especially in presence of low glucose availability [88]; whereas, degueling, a complex 1 inhibitor, was recently reported to act as an effective metabolic regulator by inducing energy starvation and cell death in drug-resistant melanoma cells [89].
Mitochondrial tricarbossilic acid cycle (TCA) intermediates play a crucial role non only for the production of energy but are required for anabolic reactions. Recent studies have proven that cancer cells can uncouple glycolysis from the TCA cycle, granting the consumption of additional fuel

resources, such as glutamine, to fulfill their increased metabolic demands [90]. Therefore, strategies targeting TCA intermediates seem an additional interesting approach in impairing cancer cell survival [90, 91].

In addition to the aforementioned strategies, targeting the mitochondrial redox capacity in cancer cells seems another interesting strategy. It is well established that the high metabolic activity characterizing proliferative cancer cells is associated with elevated production of ROS [92]. In order to balance the high production of mitochondrial ROS, tumor cells have evolved adaptive strategies to improve their antioxidant systems and to employ ROS in triggering pathways advantageous for cancer cell adaptation and survival to environmental changes, as well as cell proliferation and metastasis [83, 92]. Thus, further studies are needed to elucidate antioxidant defense systems in cancer cells to develop adjuvant therapies, that in combination with chemo- and radiotherapy, could enhance present-day therapeutic strategies.

Historically, necrosis has been viewed as an uncontrollable form of cell death with default status. However, more recent studies have shown that, under certain cellular contexts, necrosis can be a highly regulated form of cell death in adult vertebrate organisms. Regulated necrosis is simply defined as caspase-independent cell death that has all the morphological hallmarks of classical necrosis but that can be inhibited or accelerated by affecting one or more key molecular components.

In recent years, attention has been growing towards the role of the mitochondria in inducing death with a necrotic morphotype [72]. This mechanism of cell death is caused by the rapid dissipation of the mitochondrial membrane potential ($\Delta\psi_m$), loss of ATP production, and the osmotic collapse of mitochondria, caused by openings of the mitochondrial permeability transition pore (MPTP) and triggered by specific perturbation of the intracellular environment, including Ca^{2+} overload or severe oxidative stress [93] (**Figure 6**).

Caspase activation, which is necessary for apoptosis, is ATP dependent and typically requires some degree of mitochondrial function, while necrosis is an ATP independent process where it progresses in conjunction with a complete loss of mitochondrial function [94]. MPTP opening and mitochondrial swelling and rupture also cause the release of apoptogenic factors such as cytochrome c; but, in the absence of sufficient ATP, the formation of the apoptosome and caspase activation is blocked so that the cell perishes through a necrotic process [95].

The MPTP forms within the inner membrane of the mitochondrion where it permits the diffusion of molecules up to 1.5 kDa [96]. The classical model of the MPTP was proposed to be a contiguous pore spanning the outer and inner mitochondrial membranes and consisting of the voltage-dependent anion channel (VDAC, outer membrane) and adenine nucleotide translocator (ANT, inner membrane), regulated by the peptidylprolyl isomerase F (PPIF; also identified as cyclophilin D, CypD) within the

mitochondrial matrix. More recently, evidence has emerged that both ANT and VDAC are not direct components of the MPTP, whereas the mitochondrial F_1F_0 ATP synthase and CypD serve as the core component of the MPTP within the inner membrane [97]. In fact, MPTP-driven necrosis is limited by CYPD inhibitors, such as cyclosporin A (CsA), JW47 and sanglifehrin A (SfA) [72], whereas purified components of the F_1F_0 ATP synthase reconstituted into lipid bilayers could recapitulate pore activity similar to that of the MPTP [98].

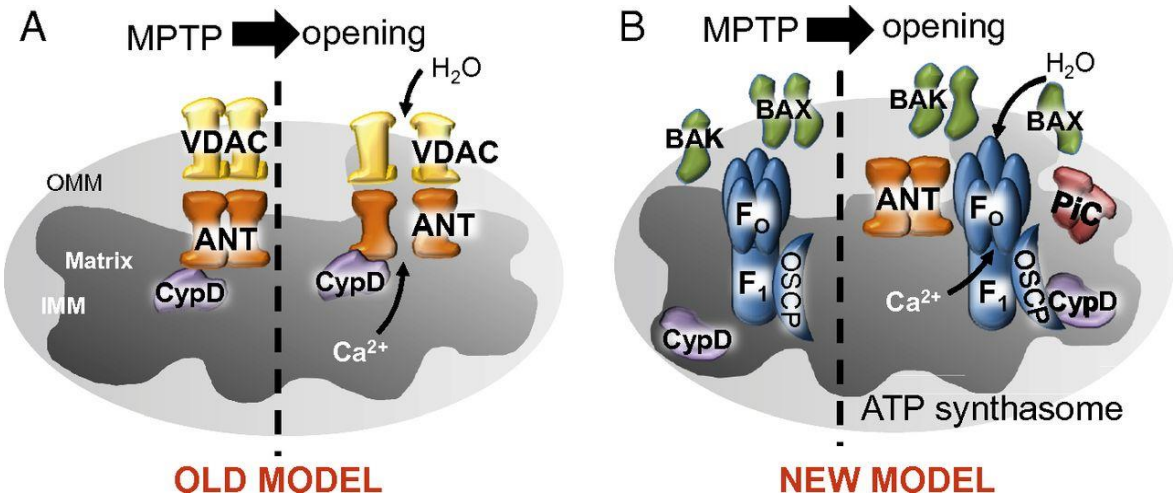

Figure 6 **Structure of the mitochondrial permeability transition pore (MPTP)**. Schematic representation of the original model of the MPTP as a contiguous pore composed of VDAC and ANT regulated by CypD (**A**). Schematic image of the new model of the MPTP consisting of Bax/Bak on the outer mitochondrial membrane and the F_1F_O ATP synthase regulated by CypD in the matrix (*Adapted from Karch et al 2004*)

The MTPT-driven necrosis is regulated by several PTPC interactors, including the BCL2 family members [99], p53 [100], but also by the dynamin-related protein 1 (DRP1), which triggers PTPC opening when phosphorylated by calcium/calmodulin-dependent protein kinase II (CAMKII), after chronic activation of the β adrenergic receptor [101].

Moreover, the latest evidence highlight the importance of tight Ca^{2+} mitochondrial homeostasis for cellular survival, by identifying a possible role of the IMM Ca^{2+} uniporter (MCU) in MPTP-driven necrosis [102].

In summary, the understanding of mitochondria biology and the development of therapies aiming to directly target the powerhouse of the cell could represent a new strategy in order to target apoptotic-resistant cancer cells.

1.3.3 Role of autophagy in cancer treatment

Autophagy is an evolutionary conserved pro-survival stress response, through which cellular contents are degraded after uptake into autophagosomes that subsequently fuse with lysosomes for cargo degradation [103]. Autophagy will be activated under situations of nutrient deprivation to maintain

cellular homeostasis by enriching nutrient pools. Autophagy also serves to remove damaged and potentially harmful organelles, thereby supporting cell survival. Up to date, three different types of autophagy are known: micro-autophagy that is characterized by direct engulfment of material by the lysosome; chaperone-mediated autophagy that requires the recognition by the heat shock protein (hsp70) of the amino acid motif (KFERQ) and the delivery to the lysosome through the lysosomal protein LAMP2A; macro-autophagy, the best characterized, which requires the formation of double-membrane vesicle named autophagosomes [104].

Macro-autophagy (hereafter mentioned as autophagy) is a complex mechanism usually induced by nutrient deprivation and/or other stress conditions such as hypoxia or endoplasmic reticulum (ER) stress [105], in mammal it is regulated by an intricate network of signaling pathways among which AMPK and PI3K/mTORC1 pathways play a pivotal role (**Figure 7**).

The first step of autophagy is represented by the formation of the phagophore, a double membrane vesicle deriving from small membranous portions of broken organelles, further elongated and closed by the autophagy-related protein (ATG) complexes. Among these complexes, the Unc-51-Like Kinase (ULK) complex (composed of the ULK1/2 protein kinase, the FIP200 scaffold protein, ATG13 and ATG101) [106] leads to the activation of class III PI3K complex (composed of the VPS34 lipid kinase, VPS15, Beclin and ATG14). PI3K, in turn, produces phosphatidylinositol-3-phosphate, necessary for elongation of the phagosome [107].

Autophagosome formation involves two successive ubiquitin-like reactions. The first reaction employs the E1-like ATG7 and the E2-like ATG10 enzymes, which conjugate the ubiquitin-like ATG12 to ATG5. This conjugate then forms a complex with ATG16L1. The second set of reactions involves the ubiquitin-like LC3 protein family. LC3-I is generated by proteolytic cleavage of pro-LC3 by ATG4, which exposes a C-terminal glycine that is amenable to conjugation. ATG7, the E1-like enzyme, ATG3, an E2-like enzyme, and the ATG5-12-16L1 complex as the E3-like enzyme then conjugate LC3 family members to phosphatidylethanolamine (PE) on the surface of nascent autophagosomes [108].

The autophagic system also requires proteins known as autophagy receptors, which increase the selectivity of the autophagic process by facilitating the engulfment of certain cargoes by the growing autophagosomes [109]. The most widely studied autophagy receptors are p62/SQSTM-1 (sequestosome-1) and BRCA1 [107, 110]. The autophagy receptor proteins share a common domain organization containing both a ubiquitin-binding domain (UBD) and an LC3-interacting region, which allow them to act as bridging molecules recognizing the degradation signal on the autophagic cargo on the one hand, and binding LC3 on the growing autophagosomal membrane on the other.

During autophagosome maturation, the cytosolic phagosomes are directed, through microtubules and actin filaments, to the perinuclear region, where lysosomes are mainly localized. Subsequently, the fusion of the autophagosome with the lysosome is mediated by several complexes including tethering factors, Rab GTPases, and SNAP receptors complexes (SNAREs). While SNAREs proteins are mainly localized on the autophagosomal membrane, Rab GTPases (RAB2 and RAB21) are located on the lysosomal membrane [111]. This fusion results in the formation of the autolysosome, the structure designated to the degradation and the recycling of autophagosome contents [104].

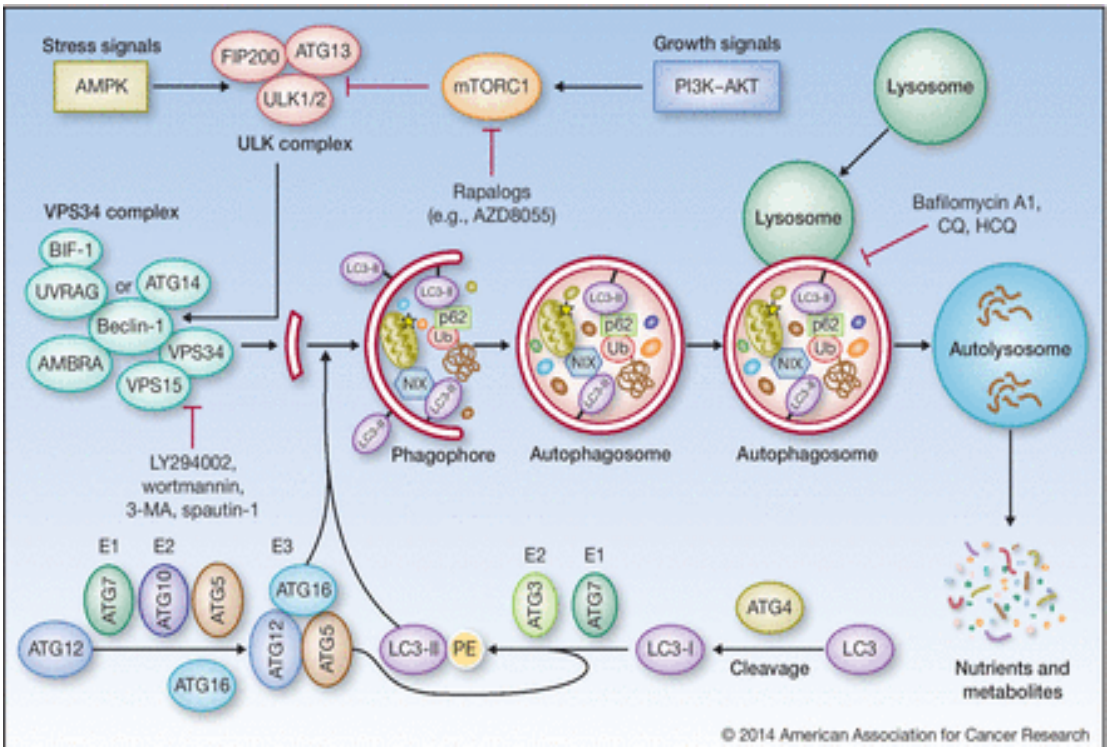

Figure 7 **Schematic representation of the autophagic process.** (*Adapted from Cicchini et al., 2015*)

In the context of cancer, the role of autophagy is still controversial since, unlike apoptotic or necrotic programmed cell death, autophagy can play a context-dependent tumor-suppressive or pro-survival role [104, 112].

Autophagy is active in many types of cancer and is required for cancer progression by promoting survival during nutrient stress and allowing the recycling of cell components to support a transformed phenotype [113–115]. Moreover, autophagy can help tumor cells to overcome the cytotoxicity of chemotherapy [116, 117]. In this regard, several autophagy-targeting drugs are under study in ongoing clinical trials [118]. For instance, chloroquine (CQ) and hydroxychloroquine (HCQ), are well known anti-malarial drugs with the ability to inhibit lysosome acidification, resulting in the block of the last steps of autophagy in cancer cells [119]. These drugs revealed their efficacy *in vivo* and several clinical trials are ongoing to identify efficient chemotherapy combinations to use with these

compounds [120]. Nowadays, many other drugs are under investigation, including ULK inhibitors (ULK100 and ULK101) [121], and ATG inhibitors (UAMC-2526and LV-320) [118]. However, further pre-clinical studies must be conducted to define their clinical efficacy.

Conversely, several studies reported that autophagy induction in cancer cells can improve chemotherapy, especially in chemoresistant cells. In this context, the administration of the mTOR inhibitor rapamycin had been proven to possibly reverse resistance to trastuzumab in patients with HER2+ metastatic breast cancers [122, 123]. Moreover, the mTOR inhibitor AZD8055 was reported to display antitumor effects in colon cancer cells [124]. These results support the existence of autophagy-dependent cell death, a type of cell death that requires autophagic machinery and is characterized by the absence of chromatin condensation and caspase activation, and the presence of several autophagosomes with wide degradation of cytoplasmic material [72, 125].

1.3.3.1 Lysosomes and cancer

Lysosomes are conservative organelles with an indispensable role in cellular degradation and the recycling of macromolecules whose role, in cancer cells, extends far beyond cellular catabolism and includes a variety of cellular pathways, such as proliferation, metastatic potential, and drug resistance [126].

The vacuolar ATPase (V-ATPase) pumps protons into the lysosome to create an acidic compartment (pH approximately 4.5–5.0) enclosed by a phospholipid membrane where nearly 60 acid hydrolases, including lipases, peptidases, nucleases, glycosidases, phosphatases, and sulfatases, cooperate to regulate nutrient homeostasis, extracellular matrix degradation, cell signaling regulation and cell death [127].

In cancer, cell transformation increases the requirement for new biomass production, and lysosome function to provide energy and metabolic precursors for macromolecular synthesis. Recycling of intracellular materials or uptake and catabolism of extracellular proteins and lipids can act as sources of these nutrients [128]. Since lysosomes display the ability to regulate metabolic homeostasis by perceiving energy, growth factor signals, and nutrients availability, they are considered an important hub for different signaling pathways. The main pathways are represented by the mammalian target of rapamycin complex 1 (mTORC1) and AMPK, key regulators of autophagy and catabolic and anabolic processes [129].

In addition to recycling macromolecules, lysosomes are capable of fusing and catabolizing entire organelles. This process is best described for mitochondria via a distinct process termed mitophagy

[130], but the emerging roles played by the lysosome in nucleophagy, pexophagy, and other forms of organellophagy are also of potential therapeutic interest [131].

Lysosome function is also involved in membrane remodeling to allow cell shape changes that enable invasion through the basement membrane. Exocytosis of lysosome-derived heparanase and cathepsins affects cell shape and favors the degradation of extracellular matrix to prime local invasion [132].

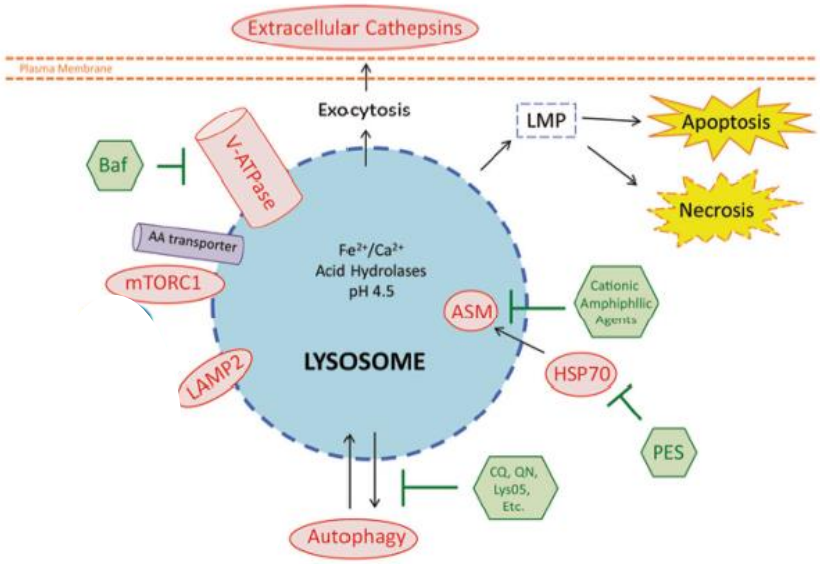

Figure 8 **Key elements involved in lysosomal biology in cancer**. *In red*: factors that can play roles in cancer progression. *In green*: various drugs that target the lysosome or cellular components link to the lysosome that can destabilize the organelle leading to LMP. *In yellow*: activation of cell death pathways. (aa amino acid, ASM acid sphingomyelinase, Baf Bafilomycin A 1, CQ chloroquine, ECM extracellular matrix, HSP70 70-kDa heat shock proteins, LAMP lysosome associated membrane glycoproteins, LMP lysosomal membrane permeabilization, mTORC1 mammalian target of rapamycin complex 1/mechanistic target of rapamycin, PES phenylethynesulfonamide, QN quinacrine, ROS reactive oxygen species, TFEB transcription factor EB, V-ATPase Vacuolar-type H+ATPase) (*Adapted from Fennelly et al., 2017*)

The lysosome is more than just the recycling center for the cell, and an improved understanding of how this organelle participates in tumor initiation and progression will be an exciting area of biology that could lead to the development of new therapeutic strategies for cancer (**Figure 8**).

Indeed, the activation of lysosomes during malignant transformation does not come without a price. The cancer-associated changes in lysosomal composition result in reduced lysosomal membrane stability, thereby sensitizing cells to lysosome-dependent cell death, a mechanism of regulated cell death that results in the permeabilization of the lysosomal membrane [133, 134]. At the biochemical level, this mechanism of cell death starts with lysosomal membrane permeabilization (LMP) and results in the release of lysosomal content, including cathepsins, into the cytoplasm; once released,

cathepsins can lead to apoptosis induction, by proteolytic regulation of factors such as BAX, BID, XIAP, BCL2 [72, 135].

The molecular pathways upstream LMP are still unclear. Some studies reported a link between lysosomes and mitochondria suggesting that LMP occurs after MOMP and considering LMP as a consequence of intrinsic apoptosis [136], whereas other findings demonstrate that LMP arises before mitochondrial permeabilization, through the pore-forming activity of BAX at the lysosomal membrane [137, 138]. Despite these observations, lysosomal-dependent cell death does not necessarily rely on caspase and MOMP and it does not result always in apoptosis [139, 140].

Oxidative stress seems to play an important role in LMP mainly by the production of H_2O_2 and hydroxyl radicals that cause lipid peroxidation of the lysosomal membrane, and activation of lysosomal Ca^{2+} channels [141, 142]. Moreover, physiological lysosomotropic agents including sphingosine and calpains were reported to induce LMP. These molecules display an affinity for the acidic lysosomal environment of the lysosome in which they accumulate, till they reach a limit concentration that destabilizes the membrane of the lysosome [143].

From cancer therapy, lysosomal-dependent cell death represents a good strategy in targeting apoptotic-resistant tumor cells [133, 144]. Many studies report that neoplastic cells are usually more sensitive to lysosomotropic agents and compounds causing lysosomal cell death because of their enlarged lysosomal system [145]. Moreover, it was demonstrated that targeting of lysosome during chemotherapy could result in improved outcomes, since it reduces chemotherapy agents accumulation in the lysosomes, resulting in more effective action in the cytosol and the nucleus [146, 147].

1.3.4 Endoplasmic reticulum stress induction

The endoplasmic reticulum (ER) is a multifunctional organelle, involved in Ca^{2+} storage or release, lipid biosynthesis and protein folding [148]. Alterations in ER homeostasis, caused by Ca^{2+} depletion, hypoxia, oxidative damage, hypoglycemia, and viral infections, trigger the accumulation of unfolded or misfolded proteins that results in the so-called ER stress, which induces the activation of the unfolded protein response (UPR) an adaptive response that leads to the reduction of unfolded proteins to favor cell functions recovery [149–152].

Although the UPR is an essential adaptive mechanism that promotes cell survival, in case of severe or irreparable damage, prolonged UPR switches from pro-survival signaling to pro-death signaling leading to activation of intrinsic apoptotic and autophagy pathways [153].

UPR is mediated by three different signaling cascades associated with three distinct ER stress sensors: protein kinase R (PKR)-like ER kinase (PERK), inositol requiring enzyme 1 (IRE1), and activating

transcription factor 6 (ATF6) [154] (**Figure 9**). In physiological conditions, these sensors are inactive and bind the chaperone GRP78 (also known as BiP). On the contrary, when the stress condition directly affects the ER, the inhibitory function of GRP78 is titrated down by the accumulation of unfolded or misfolded proteins inside the ER lumen. This event results in the activation of serine/threonine kinase activity of PERK that phosphorylates eukaryotic initiation factor 2 alpha (EIF2α) and nuclear factor E2-related factor 2 (NRF2) resulting in the upregulation of chaperones factors involved in oxidative stress response and inhibition of protein synthesis [154, 155].

Additionally, the stimulation of IRE1 results in its dimerization and auto-transphosphorylation and results in the splicing of the unspliced X box-binding protein 1 (uXBP1), in the active transcription factor, spliced XBP1 (sXBP1) involved in the transcriptional response aiming to alleviate the intracellular misfolded protein burden [149]. These events result in the transcription of genes encoding proteins involved in protein folding and oxidative stress response, but also ER-associated degradation (ERAD), a crucial event for cell survival under ER stress conditions [156, 157].

Lastly, ATF6 activation, mediated by the dissociation from BiP/GRP78, upregulates genes associated with ERAD and mediates their binding to XBP1s. These events are essential for the transcription of ER quality control genes including ERdj3/HEDJ, EDEM, ERdj4, RAMP4 and p58IPK [158].

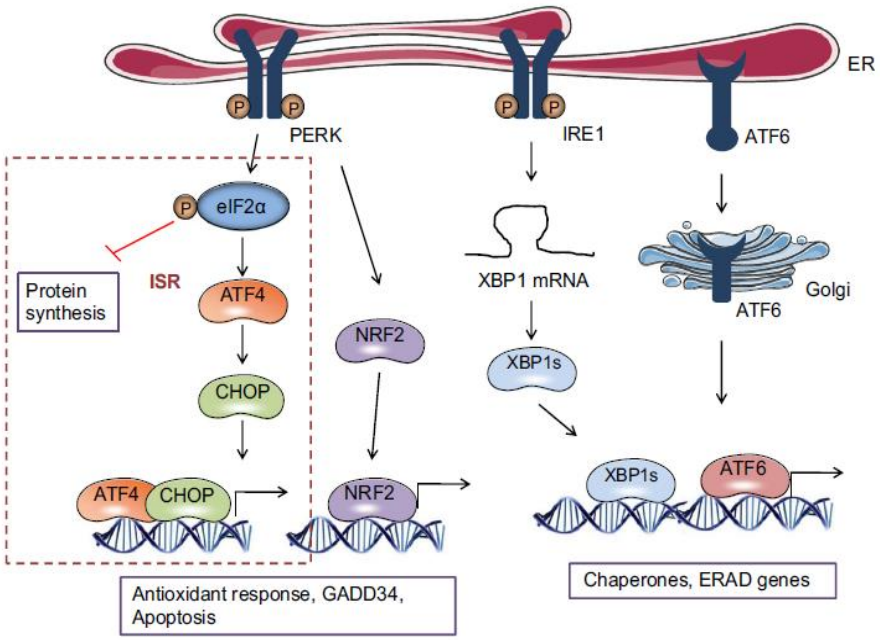

Figure 9 **Representation of the UPR.** Three different signaling cascades associated to three distinct ER stress sensors (*Adapted from Iurlaro et al., 2015*)

When the primary stimulus responsible for ER stress is prolonged or excessive, the adaptive mechanisms of the UPR fail to restore physiological homeostasis, and cell death is usually induced by inhibition of cell cycle and apoptosis induction [153]. The mechanism behind this switch is still

not well defined, although experimental evidence suggests that, at least in part, it's mediated by the sustained activation of eIF2a, and by the expression of ATF4 and C/EBP homologous protein CHOP [151]. CHOP is the main effector of the pro-death side of the UPR as it upregulates some pro-apoptotic proteins and regulates the intrinsic apoptotic pathway by inducing autophagy and caspase 4 activation [153]. Finally, IRE1, with its kinase activity, can induce ER collapse activating JNK and P38 MAPK pathways [152] (**Figure 10**).

In the context of cancer, ER stress has always been considered a double-edged sword due to its ability to induce both cell survival and cell death [159]. Since high proliferative cancers are frequently exposed to alteration in protein homeostasis and ER stress, the upregulation of UPR is required for the maintenance of proteostasis to sustain tumor growth. However, under chronic and severe ER stress, cancer cells can fail to restore ER homeostasis via UPR, with the consequent switch from pro-survival to pro-death conditions [160]. In this context, studies are ongoing to determine the mechanisms involved in ER-stress dependent cell death [161, 162].

Nowadays it is possible to identify two ways of cell death under chronic ER-stress: the UPR dependent and the UPR independent. As previously mentioned, UPR dependent cell death is mainly mediated by CHOP, induced via the IRE1α / Apoptotic-Signaling Kinase-1 (ASK1) / JNK and p38 MAPKs pathway and through PERK/ eIF2α. CHOP targets are GADD34 (growth arrest and DNA damage-inducible 34), the cell surface death receptor of the TNFR family DR5 (TRAIL Receptor-2), and Ero1α (endoplasmic reticulum oxidoreductase-1), which hyperoxidizes the ER leading to cell death [161]. Moreover, Ero1α can activate inositol triphosphate receptor (IP_3R), stimulation that promotes extreme Ca^{2+} release from the ER to the mitochondria resulting in cell death [163].

Conversely, UPR-independent ER stress-related cell death could be driven by different causes, which include alterations in Ca^{2+} dynamics [164, 165]. Acute release of Ca^{2+} from ER was reported as a leading mechanism of Ca^{2+} - mediated mitochondrial cell death [166]. Additionally, it was reported that Bak and Bax play a crucial role in ER Ca^{2+}-mediated apoptosis. A temporary overexpression of Bax can induce Ca^{2+} release from the ER, resulting in a mitochondrial overload of Ca^{2+} and cytochrome c release [167].

Furthermore, UPR independent ER stress cell death could also be driven by ER-membrane reorganization. With the help of informatic tools researchers identified that this stress response was caused by a different variety of drugs including antimalarials, antipsychotics and antihistamines [168].

Altogether, these pieces of evidence suggest that both the inhibition and the enhancement of the ER stress and UPR could show potential in the identification of an alternative regimen in targeting chemoresistant cancer cells.

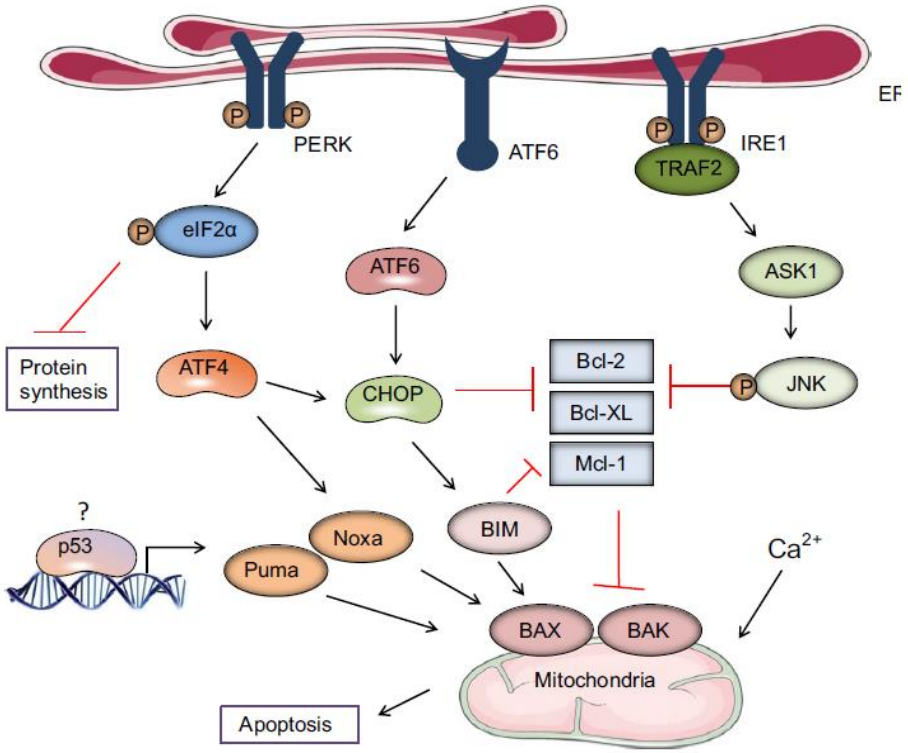

Figure 10 **Schematic representation of ER stress-induced cell death** (*Adapted from Iurlaro et al., 2015*)

1.3.5 Intracellular Ca^{2+} dynamics in cancer

Ca^{2+} homeostasis is of pivotal interest for the cell, reflecting the central importance of Ca^{2+} as a second messenger, regulating a variety of cellular processes such as cell motility, metabolism, gene transcription, cell proliferation, division and differentiation, and cell death [169]. Therefore, several transport systems including the sarco/endoplasmic Ca^{2+}-ATPases (SERCAs), the plasma membrane Ca^{2+}-ATPases (PMCAs) and the Na^{+}/Ca^{2+} exchangers (NCX, NCKX) strictly maintain the electrochemical Ca^{2+} gradients between cytosol (~100 nM), extracellular environment (> 1 mM) and intracellular Ca^{2+} stores of the sarco/endoplasmic reticulum (> 100 μM) [170].

Modification in the $[Ca^{2+}]_{cyt}$ can occur not only after the opening of plasma membrane channels such as voltage-operated channels, receptor-operated channels (NMDA and ATP receptors), and second messenger-operated channels, but also through the opening of inositol-1,4,5-trisphosphate receptors (IP_3Rs) downstream receptor tyrosine kinases (RTKs) or G-protein coupled receptors (GPCRs), coupled to phospholipase C (PLC) activation [169]. Furthermore, internal Ca^{2+} release can be also modulated by other second messengers such as cyclic ADP ribose (cADPR), nicotinic acid adenine dinucleotide phosphate (NAADP), sphingosine-1-phosphate (S1P) and Ca^{2+} itself [171]. $[Ca^{2+}]_{cyt}$

variations can occur as global constant or transient increases, or tightly localized such as Ca^{2+} sparks, or can arise as oscillations or waves. These modifications are decoded by the cells and result in the regulation of several processes [172].

Numerous studies reported that deregulation in Ca^{2+} homeostasis mechanisms can lead to the development of several diseases including cancer [169, 170, 172]. Cancer cells are usually characterized by aberrant intracellular Ca^{2+} levels or Ca^{2+} regulating protein expression. In proliferating cells, mitogenic growth signals lead to the activation of Ca^{2+} effectors, including calmodulin-dependent protein kinases II (CaMKII), calcineurin and protein kinase C (PKC), resulting in cell cycle progression [173]. Moreover, these mechanisms are further sustained in cancer cells by the activation of Ca^{2+}-dependent transcription factors, including c-Jun, c-Myc and c-Fos, that lead to the hypertrophic growth through the expression of cyclin D, cyclin E and cyclin-dependent kinases, that regulates the phases G1 and G1/S of the cell cycle [174].

Furthermore, several studies demonstrate that a modified regulation of $[Ca^{2+}]_{cyt}$ during cancer progression could result in apoptosis resistance [175]. In fact, tumor cells can display mechanisms of cell adaptation also in a condition of reduced $[Ca^{2+}]_{ER}$ by modulating he expression of crucial components of the store-operated calcium entry (SOCE) response including ORAI1 and STIM1, but also by downregulating the expression or the activation of IP_3R, resulting in decreased Ca^{2+}-signal transmission in the ER-mitochondrial contact sites and blocked MTP-driven cell death [173].

Altogether these findings highlight the fact that disrupting intracellular Ca^{2+} dynamics could represent an effective strategy in targeting tumor cells [175, 176]. In this context, many drugs already in use for cancer treatment target these mechanisms (**Table 2**) and several studies are ongoing for the identification of new compounds that can alter the regulation of $[Ca^{2+}]_{cyt}$ during cancer progression [169].

Table 2 **Summary of the principal compounds targeting Ca^{2+} channels/transporters/pumps in cancer** (*Adapted from Patergnani et al., 2020*)

Channel/Transporter/Pump	Compound	Cancer
TRPCs	20-GPPD	Colorectal
	SKF96365	Glioblastoma
	Carvacrol	Glioma
	D-3263	Prostate, colon, breast, lung, pancreas, leiomyosarcoma, and Kaposi's sarcoma
	Capsaicin	Prostate
	Cannabidiol	Bladder
	SOR-C13	Ovarian and prostate
	Dexamethasone	Leukemia
VGGCs	Mibefradil	Esophageal, colon, glioblastoma, and ovarian
	NNC-55-096	Glioblastoma and ovarian
Purinergic P2 receptors	BIL010t	Basal cell carcinoma
	BIL06v	Advanced or metastatic solid tumors
	AR-C118925XX	Pancreatic ductal adenocarcinoma
ORAI and STIM	SKF96365	Breast
	DPB-162AE/-163AE	Colon and glioma
	ML-9	Prostate
	GA101/obinutuzumab	Non-Hodgkin lymphoma and leukemia
	5-Fluorouracil	Hepatocarcinoma
SERCA	Mipsargargin	Prostate cancers, glioblastoma, kidney, and hepatocellular carcinoma
	Curcumin	Breast, lung, ovarian, and colon
PMCA	Pt(O,O0-acac)(γ-acac)(DMS)	Breast
	Resveratrol	Prostate
IP3R3	Paclitaxel	Ovarian, breast, neck and head
VDAC	R-Tf-D-LP4	Glioblastoma, lung, and breast

1.4 Drug repurposing: psychotropic drugs and cancer

Despite increasing efforts in research and development, successful cancer drug development has proven difficult. The average period from preclinical experiments to completed regulatory review vary between 10-17 years [177], whereas estimates of capitalized costs range from 161 to 1800 million dollars per drug [178] (**Figure 12**).

Currently, there are more than 10.000 clinical trials investigating drug interventions in cancer registered at www.clinicaltrials.gov. However, the approval rate of cancer drugs entering phase I trials is very low [179]. The 'classical' process of drug development is estimated to have an approximately 90% attrition rate, meaning that 90% of those drug candidates that have been extensively studied in preclinical models, lack toxicity in rodents and large animals and are well tolerated by humans do not reach drug approval stage [180–182]

For oncology drugs that receive marketing approval, prices have risen steeply in recent years, increasing significantly the burden on health economies worldwide. Whereas basic drug discovery for a large part receives public funding and financial support from nonprofit organizations, late-stage development is mostly driven by the pharmaceutical industry and venture capital. Given the profit-based incentives of this funding model, drugs that ultimately receive clinical approval are highly-priced to cover overall investments − both for failed and successful drug candidates [183] (**Figure 12**).

For all these reasons, drug repurposing (also known as repositioning) has received in the last years increasing interest as an alternative strategy to de novo drug synthesis, and it consists of using an already approved drug for a different application than the one for what it was originally approved. Drug repurposing grants the possibility to develop a new therapeutic option in a shorter time, because of the great quantity of data already available about safety and toxicity, even though a new clinical trial to approve repositioning is required [184].

By now, many common drugs have been repositioned in cancer either for prevention or therapy Examples are aspirin, statins and metformin [185–187]. And many others are under investigation for their repurposing including cardiovascular drugs such as beta-blockers, digoxin, antipsychotic drugs (chlorpromazine, fluspirilene and penfluridol), tricyclic antidepressant, the anti-epilepsy valproic acid and thalidomide [184, 188].

Among these categories, antipsychotic drugs are proving to be a good option in repurposing due to safety and long clinical use [189]. It has long been suggested that individuals affected by psychosis, schizophrenia or bipolar disturbs exhibit reduced tumor incidences after receiving long-term drug treatment compared to the general population [190–193] and neuroleptics have been suggested as

possible mediators of this effect [192]. This reduction has been found in men for smoking-related cancers [194], prostate [194, 195] and CRC [194, 196].

Many antipsychotic drugs have demonstrated in vitro antitumoral activities [184] (**Table 3**). In this context, the antipsychotic chlopromazine (CPZ) that has been reported to be associated with a lower risk of prostate cancer in men [197], upregulates cyclin-dependent kinase inhibitor p21 and autophagic flux by inhibiting Akt/mTOR pathway in glioblastoma cell lines [198, 199]and induces apoptosis via TP53 upregulation in CRC [200]. Besides, penfluridol was found to inhibits pancreatic tumor increasing autophagy [201].

Furthermore, recent data have revealed that antipsychotic drugs display a potential value in eradicating not only the bulk of the tumor but also CSCs. For example, pimozide was reported to reduce cell proliferation and to promote CSCs differentiation in many cancer types [202]. CSCs differentiation represents a new therapeutic strategy whose objective is to force CSCs to differentiate into cell types lacking self-renewal, malignancy, and proliferation ability, thus preventing tumor relapse, and making them more susceptible to present-day chemotherapy [58, 203].

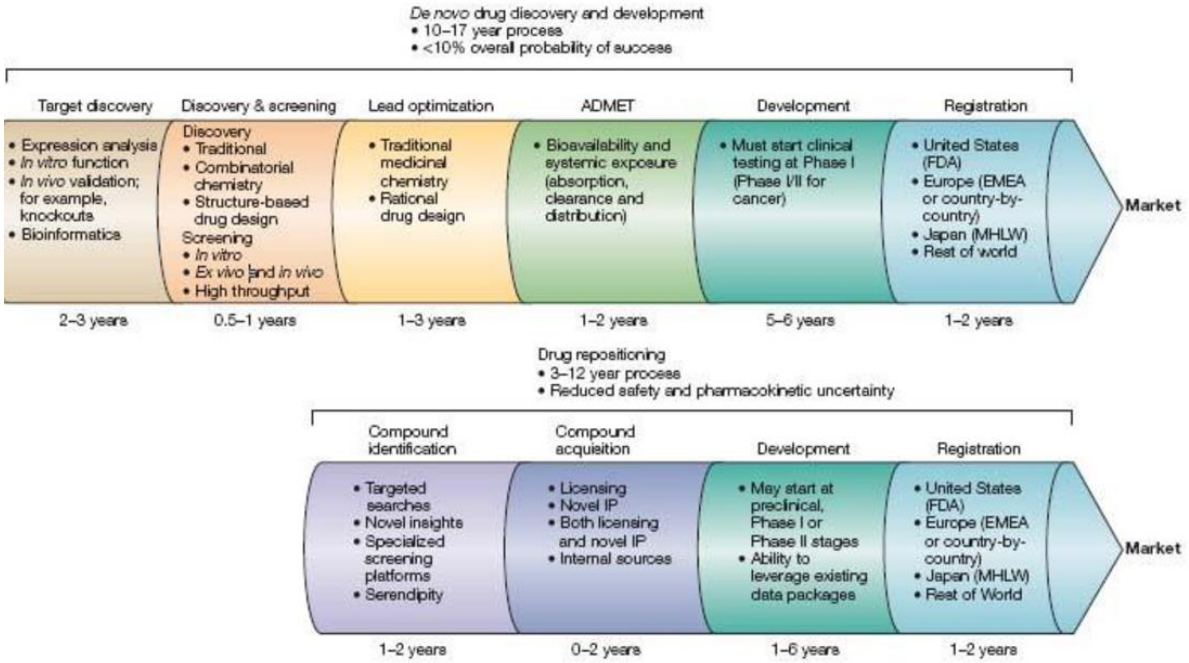

Figure 11 **Pipelines representing *de novo* drug discovery versus drug repurposing** (*Adapted from Deotarse et al., 2015*)

Table 3 **Psychiatric drugs with potential anti-neoplastic effects** (*Adapted from Huang et al., 2018*)

Class Drug	Primary indications for use	Primary mechanism of action	Mechanism of anti-cancer effects
Valproic acid (Valproate, VPA)	Bipolar disorder Epilepsy Migraine headaches	Blockade of voltage-gated sodium, potassium, and calcium channels and inhibition the re-uptake of GABA.	Inhibits histone deacetylase to reduce cancer cell proliferation and induce apoptosis; induces differentiation and inhibits angiogenesis.
Phenothiazines Chloropromazine Levomepromazine Thioridazine	Schizophrenia Psychosis Antiemetic	Dopamine receptor antagonists	Promotes cancer stem cell differentiation through dopamine receptor pathway; inhibits mitochondrial DNA polymerase and decreases ATP production with selectively cytotoxicity and antiproliferative activity in leukemic cells.
Olanzapine Pimozide	Schizophrenia Bipolar disorder Tourette syndrome Resistant tics	An antagonist of the D2, D3, and D4 receptors and the 5-HT7 receptor	Disrupts cholesterol homeostasis to kill cancer cells.
Selective serotonin reuptake inhibitors (SSRI) Citalopram Fluoxetine Paroxetine Sertraline	Depression Generalized anxiety disorder Obsessive–compulsive disorder Eating disorders Stroke recovery Premature ejaculation	Serotonin reuptake inhibition	Reduces proliferation and induce apoptosis in cancer cells; down-regulates pAKT to mediate the synergistic anti-proliferative interaction with other chemo-drugs.
Tricyclic antidepressants Imipramine Trimipramine Amitriptyline	Major depression Attention-deficit hyperactivity disorder Insomnia Chronic pain	Serotonin and norepinephrine transporter blockage to enhance neurotransmission.	Inhibits cellular proliferation and induces cell apoptosis in different tumors including neuroendocrine tumors; improves the effectiveness of other chemotherapeutic agents.
MAO inhibitors Selegiline Phenelzine Tranylcypromine	Atypical depression Panic disorder Borderline personality disorder	Inhibition of monoamine oxidase, thus preventing the breakdown of monoamine neurotransmitters.	Inhibits BHC110/LSD1, as an important chromatin modification enzyme capable of demethylating histone.

2. Aim of the study

In this Ph.D. dissertation, I intended to describe the identification of psychotropic drugs with cytotoxic activity in several cancer cell lines and to elucidate their pharmacological properties supporting their possible applications in cancer treatment.

This first part of the research project led to the identification of a group of drugs displaying cationic amphiphilic properties (CADs) reducing tumor cell viability at clinically relevant concentrations, by impairing both mitochondrial and lysosomal function. These data resulted in one publication that is attached at the end of this thesis; also, the results related to this first part can be found in section *4.1 Psychotropic drugs show anticancer activity by disrupting mitochondrial and lysosomal function* of this thesis.

Besides, I included in this dissertation our ongoing investigation which aims to dissect the molecular mechanism through which spiperone, one of the psychotropic drugs identified through the aforementioned screening, proves cytotoxicity in colorectal cancer cells. These unpublished data can be found in section *4.2 Effective cytotoxic activity of spiperone on human colorectal cancer cells*.

Supplementary material is listed in paragraph *8 Supplementary material*.

3. Materials and methods

3.1 Cell culture

The human differentiated cell line: HCT116, SW620, MCF7, MDA-MB-231, U87 and U251 cell lines were purchased from the American Type Culture Collection (ATCC), while human dermal fibroblast cell line (HDF) was a kind gift from Dr. Barbara Azzimonti (Department of Health Sciences, University of Piemonte Orientale). MCF7, HCT1116, HDF, vAT-MSC and U251cells were cultured in Dulbecco's Modified Eagle Medium (DMEM, Gibco), whereas HCT8, SW620 and MDA-MB-213 cells were maintained in RPMI-1620 (Gibco). U87 cells were cultured in Minimum Essential Medium (MEM, Gibco). All culture media were supplemented with 10% Fetal Bovine Serum (FBS, Euroclone) and 1% antibiotics-antimycotics (Penicillin, Streptomicyn, Amphotericyn, Sigma).

Peripheral blood mononuclear cells (PBMCs) were isolated from human blood by ficoll density gradient centrifugation and were stimulated for 24 hours with 10 μmol/L phytoheamoagglutin (PHA, Sigma) in RPMI-1620 (Gibco) supplemented with 10% heat inactivated FBS (Euroclone). Subsequently, cells were cultured for 48 hours in fresh RPMI containing interleukin 2 (IL-2, Peprotech). Lastly, cells were harvested and plated for viability assay.

Human CRC stem cell lines (CRC-SCs) 511, DA13, CCO9 and Me52 were kindly provided by Prof. Giorgio Stassi (Department of Surgical, Oncological and Stomatological Sciences, University of Palermo). These cell lines were cultured in suspension as colonospheres in stem cell medium (DMEM/F12, Gibco) supplemented with EGF (10 μg/ml, Peprotech) and FGF (20 μg /ml, Peprotech), B27 and N2 (Gibco), 1 mmol/L nicotinamide (Sigma Aldrich) and 1% antibiotics-antimycotics (Penicillin, Streptomicyn, Amphotericyn, Sigma). All the cell lines were cultured at controlled temperature and atmosphere in a humidified incubator (37°C, 5% CO_2).

3.2 Psychotropic drugs

Psychotropic drugs used in the screening were purchased from Cayman Chemicals, Sigma, TCI Chemicals and Selleck Chemicals. List of drugs used: aripiprazole, brexpiprazole, cetirizine, diphenhydramine, droperidol, ebastine, fluoxetine, fluspirilene, haloperidol, iloperidone, ketanserin, metoclopramide, nefazodone, paliperidone, penfluridol, pimozide, pipamperone, R59022, R59949, risperidone, ritanserin, spiperone, trazodone, urapidil, way-100135 and ziprasidone. All drugs were dissolved in DMSO at a 10 mmol/L concentration and stored, in small aliquots at -20°C.

3.3 MTT (Thiazolyl blue tetrazolium bromide) viability assay

For each cell line, 1,000 cells/well were plated (only for PBMCs 10,000 cells/well were plated) in a volume of 100 µL in 96 wells plate. Cells were treated with different concentration of drug and incubated for 72 hours. For each concentration of drug, the same concentration of vehicle (DMSO) was used as control. MTT (Thiazolyl blue tetrazolium bromide, Sigma) 0,5 mg/ml was, then, added to each well and incubated for 4 hours at 37°C and 5% CO_2. Crystals were dissolved using 100 µl of acidic isopropanol (4 mmol/L HCl) and the absorbance (570 nm and 650 nm) was read at the spectrophotometer (Victor, PerkinElmer).

To perform viability assay with biogenic amines 4,000 cells/well from MCF7 and HCT116 were plated in 96 wells plate. Cells were treated with different doses of serotonin, dopamine and histamine (Cayman Chemicals) in DMEM 0% FBS and viability was evaluated after 24- and 48-hours treatment by MTT assay.

3.4 Viability rescue assay

To perform viability rescue experiments, 1,500 cells were plated in 96 wells plate and treated with spiperone, nefazodone, fluoxetine, fluspirilene, ebastine, pimozide or penfluridol in combination with vehicle alone (DMSO), or with 5 µmol/L carbobenzoxy-valyl-alanyl-aspartyl- [O-methyl]fluoromethylketone (zVAD-fmk, AdipoGen), 2.5 mmol/L 3-methyladenine (3-MA, AdipoGen), 5 mmol/L N-[[(2S,3S)-3-[(propylamino) arbonyl]-2-oxiranyl]carbonyl]-L-isoleucyl-L-proline, methyl ester (CA-074 me, Cayman Chemical), 5 µmol/L cyclosporin A (Cayman Chemical) and 5 µmol/L N-Acetyl-L-cysteine (NAC, Sigma Aldrich), 1 µmol/L BAPTA-AM, 5 µmol/L U-73122 . MTT viability assay was performed after 16 or 72 h as previously described, except for NAC where, prior to MTT adding, medium was removed, and each well was washed with 100 µL of phosphate buffered saline.

For biogenic amines viability rescue, 1,500 MCF7 cells were seeded in 96 wells plate and treated with IC_{50} concentration of the following drugs: spiperone, nefazodone, fluoxetine, fluspirilene, ebastine, pimozide, penfluridol in combination with vehicle (DMSO) or 5 µmol/L dopamine, serotonin, or histamine. MTT viability assay was performed as described before after 24, 48, and 72 hours.

3.5 Apoptosis assay

50,000 MCF7, HCT116, SW620 cells and 100,000 CRC-SCs were plated in 24 wells plate and treated for different time points with 10 μmol/L fluoxetine, ebastine, pimozide, fluspirilene, nefazodone, 5 μmol/L penfluridol and different concentrations of spiperone ranging from 2.5 to 20 μmol/L.
Cells were, then, stained following manufacturer's instruction (AdipoGen). Briefly, cells were incubated for 10 minutes at room temperature with annexin binding buffer (10 mmol/L HEPES/NaOH, pH 7.4, 140 mmol/L NaCl, 2.5 mmol/L $CaCl_2$) containing Annexin V-FITC. Lastly, cells were washed and resuspended in annexin binding buffer. Propidium iodide was added to all the samples 5 minutes before FACS analysis (Attune Nxt, Flow Cytometer, Thermo Fisher Scientific). Data were analyzed with FlowJo, LLC.

3.6 Migration assay

Migration assay was performed using Culture-Insert 2 well in μ-dish (ibidi GmbH, Martinsried, Germany) as previously described [204]. Briefly 30,000 HCT116 cells and 25,000 MCF7 cells were plated in each side of the insert in 24 well plate. After 24 hours, inserts were removed, and cells were treated with respective psychotropic drug (5 μmol/L) or DMSO (0.05%) in complete medium. Images were acquired at 0 hours and 24 hours after treatment, with phase contrast microscope and analyzed through ImageJ software (NIH, USA). Data were shown as % of closure rate relative to time 0.

3.7 Vacuolization assay

25,000 cells were plated in 48 wells plate and then treated with fluoxetine, ebastine, penfluridol, pimozide, fluspirilene, spiperone, nefazodone at the concentration of 5 μmol/L and rapamycin (10 μmol/L). After 2 hours treatment one well from each treatment was treated with bafilomycin A1 (50 nmol/L) or 3-MA (1 mmol/L). Pictures were acquired with a phase contrast microscope 4 and 6 hours after treatment, images were analyzed by ImageJ software. Analysis shows percentage of vacuolization rate for each treatment.

3.8 Mitochondrial membrane potential analysis

20,000 cells were plated in 48 wells plate and treated with 5 μmol/L fluoxetine, ebastine, fluspirilene, nefazodone penfluridol, pimozide, and 5 - 10 μmol/L spiperone. DMSO 0.05% was used as negative

control. After treatment, cells were stained with 10 µg/ml JC-1 dye (Adipogen) in PBS for 30 minutes in the dark at 37°C. FCCP (Cayman chemicals) was added for 15 minutes after the staining as positive control. Signals were acquired with a fluorescence microscope (FLoid Cell Imaging Station, Life Technology) and images were analyzed by ImageJ software calculating red/green fluorescence ratio.

3.9 Lysotracker assay

20,000 cells were plated in 48 wells plate and treated with 5 µmol/L fluoxetine, ebastine, fluspirilene, nefazodone penfluridol, pimozide, spiperone or 10 µmol/L rapamycin for 16 hours. After the treatment medium was removed and cells were stained with Lysotracker Deep Red (Invitrogen, 50 nmol/L) and Hoechst 33342 (5 µg/ml) for nuclei staining, in the dark at 37°C for 30 minutes. Signals were acquired with a fluorescence microscope (FLoid Cell Imaging Station, Life Technology). Lysotracker red signal/blue nuclei signal was analyzed by ImageJ software.

3.10 Phospholipidosis assay

20,000 cells were plated in 48 wells plate and treated with 5 µmol/L ebastine, fluoxetine, fluspirilene, nefazodone penfluridol, pimozide, 5 or 10 µmol/L spiperone or 10 µmol/L rapamycin and stained with 1X LipidTox green (Thermo Fisher Scientific) for 16 hours.
Subsequently, nuclei were stained using Hoechst 33342 (5 µg/ml) and plate was incubated for 30 minutes in the dark at 37°C. Afterwards, cells were washed with PBS and fixed with paraformaldehyde 4% for 15 minutes in the dark. Signals were acquired with a fluorescence microscope (FLoid Cell Imaging Station, Life Technology) and images were analyzed by ImageJ software.

3.11 Western blotting

150,000 cells were plated in 6 wells plate and treated with 5 µmol/L ebastine, fluoxetine, fluspirilene, nefazodone penfluridol, pimozide, spiperone for 16 hours.
For experiment of autophagic flux two conditions were carried out for each drug: drug alone and cotreatment of drug and chloroquine 50 µmol/L.
For spiperone signaling experiment, 300,000 cells/well of HCT116 were plated in six wells plate and starved overnight with DMEM without FBS. The day after, cells were stimulated with spiperone for

5, 30 and 60 minutes keeping one well unstimulated as control; a second experiment was then performed in the same conditions with a 30 minutes pretreatment with PLC inhibitor U-73122 10 μmol/L.

To evaluate spiperone induction of ER stress HCT116 were plated 300000 cells/well in six well plate. The day after, cells were treated with spiperone 10 μmol/L for 2, 4 and 8 hours. One well was kept unstimulated (negative control) and 2 were treated with DTT 1 or 2 mM as positive control of ER stress.

After treatments, whole cell lysates were prepared using RIPA lysis buffer (25 mmol/L Hepes pH 8, 135 mmol/L NaCl, 5 mmol/L EDTA, 1 mmol/L EGTA, 1 mmol/L ZnCl2, 50 mmol/L NaF, 1% Nonidet P40, 10% glycerol) with protease inhibitors (AEBSF, aprotinin, bestatin, E-64, EDTA, leupeptin, Sigma-Aldrich) and orthovanadate. Lysates were then kept on a wheel for 20 minutes at 4°C and after centrifuged at 12,500 g for 15 minutes. Proteins contained in the samples were collected and quantified using Pierce BCA protein assay kit (Thermo Fisher Scientific). Successively, proteins were denatured at 95°C for 5 minutes in presence of 2% Sodium Dodecyl Sulfate (SDS), 150 mmol/L dithiothreitol (DTT) and 0,01% bromophenol blue. Electrophoresis of the samples was performed using 6%, 8 %, 10 % or 15% polyacrylamide gels and proteins were transferred from the gel to a PolyVinylidene DiFluoride membrane (PVDF, Amersham). Lastly, the membrane was saturated using 3% Bovine Serum Albumin (BSA, Sigma) in TBS/Tween-20 0.1% [Tris Buffered Saline 1X containing Trizma base 50 mmol/L, NaCl 120 mmol/L, 0,1% Polyethylene glycol sorbitan monolaurate (Tween-20)] for 1 hour and incubated with primary antibody dissolved in the same buffer with sodium azide 0,01%. Primary antibodies were anti-LC3B (Thermo Scientific), anti-P-P70S6K T389 (Cell Signaling Technology), P70S6K (Cell Signaling Technology), anti-P-S6 S235/236 (Cell Signaling Technology), anti-S6 (Cell Signaling Technology) anti-P-AMPKα T172 (Cell Signaling Technology), anti-AMPK (Cell Signaling Technology), anti-GAPDH (Cell Signaling Technology) P-(S)-PKC substrate, anti-P-Akt S473 (Cell Signaling Technologies, CST), anti-P-Akt T308 (Cell Signaling Technologies, CST), anti-Akt (Cell Signaling Technologies, CST), anti-P-p44/42 MAPK (Erk1/2) T202/Y204 (Cell Signaling Technologies, CST), anti-p44/42 MAPK (Erk 1/2) , anti-P-P38 MAPK T180/Y182 (Cell Signaling Technologies, CST), anti-P38 MAPK (Cell Signaling Technologies, CST), anti-vinculin , anti-P-eIF2a (Santa Cruz), anti-P-JNK (Santa Cruz), anti-JNK (Santa Cruz) and anti-Lamin A/C (BD Biosciences). The day after, primary antibody was removed, and the membrane was washed with TBS-Tween-20 0,1% for 15 minutes 3 times and then incubated with horseradish peroxidase conjugated secondary anti-mouse or anti-rabbit antibody (Perkin Elmer Life Science) diluted 1:3000 in TBS-Tween-20 0,1% for 45 minutes. After washing,

reading of the membrane was performed using ECL Western Lightning Chemiluminescence Reagent Plus (Perkin Elmer Life Science) and images acquired with the Chemidoc Touch (Bio-Rad).

3.12 Immunofluorescence microscopy analysis

50,000 cells/well were seeded onto glass coverslips and treated with 5 µmol/L fluoxetine, ebastine, penfluridol, pimozide, fluspirilene, nefazodone and 5 - 10 µmol/L spiperone. After the treatment, cells were washed with PBS and fixed with PFA 4% for 10 minutes at room temperature and washed with PBS. Then cells were permeabilized incubating with cold HEPES-Triton X-100 (20 mM HEPES pH 7.4, 300 mM sucrose, 50 mM NaCl, 3 mM MgCl2, 0,5% Triton X-100) for 5 minutes at 4°C. Cells were washed with 0,2% PBS-BSA and saturated using 2% PBS-BSA for 15 minutes before placing primary antibodies.

Antibodies used in these experiments were anti-mTOR (Cell Signaling Technology), anti-Galectin-1 (Santa Cruz Biotechnology), anti-LAMP1 (Santa Cruz Biotechnology), anti-Cathepsin B (Cell Signaling Technology). For MitoTracker assay instead of antibody, MitoTracker dye 100 nmol/L was used. Cells were incubated with primary antibodies for 30 minutes, then washed, saturated with 2% PBS-BSA and incubated with secondary antibodies conjugated with Alexa Fluor-488, -536 (Invitrogen) and DAPI for 30 minutes.

After the incubation, glasses were mounted on glass slides using Mowiol (20% Mowiol 4-88, 2,5% DABCO in PBS, pH 7.4). Images were acquired at confocal microscope Leica TCS SP8 or fluorescence microscope DM5500B (Leica) and analyzed using ImageJ software.

3.13 Compounds chemical analysis

The properties of the compounds (LogP and basic pKa) were investigated using ACD/ LAB software. As reported in the publication of Muehlbacher [205] there is not a clear CADs classification based of chemical properties. We decided to apply the same parameters based on LogP and pKa applied in the Muehlbacher's manuscript. Compounds were considered CADs when LogP > 3, for the amphiphilic characteristics, and a PKa > 7.4 for the cationic characteristics.

3.14 Cell cycle analysis

Cell cycle analysis was performed through DNA content measurement. 60,000 HCT116 cells/well were plated in a 12-well plate and starved for 16 hours (DMEM without FBS). After starvation, cells were treated with spiperone for 24 and 48 hours in DMEM supplemented with 10% FBS. Subsequently, cells were harvested and fixed with 70% ethanol for 30 minutes. Then, cells were treated with 20 µg/ml RNAse A (Sigma) for 45 minutes at 37°C. Finally, cells were stained with PI (50 µg/ml, sigma) and the fluorescence was acquired through cytofluorimeter (Attune Nxt, Flow Cytometer, Thermo Fisher Scientific). Data analysis was performed using FlowJo, LLC software.

3.15 Intracellular Ca^{2+} concentration measurements

To investigate Ca^{2+} concentration, 300,000 HCT116 cells were harvested for each condition and resuspended in 300 µl of Krebs-Ringer Buffer (KRB) containing 135 mmol/L NaCl, 5 mmol/L KCl, 0,4 mmol/L KH_2PO_4, 1 mmol/L $MgSO_4$, 20 mmol/L HEPES, 2 mmol/L $CaCl_2$. The samples were incubated with Fluo 4-AM (Molecular Probes, Invitrogen) 2,5 µmol/L at room temperature, in the dark for 30 minutes, then washed with KRB and re-incubated in 2 mmol/L $CaCl_2$ KRB at room temperature other 30 minutes.

After incubation all the samples were resuspended in 2 mmol/L $CaCl_2$ KRB, in 2 mmol/L EGTA KRB or 2 mmol/L EGTA KRB with10 µmol/L U-73122 (Sigma) or U-73443 (Caymann chemicals) for 10 minutes, depending on the experimental conditions.

Finally, fluorescence emission was acquired for each sample by flow cytometry (FACScalibur, BD Biosciences). Data analysis was performed using FlowJo, LLC software.

The same protocol was used to investigate intracellular Ca^{2+} concentration through microscopy analysis, but cells were stained in adherent condition and fixed with PFA 1%.

3.16 RNA extraction and real time PCR

In order to perform RNA extraction 300,000 HCT116 and CC09 cells were plated in each well and treated with different concentrations of spiperone (2,5 µmol/L, 5 µmol/L, 10 µmol/L) for 24 hours. After the treatment, RNA was extracted using phenol/chlorophorm method (RNAzol, Sigma Aldrich) and isopropanol precipitation following manufacturer's instructions. Then, precipitated RNA was washed with 75% ice-cold ethanol and resuspended in 30 µl of water.

RNA samples were quantified at NanoDrop 2000 and then reverse transcribed into cDNA using recombinant *moloney murine leukemia* virus reverse transcriptase (MultiScribe Reverse Trascriptase, Biorad) and iScript cDNA Synthesis kit (Biorad).

The genes analyzed by real time PCR using SsoAdvanced Universal SYBR Green Supermix kit (Bio rad) were: GRP78, c-MYC, CDKN1A, CHOP, BIRC5, AXIN2 and GUSB as control gene (**Table 4**). Relative quantification was determined using the ΔΔCt algorithm [206].

Table 4 **Oligo sequences for the genes investigated**

Gene	Forward	Reverse
GRP78	5’ GTT CTT GCC GTT CAA GGT GG 3’	5’ TGG TAC AGT AAC AAC TGC ATG 3’
c-MYC	5’ GAT TCT CTG CTC TCC TCG AC 3’	5’ ACC CTC TTG GCA GCA GGA TA 3’
CHOP	5’CAT CAC CAC ACC TGA AAG CA3’	5’TCA GCT GCC ATC TCT GCA G 3’
BIRC5	5’ACC GCA TCT CTA CAT TCA AG 3’	5’CTT TCT TCG CAG TTT CCT C3’
AXIN2	5’AGA GCA GCT CAG CAA AAA GG 3’	5’CCT TCA TAC ATC GGG AGC AC3’
GUSB	5’ ATC GCC ATC AAC AAC ACA 3’	5’ CTT GGG ATA CTT GGA GGT G 3’

3.17 Analysis of XBP1 splicing variants

To evaluate XBP1 alternative splicing cDNA was used as a template for PCR amplification using XBP1 specific primers (forward: 5’ TTA CGA GAG AAA ACT CAT GGC C 3’; reverse: 5’ GGG TCC AAG TTG TCC AGA ATG C 3’). PCR was performed using Taq polymerase (Biorad), the products were separated by agarose gel electrophoresis and visualized with GelGreen™ (Invitrogen). Results were acquired at ChemiDoc touch (Biorad).

3.18 Extreme limiting dilution assay

CC09 cells were plated at a number of 3 and 1 cell/well in an ultra-low attachment 96-well plate in 50 μL of complete stem cell medium, and then treated with 50 μL of medium containing 1 μmol/L spiperone or same concentration of DMSO. Tumor sphere growth was monitored using a phase contrast microscope, and picture were acquired 15 days after plating. Data were analyzed using the free ELDA software (http://bioinf.wehi.edu.au/software/elda/).

3.19 Statistical analysis

Prism 8.0 software was used for statistical analysis (GraphPad software Inc., San Diego, CA). In viability assays, IC50 was determined using a variable slope model referring to the values obtained during the assay; a semi-logarithmic dose-response curve was created.

Statistical significance was analyzed using Student's t-test with $p < 0.05$ as the criterion of significance when two groups were compared. Analysis of contingency tables were performed using Prism 8.0 software (GraphPad software Inc., San Diego, CA) and statistical significance was evaluated using Fisher exact test with $p < 0.05$.

In section *4.2* of *Results*, data were analyzed by using mixed one-way ANOVA with Dunett's multiple comparisons correction using GraphPad PRISM 8.0 software. While for apoptosis assay and cell cycle analysis, statistical significance was evaluated through mixed two-way ANOVA with Dunett's multiple comparisons using GraphPad PRISM 8.0 software. Error bars are described in Figure legends as ± SD. A single, double, triple and four asterisks denote their significance of a p-value ≤ 0.05, ≤ 0.01, ≤ 0.001 and ≤ 0.0001 respectively in all experiments.

4. Results

4.1 Psychotropic drugs show anticancer activity by disrupting mitochondrial and lysosomal function

4.1.2 The antitumoral activity of psychotropic drugs transcends the conventional therapeutic classes and tumor type

To identify compounds with potential, clinically relevant, anticancer activity we first assessed their effect on six different tumor types represented by two CRC (HCT116 and SW620), two breast cancer (BC, MCF7 and MDA-MB-231) and two glioblastoma (GB; U87MG and U251) cell lines. Cells were treated for 72h with scalar doses of drugs ranging from 10 to 160 μmol/L. The screened drugs (N=26) were represented by antipsychotics (n=14), antidepressant (n=2), antihistamines (n=3) and three compounds used in scientific research with reported serotonin receptors antagonistic activity (**Figure 13**; **Figure S1**; **Table 5**). For drugs that induced more than 50% cell viability reduction at a concentration lower that 100 μmol/L, in a dose-dependent manner, the IC_{50} values were calculated (**Figure S2**; **Table 5**).

The most effective drugs in all cell lines tested belonged to all three pharmacological classes investigated (antipsychotics, antidepressants, and antihistamines) (**Figure 13**; **Figure S1**; **Figure S2**; **Table 5**). The six most potent drugs induced more than 50% cell viability reduction at a concentration lower that 10 μmol/L (penfluridol, ebastine), 15 μmol/L (pimozide and fluoxetine) or 25 μmol/L (fluspirilene and nefazodone) in all cell lines tested; spiperone and brexpiprazole proved to be highly effective in both CRC and BC (with IC50 <10 μmol/L and 10 <IC50< 20 μmol/L, respectively) whereas their cytotoxicity was negligible in GB. A tendency for the diphenylbutylpiperidines pimozide, fluspirilene and penfluridol to be more effective in BC and CRC than in GB was also observed (Table 5). Aripiprazole and ritanserin demonstrated a moderate cytotoxicity, whereas droperidol, haloperidol and iloperidone showed a weak effect only in a fraction of cell lines. Notably, in the lower range of concentrations, some compounds induced a moderate increase in cell viability reflecting cell proliferation: haloperidol in all cell lines tested; ritanserin and the two structurally related R59022 and R5949 in CRC cell lines only, whereas iloperidone in MCF7 and U87MG cell lines (Figure S1).

Eight compounds, represented by the antihistamines cetirizine and diphenhydramine, the antipsychotics paliperidone, pipamperone and risperidone, the antihypertensives ketanserin and urapidil, and the antiemetic metoclopramide showed no cytotoxicity, or caused a reduction of at least 50% of cell viability only at very high concentration (>60 μmol/L) (**Figure S1**, **Table 5**). A few of

these drugs i.e. urapidil, cetirizine, diphenhydramine and metoclopramide even induced cell growth in one or more cell lines tested (**Figure S1**). These results clearly suggest that the cytotoxic effect of these compounds in the micromolar range is not associated with their conventional pharmacological properties and clinical use.

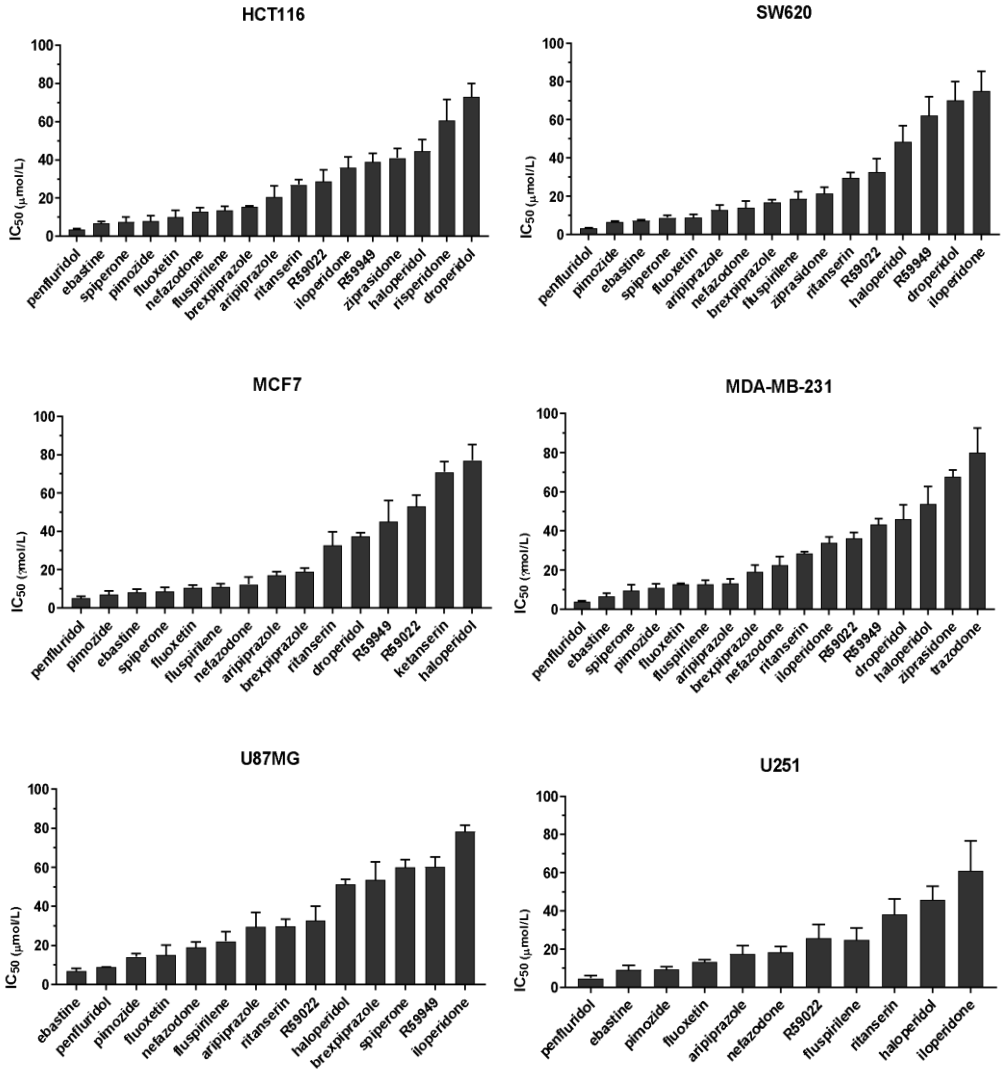

Figure 12 **Anticancer activity of psychotropic drugs**. Two CRC (HCT116 and SW620), 2 BC (MCF7 and MDA-MB-231) and 2 GB (U87MG and U251) cell lines were treated for 72 h with scalar doses of drugs ranging from 10 to 160 μmol/L. The screened drugs included antipsychotics, antidepressant, antihistamines, and three compounds used in scientific research with reported serotonin receptors antagonistic activity (R59949, R59022; WAY-100135). Viabilities were assessed by MTT assay. Data are presented as mean IC50 ± standard error of the mean (SEM) from three-five independent experiments, each performed in quadruplicate. IC50, drug concentration reducing by 50% viability compared to control. Histograms show drugs with IC50 < 100 μmol/L

Table 5 **Summary of psychotropic drugs IC50 value measured by viability assay in different cancer**

Compound	Therapeutic class	Taxonomy	Cell lines (IC_{50} ± SEM, µmol/L)					
			HCT116	SW620	MCF7	MDA-MB-231	U87MG	U251
aripiprazole	antipsychotic	arylpiperazine, hydroquinolone	20.2 ± 2.36	12.7 ± 1.48	17.1 ± 1.48	13.2 ± 1.24	29.2 ± 2.9	17.5 ± 2.45
brexpiprazole	antipsychotic	arylpiperazine, hydroquinolone	15.3 ± 2.45	16.7 ± 0.24	18.8 ± 1.45	19.1 ± 2.157	53.7 ± 5.26	>100
cetirizine	antihistamine	diphenylmethane, N-alkylpiperazine	>100	>100	>100	>100	>100	>100
diphenhydramine	antihistamine	diphenylmethane, benzylether	>100	>100	>100	>100	>100	>100
droperidol	antipsychotic	alkil-phenylchetone, phenylbutylamine, **butyrophenone**, benzimidazole	72.8 ± 4.94	70.2 ± 9.38	37.3 ± 1.25	46.1 ± 5.10	>100	>100
ebastine	antihistamine	diphenylmethane, alkyl-phenylketones, phenylbutylamine, **butyrophenone**	6.77 ± 0.621	7.32± 0.220	8.28 ± 0.922	6.63 ± 2.1	6.84 + 1.375	9.15 ± 0.691
fluoxetine	antidepressant, SSRI	trifluoromethylbenzene	10.0 ± 1.70	8.80 ± 1.16	10.4 ± 1.14	12.7 ± 0.378	15.1 ± 2.94	13.3 ± 3.38
fluspirilene	antipsychotic	diphenylbutylpiperidine	13.4 ± 1.23	18.7 ± 2.5	11.2 ± 0.12	12.7 ± 1.24	22.3 ± 4.6	25.8 ± 2.94
Haloperidol	antipsychotic	alkyl-phenylketone,phenylpiperidine, **butyrophenone**	44.6 ± 3.56	48.4 ± 0.505	77.0 ± 4.83	54.0 ± 6.76	51.1 ± 1.36	45.7 ± 4.27
Iloperidone	antipsychotic	alkyl-phenylketone, acetophenone, benzisoxazole	35.9 ± 3.90	75.2 ± 8.21	>100	33.9 ± 3.6	78.4 ± 9.7	61.1 ± 8.5
ketanserin	antihypertensive	alkyl-phenylketone	>100	>100	71.0 ± 1.32	>100	>100	>100
metoclopramide	propulsive	aminophenyl ether, methoxyaniline, benzamide	>100	>100	>100	>100	>100	>100
nefazodone	antidepressant	phenylpiperazine	13.0 ± 0.877	14.0 ± 1.96	12.3 ± 2.15	22.5 ± 3.54	19.2 ± 3.41	18.5 ± 1.46
paliperidone	antipsychotic	pyridopyrimidine, benzisoxazole	>100	>100	>100	>100	>100	>100
penfluridol	antipsychotic	**diphenylbutylpiperidine**	3.48 ± 0.285	3.18 ± 0.142	5.18 ± 2.05	3.86 ± 0.824	9.04 ± 0.31	4.68 ± 0.319
pimozide	antipsychotic	diphenylmethane, **diphenylbutylpiperidine**	8.21 ± 2.81	6.48 ± 0.513	7.04 ± 0.816	11.1 ± 0.8	14.1 ± 2.60	9.38 ± 0.854
pipamperone	antipsychotic	alkyl-phenylketone, **butyrophenone**	>100	>100	>100	>100	>100	>100
R59022	-	diphenylmethane/thiazolopyrimidine (?)	28.6 ± 1.29	32.5 ± 4.09	53.1 ± 1.91	36.4 ± 2.71	32.7 ± 7.63	25.7 ± 2.24
R59949	-	diphenylmethane/thiazolopyrimidine (?)	38.8 ± 2.12	62.2 ± 9.74	45.3 ± 7.12	42.3 ± 2.47	60.0 ± 2.81	>100
risperidone	antipsychotic	pyridopyrimidine, benzisoxazole	60.7 ± 7.99	>100	>100	>100	>100	>101
ritanserin	antipsychotic	diphenylmethane/pyrimidone	27.0 ± 2.00	29.6 ± 2.70	32.9 ± 2.61	28.5 ± 0.735	29.8 ± 2.44	38.1 ± 4.38
spiperone	antipsychotic	**butyrophenone**	7.59 ± 1.39	8.74 ± 0.92	8.70 ± 0.86	9.80 + 1.42	60.1 ± 3.95	>100
trazodone	antidepressant	phenylpiperazine	>100	>100	>100	80.1 ± 8.85	>100	>100
urapidil	antihypertensive	phenylpiperazine	>100	>100	>100	>100	>100	>100
WAY-100135	-	phenylpiperazine	>100	>100	>100	>100	>100	>100
ziprasidone	antipsychotic	arylpiperazine, benzothiazole, phenethylamine, indole derivative	40.9 ± 1.45	21.3 ± 1.2	>100	67.8 + 7.64	>100	>100

4.1.3 Cytotoxicity of psychotropic drugs is not mediated by biogenic amine receptors

At therapeutic concentrations, the main pharmacological targets of these compounds are biogenic amines receptors [207, 208]. The precise role of biogenic amines such as histamine, dopamine and serotonin in cancer is still debated [209–211]. To test biogenic amines in our cell lines modes, we treated HCT116 and MCF7 cells with a wide range of concentrations of serotonin, dopamine and histamine and evaluated viabilities after 24 and 48 hours. In our assay conditions we observed only a mild positive effect on cell proliferation even at very high doses (**Figure 14**). Long term treatment of MCF7 cells with the strongest cytotoxic compounds penfluridol, ebastine, pimozide or fluoxetine at

clinically significant concentrations determined only a modest increase of drugs efficacy, with IC50 values that remained above 3 μmol/L even after 6 days of treatment (**Figure S3**).

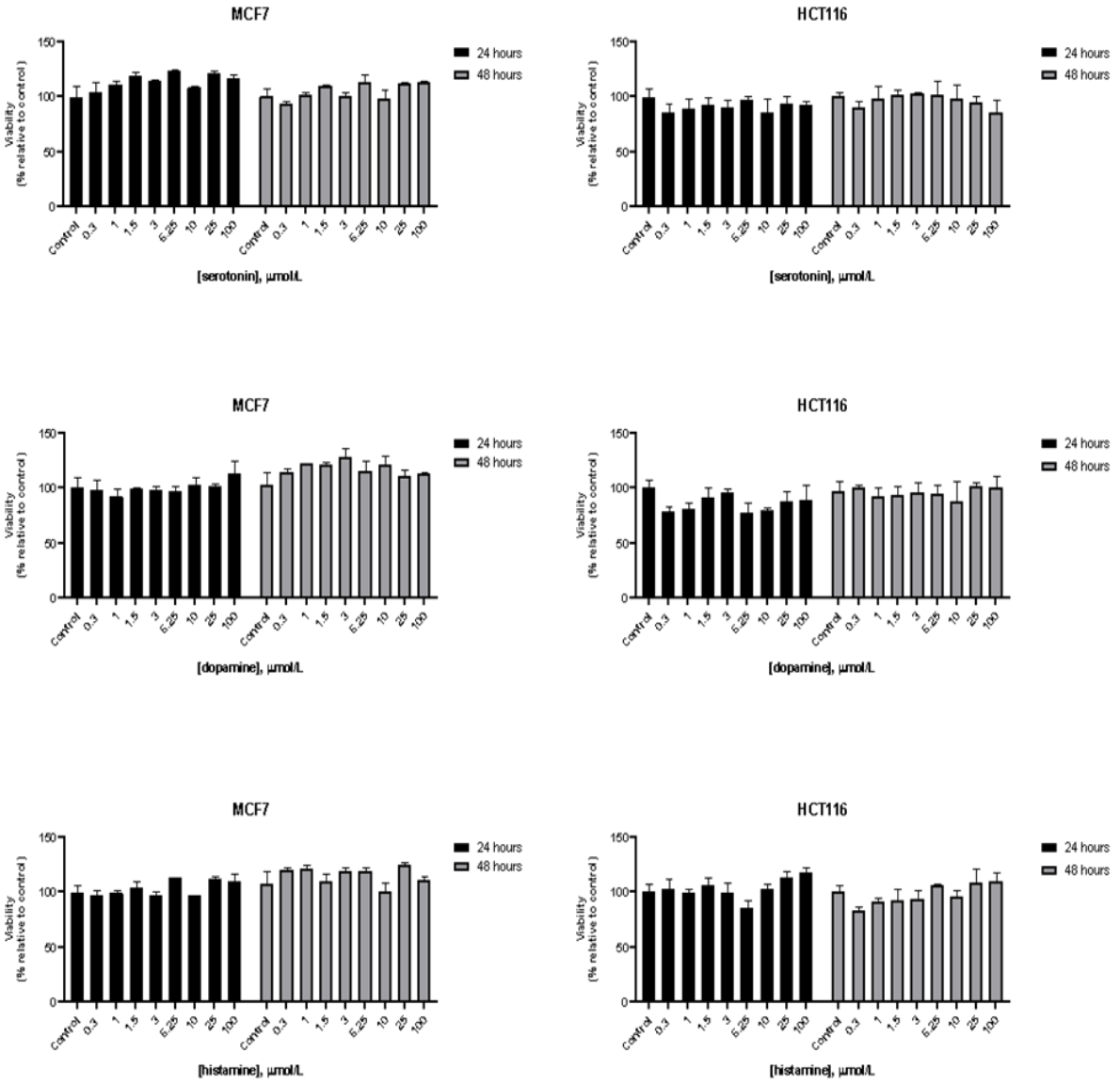

Figure 13 **Effect of biogenic amines on HCT116 and MCF7 cell viability**. MCF7 and HCT116 cells were grown for 24 or 48 h in serum-free medium in presence of viable cells vs control. Data show mean ± SD of one representative experiment out of three independent experiments performed in quadruplicate.

Notably, neither dopamine, nor serotonin and histamine, added to the culture media, were able to rescue the cytotoxic effect of these drugs (**Figure 15**).

These data further support the hypothesis that these compounds affect tumor cell viability through a mechanism that is not mediated by the major neuroreceptor systems implicated in their psychotropic effects.

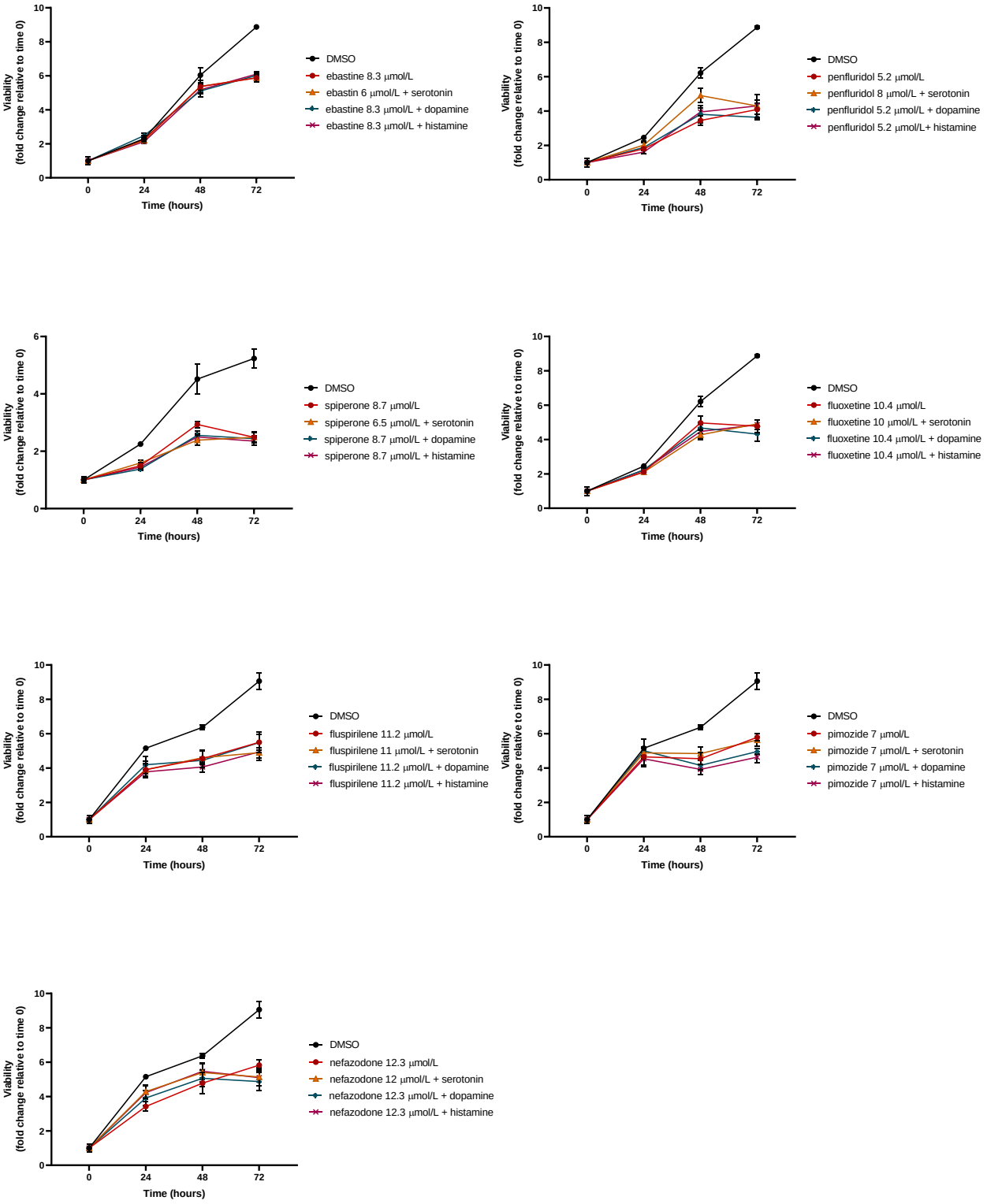

Figure 14 **The cytotoxic effect of psychotropic drugs is not reduced by co-treatment with biogenic amines**. MCF7 cells were treated with psychotropic drugs alone (at a concentration equivalent to IC50) or in presence of 5 µmol/L biogenic amines serotonin, dopamine or histamine. Viabilities were assessed by MTT assay at different time points and presented as fold change relative to control cells treated with vehicle only. Data show mean ± SD of one representative experiment out of three independent experiments performed in quadruplicate.

4.1.4 Psychotropic drugs affect tumor cell migration

To determine the effect of psychotropic drugs on the motility of cancer cells, we assessed MCF7 and HCT116 cells migration by the wound-healing assay (**Figure 16**). All active drugs caused a reduction in the motility of MCF7 cells with the strongest effects observed with penfluridol, spiperone, urapidil and brexpiprazole (**Figure 16A**). On the contrary, the migration rate of HCT116 cells was unexpectedly increased by the cytotoxic compounds ebastine and penfluridol, as well as by different other compounds such as urapidil, diphenhydramine, ritanserin, R59022 and R59949; spiperone, and to a lesser extent, ketanserin and trazodone reduced HCT116 cells motility (**Figure 16B**). Overall, these results show that: i) the impact of the different compounds on the migration rate is not strictly associated with their cytotoxic effect or their conventional pharmacological properties and clinical use; ii) the effect of the compounds on cell motility is cell line specific.

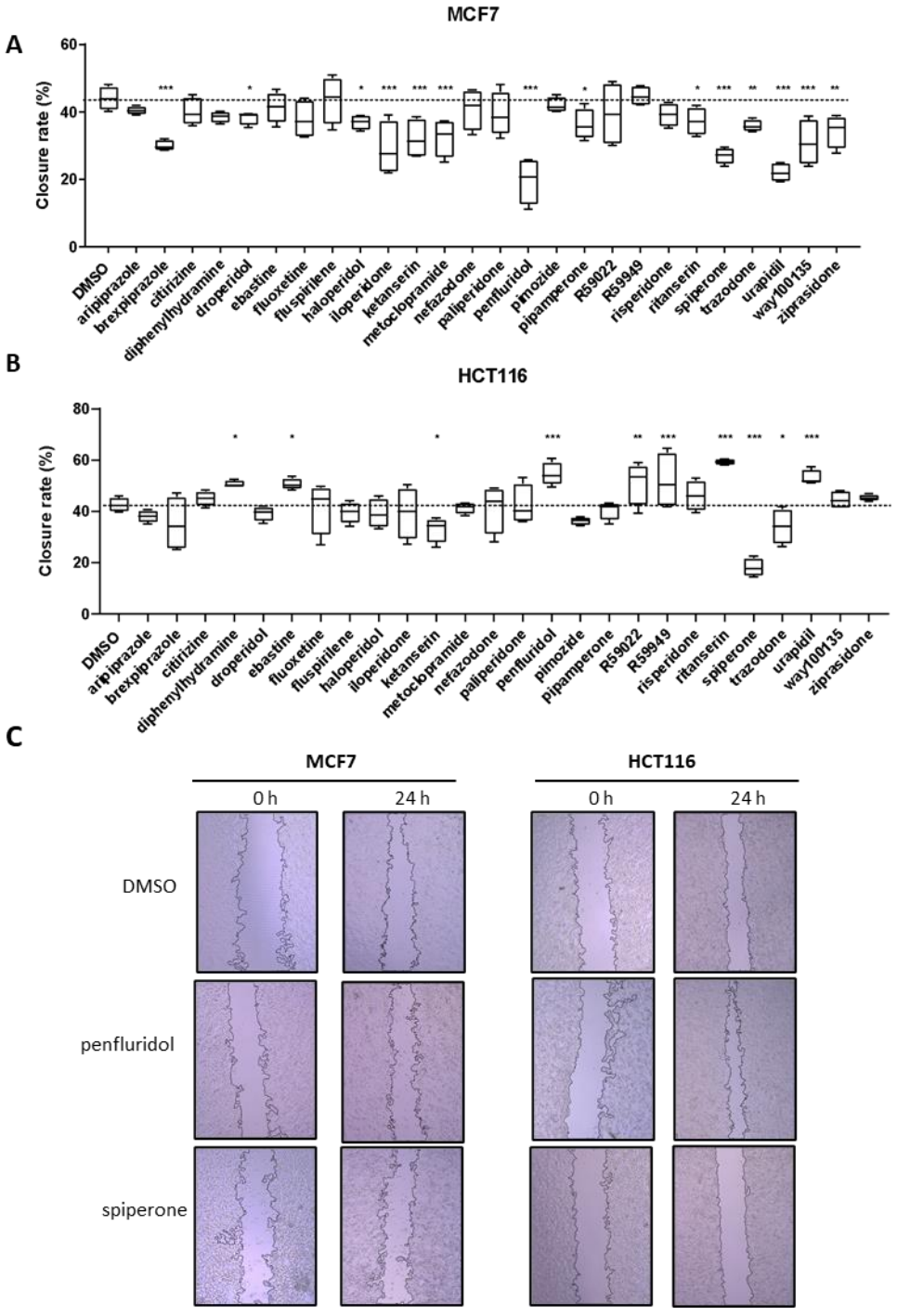

Figure 15 **Effect of psychotropic drugs on cancer cells migration.** Cell motility was evaluated by wound healing assay. MCF7 (**A**) and HCT116 (**B**) cells were plated in 2 wells IBIDI chambers. After removing the insert, cells were treated with drugs (5µmol/L) in DMEM 10% FBS. The widths of wounds were measured at 0 and 24 hours. Graphs show the closure rate. Data are presented as mean ± SD from three independent experiments, each performed in triplicate. *, Student's T-test $p < 0.05$; **, Student's T-test $p < 0.01$; ***, Student's T-test $p < 0.001$. Representative images of MCF7 and HCT116 wounds after treatment with penfluridol, spiperone and DMSO (**C**)

4.1.5 Psychotropic drugs with significant antitumoral activity display a cationic amphiphilic structure

Cationic amphiphilic drugs (CADs) are defined as chemical compounds with the ability to passively diffuse through lipid bilayers stacking in acid organelles such as lysosomes [212]. These compounds contain both a hydrophobic and a hydrophilic domain; the hydrophobic domain contains one or more aromatic rings whereas the hydrophilic part contains a functional amine group that can be ionized [213]. CADs family comprises a broad spectrum of compound classes, including dozens of approved drugs that are used to treat a wide range of diseases including allergies, heart diseases, and psychiatric disorders [214, 215]. Since the antitumoral activity of compounds investigated in this study is not apparently related to their conventional pharmacological properties and clinical use, we investigated CADs properties of psychotropic drugs used in our screening evaluating their chemical structure, logP and PKa in comparison to the well-known CADs compounds amiodarone, chlorpromazine and chloroquine (**Table 6**) [216, 217]. Since there is not a clear CADs classification based on chemical properties, we set LogP and pKa cut as suggested by Muehlbacher [205]. Overall, 14 psychotropic drugs out of 26 were classified as CADs. Five out of seven most cytotoxic drugs in MCF7 (IC50<15 μmol/L) were CADs, whereas spiperone and nefazodone, were excluded from CAD classification just because of a LogP or pKa value below the selected cut off (**Figure S4, Table 6**). Since CADs were represented also among drugs without cytotoxic activity (e.g. haloperidol, iloperidone or ritanserin), cationic amphiphilic characteristics contribute strongly, but are not sufficient to confer significant antitumoral activity to psychotropic compounds.

Table 6 **List of psychotropic drugs value of LogP and Pka**

Compound	Log P*	Basic pKa	Compound	Log P*	Basic pKa
amiodarone	6.94	8.47	nefazodone	3,55	7,09
chloropromazine	4.89	9.20	paliperidone	3,08	8,76
chloroquine	4.81	10.32	penfluridol	7,53	8,96
aripiprazole	4,68	7,767	pimozide	5,86	8,83
brexpiprazole	4,72	8,4	pipamperone	2,59	8,39
cetirizine	3,15	7,42	R59022	5,04	7,95
diphenhydramine	3,35	8,87	R59949	5,94	7,73
droperidol	3,68	6,75	risperidone	3,59	8,76
ebastine	7,22	8,43	ritanserin	5,48	8
fluoxetine	4,44	9,8	spiperone	3,22	8,28
fluspirilene	5,31	9,31	trazodone	2,36	7,09
Haloperidol	4,43	8,05	urapidil	0,72	7,81
Iloperidone	4,83	7,91	WAY-100135	3,52	8,12
ketanserin	2,42	7,29	ziprasidone	3,81	7,09
metoclopramide	2	9,04	* Log10 (partition coefficient) Partition Coefficient, P = [organic]/[aqueous]		

4.1.6 Psychotropic drugs cause mitochondrial membrane depolarization

CADs can readily pass through phospholipids bilayers, particularly through membranes with a large transmembrane potential such as the mitochondrial inner membrane. They readily accumulate in the mitochondrial matrix, causing mitochondrial membrane depolarization [215, 217, 218]. Therefore, we evaluated the alteration in mitochondrial membrane potential (Δψm) as a function of drugs treatment, using the lipophilic cationic dye JC-1 [219]. MCF7 cells were treated, for 16 h, with 5 µmol/L of each drug or with FCCP, used as positive control. A significant reduction in Δψm was observed after treatment with ebastine, fluoxetine, penfluridol, pimozide, nefazodone and fluspirilene, but not with spiperone (**Figure 17**).

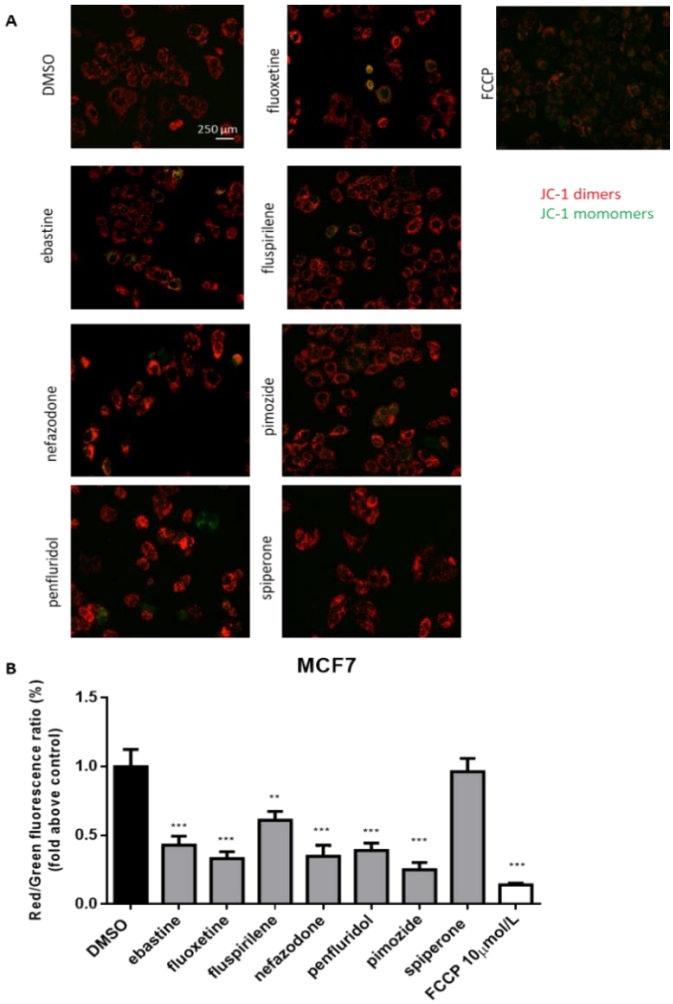

Figure 16 **Psychotropic drugs induce mitochondrial membrane depolarization**. Mitochondrial membrane potential depolarization was evaluated by JC-1 staining after overnight treatment with psychotropic compounds (5 µmol/L) in MCF7 cells. Pictures were acquired by fluorescence microscopy. Representative images of cell treated with the negative control DMSO, FCCP positive control, ebastine, fluoxetine, fluspirilene, nefazodone, penfluridol, pimozide, and spiperone (**A**). Histogram showing quantification of red/green fluorescent ratio as fold change relative to control (**B**). Data are presented as mean ± SD from three independent experiments, each performed in triplicate. **, Student's T-test $p < 0.01$; ***, Student's T-test $p < 0.001$.

4.1.7 Psychotropics drugs induce vacuolization and increase acidic compartments

CADs are known to concentrate in acidic cell compartments because the retro-diffusion of the protonated form is inefficient (mechanism known as ion-trapping or pH partitioning). If sufficiently intense, this sequestration results in the osmotic formation of numerous large, fluid-filled vacuoles already after short term exposure to drugs [216]. These molecules are collectively referred as lysosomotropic agents, for their propensity to concentrate into lysosomes [220]. To test the hypothesis that cytotoxic psychotropic drugs concentrate in MCF7 cells by this mechanism, MCF7 were cultured in the presence of 10% FBS and treated with drugs alone or in the presence of the V-ATPase inhibitor bafilomycin A1 or class III PI3K inhibitor 3-MA (**Figure 18**, **Figure S5**). Fluoxetine induced a strong vacuolar morphology already 6 hours after treatment as previously reported [216] (**Figure S5A**); a less prominent, but still significant increase of vacuolar structures was also observed after treatment with fluspirilene, ebastine, pimozide, penfluridol and nefazodone, whereas increase of vacuoles was not observed with spiperone (**Figure S5**). The mTOR inhibitor rapamycin used as a positive control of autophagy induced a mild vacuolar morphology.

In the presence of bafilomycin A1, a significant reduction of vacuoles formation was observed with fluoxetine, ebastine, fluspirilene, pimozide, and nefazodone, suggesting that these drugs require an acidic environment to accumulate and induce vesicles formation; on the contrary, a higher number of vesicles was observed after treatment with penfluridol and spiperone, suggesting that these drugs do not require pre-existing acidic compartments to induce vacuolization although they can cause the formation of autophagosome structures that accumulate after inhibition of autophagosome-lysosome fusion and autolysosome acidification by bafilomycin A1 (**Figure 18**). The autophagosome nature of vacuoles induced by all these compounds was suggested the reduction of the number of vesicles in the presence the inhibitor of class III PI3K, 3-MA (**Figure 18**).

The nature of the vacuoles induced by psychotropic drugs was further investigated by staining MCF7 cells with the LysoTracker dye, which is a highly soluble small molecule that is retained in acidic subcellular compartments, such as late endosomes and lysosomes, whose presence is an indirect indication for autophagic activity [221]. In agreement with data described above, LysoTracker dye staining clearly show a strong increase of acidic compartments after long-term treatment with all drug tested consistent with increased autophagosome-lysosome acidic structures (**Figure 19**; **Figure S6**).

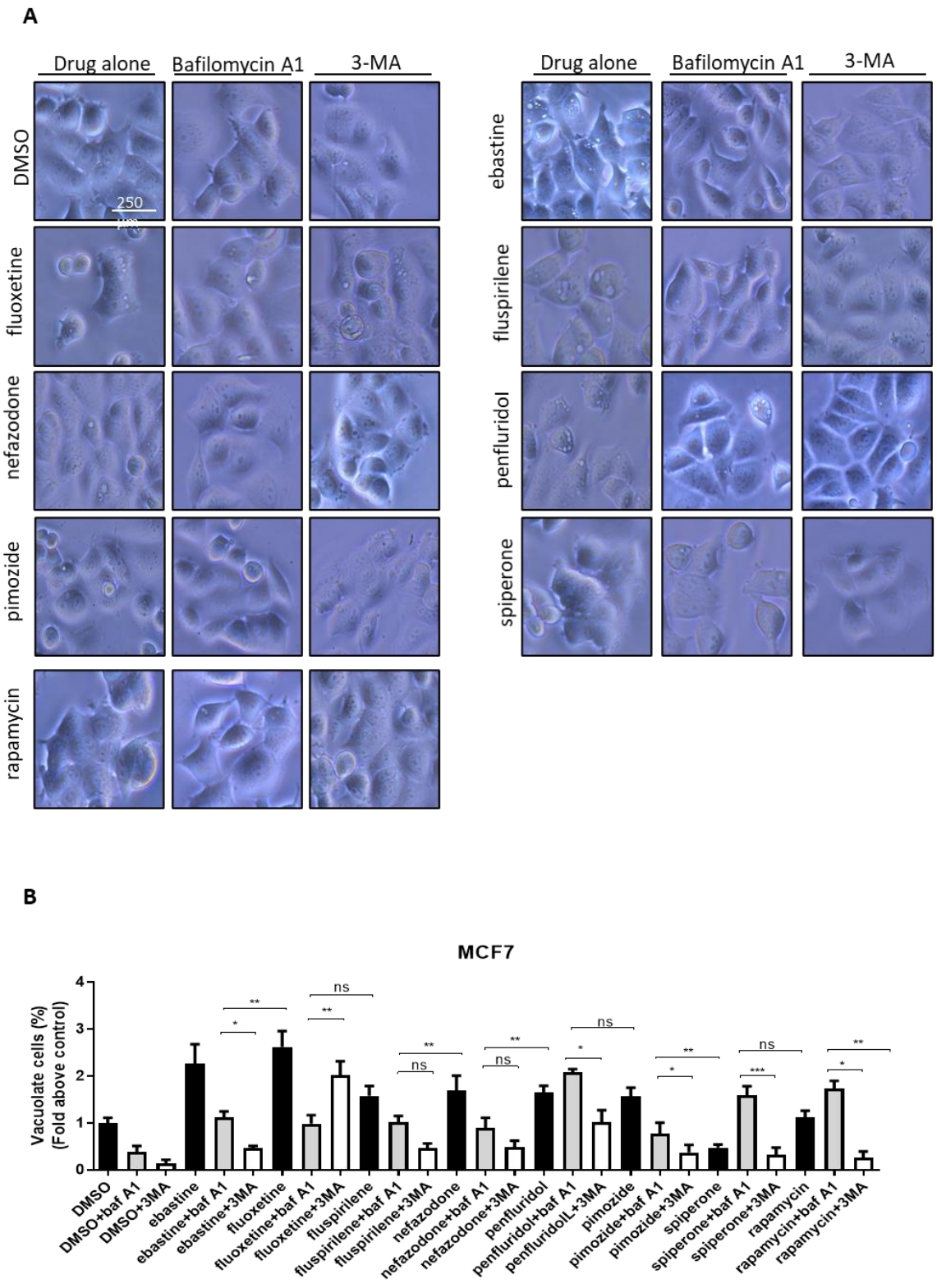

Figure 17 **Vacuolar structures formation after treatment of MCF7 cells with psychotropic drugs**. Morphological alterations associated with psychotropic drugs treatment in MCF7 were investigated after 4 h exposure by phase contrast microscopy. Representative images of cells treated with the negative control DMSO, ebastine, fluoxetine, fluspirilene, nefazodone, penfluridol, pimozide and spiperone and rapamycin alone or with bafilomycin A1 and 3-MA (**A**). Histogram showing quantification of vacuoles as fold change relative to control (**B**). Data are expressed as the mean ± SD of a representative experiment out of three independent experiments performed in triplicate. *p < 0.05; **, Student's T-test p < 0.01; ***, Student's T-test p < 0.001.

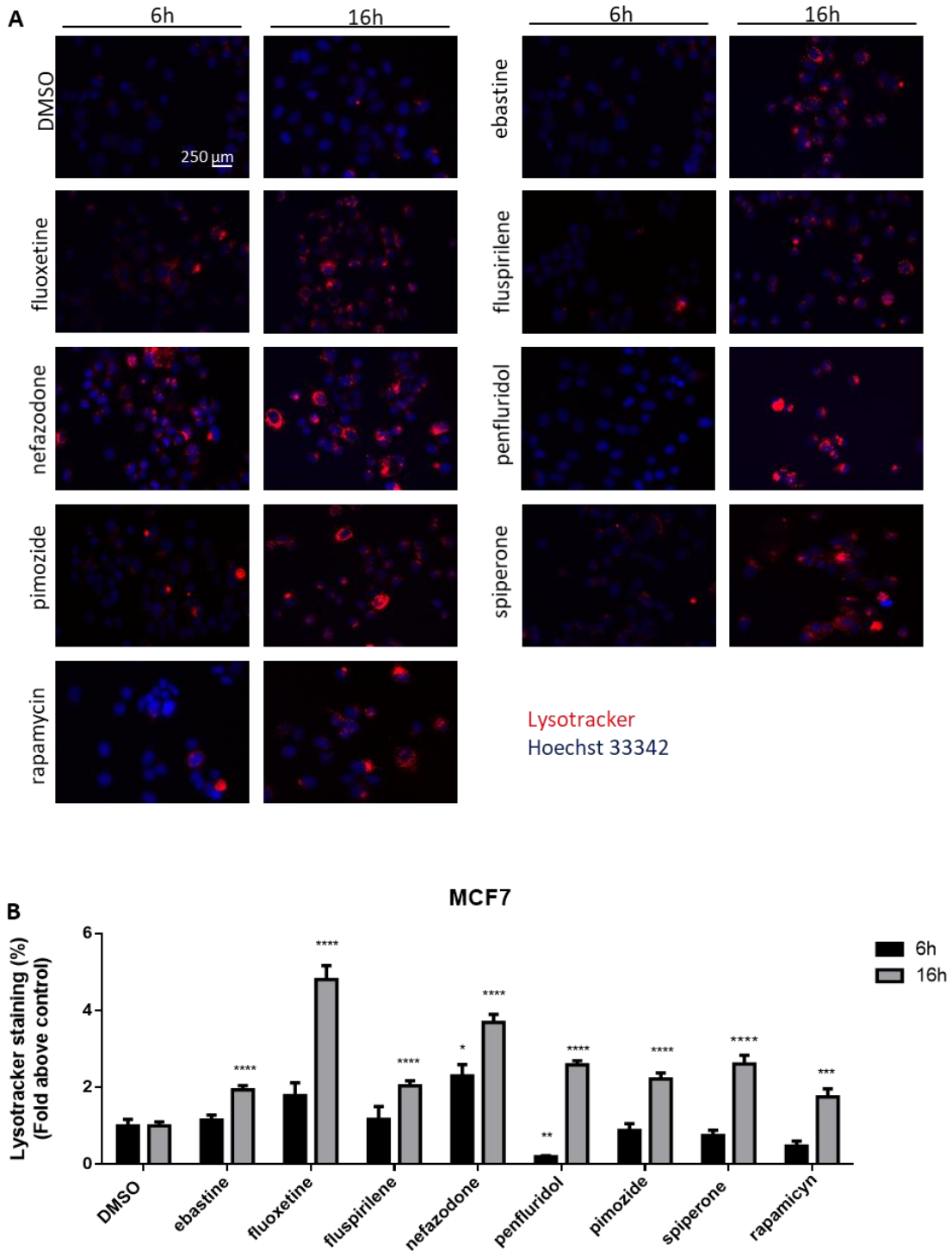

Figure 18 **Psychotropic drugs induce acidic compartment formation perturbing lysosomal and autophagic functioning**. Effects of psychotropic drugs on intracellular acidic compartments were evaluated by Lysotracker Deep Red staining after 6 and 16 h of treatment. Nuclei were stained using Hoechst 33342. Pictures were acquired by fluorescence microscopy (magnification: 20×). Representative images of cells treated with DMSO, negative control, rapamycin, positive control, ebastine, fluoxetine, fluspirilene, nefazodone, penfluridol, pimozide, and spiperone (**A**). Graphs showing quantification of red lysotracker staining/blue nuclei staining ratio as fold change relative to negative control (**B**). Data are expressed as the mean ± SD of a representative experiment out of three independent experiments performed in triplicate. *p < 0.05; **, Student's T-test p < 0.01; ***, Student's T-test p < 0.001; ****p < 0.0001.

4.1.8 Psychotropic drugs alter autophagy flux by affecting mTOR pathway

In addition to autophagy, the increase of acidic structures could reflect reduced turnover in the autophagosomal compartment caused by impaired autophagosome-lysosome fusion and/or lysosomal function. In order to clarify this issue, we investigated mTOR pathway and AMPK, the main regulators of autophagy (**Figure 20**). Starvation, a strong inducer of autophagy was used as positive control. Western blot analysis showed a strong reduction of P70S6K T389 phosphorylation in cells treated with penfluridol and spiperone whereas a mild reduction of this phosphorylation was observed in cells treated with ebastine and fluoxetine; on the contrary, treatment with fluspirilene, nefazodone and pimozide showed no effect on P70S6K phosphorylation (**Figure 20A**,**B**). Phosphorylation in serine 235/236 of ribosomal protein S6, was strongly reduced in cell treated with penfluridol, and mildly reduced with all other drugs (**Figure 20A**,**C**). Those drugs likely downregulate other pathways upstream other kinases that phosphorylate this position, including PKC, PKA, RSK1 and death associated protein kinase (DAPK) [222]. A mild increase of AMPK phosphorylation in the activation site T172, comparable to that induced by starvation, was observed after treatment with penfluridol and spiperone, whereas it was unaffected or slightly reduced after treatment with all other compounds (**Figure 20A**,**D**).

The conversion of the cytosolic LC3B form, LC3B-I, into the faster migrating, phosphatidylethanolamine-conjugated, LC3B-II form, a marker of autophagy induction [223] was strongly enhanced in cells treated with penfluridol and spiperone and a lower but significant increase was also observed in cells treated with pimozide (**Figure 20E**,**F**).

Notably, treatment with both penfluridol and spiperone also caused a partial delocalization of mTOR from the lysosomal membrane, supporting the hypothesis that these drugs can induce mTORC1 downregulation and activation of autophagy (**Figure 20G**, **Figure S7**).

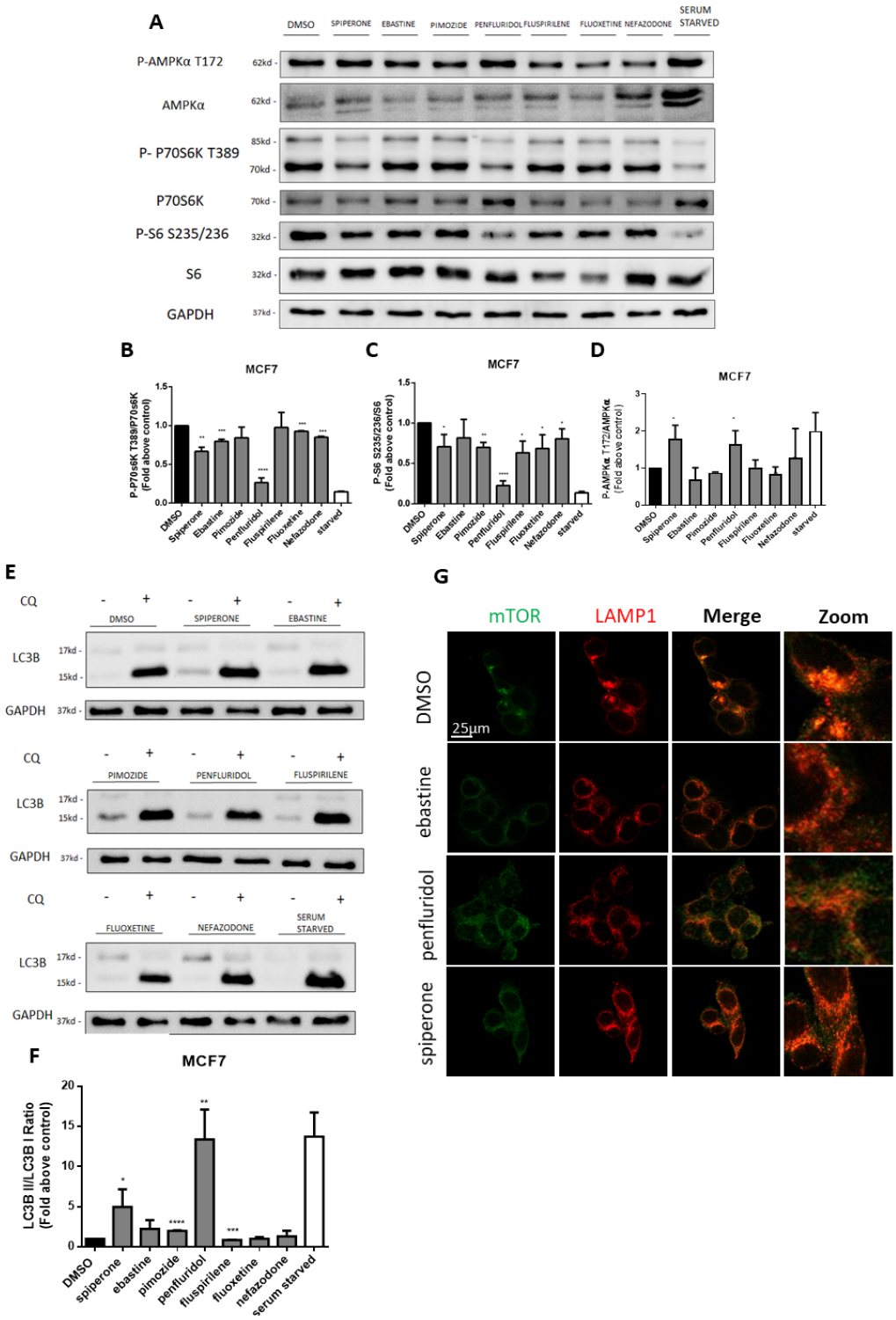

Figure 19 **Effect of psychotropic drugs on mTOR and AMPK pathways and autophagic flux.** Western blot analysis of MCF7 cells after 16 h treatment with psychotropic drugs. Lysates were analyzed for p AMPKa T172, AMPKa, p-P70S6K T389, P70S6K, P-S6 S235/236, S6, LC3B, and GAPDH (**A**). Histogram showing quantification of P70S6K (**B**), S6 (**C**) and AMPK (**D**) phosphorylation normalized on total protein P70S6K, S6 and AMPKa, respectively. WB (**E**) and histogram (**F**) showing the relative expression of LC3B II/I upon chloroquine treatment. Densitometric analyses mean ± SD of 3 independent experiments performed in triplicate. * Student's *T*-test $p < 0.05$ **, Student's *T*-test $p < 0.01$; ***, Student's *T*-test $p < 0.001$, ****$p <$ 0.0001. Delocalization of mTOR from the lysosomal membrane was evaluated in MCF7 after 16 h treatment with psychotropic drugs. mTOR was stained using mTOR primary antibody and Alexa Fluor 488 secondary antibody (green). Lysosomes were stained using LAMP1 primary antibody and Alexa Fluor 536 secondary antibody (red). Representative images of DMSO, negative control, ebastine, penfluridol, and spiperone (**G**).

4.1.9 Psychotropic drugs cause lysosomal disruption

CADs can accumulate into lysosomes and impair lysosomal enzymatic activities [214, 224]. Lysosomes are a major site of cellular phospholipid metabolism and the hallmark of drug-induced lysosomal impairment is accumulation of phospholipids [212, 225]. It has also been shown that some antipsychotic and antidepressant drugs extensively accumulate in lysosomes and it is thought that this accumulation could contribute to the mechanism of action of these agents through inhibition of acid sphingomyelinase and phospholipases [205, 226]. Therefore, we investigated whether the antitumoral activity of psychotropic drugs was associated with lysosomal impairment by incubating cells in the presence of phospholipids conjugated to fluorescent dye. After incubation for 24 h with LipidTOX, MCF7 cells treated with ebastine, fluspirilene, fluoxetine, pimozide and penfluridol showed a strong increase of phospholipids aggregates; on the contrary, this phenotype was not observed after treatment with spiperone, nefazodone and with the inducer of autophagy rapamycin (**Figure 21A**,**B**). Drugs with cationic amphiphilic properties accumulating into lysosomes can also induce LMP. This phenomenon leads to the release of lysosomal enzymes inside the cytoplasm and possibly cell death [144]. Galectin-1 is a small protein normally located in the cytoplasm and in the nucleus, that accumulates and forms complexes to the lysosomal membrane in case of LMP and rupture [227]. To evaluate LMP and lysosomal damage in response to psychotropic drug treatment we investigated galectin-1 complex formation by immunofluorescence. All the drugs tested, apart from nefazodone, induced the formation of galectin-1 complexes and possibly a damage to the lysosomal membranes (**Figure 22 A**,**B**)

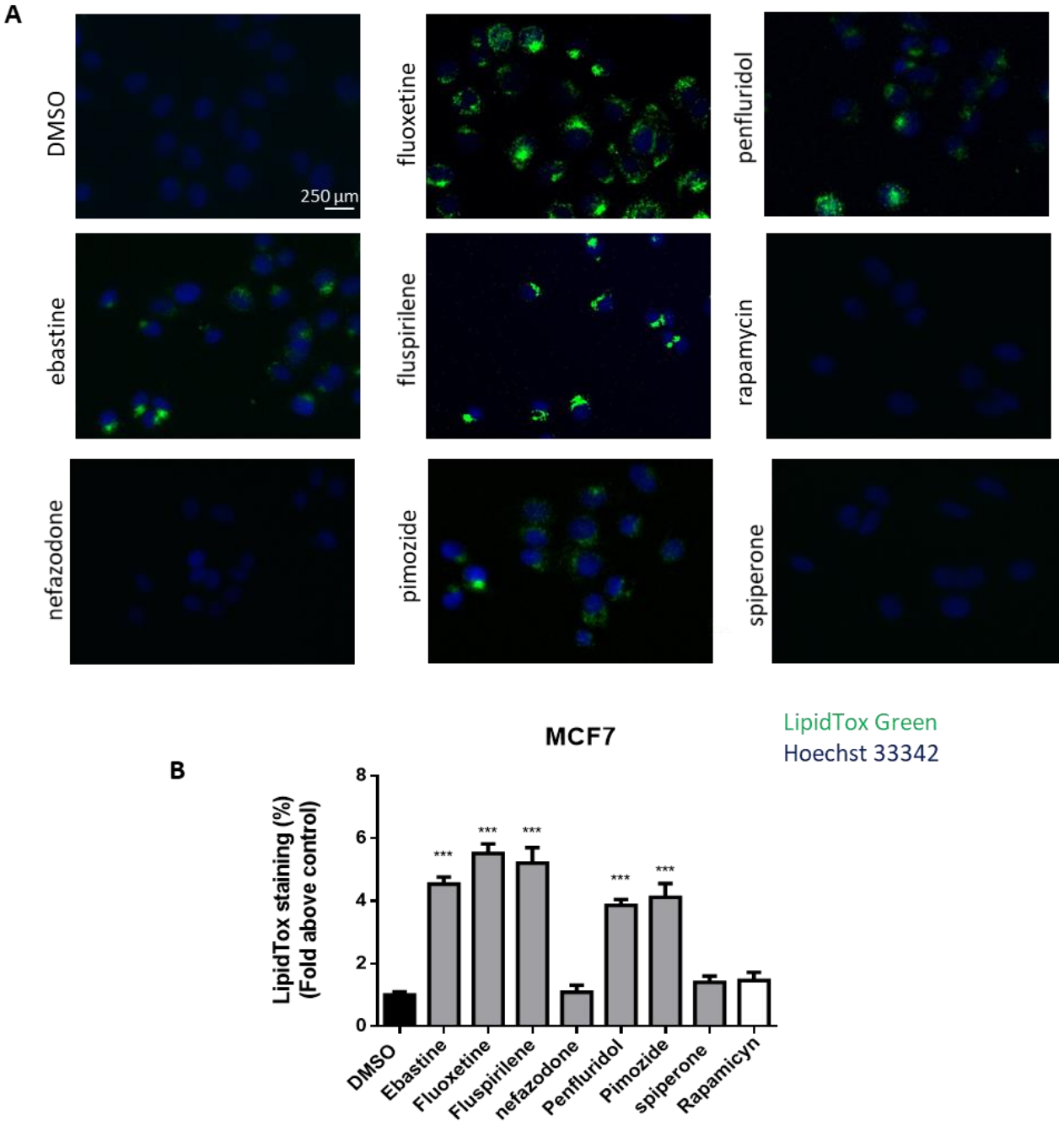

Figure 20 **Treatment with psychotropic drugs induces phospholipidosis in MCF7 cells**. Accumulation of phospholipids in MCF7 cell line was evaluated after 16 h treatment with drugs using LipidTox green staining. Nuclei were stained using Hoechst 33342. Pictures were acquired by fluorescence microscopy (magnification: 20×). Representative images of cells treated with DMSO, negative control, ebastine, fluoxetine, fluspirilene, nefazodone, penfluridol, pimozide, spiperone, and rapamycin (**A**). Histogram showing quantification of Green LipidTox staining/blue nuclei staining ratio as fold change relative to control (**B**). Data are presented as mean ± SD from three independent experiments, each performed in triplicate. ***, Student's T-test $p < 0.001$.

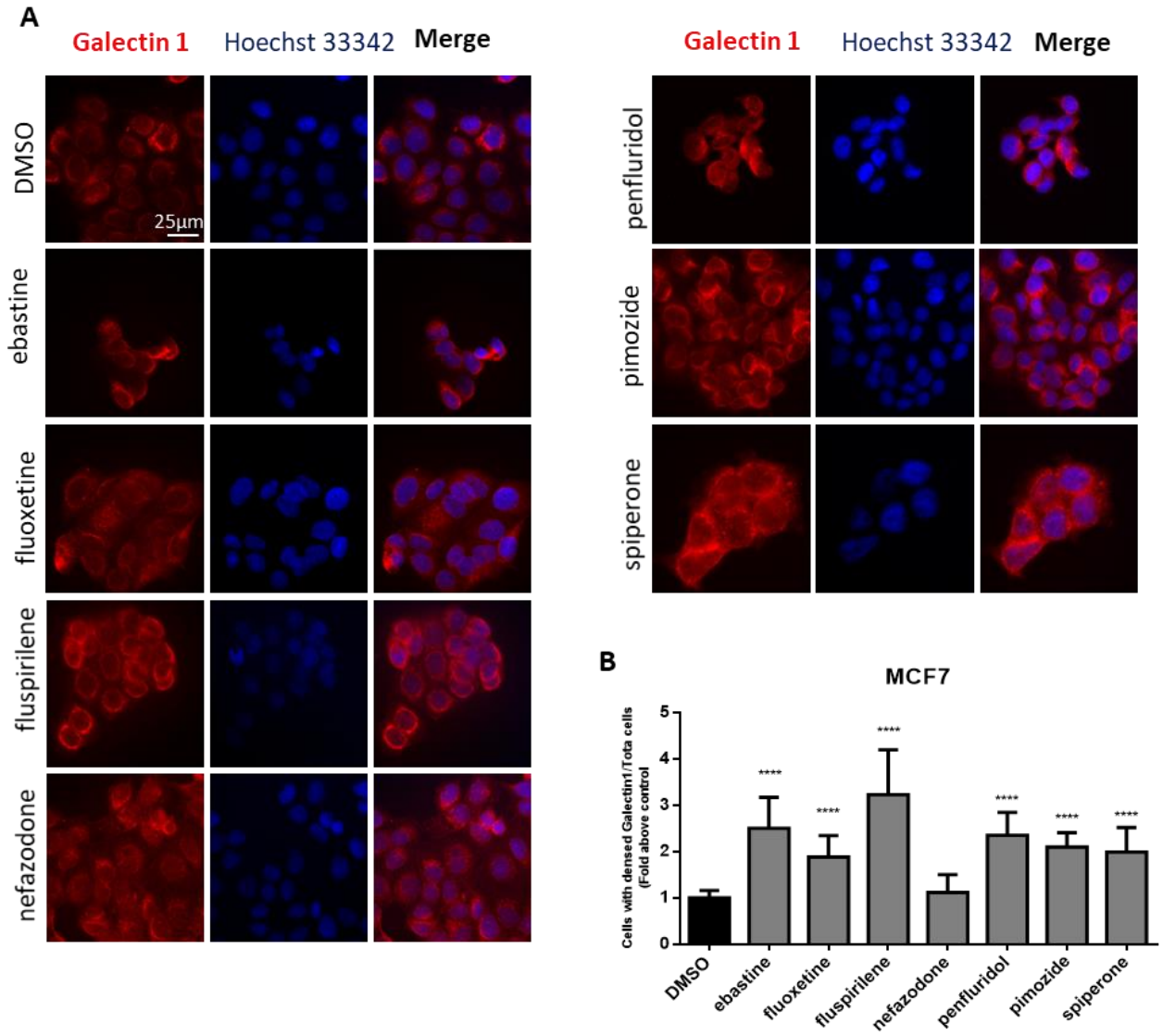

Figure 21 **Treatment with psychotropic drugs induced formation of galectin-1 complexes.** Formation of galectin-1 complexes in MCF7 after 16 h treatment with psychotropic drugs was observed by fluorescence microscopy (magnification: 63X). Galectin-1 was stained with anti galectin-1 primary antibody and Alexa Fluor 563 secondary antibody. Nuclei were stained using DAPI. Representative images showing cells treated with psychotropic drugs: DMSO, ebastine, fluoxetine, fluspirilene, nefazodone, penfluridol, pimozide, and spiperone (**A**). Histogram showing the number of cells presenting galectin-1 complexes/total number of cells ratio as fold change relative to control (**B**) Data are presented as mean ± SD from three independent experiments, each performed in triplicate. ****$p < 0.0001$.

4.1.10 Psychotropic drugs induce different types of cell death

To assess if apoptosis is involved in psychotropic drugs-induced cell death we performed PI/Annexin V staining in MCF7 cells. FACS analysis at different time points showed an increase in necrosis cells with all the drugs but a significant induction of apoptosis after 48 hours of treatment with the sole spiperone (**Figure S11**). These data were further confirmed by viability rescue experiments with a pan caspase inhibitor zVAD-fmk. As shown in **Figure 23A**, zVAD-fmk significantly rescued cell death only in cells treated with spiperone, whereas it was ineffective with the other drugs.

Since apoptosis is not the primary mechanism of death elicited by cytotoxic psychotropic drugs, except for spiperone, we investigated the role of autophagy by treating cells with the autophagy inhibitor 3-MA [228]. As shown in **Figure 23B**, 3-MA co-treatment significantly rescued cell viability in cells treated with rapamycin and in cells treated with spiperone and pimozide. Conversely, 3-MA enhanced penfluridol cytotoxicity, whereas it did not show any effect in combination with ebastine, fluoxetine, nefazodone and fluspirilene. However, since it was reported that in particular conditions 3-MA could induce autophagy [228] we performed western blot analysis to investigate the conversion of the cytosolic LC3 I to II form in MCF7 cells treated with spiperone and penfluridol alone or in

combination with 3-MA (**Figure S9**). Our data indicate that in our experimental set-up 3-MA does not induce autophagy, on the contrary it is effective in suppressing LC3 II conversion.

To further investigate the mechanism of the observed cytotoxicity we assessed whether inhibition of lysosomal cathepsins B and L rescued cell viability in MCF7 cells, for this purpose we performed experiments with the inhibitor CA-074 me [229]. As displayed in **Figure 23C** CA-074 me significantly rescued cell death induced by ebastine, penfluridol, pimozide and spiperone, while a mild but not significant effect was observed in cells co-treated with fluoxetine. Additionally, in order to clarify if oxidative stress was involved in psychotropic drugs-induced cell death, we cotreated MCF7 cells with the antioxidant NAC, however no significant effect was observed in terms of viability rescue (**Figure 23D**). With cyclosporin A, an inhibitor of the mitochondrial permeability transition pore (mPTP), an additive cytotoxic effect was observed with all drugs tested (**Figure 23E**). Cyclosporin A has been reported to be a broad-spectrum multidrug resistance modulator [230] and this activity possibly induces psychotropic drugs retention resulting in a boost of cytotoxicity.

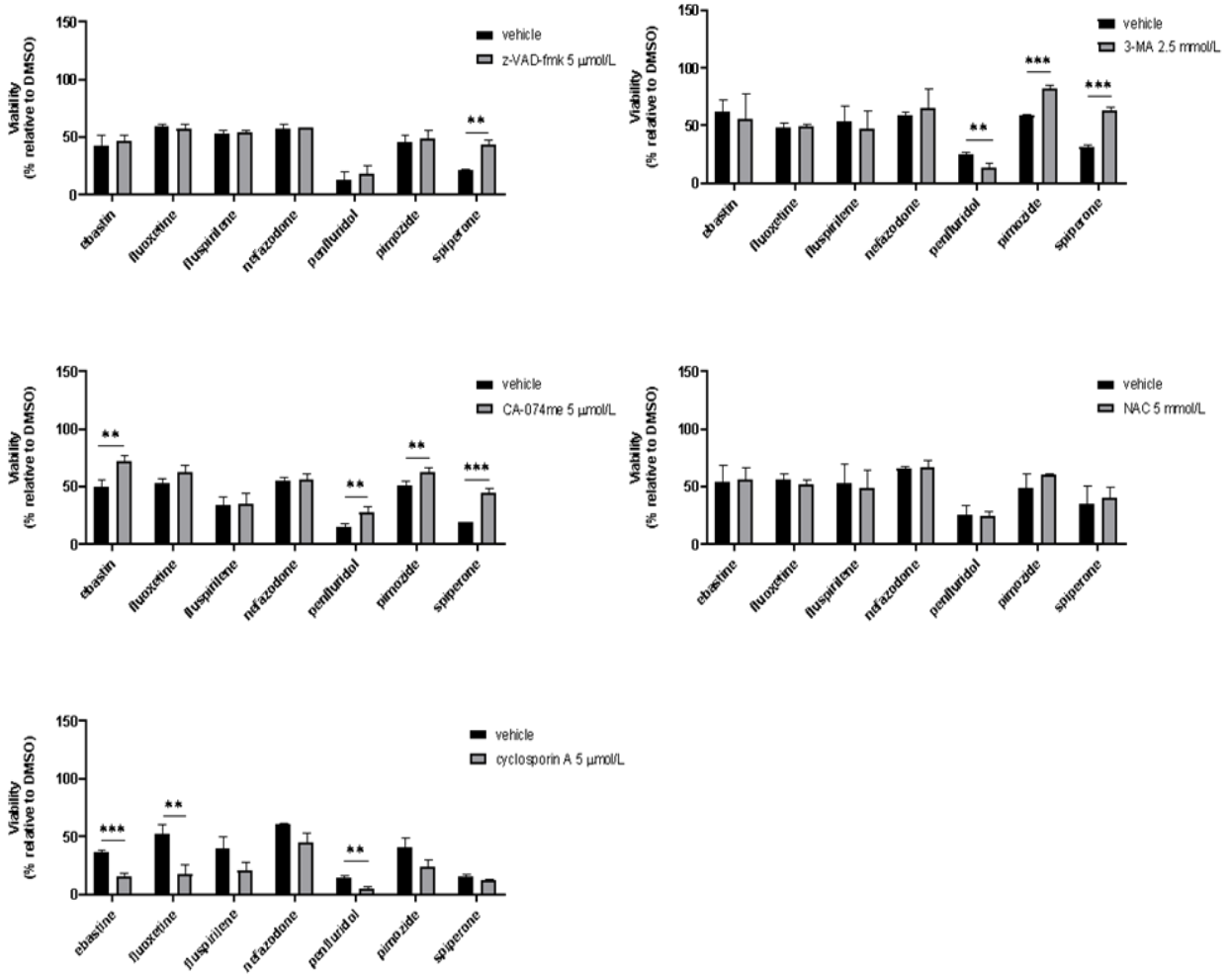

Figure 22 **Effect of co-treatment of psychotropic drugs and the pan-caspase inhibitor zVAD-fmk, the autophagy inhibitor 3-MA, the cathepsin inhibitor CA-074 me, the antioxidant NAC or the inhibitor of mitochondrial membrane depolarization cyclosporin A**. MCF7 cells were treated for 72 h with vehicle or psychotropic drugs (all 10 µmol/L except penfluridol, 5 µmol/L) alone, or in combination with zVAD-fmk, 5 µmol/L (**A**), 3-MA, 2.5 mmol/L (**B**), CA-075 me, 5 µmol/L (**C**), NAC, 5 mmol/L (**D**), cyclosporin A, 5 µmol/L (**E**) Data show mean ± SD of at least three independent experiments performed in triplicate. The graphs show cell viability as the percentage of viable cells vs. control. **, Student's T-test $p < 0.01$; ***, Student's T-test $p < 0.001$.

4.2 Effective cytotoxic activity of spiperone on human colorectal cancer cells

4.2.1 Spiperone is cytotoxic for CRC cells and impairs the clonogenic potential of CRC-SC

We have recently demonstrated the cytotoxic effect of the antipsychotic spiperone at clinically relevant concentrations (IC_{50} < 10 μmol/L) on breast and CRC cell lines [231]. In this part of the study we further confirm the antineoplastic activity of this compound on CRC cell lines and validate its specific activity against neoplastic cells. CRC cells exposed for 72 hours to spiperone showed a dose-dependent reduction of viability, with an IC_{50} <10 μmol/L. On the contrary, spiperone toxicity was negligible for non-neoplastic PBMC (IC50 > 30 μmol/L), primary human dermal fibroblasts (hDF1 IC50 > 90 μmol/L) and visceral adipose tissue-derived mesenchymal stem cells (vAT-MSC; IC_{50} > 80 μmol/L) (**Table 7**, **Figure 24A**).

Table 7 **Summary of spiperone IC50 value measured by viability assay in different cell lines**

Cell line	**IC_{50} 72 hours spiperone Mean ± SEM (μmol/L)**
HCT116	7.1 ± 0.83
SW620	7.2 ± 1.2
HCT8	6.5 ± 0.48
CC09	3.76 ± 0.86
DA13	8.4 ± 0.94
511	4.2 ± 0.21
Me59	3.5 ± 0.42
PBMC	32 ± 4.7
hDF1	98 ± 9.7
vAT-MSC	81 ± 7.8

We further investigated the efficacy of spiperone on CRC-SCs. Hence, viability assay was performed on four different CRC-SCs lines derived from human primary tumors and grown as colonospheres in stem cell medium (**Figure 24B**). A significant reduction in cell viability was measured after 72 hours of treatment with scalar doses of the drug, with an IC_{50} < 5 μmol/L in three out of four investigated cell lines (**Table 7**, **Figure 24A**).

The efficacy of spiperone against colonospheres, prompted us to assess the effect of the drug on the clonogenic potential of CSC-SCs. The extreme limiting dilution assay (ELDA) demonstrated a significant reduction of colonosphere formation in CC09 cells treated with 1 μmol/L spiperone, with an estimated stem cell frequency reduction from 1/1.49 in controls to 1/3.16 in treated cells (**Figure 25**).

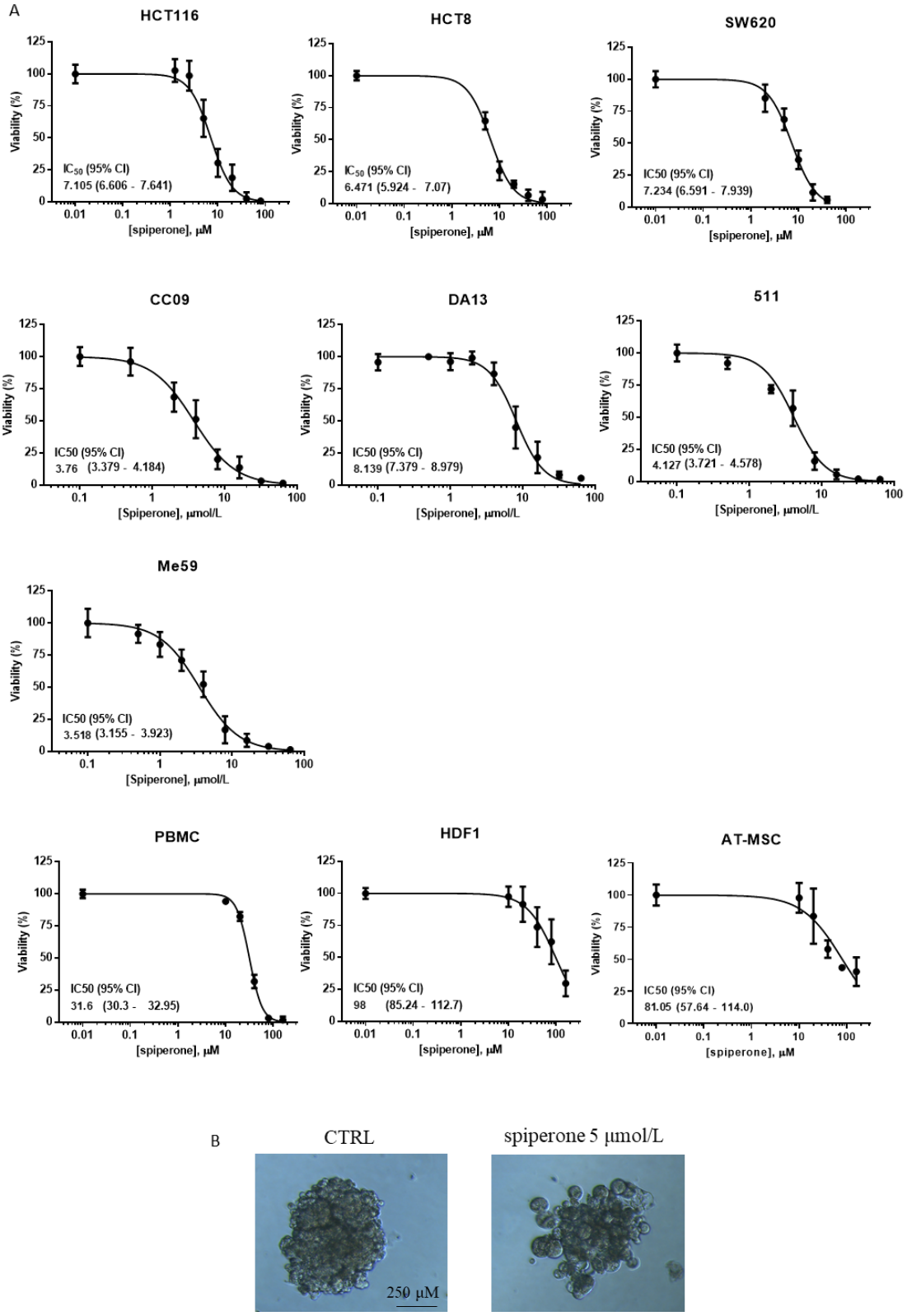

Figure 23 **Spiperone reduces cell viability of CRC cell lines**. Nonlinear regression (dose-response curves) viability analysis of adherent CRC cells (HCT116, HCT8, SW62), CRC-SCs (CC09, DA13, 511, Me59) and non-neoplastic (hDF, PBMC, vAT-MSC) treated with scalar concentration of spiperone for 72 h (mean IC_{50} ± SD, from 3 independent experiments) (**A**). Representative images of CC09 colonospheres control vs treated with spiperone for 48 hours (**B**)

A

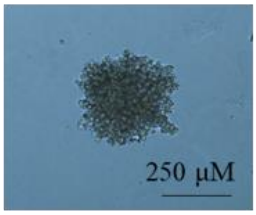

B

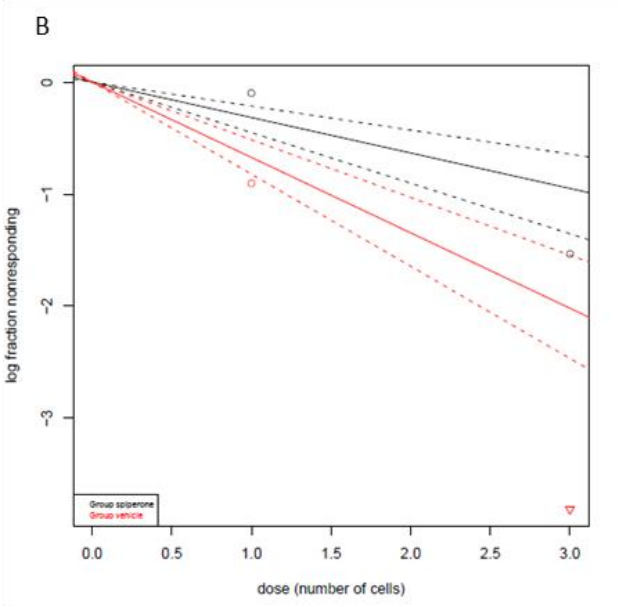

C

Group	Lower	Estimate	Upper
spiperone	4.67	3.16	2.22
vehicle	1.94	1.49	1.22

D

Chisq	DF	P.value
11.1	1	0.00085

E

Test	Chisq	DF	P Value
Likelihood ratio test of single-hit model	6.25	1	0.0125
Score test of heterogeneity	4.59	1	0.0322

Figure 24 **In vitro analysis of CRC-SCs self-renewal using the limiting dilution assay**. CRC-SCs were dissociated into single cells and plated into 96 wells plate. The number of wells containing spheres was then evaluated and micrographs are obtained to visualize sphere morphology. In the examples provided, sphere formation assays are performed on CRC-SCs populations to evaluate their stemness and clonogenic potential. Representative image of CC09 colonosphere (**A**). The amount of initially seeded cells (x-axis) is plotted against the log fraction of non-responders corresponding to wells without any detected spheres (y-axis). The slope of the line represents the log-active cell fraction (**B**). The number of lines of data entered (**C**), confidence intervals for 1/(stem cell frequency)(**D**). Goodness of fit tests (**E**).

4.2.2 Spiperone induces cell cycle arrest resulting in apoptotic cell death

To investigate the mechanism of cell death induced by spiperone, propidium iodide (PI) / annexin V (Ax) staining was performed in different cell lines. We observed a significant, time- and dose-dependent increase of apoptosis in HCT116 and SW620 cells treated with 5, 10 and 20 μmol/L spiperone (**Figure 26A-D**). Similarly, apoptosis was also observed in CRC-SCs with a two-fold increase of apoptotic cells after 24 hours exposure to 2.5 μmol/L and a progressive rise of late apoptotic/necrotic cells after exposure to increasing doses of drug (**Figure 27A-D**).

We also performed a cell cycle analysis of HCT116 cells treated with spiperone. A significant increase of cells in the G1 phase, together with a decrease in the S/G2 phases, was observed to occur in a dose-dependent manner both after 24- and 48-hours treatments (**Figure 28A,B**). G1 phase arrest was associated with increased expression of CDKN1A both in HCT116 and CC09 cells treated for 24 with spiperone (**Figure 28C**). Altogether these data suggest that spiperone is capable of causing G1-phase cell cycle arrest and apoptosis in CRC cells.

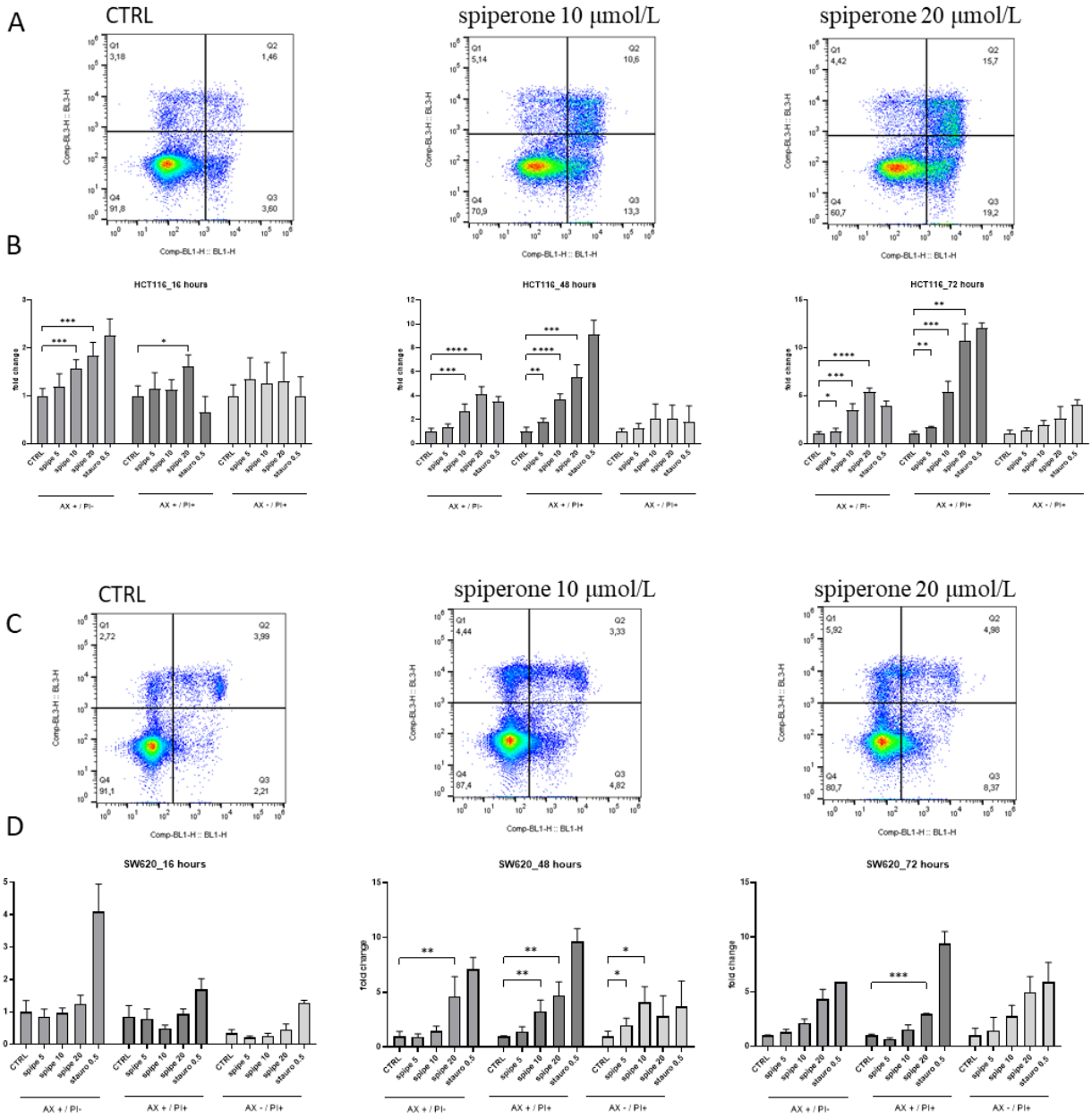

Figure 25 **Spiperone induces apoptosis in CRC cells**. Representative dot plots showing cell distribution of HCT116 (**A**) and SW620 (**C**) after annexin V/PI staining. Graph showing the analysis of the HCT116 (**B**) and SW620 (**D**) treated with different concentration of spiperone at different time points. Staurosporine was used as positive control. Cells populations are indicated as Ax+/ PI– (apoptotic), Ax+/PI+ (late apoptotic/necrotic), and Ax-/PI+ (necrotic). Data are presented as mean ± SD from three independent experiments, each performed in triplicate. *,p< 0.05; **, p< 0.01; ***, p<0.001; ****, p< 0.0001.

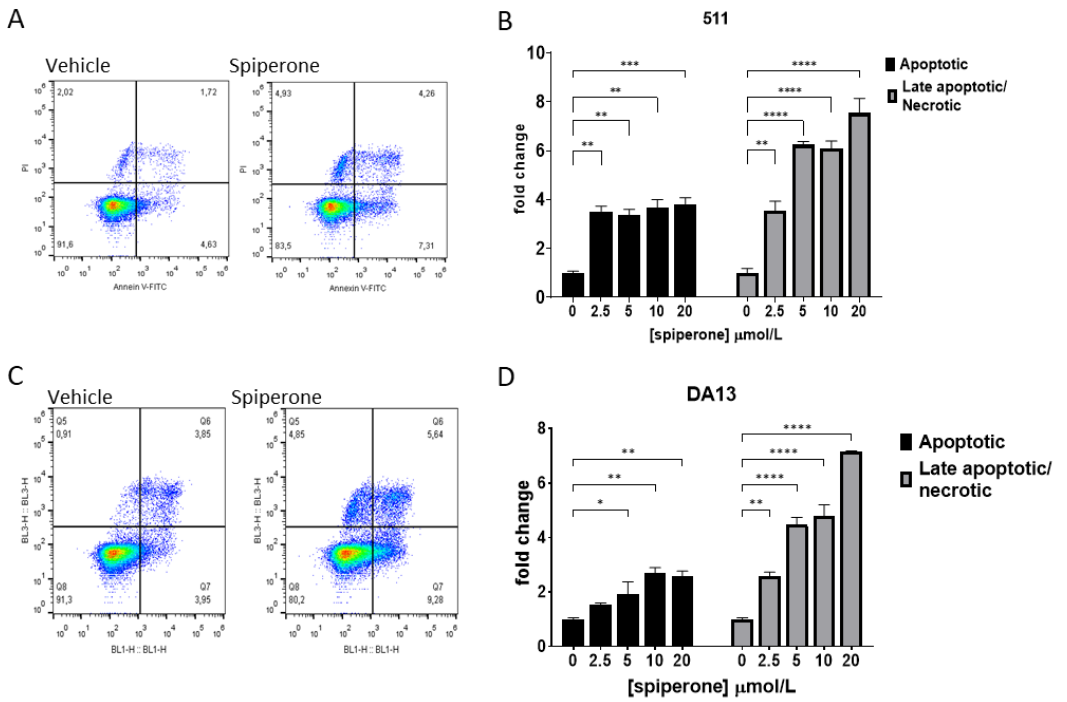

Figure 26 **Spiperone induces apoptosis in CRC-SCs**. Representative dot plot showing cell distribution of 511 (**A**) and DA13 (**C**) CRC-SC lines after AX/PI staining in control cells and in cells treated with spiperone. Graphs showing the analysis of the 511 (**B**) and DA13 (**D**) cells treated with different concentration of spiperone for 24 hours. Cells populations are indicated as apoptotic (Ax+/PI–) and late apoptotic/necrotic (Ax+/PI+ and Ax-/PI+). Data are presented as mean ± SD from three independent experiments, each performed in triplicate. *, p<0.05; **, p< 0.01; ****, p< 0.0001.

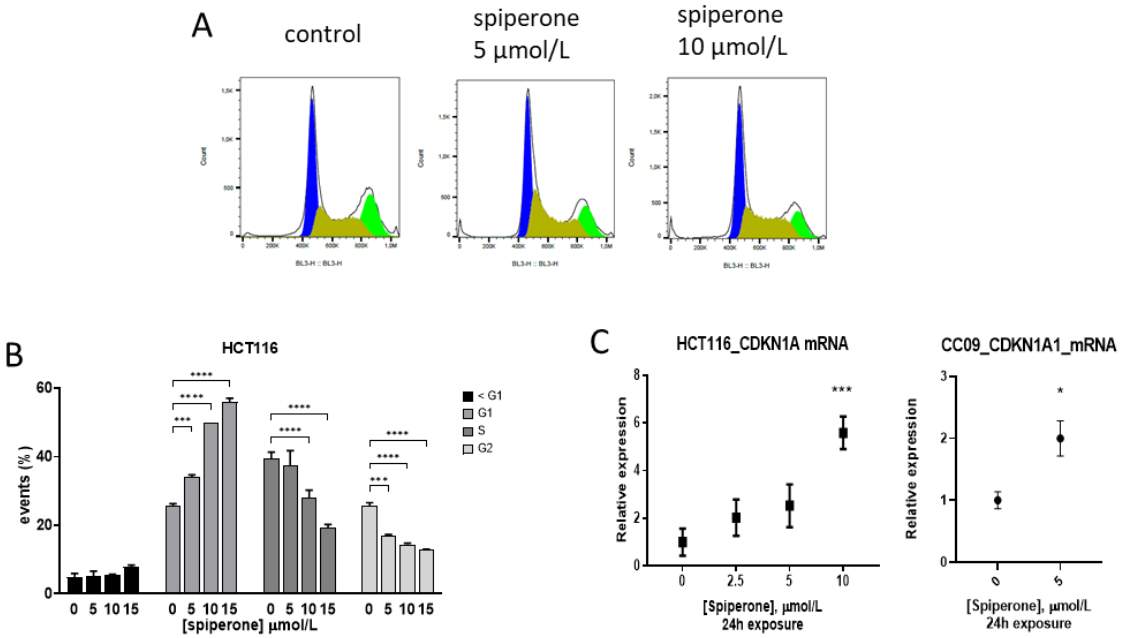

Figure 27 **Spiperone induces cell cycle arrest in G1 phase**. Representative frequencies distributions of PI staining analyzed by flow cytometry (**A**). The number of cells in G0, G1, S and G2 phase of cell cycle after 24 hours treatment with scalar doses of spiperone were quantified (**B**). Gene expression analysis of CDKN1A by RTQ-PCR, relative expressions were determined by the ΔΔCt method and normalized with the control gene GUSB (**C**). Data are presented as mean ± SD from three independent experiments, each performed in triplicate *p< 0.05; ***, p< 0.001; ****, p< 0.0001.

4.2.3 Spiperone does not induce lysosomal disruption in CRC cells

We previously showed that spiperone induces lysosomal damage and cathepsin-mediated cell death in MCF7 cells (**Figure 23**). To evaluate the role of lysosomes in CRC cells death induced by spiperone, LipidTox green staining was performed on three different CRC cell lines. While treatment with 5 μmol/L fluoxetine caused a significant increase in LipidTox staining, treatment with 5 and 10 μmol/L spiperone did not induce phospholipidosis in CRC cell lines, similarly to what previously observed in MCF7 cells (**Figure 21**; **Figure 29A,B**). We then investigated if spiperone treatment induced the release of lysosomal cysteine protease cathepsin B, in the cytosol. After a 16-hour treatment, cathepsin B strictly colocalized with LAMP-1, suggesting that spiperone toxicity is not related to lysosomal membrane damage and cathepsin B release (**Figure 29C**).

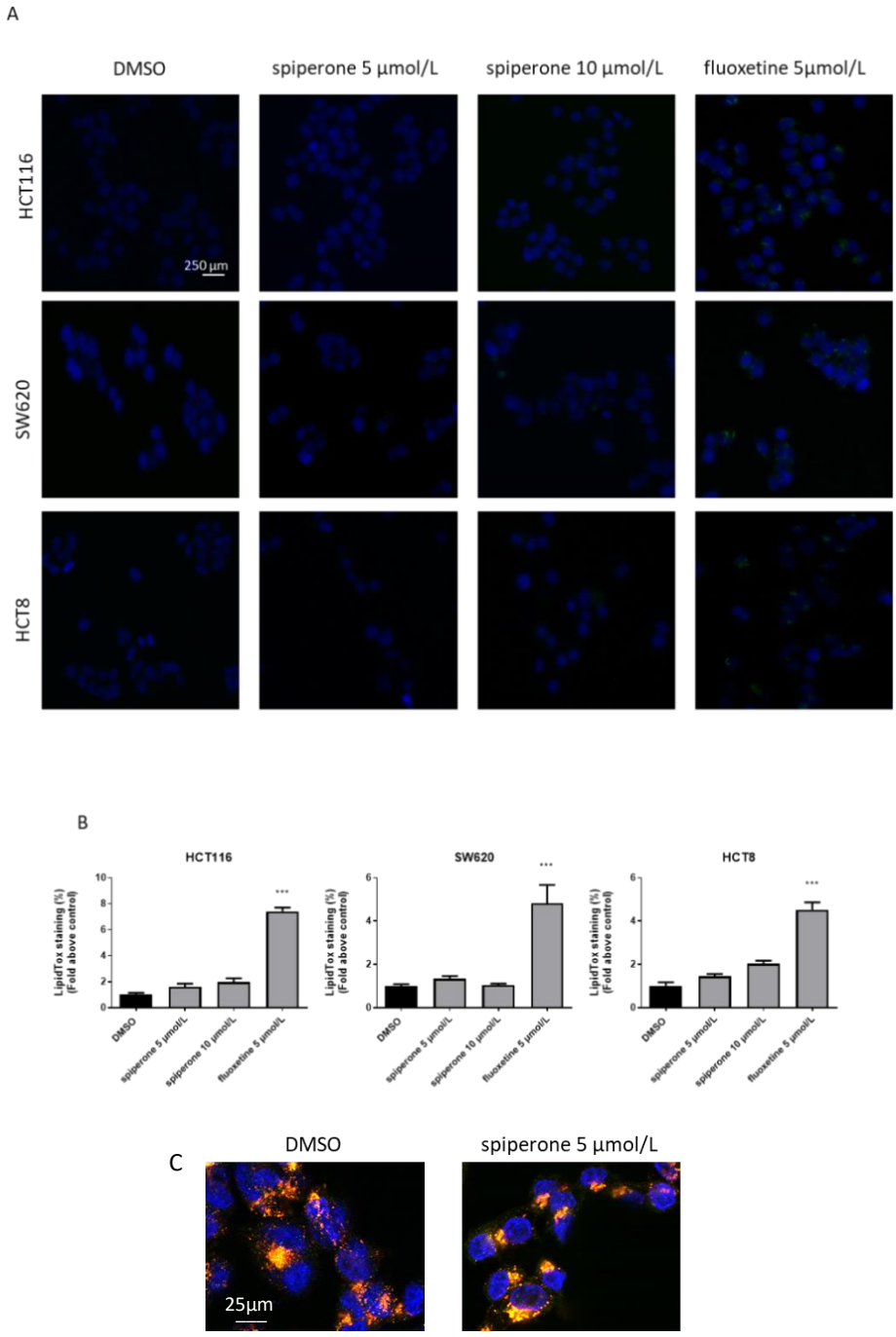

Figure 28 **Treatment with spiperone does not induce phospholipidosis and lysosomal damage in CRC cells**. Accumulation of phospholipids was evaluated after 16 hours treatment with drugs using LipidTox green staining. Nuclei were stained using Hoechst 33342. Pictures were acquired by fluorescence microscopy (magnification: 20x). Representative images of cells treated with DMSO, spiperone 5 and 10 µmol/L (**A**). Histogram showing quantification of Green LipidTox staining/blue nuclei staining ratio as fold change relative to control. Data are presented as mean ± SD from three independent experiments, each performed in triplicate. ***, Student's T-test $p < 0.001$ (**B**). Colocalization of cathepsin B and lysosomes was evaluated by using cathepsin B (green) and LAMP1 (red) antibodies after 16 hours treatment with spiperone. Nuclei were stained using DAPI. Pictures were acquired by confocal microscope Leica SP8 (magnification: 60x) (**C**).

4.2.4 Spiperone induces endoplasmic reticulum (ER) Ca^{2+} release resulting in a Ca^{2+}- mediated activation of PKC

In 2009 Lu and collaborators performed a screening of 960 drugs in HEK297 cells and identified spiperone as a molecule effective in inhibiting the WNT signaling pathway [232]. Since their results suggested that the inhibitory effect of spiperone was likely associated with its capacity to induce intracellular Ca^{2+} mobilization, we evaluated intracellular Ca^{2+} kinetics in response to spiperone treatment in CRC cells. To this end, HCT116 cells were incubated with the FLUO 4-AM Ca^{2+} flux fluorescent probe and Ca^{2+} kinetic was analyzed by flow cytometry after stimulation with spiperone. In samples treated with 20 μmol/L spiperone we observed a strong increase of the fluorescence, indicative of an increase in cytoplasmatic Ca^{2+} concentration ($[Ca^{2+}]_{cyt}$) (**Figure 30A**). A similar increase of fluorescence was also observed in cells resuspended in KRB buffer containing the extracellular Ca^{2+} chelator ethylene glycol tetraacetic acid (EGTA) (**Figure 30B**). These results indicate that, in CRC cells, spiperone enhances cytosolic Ca^{2+} levels by inducing its release from the intracellular storages.

Ca^{2+} acts inside the cell as a ubiquitous second messenger and one of its first interacting protein is protein kinase C (PKC), a class of protein kinases involved in many cellular functions, including receptors desensitization and cell growth [233]. To understand if spiperone treatment affected PKCs activity, HCT116 cells were treated with 10 μmol/L spiperone for 5, 30 and 60 minutes and levels of PKC activation were examined. Western blot analysis shows the increase of PKC substrates phosphorylation already at 5 minutes after stimulation and which still remains elevated at 60 after treatment.

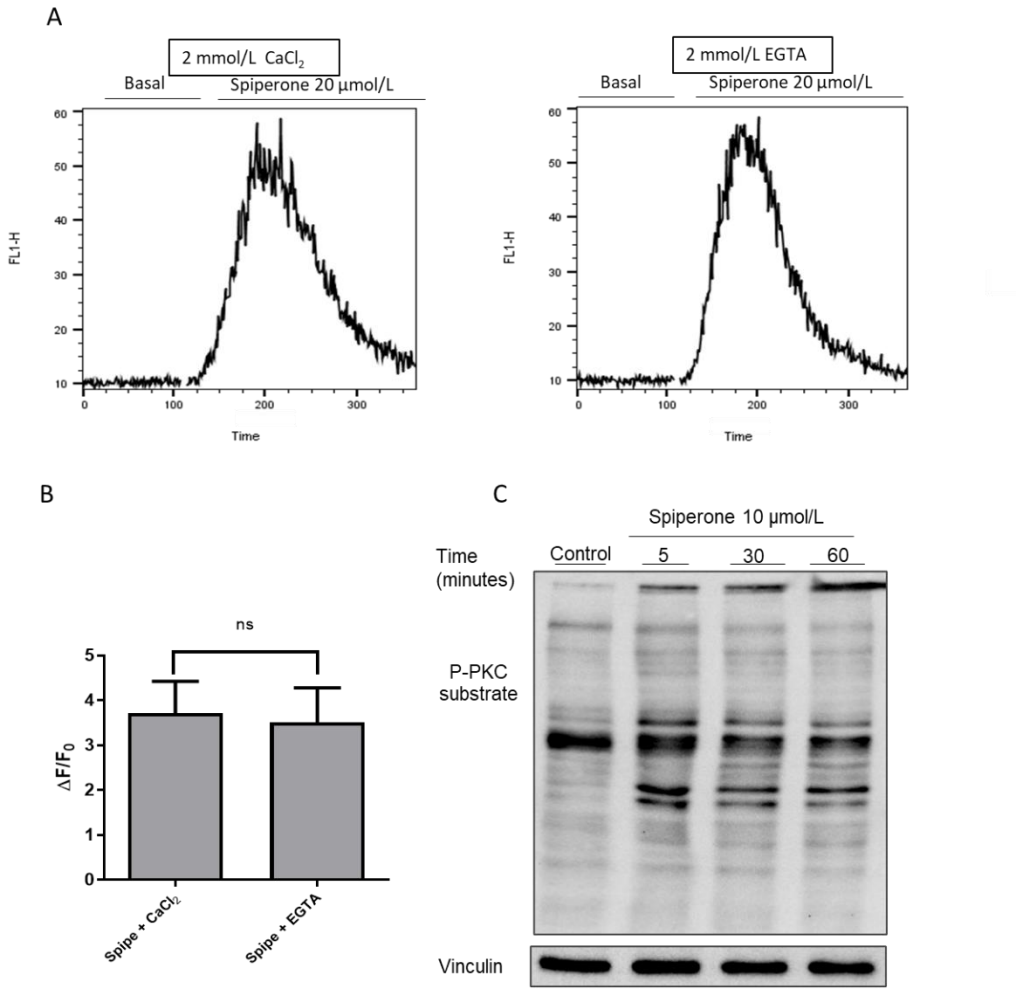

Figure 29 **Spiperone induces ER Ca^{2+} release and Ca^{2+} mediated activation of PKCs**. Representative graphs of FLUO4-am fluorescence over time with or without extracellular Ca^{2+} (**A**) Fluorescence peaks quantification, values were normalized on the basal signal (ΔF/Fo) (**B**). Western blot performed on HCT116 treated with spiperone for 5, 30, 60 minutes. Lysates were analyzed for P-(S)-PKC substrates and vinculin (**C**) Data are presented as mean ± SD from three independent experiments, each performed in triplicate.

4.2.5 Spiperone-mediated calcium increase in CRC cells is a PLC dependent process

The major Ca^{2+} store in eukaryotic cells is ER, which is characterized by the presence of various ion channels, among which inositol 1,4,5-trisphosphate receptors (IP_3Rs) constitute a family widely expressed in nearly all cell types [234]. The major agonist of IP_3R is inositol 1,4,5-trisphosphate (IP_3), produced by phospholipase C (PLC), through the hydrolysis of phosphatidylinositol-4, 5-bisphosphate (PIP_2) into diacylglycerol (DAG) and IP_3.

To evaluate the possible role of PLC in spiperone signaling in CRC cells, we repeated intracellular Ca^{2+} measurement and western blot analysis by pre-treating cells with PLC inhibitor U-73122 and its inert analogue U-73433, at the concentration of 10 μmol/L for 30 minutes. Results showed that U-73122 pretreatment abolished both the increase of $[Ca^{2+}]_{cyt}$ and the PKC activation under spiperone treatment, whereas there was no difference between fluorescence detected in cells treated with U-73433 and the control (**Figure 31A,B**). These data further confirm that in CRC spiperone-mediated Ca^{2+} release is PLC dependent (**Figure 31C**).

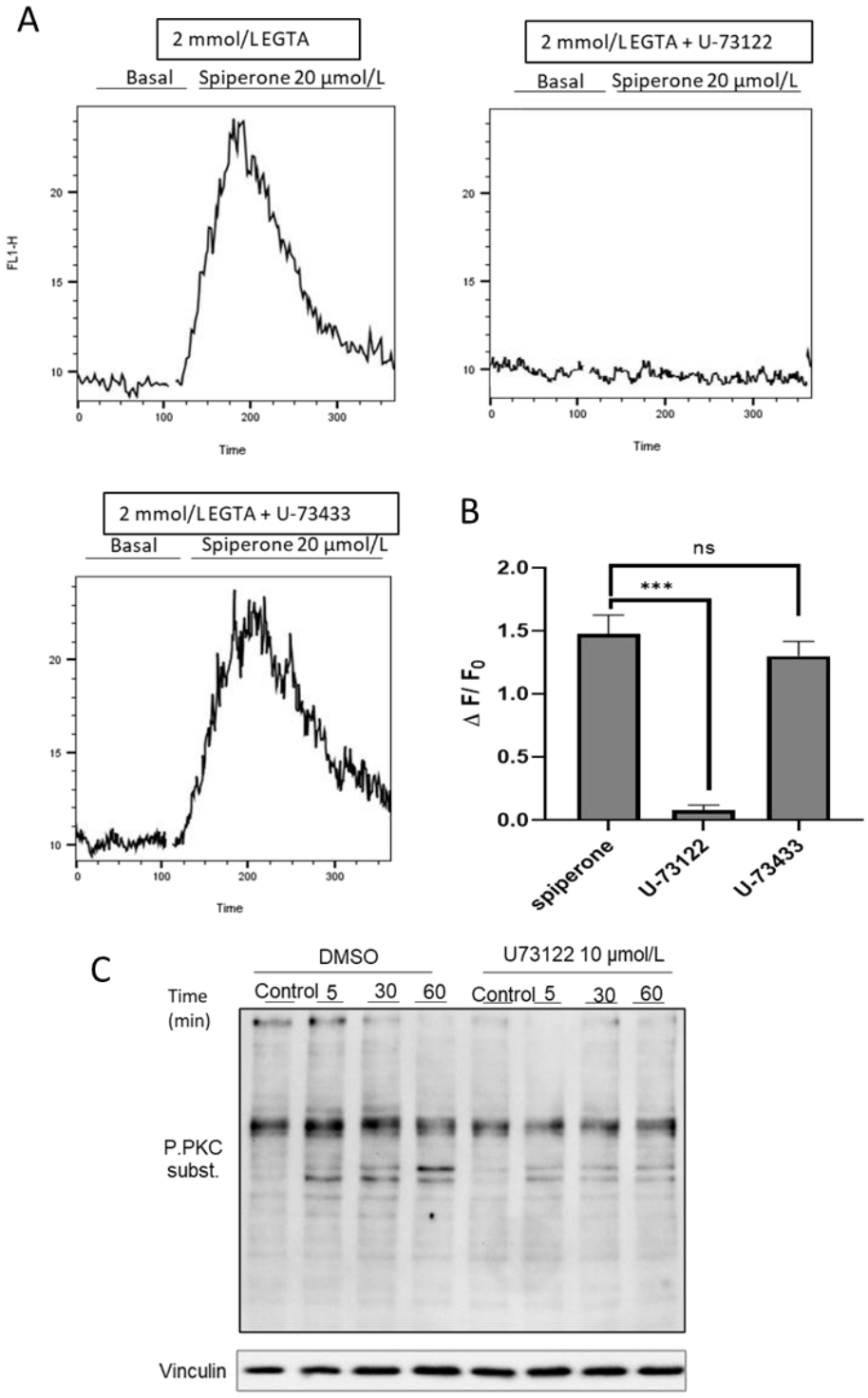

Figure 30 **Spiperone-induced calcium increase is a PLC-dependent process**. Representative graphs of FLUO4-am fluorescence over time in cells treated with spiperone, U73122 and U73433 (**A**). Graph showing the quantification of the fluorescence peaks detected in the experiment; ΔF/Fo, normalized fluorescence values (**B**). Western blot performed on HCT116 cells pretreated with U73122 and stimulated with spiperone at different times points. Lysates analyzed for P-(S)-PKC substrate and vinculin (**C**) Data are presented as mean ± SD from three independent experiments, each performed in triplicate; ***, p< 0.001.

4.2.6 Spiperone induces ER stress

ER is a multifunctional organelle and its function is not limited to Ca^{2+} storage or release, but it is also the place where lipid biosynthesis and protein folding take place [148]. Alteration in ER homeostasis causes the accumulation of unfolded or misfolded proteins that results in ER stress, which induces the activation of the unfolded protein response (UPR), an adaptive response that leads to the reduction of unfolded proteins in favor of cell function and viability [149].

Considering the link between Ca^{2+} release and UPR [235], we investigated markers of UPR activation to evaluate if spiperone-mediated Ca^{2+} release could induce ER stress in CRC.

Firstly, we investigated the splicing of XBP1 mRNA, involved in the transcriptional response aiming to alleviate the intracellular misfolded protein burden [149]. PCR analysis demonstrated the induction of the spliced form of XBP1 (XBP1s) already after 8 hours of treatment with 2.5 μmol/L of spiperone (**Figure 32A**). Spicing of XBP1 is a key event downstream IRE1α dimerization and auto-transphosphorylation that triggers not only the transcription of genes involved in protein folding but also in ER-associated degradation (ERAD), a crucial event for cell survival under ER stress conditions [156].

Then we investigated the mRNA expression of the glucose-regulated protein, 78 kDa (GRP78), a chaperone induced in the first phase of ER stress, which sustains survival and restore normal cellular functions, the phosphorylation of eukaryotic initiation factor 2α (eIF2a), involved in protein translation regulation, and the phosphorylation of JNK and P38, involved in stress response and apoptosis induction. These signal transduction factors are commonly associated with cellular stress and are activated in response to the UPR-induced alarm [152].

RTQ-PCR analysis demonstrated a significant, dose-dependent increase of GRP78 mRNA after 24 hours of treatment in HCT116 cells while a significant three-fold increase was observed in CC09 stem cells treated with 5 μmol/L spiperone (**Figure 32B**). Western blot results showed strong phosphorylation of eIF2a, P38 and JNK already after 2 hours of exposure to spiperone (**Figure 32C**), confirming UPR activation upon spiperone treatment.

When the adaptive mechanisms of the UPR fail to compensate, when the primary cause of ER stress is prolonged or excessive, cell death is induced, typically, by apoptosis [236]. For this reason, we investigated the mRNA expression of CHOP a major player in cell death induction downstream UPR [153]. In HCT116 cells we observed a 3-fold and 7-fold increase of CHOP mRNA after treatment with 5 and10 μmol/L spiperone, respectively (**Figure 32D**). Similarly, a 2.5-fold increase of CHOP mRNA was observed in CC09 cells treated, for 24 hours, with 5 μmol/L spiperone (**Figure 32D**). Altogether these data strongly suggest that spiperone induces ER stress and that this mechanism is likely to contribute to spiperone cytotoxicity in CRC cells.

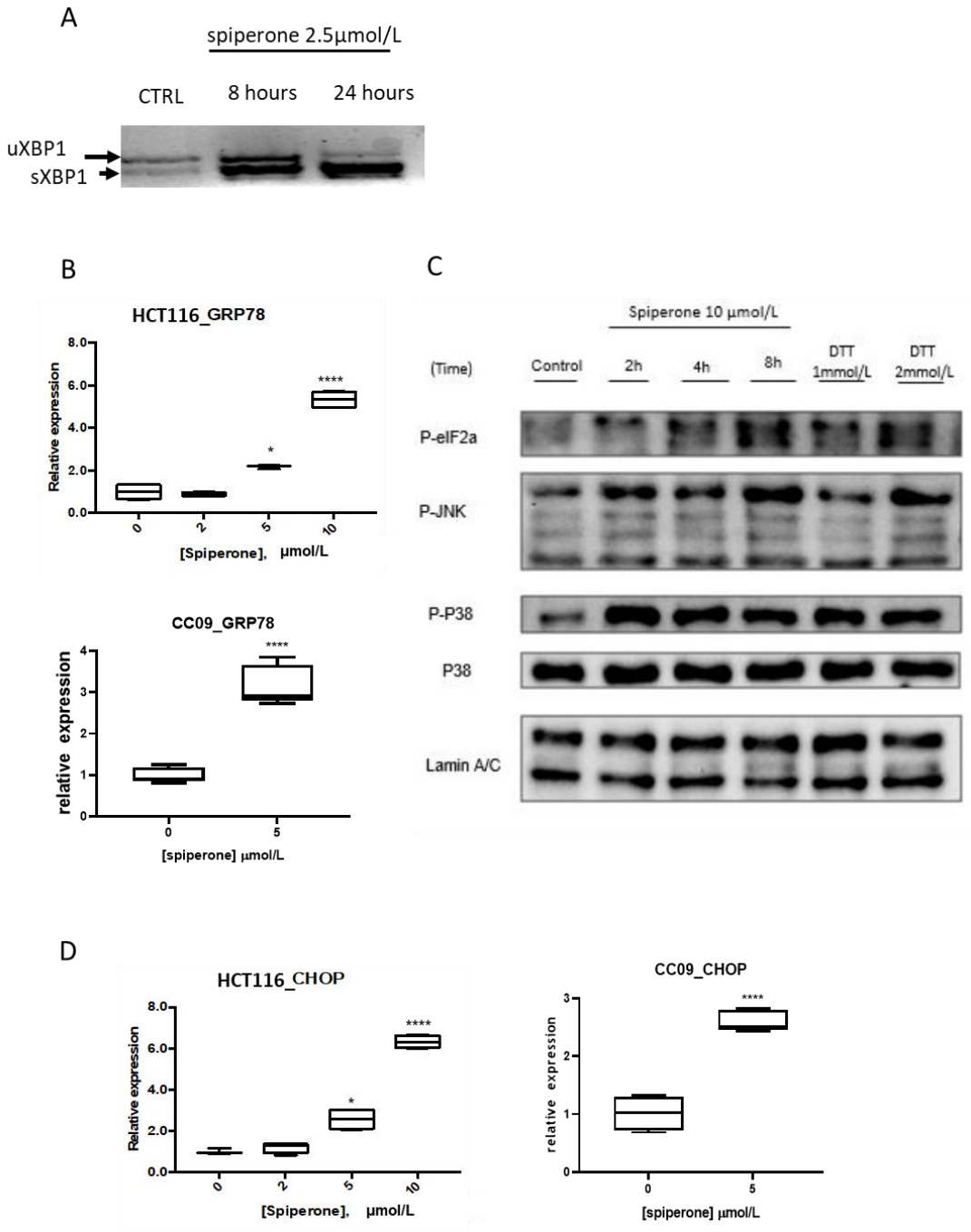

Figure 31 **Spiperone induces ER stress**. XBP1 splicing analysis; uXBP1, unspliced; sXBP1, spliced form of XBP1 after different time points (**A**). Analysis of mRNA levels of GRP78 in HCT116 and CC09 at 24 hours, relative expressions were determined by the ΔΔCt method and normalized with the control gene GUSB. (**B**). Western blot analysis of HCT116 treated with spiperone for different times and with DTT (positive control). Lysates analyzed for P-eIF2a S51, P-P38 T180/Y182, P38, P-JNK T183/Y185 and Lamin A/C (**C**). Analysis of mRNA levels of GRP78 in HCT116 and CC09 at 24 hours, relative expressions were determined by the ΔΔCt method and normalized with the control gene GUSB (**D**). Data are presented as mean ± SD from three independent experiments, each performed in triplicate *p< 0.05, **** p< 0.0001.

4.2.7 Spiperone induces mitochondrial damage

In the context of ER stress induced apoptosis, increasing evidence indicates that ER and mitochondria cooperate to induce cell death. It was reported that the tight functional network along with the controlled Ca^{2+} transfer between mitochondria and ER at the MAMs (mitochondria-associated ER membranes), is crucial in the control of cellular homeostasis and the decision of cell fate [237]. Besides, it is now well established that elevated and dysregulated increase of $[Ca^{2+}]_{cyt}$ leads to mitochondrial Ca^{2+} overload resulting in a rapid increase in the IMM permeability and collapse of the proton gradient [238].

Thus, we investigated whether spiperone was able to induce an increase of $[Ca^{2+}]_{cyt}$ and mitochondrial Ca^{2+} concentration ($[Ca^{2+}]_{mit}$). For this purpose, HCT116 cells treated with 10 μmol/L spiperone were loaded with probe FLUO-4 am along with MitoTracker to monitor $[Ca^{2+}]_{mit}$ at different time points. Our results show that spiperone causes the increase of $[Ca^{2+}]_{cyt}$ in a time-dependent manner (**Figure 33A,B**). Moreover, colocalization data indicate that long-term exposure to spiperone causes also a significant increase of $[Ca^{2+}]_{mit}$ (**Figure 33C**).

In order to determine if increased $[Ca^{2+}]_{mit}$ was impairing mitochondrial functions, cells were treated with spiperone for 16 hours and then stained with JC-1 to evaluate mitochondrial membrane depolarization. From the pictures, it is possible to observe the reduction of nearly 50% of the red/green fluorescent ratio in spiperone-treated cells compared to controls, indicating a strong depolarization of the mitochondrial membrane in spiperone-treated cells (**Figure 34A,B**).

To validate the hypothesis that mitochondrial depolarization is induced by mitochondrial Ca^{2+} overload, we performed JC-1 staining in cells treated with spiperone alone or in combination with the intracellular Ca^{2+} chelator, BAPTA-AM. Our data show that BAPTA-AM significantly rescues spiperone induced mitochondrial depolarization (**Figure 34C**).

Altogether these results show that spiperone causes the disruption of intracellular Ca^{2+} homeostasis that compromises mitochondrial function.

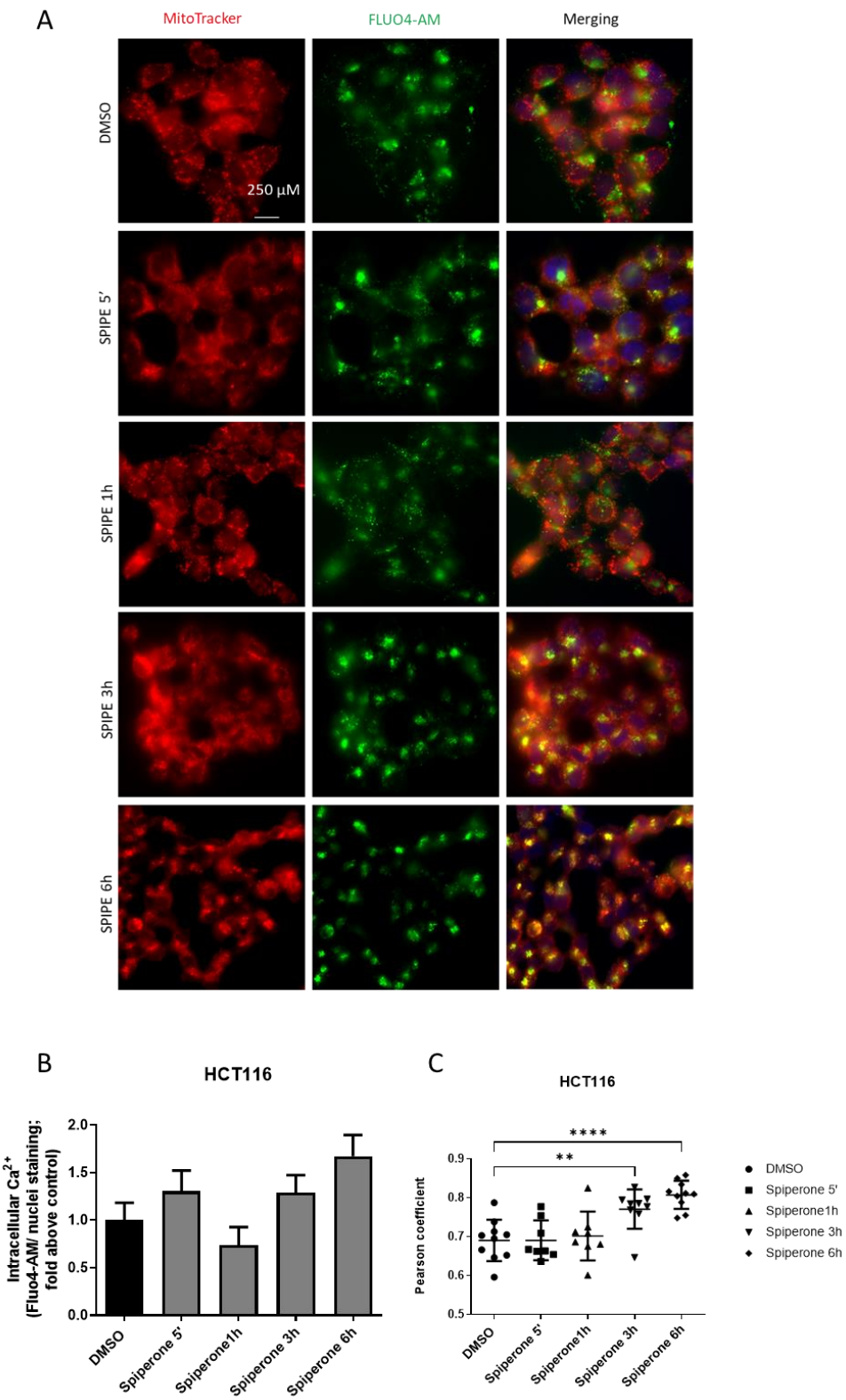

Figure 32 **Spiperone induces $[Ca^{2+}]_{cyt}$ increase resulting in $[Ca^{2+}]_{mit}$ rise**. $[Ca^{2+}]_{cyt}$ increase in response to spiperone was evaluated at different time points using FLUOA-AM, green staining. Nuclei were stained using Hoechst 33342 (blue). Mitochondria were stained with MitoTracker (red). Pictures were acquired by fluorescence microscopy (magnification: 20x). Representative images of cells treated with DMSO and 10 µmol/L spiperone (**A**). Histogram showing quantification of intracellular Ca^{2+} FLUO4-AM/blue nuclei staining ratio as fold change relative to control (**B**). Pearson coefficient of FLUO4-AM and mitochondria colocalization (**C**). Data are presented as mean ± SD from two independent experiments, each performed in triplicate. **, p< 0.01; ****, p< 0.0001.

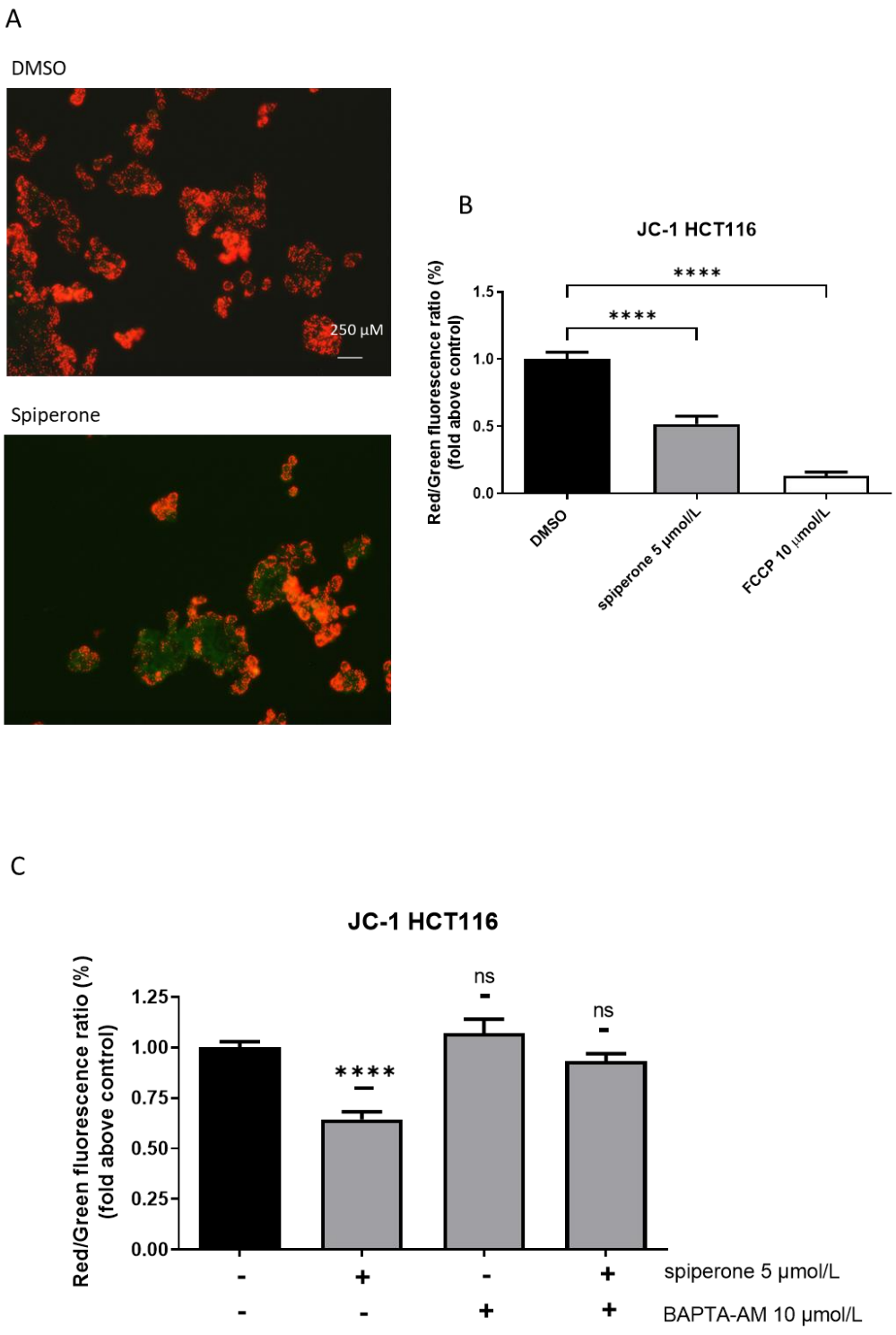

Figure 33 **Spiperone induces mitochondrial impairment.** Representative images obtained by fluorescence microscopy that show red J-aggregate in cells treated for 24 hours with vehicle or spiperone (**A**). Graph showing the reduction in red/green fluorescence ratio (**B**). Graph showing the red/green fluorescence ratio of cells treated with spiperone alone or in combination with BAPTA-AM (significance of each treatment versus control) (**C**). Data are presented as mean ± SD of three independent experiment performed in triplicate. **, p<0.01; ****, p<0.0001.

4.2.8 Intracellular Ca^{2+} chelation and PLC inhibition protects from cell death

Since we demonstrated that spiperone induces cell death of both stem-like and differentiated CRC cells, and that this cytotoxicity is associated with PLC activation and alteration in Ca^{2+} homeostasis, we investigated the role of PLC and Ca^{2+} in spiperone antitumor activity. For this purpose, we evaluated the cytotoxic activity of spiperone in the presence of the PLC inhibitor U-73122 or the intracellular Ca^{2+} chelator BAPTA-AM (**Figure 35AB**). Our results demonstrate a significant cell viability rescue in cells cotreated with both spiperone and U-73122 or BAPTA, confirming definitively that spiperone mediated CRC cell death is PLC and Ca^{2+}-dependent.

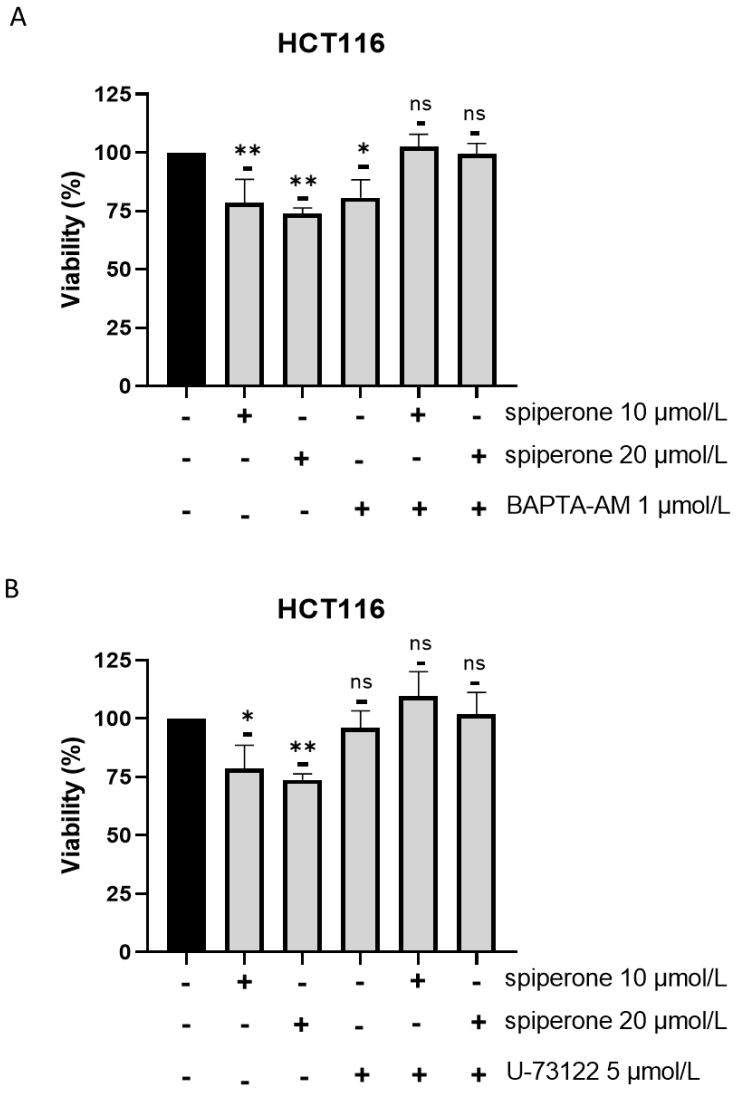

Figure 34 **Intracellular Ca^{2+} chelation and PLC inhibition prevent cell death.** Viability analysis of HCT116 cells treated with spiperone along with BAPTA-AM 1 µmol/L (**A**) and U-73122 5 µmol/L (**B**). Data represent the mean ± SD of three indipendent experiment performed in quadruplicate. Graph showing the significance of each treatment versus control. * P<0.05, ** P<0.01

5. Discussion

Although cancer treatment has witnessed remarkable progress over the past few decades, cancer remains a major threat to humans, with total cure remaining elusive. Repurposing of well-characterized and well-tolerated drugs for cancer therapy has emerged as an attractive alternative for a long and costly process of drug development [184]. Psychotropic drugs are revealing promising candidates for drug repositioning in cancer. Although several in vitro and in vivo models reported the efficacy of this family of drugs in reducing cancer cell viability and tumor growth [189, 239, 240], the pharmacological properties underpinning the possible clinical application of psychotropic drugs for cancer therapy remain poorly understood. In this study we investigated a large panel of psychotropic drugs for their potential anti-tumoral activity evaluating their cytotoxic effect in six cell lines derived from three different tumor types. By using stringent screening conditions, we identified only a few compounds that significantly reduced cell viability at clinically relevant concentrations. These were represented by the antipsychotics penfluridol, pimozide, fluspirilene, nefazodone and spiperone, the antidepressant fluoxetine and the antihistamine ebastine. Except for spiperone, whose cytotoxicity was negligible in GB, all the other compounds showed cytotoxic activity in all cell lines tested.

The comparable efficacy, in three different tumor types, of compounds with clinically different indications allows us to speculate a common mechanism of action independent from the phenotypic and molecular profile of the tumor and not associated with the conventional pharmacological properties and clinical use of these compounds. This hypothesis is corroborated by the negligible cytotoxicity observed with other drugs with superimposable biogenic amine receptors targeting, by the lack of rescue of cell viability after co-treatment with biogenic amines and by the drug concentration necessary to observe a biologic effect, that it is at least one order of magnitude higher than that needed for their conventional pharmacological targets [241].

Based on the analysis of structure and chemical-physical properties, most psychotropic compounds with a significant cytotoxic activity can be classified as CADs [205, 213]. It is well demonstrated the formation of cytoplasmic vesicles in cells exposed to CADs results from extensive ion-trapping-based accumulation of lysosomotropic weak bases in acidic compartments [205, 224]. Vacuoles formation, inhibited by the disruption of the lysosomal V-ATPase, was observed after short term exposure of MCF7 cells to CADs fluoxetine, ebastine, fluspirilene, pimozide but also to nefazodone, that is not formally a CAD but might display some of their features. Accumulation of vacuoles in the presence of bafilomycin A1 was instead observed after treatment with penfluridol and spiperone, suggesting that the formation of vesicles by these drugs does not necessarily depend on ion-trapping in acidic compartments, but is favored by the block of lysosomal activity. The acidic autophagosome nature of these vesicles was confirmed by the requirement of class III PI3K for their formation and by the

positive staining with the lysosomotropic dye LysoTracker. Notably, both spiperone and penfluridol, that induced the formation of autophagosome structures independently from the ion-trapping mechanism are likely true activator of autophagy, as demonstrated by stimulation of AMPK and LC3B conversion and downregulation of mTOR pathway observed in MCF7 cells.

Although lysosomotropic CADs can increase lysosomal pH after compound sequestration which could lead to suboptimal conditions for lysosomal digestion [242, 243], lysosomal pH increase may be a transient change and pH could be restored after extended exposure to lysosomotropic compounds [217, 244, 245]. The increased LysoTracker dye staining we observed after overnight treatment with drugs indicates a pH recovery after compound sequestration and reflects the increased lysosomal volume, suggestive of the occurrence of lysosome biogenesis induced by lysosomotropic drugs. Moreover, drug interactions with the lysosomal lipid bilayer and membrane proteins could influence the dynamics of membrane fusion and/or fission, thereby affecting trafficking steps and lysosomal egress [245], causing a reduction in autophagic flux and lysosomal enlargement.

Due to their chemical structure, CADs can accumulate in acidic lysosomes [216] and incorporate to luminal membranes where they function as effective inhibitors of acid sphingomyelinase and other lysosomal lipases [205, 214]. At therapeutically relevant concentrations, CADs have been shown to cause the lysosomal accumulation of various lipid species, including sphingomyelin, phosphatidylethanolamine, phosphatidylserine, phosphatidylcholine, lysophosphatidic acid and cholesterol, with induction of phospholipidosis [212, 226]. In our experimental model, CADs ebastine, fluspirilene, fluoxetine and pimozide, that very rapidly accumulated in cells by ion-trapping, caused a strong increase of phospholipids aggregates. Our observations are supported by papers reporting the capacity of these compounds to induce phospholipidosis. Gonzalez-Rothi in 1995 first described the complication of pulmonary phospholipidosis in a patient with manic-depressive illness after treatment with fluoxetine [246]; penfluridol, pimozide and fluspirilene have been reported in a screening of drugs capable to inhibit sphingomyelinase and were found to induce phospholipidosis in neuroglioma H4 cells [205, 214] whereas ebastine was identified by electron microscope screening to evaluate chemicals for drug-induced phospholipidosis [247]. Our results demonstrate that, also in cancer cells, ebastine, fluspirilene, fluoxetine and pimozide act as typical CADs, impairing lysosomal activity.

Some compounds investigated in this study, including the antipsychotics diphenylbutylpiperidines fluspirilene, penfluridol, and pimozide and antidepressants such as fluoxetine have been previously reported as autophagy inducers in neurons and in different cancer cell types such as BC and GB by affecting a variety of targets [248–251]. Our study shows that the cytotoxic activity of most of these compounds is essentially based on their common cationic amphiphilic properties and their capacity

to perturb acidic intracellular compartments. Moreover, although all investigated drugs caused the formation of acidic structures, apparently inducing the autophagic flux, only spiperone, penfluridol and, potentially, pimozide can be considered true autophagy activators. Overall, these data raise a critical issue related to clinical use of these compounds as autophagy enhancers, but they also reveal interesting therapeutic implications for compounds that transiently increase upstream autophagic flow while compromising downstream lysosomal function.

The lysosome is emerging as a driving force in the progression of numerous human cancers, in which enhanced function of the autophagy–lysosome system enables efficient nutrient scavenging and growth in nutrient-poor microenvironments, promote the metastatic potential and treatment resistance [115]. But lysosomal activation in aggressive cancers can lead to alterations in lysosomal structure and function, which, paradoxically, renders cancer cells more sensitive to lysosomal destabilization [252, 253]. This frailty can be targeted by lysosomotropic compound that may have an antitumor effect preferentially killing the more sensitive cancer cells by inducing dysregulation of lysosomal lipid metabolism and LMP with release into the cytosol of cathepsins, potent inducers of cell death [134, 254, 255]. In our study, we observed increased Lysotracker staining, suggestive of lysosomal swelling that is considered a typical condition preceding LMP [134, 138, 256, 257] and galectin-1 complexes, a surrogate marker of lysosomal membrane damage [227], suggesting a possible role of lysosomes in cancer cell death. This was confirmed for ebastine, penfluridol, pimozide, and fluoxetine, whose cytotoxic activity was partially rescued by inhibitor of cathepsins B and L but not by treatment with both apoptosis or autophagy inhibitors.

Inhibition of apoptosis and autophagy were also ineffective in reducing cell death induced by nefazodone and fluspirilene and further experiments are required to clarify the mechanisms of cell death induced by these drugs.

Notably, while inhibition of autophagy significantly rescued pimozide and spiperone cytotoxicity, it further increased cell death induced by penfluridol, the compound that demonstrated the highest cytotoxicity in all cell lines tested. The strong antitumoral activity of penfluridol may be due to its ability to induce both ADCD and LMP. Most of the known compounds that affect autophagy in neoplastic cells are either inducers or inhibitors of this process [119, 258]**.** However, molecules that can modulate autophagy in a dual mode, by both inducing and inhibiting the process, seem to represent a novel and effective strategy for anticancer therapy [259, 260].

Finally, all psychotropic compounds with cationic amphiphilic properties caused a significant reduction in $\Delta\psi m$. Since oncogenic activation leads to increased mitochondrial metabolism and higher $\Delta\psi m$ compared to that of non-cancer cells [261] and experimental evidence demonstrates that irreversible mitochondrial membrane depolarization can induce cell death also in apoptotic resistant

cells [262], CADs appear excellent candidates for mitochondrial targeting in cancer, as they can easily diffuse in tumor tissues and interact with negatively charged mitochondrial membranes [215, 261, 263]. Since in our cell line model cytotoxicity of psychotropic drugs was not mediated by ROS and thiols oxidation whereas apoptosis has been demonstrated only in cells treated with spiperone, studies are underway to explore the molecular mechanisms underlying CADs induced mitochondrial membrane depolarization and its role in inducing cancer cell death.

In addition to acute cytotoxicity, observed, in vitro, at lower micromolar concentrations, in vivo psychotropic drugs with cationic amphiphilic properties can also impair cancer cell metabolism and sensitize tumors to chemotherapy at plasma concentrations achieved with standard therapeutic regimens [264, 265]. Suggestive of their efficacy in human clinical setting, epidemiologic studies have reported a reduced incidence of glioma and CRC among users of tricyclic antidepressants [266], a lower CRC risk under therapy with fluoxetine [267, 268] and an association between post diagnostic use of cationic amphiphilic antihistamines and reduced cancer mortality as compared with similar use of antihistamines that do not classify as CADs [269].

Altogether, the data presented above identify a subset of psychotropic drugs as putative anticancer agents and open a feasible, safe, and economically sound possibility to test the clinical anticancer efficacy of this therapeutic class of compounds. In particular, the cytotoxicity of psychotropic drugs with cationic amphiphilic structures relied on simultaneous mitochondrial and lysosomal disruption and induction of cell death that not necessarily requires apoptosis.

CRC represents the third most diagnosed malignancy and the fourth leading cause of cancer death in the world [270]. More than 50% of the patients develop chemoresistant metastasis and, despite improvements in cytotoxic and targeted therapy, metastatic disease is still incurable, with a survival rate of more than 5 years in only 20% of cases [271]. This has raised concerns over the progress of CRC therapy and implies that alternative conceptual and practical approaches are required for the treatment of advanced-stage CRC [272]. Repurposing might represent a valid therapeutic option, especially in frail patients who are no longer candidates for aggressive therapeutic approaches, and psychotropic medications are promising as a new generation of cancer chemotherapies [239]. Notably, epidemiological data support reduced risks for rectal cancer among male patients with schizophrenia [273], colon cancer in female neuroleptic users [274] and colorectal cancer in antidepressant users [268].

In this study, we identified spiperone, a typical antipsychotic, belonging to the butyrophenone family, approved in Japan in 1969 for the treatment of schizophrenia [275] as a promising compound for CRC therapy.

Viability assays demonstrated a potent *in vitro* antitumor activity of spiperone at low micromolar concentrations, compatible with therapeutic concentrations in humans [276], whereas viability of normal, non-cancerous cells was only slightly affected by very high doses of the drug. Remarkably, spiperone induced apoptosis and reduced the clonogenic potential of undifferentiated CRC grown in colonospheres, suggesting that spiperone can target CRC-SCs, which represent the main cause of tumor growth, metastasis formation and relapse [277].

Unlike other antipsychotic drugs displaying cationic amphiphilic properties, spiperone cytotoxicity was associated neither with phospholipidosis nor with lysosomal damage. In CRC cells, instead, we observed a PLC-dependent increase of $[Ca^{2+}]_{cyt}$ after spiperone treatment, confirming previous pieces of evidence in embryonic kidney 293 (HEK293) cells and in cystic fibrosis models showing that spiperone could modulate $[Ca^{2+}]_{cyt}$ in a PLC-dependent manner [232, 278].

Currently, known targets of spiperone are serotonin (5-HT1A, 5-HT2A) and dopamine (D2,3,4) receptors [279, 280], however, our results suggest the possible involvement of other still unknown targets. The concept of polypharmacology, which involves the interaction of drug molecules with multiple targets, is recurrent among neuroleptics, that can recognize multiple aminergic GPCR in addition to dopamine receptors [281]. Since many isoforms of PLC exist and can be activated downstream receptor tyrosine kinase (RTKs), G protein-coupled receptors (GPCRs) and small GTPases [282], the identification of the PLC isoform involved in spiperone induced calcium release could help to clarify the molecular pathway involved in spiperone antitumor activity.

Although spike calcium release and PKC activation may represent a short term physiological response downstream spiperone receptor activation, long term treatment with the drug induces a long-lasting increase of $[Ca^{2+}]_{cyt}$. A well-known consequence of intracellular Ca^{2+}perturbation is ER stress [165] and activation of UPR [283]. Although the UPR is an essential adaptive mechanism that promotes cell survival, in case of severe or irreparable damage, prolonged UPR switches from pro-survival signaling to pro-death signaling leading to activation of intrinsic apoptotic and autophagy pathways [153]. In CRC, spiperone induces UPR already after two hours of treatment, with activation of both PERK and IRE1 signaling branches. The expression of CHOP and phosphorylation of JNK/P38 MAPK, link spiperone-induced ER stress to cell death. In particular, CHOP is known to induce the overexpression of proapoptotic proteins of the BCL2 family, resulting in mitochondrial impairment, release of cytochrome C and caspases activation [284]. CHOP mediates apoptosis also through other pathways. CHOP can increase the expression of the ERO1α (ER reductase) gene, which catalyzes the oxidation of protein disulfide isomerase (PDI), resulting in the production of ROS [285, 286]. Additionally, CHOP directly activates GADD34 (DNA damage protein), which combines with phosphatase 1 protein (PP1) and dephosphorylates eIF2α, resulting in protein translation recovery

and increase of ER stress and cell apoptosis [287]. Further studies are ongoing to investigate these multiple pathways to clarify the role of ER stress in spiperone-induced cell death.

While, in physiological conditions, Ca^{2+} resides mainly within the lumen of the ER, and it is released only during cellular events requiring Ca^{2+} signal; alterations in intracellular Ca^{2+} homeostasis leads to massive and/or a prolonged-release resulting in mitochondrial membrane depolarization and Ca^{2+} overload, crucial events that trigger apoptosis [237, 238, 288, 289].

We observed $[Ca^{2+}]_{cyt}$ increase already after 5 minutes of treatment, while mitochondrial overload occurred after 3 hours. Our data suggest that this prolonged Ca^{2+} increase, which occurs after either ER release or membrane channel activation, is likely to trigger not only mitochondrial membrane depolarization but also cell death, as verified by membrane depolarization and viability rescue with the intracellular Ca^{2+} chelator BAPTA-AM.

However, in order to better determine the mechanism through which spiperone triggers long term $[Ca^{2+}]_{cyt}$ increase, further experiments will be performed to clarify the involvement of membrane receptors. In addition, considering the tight link between ER and mitochondria [237], a clearer comprehension of spiperone activity at the MAM will further characterize the connection between ER stress, mitochondrial depolarization, Ca^{2+} dynamics and cell death in CRC cells.

In conclusion, altogether these results highlight the fact that dual targeting of lysosomes and mitochondria constitutes a new promising therapeutic approach for cancer, particularly those in which the apoptotic machinery is defective. Moreover, the individuation of drugs, such as spiperone, that prove effective in inducing selectively ER stress, UPR activation along with intracellular Ca^{2+} homeostasis dysregulation, could represent a crucial step in the development of new therapeutic strategies in cancer treatment.

Notably, it was previously reported spiperone efficacy in inhibiting the Wnt pathway, targeting the Wnt1/LRP6 and Wnt3/LPR6 complexes and leading to ubiquitination and degradation of β-catenin, [232]. Considering the dependence of CRC cells on the Wnt/β-catenin pathway, the observed reduction of CRC viability upon spiperone treatment could be also linked to the inhibition of this pathway. Further experiments will be performed in order to understand the role of spiperone in the Wnt/β-Catenin pathway and how this drug can alter the functioning of β-catenin. Spiperone, in fact, could induce β-Catenin degradation or interfere with its nuclear translocation, which is an essential event for gene transcription and cancer progression [290].

6. References

[1] Essue, B. M.; Laba, T.-L.; Knaul, F.; Chu, A.; Minh, H. Van; Nguyen, T. K. P.; Jan, S. Economic Burden of Chronic Ill Health and Injuries for Households in Low- and Middle-Income Countries. In *Disease Control Priorities, Third Edition (Volume 9): Improving Health and Reducing Poverty*; The World Bank, 2017; pp 121–143. https://doi.org/10.1596/978-1-4648-0527-1_ch6.

[2] Bray, F.; Ferlay, J.; Soerjomataram, I.; Siegel, R. L.; Torre, L. A.; Jemal, A. Global Cancer Statistics 2018: GLOBOCAN Estimates of Incidence and Mortality Worldwide for 36 Cancers in 185 Countries. *CA. Cancer J. Clin.*, 2018, *68* (6), 394–424. https://doi.org/10.3322/caac.21492.

[3] Ferlay, J.; Colombet, M.; Soerjomataram, I.; Mathers, C.; Parkin, D. M.; Piñeros, M.; Znaor, A.; Bray, F. Estimating the Global Cancer Incidence and Mortality in 2018: GLOBOCAN Sources and Methods. *International Journal of Cancer*. Wiley-Liss Inc. April 15, 2019, pp 1941–1953. https://doi.org/10.1002/ijc.31937.

[4] Belgioia, L.; Desideri, I.; Errico, A.; Franzese, C.; Daidone, A.; Marino, L.; Fiore, M.; Borghetti, P.; Greto, D.; Fiorentino, A. Safety and Efficacy of Combined Radiotherapy, Immunotherapy and Targeted Agents in Elderly Patients: A Literature Review. *Critical Reviews in Oncology/Hematology*. Elsevier Ireland Ltd January 1, 2019, pp 163–170. https://doi.org/10.1016/j.critrevonc.2018.11.009.

[5] Harbeck, N.; Gnant, M. Breast Cancer. *The Lancet*. Lancet Publishing Group March 18, 2017, pp 1134–1150. https://doi.org/10.1016/S0140-6736(16)31891-8.

[6] Sun, Y. S.; Zhao, Z.; Yang, Z. N.; Xu, F.; Lu, H. J.; Zhu, Z. Y.; Shi, W.; Jiang, J.; Yao, P. P.; Zhu, H. P. Risk Factors and Preventions of Breast Cancer. *International Journal of Biological Sciences*. Ivyspring International Publisher 2017, pp 1387–1397. https://doi.org/10.7150/ijbs.21635.

[7] Stingl, J.; Caldas, C. Molecular Heterogeneity of Breast Carcinomas and the Cancer Stem Cell Hypothesis. *Nature Reviews Cancer*. Nature Publishing Group October 2007, pp 791–799. https://doi.org/10.1038/nrc2212.

[8] Siziopikou, K. P. Ductal Carcinoma in Situ of the Breast: Current Concepts and Future Directions. *Archives of Pathology and Laboratory Medicine*. Arch Pathol Lab Med April 2013, pp 462–466. https://doi.org/10.5858/arpa.2012-0078-RA.

[9] ELSTON, C. W.; ELLIS, I. O. Pathological Prognostic Factors in Breast Cancer. I. The Value of Histological Grade in Breast Cancer: Experience from a Large Study with Long-term Follow-up. *Histopathology*, 1991, *19* (5), 403–410. https://doi.org/10.1111/j.1365-2559.1991.tb00229.x.

[10] Singletary, S. E.; Connolly, J. L. Breast Cancer Staging: Working With the Sixth Edition of the AJCC Cancer Staging Manual. *CA. Cancer J. Clin.*, 2006, *56* (1), 37–47. https://doi.org/10.3322/canjclin.56.1.37.

[11] Arvold, N. D.; Taghian, A. G.; Niemierko, A.; Abi Raad, R. F.; Sreedhara, M.; Nguyen, P. L.; Bellon, J. R.; Wong, J. S.; Smith, B. L.; Harris, J. R. Age, Breast Cancer Subtype Approximation, and Local Recurrence after Breast-Conserving Therapy. *J. Clin. Oncol.*, 2011, *29* (29), 3885–3891. https://doi.org/10.1200/JCO.2011.36.1105.

[12] Howlader, N.; Altekruse, S. F.; Li, C. I.; Chen, V. W.; Clarke, C. A.; Ries, L. A. G.; Cronin, K. A. US Incidence of Breast Cancer Subtypes Defined by Joint Hormone Receptor and HER2 Status. *J. Natl. Cancer Inst.*, 2014, *106* (5). https://doi.org/10.1093/jnci/dju055.

[13] Ades, F.; Zardavas, D.; Bozovic-Spasojevic, I.; Pugliano, L.; Fumagalli, D.; De Azambuja, E.; Viale, G.; Sotiriou, C.; Piccart, M. Luminal B Breast Cancer: Molecular Characterization, Clinical Management, and Future Perspectives. *Journal of Clinical Oncology*. American Society of Clinical Oncology September 1, 2014, pp 2794–2803. https://doi.org/10.1200/JCO.2013.54.1870.

[14] Tang, Y.; Wang, Y.; Kiani, M. F.; Wang, B. Classification, Treatment Strategy, and Associated Drug Resistance in Breast Cancer. *Clinical Breast Cancer*. Elsevier Inc. October 1, 2016, pp 335–343. https://doi.org/10.1016/j.clbc.2016.05.012.

[15] Anders, C.; Carey, L. A. Understanding and Treating Triple-Negative Breast Cancer. *Oncology*, 2008, *22* (11), 1233–1239.

[16] Curigliano, G.; Goldhirsch, A. The Triple-Negative Subtype: New Ideas for the Poorest Prognosis Breast Cancer. *J. Natl. Cancer Inst. - Monogr.*, 2011, *2011* (43), 108–110. https://doi.org/10.1093/jncimonographs/lgr038.

[17] Moo, T. A.; Sanford, R.; Dang, C.; Morrow, M. Overview of Breast Cancer Therapy. *PET Clinics*. W.B. Saunders July 1, 2018, pp 339–354. https://doi.org/10.1016/j.cpet.2018.02.006.

[18] Cameron, D.; Piccart-Gebhart, M. J.; Gelber, R. D.; Procter, M.; Goldhirsch, A.; de Azambuja, E.; Castro, G.; Untch, M.; Smith, I.; Gianni, L.; et al. 11 Years' Follow-up of Trastuzumab after Adjuvant Chemotherapy in HER2-Positive Early Breast Cancer: Final Analysis of the HERceptin Adjuvant (HERA) Trial. *Lancet*, 2017, *389* (10075), 1195–1205. https://doi.org/10.1016/S0140-6736(16)32616-2.

[19] Liu, Y. C.; Ma, Y.; An, N.; Sun, P.; Wang, Y.; Sun, C. Clinical Efficacy of Combination of Pertuzumab, Trastuzumab, and Docetaxel for Treatment of Patients with HER2-Positive Breast Cancer. *Medicine (United States)*. Lippincott Williams and Wilkins September 1, 2019. https://doi.org/10.1097/MD.0000000000017262.

[20] Nathan, M. R.; Schmid, P. A Review of Fulvestrant in Breast Cancer. *Oncol. Ther.*, 2017, *5* (1), 17–29. https://doi.org/10.1007/s40487-017-0046-2.

[21] Li, F.; Dou, J.; Wei, L.; Li, S.; Liu, J. The Selective Estrogen Receptor Modulators in Breast Cancer Prevention. *Cancer Chemotherapy and Pharmacology*. Springer Verlag January 20, 2016, pp 895–903. https://doi.org/10.1007/s00280-016-2959-0.

[22] Widakowich, C.; de Castro, G.; de Azambuja, E.; Dinh, P.; Awada, A. Review: Side Effects of Approved Molecular Targeted Therapies in Solid Cancers. *Oncologist*, 2007, *12* (12), 1443–1455. https://doi.org/10.1634/theoncologist.12-12-1443.

[23] Marley, A. R.; Nan, H. Epidemiology of Colorectal Cancer. *International Journal of Molecular Epidemiology and Genetics*. E-Century Publishing Corporation 2016, pp 105–114. https://doi.org/10.3109/9781420016307-2.

[24] Huang, D.; Sun, W.; Zhou, Y.; Li, P.; Chen, F.; Chen, H.; Xia, D.; Xu, E.; Lai, M.; Wu, Y.; et al. Mutations of Key Driver Genes in Colorectal Cancer Progression and Metastasis. *Cancer Metastasis Rev.*, 2018, *37* (1), 173–187. https://doi.org/10.1007/s10555-017-9726-5.

[25] Müller, M. F.; Ibrahim, A. E. K.; Arends, M. J. Molecular Pathological Classification of Colorectal Cancer. *Virchows Archiv*. Springer Verlag August 1, 2016, pp 125–134. https://doi.org/10.1007/s00428-016-1956-3.

[26] Nguyen, H. T.; Duong, H. Q. The Molecular Characteristics of Colorectal Cancer: Implications for Diagnosis and Therapy (Review). *Oncology Letters*. Spandidos Publications July 1, 2018,

pp 9–18. https://doi.org/10.3892/ol.2018.8679.

[27] Simon, K. Colorectal Cancer Development and Advances in Screening. *Clinical Interventions in Aging*. Dove Medical Press Ltd. July 19, 2016, pp 967–976. https://doi.org/10.2147/CIA.S109285.

[28] Stanczak, A.; Stec, R.; Bodnar, L.; Olszewski, W.; Cichowicz, M.; Kozlowski, W.; Szczylik, C.; Pietrucha, T.; Wieczorek, M.; Lamparska-Przybysz, M. Prognostic Significance of Wnt-1, β-Catenin and E-Cadherin Expression in Advanced Colorectal Carcinoma. *Pathol. Oncol. Res.*, 2011, *17* (4), 955–963. https://doi.org/10.1007/s12253-011-9409-4.

[29] Fearon, E. R.; Vogelstein, B. A Genetic Model for Colorectal Tumorigenesis. *Cell*. Cell June 1, 1990, pp 759–767. https://doi.org/10.1016/0092-8674(90)90186-I.

[30] Thiagalingam, S.; Lengauer, C.; Leach, F. S.; Schutte, M.; Hahn, S. A.; Overhauser, J.; Willson, J. K. V.; Markowitz, S.; Hamilton, S. R.; Kern, S. E.; et al. Evaluation of Candidate Tumour Suppressor Genes on Chromosome 18 in Colorectal Cancers. *Nat. Genet.*, 1996, *13* (3), 343–346. https://doi.org/10.1038/ng0796-343.

[31] Markowitz, S. D.; Bertagnolli, M. M. Molecular Basis of Colorectal Cancer. *N. Engl. J. Med.*, 2009, *361* (25), 2449–2460. https://doi.org/10.1056/nejmra0804588.

[32] Testa, U.; Pelosi, E.; Castelli, G. Colorectal Cancer: Genetic Abnormalities, Tumor Progression, Tumor Heterogeneity, Clonal Evolution and Tumor-Initiating Cells. *Med. Sci.*, 2018, *6* (2), 31. https://doi.org/10.3390/medsci6020031.

[33] Mojarad, E. N.; Kuppen, P. J. K.; Aghdaei, H. A.; Zali, M. R. The CpG Island Methylator Phenotype (CIMP) in Colorectal Cancer. *Gastroenterology and Hepatology from Bed to Bench*. Shahid Beheshti University of Medical Sciences 2013, pp 120–128. https://doi.org/10.22037/ghfbb.v6i3.383.

[34] Miller, K. D.; Nogueira, L.; Mariotto, A. B.; Rowland, J. H.; Yabroff, K. R.; Alfano, C. M.; Jemal, A.; Kramer, J. L.; Siegel, R. L. Cancer Treatment and Survivorship Statistics, 2019. *CA. Cancer J. Clin.*, 2019, *69* (5), 363–385. https://doi.org/10.3322/caac.21565.

[35] Favoriti, P.; Carbone, G.; Greco, M.; Pirozzi, F.; Pirozzi, R. E. M.; Corcione, F. Worldwide Burden of Colorectal Cancer: A Review. *Updates in Surgery*. Springer-Verlag Italia s.r.l. March 1, 2016, pp 7–11. https://doi.org/10.1007/s13304-016-0359-y.

[36] De Rosa, M.; Pace, U.; Rega, D.; Costabile, V.; Duraturo, F.; Izzo, P.; Delrio, P. Genetics, Diagnosis and Management of Colorectal Cancer (Review). *Oncol. Rep.*, 2015, *34* (3), 1087–1096. https://doi.org/10.3892/or.2015.4108.

[37] Goldberg, R. M.; Montagut, C.; Wainberg, Z. A.; Ronga, P.; Audhuy, F.; Taieb, J.; Stintzing, S.; Siena, S.; Santini, D. Optimising the Use of Cetuximab in the Continuum of Care for Patients with Metastatic Colorectal Cancer. *ESMO Open*. BMJ Publishing Group May 1, 2018. https://doi.org/10.1136/esmoopen-2018-000353.

[38] Wang, X.; Zhang, H.; Chen, X. Drug Resistance and Combating Drug Resistance in Cancer. *Cancer Drug Resist.*, 2019, *2* (2), 141–160. https://doi.org/10.20517/cdr.2019.10.

[39] Housman, G.; Byler, S.; Heerboth, S.; Lapinska, K.; Longacre, M.; Snyder, N.; Sarkar, S. Drug Resistance in Cancer: An Overview. *Cancers*. MDPI AG September 5, 2014, pp 1769–1792. https://doi.org/10.3390/cancers6031769.

[40] Nikolaou, M.; Pavlopoulou, A.; Georgakilas, A. G.; Kyrodimos, E. The Challenge of Drug Resistance in Cancer Treatment: A Current Overview. *Clin. Exp. Metastasis*, 2018, *35*

(4), 309–318. https://doi.org/10.1007/s10585-018-9903-0.

[41] Sherlach, K. S.; Roepe, P. D. “Drug Resistance Associated Membrane Proteins.” *Front. Physiol.*, 2014, *5 MAR*. https://doi.org/10.3389/fphys.2014.00108.

[42] Vasiliou, V.; Vasiliou, K.; Nebert, D. W. Human ATP-Binding Cassette (ABC) Transporter Family. *Hum. Genomics*, 2009, *3* (3), 281–290. https://doi.org/10.1186/1479-7364-3-3-281.

[43] Vaidyanathan, A.; Sawers, L.; Gannon, A. L.; Chakravarty, P.; Scott, A. L.; Bray, S. E.; Ferguson, M. J.; Smith, G. ABCB1 (MDR1) Induction Defines a Common Resistance Mechanism in Paclitaxel- and Olaparib-Resistant Ovarian Cancer Cells. *Br. J. Cancer*, 2016, *115* (4), 431–441. https://doi.org/10.1038/bjc.2016.203.

[44] Lal, S.; Wong, Z. W.; Sandanaraj, E.; Xiang, X.; Ang, P. C. S.; Lee, E. J. D.; Chowbay, B. Influence of ABCB1 and ABCG2 Polymorphisms on Doxorubicin Disposition in Asian Breast Cancer Patients. *Cancer Sci.*, 2008, *99* (4), 816–823. https://doi.org/10.1111/j.1349-7006.2008.00744.x.

[45] Satake, K.; Tsukamoto, M.; Mitani, Y.; Regasini, L. O.; Bolzani, V. D. S.; Efferth, T.; Nakagawa, H. Human ABCB1 Confers Cells Resistance to Cytotoxic Guanidine Alkaloids from Pterogyne Nitens. *Biomed. Mater. Eng.*, 2015, *25* (3), 249–256. https://doi.org/10.3233/BME-151282.

[46] Hu, J.; Li, J.; Yue, X.; Wang, J.; Liu, J.; Sun, L.; Kong, D. Expression of the Cancer Stem Cell Markers ABCG2 and OCT-4 in Right-Sided Colon Cancer Predicts Recurrence and Poor Outcomes. *Oncotarget*, 2017, *8* (17), 28463–28470. https://doi.org/10.18632/oncotarget.15307.

[47] Tiezzi, D. G.; Sicchieri, R. D.; Mouro, L. R.; Oliveira, T. M. G.; Silveira, W. A.; Antonio, H. M. R.; Muglia, V. F.; de Andrade, J. M. ABCG2 as a Potential Cancer Stem Cell Marker in Breast Cancer. *J. Clin. Oncol.*, 2013, *31* (15_suppl), e12007–e12007. https://doi.org/10.1200/jco.2013.31.15_suppl.e12007.

[48] Mao, Q.; Unadkat, J. D. Role of the Breast Cancer Resistance Protein (BCRP/ABCG2) in Drug Transport—an Update. *AAPS J.*, 2015, *17* (1), 65–82. https://doi.org/10.1208/s12248-014-9668-6.

[49] Azzarito, T.; Venturi, G.; Cesolini, A.; Fais, S. Lansoprazole Induces Sensitivity to Suboptimal Doses of Paclitaxel in Human Melanoma. 2014. https://doi.org/10.1016/j.canlet.2014.10.017.

[50] Helleday, T.; Petermann, E.; Lundin, C.; Hodgson, B.; Sharma, R. A. DNA Repair Pathways as Targets for Cancer Therapy. *Nature Reviews Cancer*. Nature Publishing Group March 2008, pp 193–204. https://doi.org/10.1038/nrc2342.

[51] De Angelis, P. M.; Kravik, K. L.; Tunheim, S. H.; Haug, T.; Reichelt, W. H. Comparison of Gene Expression in HCT116 Treatment Derivatives Generated by Two Different 5-Fluorouracil Exposure Protocols. *Mol. Cancer*, 2004, *3*. https://doi.org/10.1186/1476-4598-3-11.

[52] De Angelis, P. M.; Svendsrud, D. H.; Kravik, K. L.; Stokke, T. Cellular Response to 5-Fluorouracil (5-FU) in 5-FU-Resistant Colon Cancer Cell Lines during Treatment and Recovery. *Mol. Cancer*, 2006, *5*, 20. https://doi.org/10.1186/1476-4598-5-20.

[53] Triana-Martínez, F.; Loza, M. I.; Domínguez, E. Beyond Tumor Suppression: Senescence in Cancer Stemness and Tumor Dormancy. *Cells*, 2020, *9* (2), 346. https://doi.org/10.3390/cells9020346.

[54] Demaria, M.; O'Leary, M. N.; Chang, J.; Shao, L.; Liu, S.; Alimirah, F.; Koenig, K.; Le, C.; Mitin, N.; Deal, A. M.; et al. Cellular Senescence Promotes Adverse Effects of Chemotherapy and Cancer Relapse. *Cancer Discov.*, 2017, *7* (2), 165–176. https://doi.org/10.1158/2159-8290.CD-16-0241.

[55] Saleh, T.; Tyutyunyk-Massey, L.; Gewirtz, D. A. Controversy and Consensus Tumor Cell Escape from Therapy-Induced Senescence as a Model of Disease Recurrence after Dormancy. 2019. https://doi.org/10.1158/0008-5472.CAN-18-3437.

[56] Sieben, C. J.; Sturmlechner, I.; van de Sluis, B.; van Deursen, J. M. Two-Step Senescence-Focused Cancer Therapies. *Trends in Cell Biology*. Elsevier Ltd September 1, 2018, pp 723–737. https://doi.org/10.1016/j.tcb.2018.04.006.

[57] Bonnet, D.; medicine, J. D.-N.; 1997, undefined. Human Acute Myeloid Leukemia Is Organized as a Hierarchy That Originates from a Primitive Hematopoietic Cell. *nature.com*, 1997. https://doi.org/10.1038/nm0797-730.

[58] Jin, X.; Jin, X.; Kim, H. Cancer Stem Cells and Differentiation Therapy. *Tumor Biology*. SAGE Publications Ltd October 1, 2017, pp 1–11. https://doi.org/10.1177/1010428317729933.

[59] Kuşoğlu, A.; Biray Avcı, Ç. Cancer Stem Cells: A Brief Review of the Current Status. *Gene*. Elsevier B.V. January 10, 2019, pp 80–85. https://doi.org/10.1016/j.gene.2018.09.052.

[60] Clarke, M. F.; Dick, J. E.; Dirks, P. B.; Eaves, C. J.; Jamieson, C. H. M.; Jones, D. L.; Visvader, J.; Weissman, I. L.; Wahl, G. M. Cancer Stem Cells - Perspectives on Current Status and Future Directions: AACR Workshop on Cancer Stem Cells. In *Cancer Research*; American Association for Cancer Research, 2006; Vol. 66, pp 9339–9344. https://doi.org/10.1158/0008-5472.CAN-06-3126.

[61] Valent, P.; Bonnet, D.; De Maria, R.; Lapidot, T.; Copland, M.; Melo, J. V.; Chomienne, C.; Ishikawa, F.; Schuringa, J. J.; Stassi, G.; et al. Cancer Stem Cell Definitions and Terminology: The Devil Is in the Details. *Nature Reviews Cancer*. Nature Publishing Group November 11, 2012, pp 767–775. https://doi.org/10.1038/nrc3368.

[62] Ajani, J. A.; Song, S.; Hochster, H. S.; Steinberg, I. B. Cancer Stem Cells: The Promise and the Potential. *Semin. Oncol.*, 2015, *42* (S1), S3–S17. https://doi.org/10.1053/j.seminoncol.2015.01.001.

[63] Turdo, A.; Veschi, V.; Gaggianesi, M.; Chinnici, A.; Bianca, P.; Todaro, M.; Stassi, G. Meeting the Challenge of Targeting Cancer Stem Cells. *Front. Cell Dev. Biol.*, 2019, *7*, 16. https://doi.org/10.3389/fcell.2019.00016.

[64] Chen, W.; Dong, J.; Haiech, J.; Kilhoffer, M. C.; Zeniou, M. Cancer Stem Cell Quiescence and Plasticity as Major Challenges in Cancer Therapy. *Stem Cells International*. Hindawi Publishing Corporation 2016. https://doi.org/10.1155/2016/1740936.

[65] Kyjacova, L.; Hubackova, S.; Krejcikova, K.; Strauss, R.; Hanzlikova, H.; Dzijak, R.; Imrichova, T.; Simova, J.; Reinis, M.; Bartek, J.; et al. Radiotherapy-Induced Plasticity of Prostate Cancer Mobilizes Stem-like Non-Adherent, Erk Signaling-Dependent Cells. *Cell Death Differ.*, 2015, *22* (6), 898–911. https://doi.org/10.1038/cdd.2014.97.

[66] Radisky, D. C.; LaBarge, M. A. Epithelial-Mesenchymal Transition and the Stem Cell Phenotype. *Cell Stem Cell*. Cell Stem Cell June 5, 2008, pp 511–512. https://doi.org/10.1016/j.stem.2008.05.007.

[67] Thiery, J. P. Epithelial-Mesenchymal Transitions in Development and Pathologies. *Current Opinion in Cell Biology*. Elsevier Ltd 2003, pp 740–746. https://doi.org/10.1016/j.ceb.2003.10.006.

[68] Ingangi, V.; Minopoli, M.; Ragone, C.; Motti, M. L.; Carriero, M. V. Role of Microenvironment on the Fate of Disseminating Cancer Stem Cells. *Frontiers in Oncology*. Frontiers Media S.A. February 21, 2019, p 82. https://doi.org/10.3389/fonc.2019.00082.

[69] Ricci, M. S.; Zong, W. Chemotherapeutic Approaches for Targeting Cell Death Pathways. *Oncologist*, 2006, *11* (4), 342–357. https://doi.org/10.1634/theoncologist.11-4-342.

[70] Pfeffer, C. M.; Singh, A. T. K. Apoptosis: A Target for Anticancer Therapy. *International Journal of Molecular Sciences*. MDPI AG February 2, 2018. https://doi.org/10.3390/ijms19020448.

[71] Danial, N. N.; Korsmeyer, S. J. Cell Death: Critical Control Points. *Cell*. Cell Press January 23, 2004, pp 205–219. https://doi.org/10.1016/S0092-8674(04)00046-7.

[72] Galluzzi, L.; Vitale, I.; Aaronson, S. A.; Abrams, J. M.; Adam, D.; Agostinis, P.; Alnemri, E. S.; Altucci, L.; Amelio, I.; Andrews, D. W.; et al. Molecular Mechanisms of Cell Death: Recommendations of the Nomenclature Committee on Cell Death 2018. *Cell Death and Differentiation*. Nature Publishing Group March 1, 2018, pp 486–541. https://doi.org/10.1038/s41418-017-0012-4.

[73] Czabotar, P. E.; Lessene, G.; Strasser, A.; Adams, J. M. Control of Apoptosis by the BCL-2 Protein Family: Implications for Physiology and Therapy. *Nature Reviews Molecular Cell Biology*. Nature Publishing Group January 20, 2014, pp 49–63. https://doi.org/10.1038/nrm3722.

[74] Ren, D.; Tu, H. C.; Kim, H.; Wang, G. X.; Bean, G. R.; Takeuchi, O.; Jeffers, J. R.; Zambetti, G. P.; Hsieh, J. J. D.; Cheng, E. H. Y. BID, BIM, and PUMA Are Essential for Activation of the BAX- and BAK-Dependent Cell Death Program. *Science (80-.).*, 2010, *330* (6009), 1390–1393. https://doi.org/10.1126/science.1190217.

[75] Julien, O.; Wells, J. A. Caspases and Their Substrates. *Cell Death and Differentiation*. Nature Publishing Group August 1, 2017, pp 1380–1389. https://doi.org/10.1038/cdd.2017.44.

[76] Salvesen, G. S.; Duckett, C. S. IAP Proteins: Blocking the Road to Death's Door. *Nature Reviews Molecular Cell Biology*. Nat Rev Mol Cell Biol 2002, pp 401–410. https://doi.org/10.1038/nrm830.

[77] Huang, K.; Zhang, J.; O'Neill, K. L.; Gurumurthy, C. B.; Quadros, R. M.; Tu, Y.; Luo, X. Cleavage by Caspase 8 and Mitochondrial Membrane Association Activate the BH3-Only Protein Bid during TRAIL-Induced Apoptosis. *J. Biol. Chem.*, 2016, *291* (22), 11843–11851. https://doi.org/10.1074/jbc.M115.711051.

[78] Negulescu, A.; Mehlen, P. Dependence Receptors – the Dark Side Awakens. *FEBS J.*, 2018, *285* (21), 3909–3924. https://doi.org/10.1111/febs.14507.

[79] Goldschneider, D.; Mehlen, P. Dependence Receptors: A New Paradigm in Cell Signaling and Cancer Therapy. *Oncogene*. Oncogene April 2010, pp 1865–1882. https://doi.org/10.1038/onc.2010.13.

[80] Chen, L.; Zeng, Y.; Zhou, S.-F. Role of Apoptosis in Cancer Resistance to Chemotherapy. In *Current Understanding of Apoptosis - Programmed Cell Death*; InTech, 2018. https://doi.org/10.5772/intechopen.80056.

[81] Kale, J.; Osterlund, E. J.; Andrews, D. W. BCL-2 Family Proteins: Changing Partners in the Dance towards Death. *Cell Death and Differentiation*. Nature Publishing Group November 17, 2018, pp 65–80. https://doi.org/10.1038/cdd.2017.186.

[82] Werner, T. A.; Nolten, I.; Dizdar, L.; Riemer, J. C.; Schütte, S. C.; Verde, P. E.; Raba, K.; Schott, M.; Knoefel, W. T.; Krieg, A. IAPs Cause Resistance to TRAIL-Dependent Apoptosis in Follicular Thyroid Cancer. *Endocr. Relat. Cancer*, 2018, *25* (3), 295–308. https://doi.org/10.1530/ERC-17-0479.

[83] Weinberg, S. E.; Chandel, N. S. Targeting Mitochondria Metabolism for Cancer Therapy. *Nature Chemical Biology*. Nature Publishing Group January 1, 2015, pp 9–15. https://doi.org/10.1038/nchembio.1712.

[84] Grasso, D.; Zampieri, L. X.; Capelôa, T.; Van De Velde, J. A.; Sonveaux, P. Mitochondria in Cancer. *Cell Stress*. Shared Science Publishers OG June 1, 2020, pp 114–146. https://doi.org/10.15698/cst2020.06.221.

[85] Rumseys, W. L.; Schlossers, C.; Nuutinen$!, E. M.; Robiolios, M.; Wilsons, D. F. *Cellular Energetics and the Oxygen Dependence of Respiration in Cardiac Myocytes Isolated from Adult Rat**; Vol. 265.

[86] Engelman, J. A.; Chen, L.; Tan, X.; Crosby, K.; Guimaraes, A. R.; Upadhyay, R.; Maira, M.; McNamara, K.; Perera, S. A.; Song, Y.; et al. Effective Use of PI3K and MEK Inhibitors to Treat Mutant Kras G12D and PIK3CA H1047R Murine Lung Cancers. *Nat. Med.*, 2008, *14* (12), 1351–1356. https://doi.org/10.1038/nm.1890.

[87] Liu, Y.; Shi, Y. Mitochondria as a Target in Cancer Treatment. *MedComm*, 2020, *1* (2), 129–139. https://doi.org/10.1002/mco2.16.

[88] Zhang, X.; Fryknäs, M.; Hernlund, E.; Fayad, W.; De Milito, A.; Olofsson, M. H.; Gogvadze, V.; Dang, L.; Påhlman, S.; Schughart, L. A. K.; et al. Induction of Mitochondrial Dysfunction as a Strategy for Targeting Tumour Cells in Metabolically Compromised Microenvironments. *Nat. Commun.*, 2014, *5* (1), 1–14. https://doi.org/10.1038/ncomms4295.

[89] Carpenter, E. L.; Chagani, S.; Nelson, D.; Cassidy, P. B.; Laws, M.; Ganguli-Indra, G.; Indra, A. K. Mitochondrial Complex I Inhibitor Deguelin Induces Metabolic Reprogramming and Sensitizes Vemurafenib-Resistant BRAFV600E Mutation Bearing Metastatic Melanoma Cells. *Mol. Carcinog.*, 2019, *58* (9), 1680–1690. https://doi.org/10.1002/mc.23068.

[90] Anderson, N. M.; Mucka, P.; Kern, J. G.; Feng, H. The Emerging Role and Targetability of the TCA Cycle in Cancer Metabolism. *Protein and Cell*. Higher Education Press February 1, 2018, pp 216–237. https://doi.org/10.1007/s13238-017-0451-1.

[91] Wheaton, W. W.; Weinberg, S. E.; Hamanaka, R. B.; Soberanes, S.; Sullivan, L. B.; Anso, E.; Glasauer, A.; Dufour, E.; Mutlu, G. M.; Scott Budigner, G. R.; et al. Metformin Inhibits Mitochondrial Complex I of Cancer Cells to Reduce Tumorigenesis. *Elife*, 2014, *2014* (3). https://doi.org/10.7554/eLife.02242.

[92] Ippolito, L.; Giannoni, E.; Chiarugi, P.; Parri, M. Mitochondrial Redox Hubs as Promising Targets for Anticancer Therapy. *Frontiers in Oncology*. Frontiers Media S.A. February 28, 2020, p 256. https://doi.org/10.3389/fonc.2020.00256.

[93] Izzo, V.; Bravo-San Pedro, J. M.; Sica, V.; Kroemer, G.; Galluzzi, L. Mitochondrial Permeability Transition: New Findings and Persisting Uncertainties. *Trends in Cell Biology*. Elsevier Ltd September 1, 2016, pp 655–667. https://doi.org/10.1016/j.tcb.2016.04.006.

[94] Skulachev, V. P. Bioenergetic Aspects of Apoptosis, Necrosis and Mitoptosis. *Apoptosis*. March 2006, pp 473–485. https://doi.org/10.1007/s10495-006-5881-9.

[95] Kushnareva, Y.; Newmeyer, D. D. Bioenergetics and Cell Death. In *Annals of the New York Academy of Sciences*; Blackwell Publishing Inc., 2010; Vol. 1201, pp 50–57. https://doi.org/10.1111/j.1749-6632.2010.05633.x.

[96] Baines, C. P.; Kaiser, R. A.; Purcell, N. H.; Blair, N. S.; Osinska, H.; Hambleton, M. A.; Brunskill, E. W.; Sayen, M. R.; Gottlieb, R. A.; Dorn, G. W.; et al. Loss of Cyclophilin D Reveals a Critical Role for Mitochondrial Permeability Transition in Cell Death. *Nature*, 2005, *434* (7033), 658–662. https://doi.org/10.1038/nature03434.

[97] Karch, J.; Molkentin, J. D. Identifying the Components of the Elusive Mitochondrial Permeability Transition Pore. *Proceedings of the National Academy of Sciences of the United States of America*. National Academy of Sciences July 22, 2014, pp 10396–10397. https://doi.org/10.1073/pnas.1410104111.

[98] Giorgio, V.; Von Stockum, S.; Antoniel, M.; Fabbro, A.; Fogolari, F.; Forte, M.; Glick, G. D.; Petronilli, V.; Zoratti, M.; Szabó, I.; et al. Dimers of Mitochondrial ATP Synthase Form the Permeability Transition Pore. *Proc. Natl. Acad. Sci. U. S. A.*, 2013, *110* (15), 5887–5892. https://doi.org/10.1073/pnas.1217823110.

[99] Shimizu, S.; Narita, M.; Tsujimoto, Y. Bcl-2 Family Proteins Regulate the Release of Apoptogenic Cytochrome c by the Mitochondrial Channel VDAC. *Nature*, 1999, *399* (6735), 483–487. https://doi.org/10.1038/20959.

[100] Vaseva, A. V.; Marchenko, N. D.; Ji, K.; Tsirka, S. E.; Holzmann, S.; Moll, U. M. P53 Opens the Mitochondrial Permeability Transition Pore to Trigger Necrosis. *Cell*, 2012, *149* (7), 1536–1548. https://doi.org/10.1016/j.cell.2012.05.014.

[101] Xu, S.; Wang, P.; Zhang, H.; Gong, G.; Gutierrez Cortes, N.; Zhu, W.; Yoon, Y.; Tian, R.; Wang, W. CaMKII Induces Permeability Transition through Drp1 Phosphorylation during Chronic β-AR Stimulation. In *Nature Communications*; Nature Publishing Group, 2016; Vol. 7. https://doi.org/10.1038/ncomms13189.

[102] Antony, A. N.; Paillard, M.; Moffat, C.; Juskeviciute, E.; Correnti, J.; Bolon, B.; Rubin, E.; Csordás, G.; Seifert, E. L.; Hoek, J. B.; et al. MICU1 Regulation of Mitochondrial Ca 2+ Uptake Dictates Survival and Tissue Regeneration. *Nat. Commun.*, 2016, *7*. https://doi.org/10.1038/ncomms10955.

[103] Yu, L.; Chen, Y.; Tooze, S. A. Autophagy Pathway: Cellular and Molecular Mechanisms. *Autophagy*. Taylor and Francis Inc. February 1, 2018, pp 207–215. https://doi.org/10.1080/15548627.2017.1378838.

[104] Thorburn, A.; Thamm, D. H.; Gustafson, D. L. Autophagy and Cancer Therapy. *Molecular Pharmacology*. American Society for Pharmacology and Experimental Therapy 2014, pp 830–838. https://doi.org/10.1124/mol.114.091850.

[105] Amaravadi, R. K.; Kimmelman, A. C.; Debnath, J. Targeting Autophagy in Cancer: Recent Advances and Future Directions. *Cancer Discov.*, 2019, *9* (9), 1167–1181. https://doi.org/10.1158/2159-8290.CD-19-0292.

[106] Wong, P. M.; Puente, C.; Ganley, I. G.; Jiang, X. The ULK1 Complex Sensing Nutrient Signals for Autophagy Activation. *Autophagy*. Taylor and Francis Inc. 2013, pp 124–137. https://doi.org/10.4161/auto.23323.

[107] Zhao, Y. G.; Zhang, H. Formation and Maturation of Autophagosomes in Higher Eukaryotes: A Social Network. *Current Opinion in Cell Biology*. Elsevier Ltd August 1, 2018, pp 29–36. https://doi.org/10.1016/j.ceb.2018.04.003.

[108] Bento, C. F.; Renna, M.; Ghislat, G.; Puri, C.; Ashkenazi, A.; Vicinanza, M.; Menzies, F. M.; Rubinsztein, D. C. Mammalian Autophagy: How Does It Work? *Annu. Rev. Biochem.*, 2016, *85*, 685–713. https://doi.org/10.1146/annurev-biochem-060815-014556.

[109] Stolz, A.; Ernst, A.; Dikic, I. Cargo Recognition and Trafficking in Selective Autophagy. *Nature Cell Biology*. Nature Publishing Group 2014, pp 495–501. https://doi.org/10.1038/ncb2979.

[110] Nakatogawa, H.; Suzuki, K.; Kamada, Y.; Ohsumi, Y. Dynamics and Diversity in Autophagy Mechanisms: Lessons from Yeast. *Nature Reviews Molecular Cell Biology*. Nat Rev Mol Cell Biol July 2009, pp 458–467. https://doi.org/10.1038/nrm2708.

[111] Tilija Pun, N.; Jang, W. J.; Jeong, C. H. Role of Autophagy in Regulation of Cancer Cell Death/Apoptosis during Anti-Cancer Therapy: Focus on Autophagy Flux Blockade. *Archives of Pharmacal Research*. Pharmaceutical Society of Korea May 1, 2020, pp 475–488. https://doi.org/10.1007/s12272-020-01239-w.

[112] White, E. Deconvoluting the Context-Dependent Role for Autophagy in Cancer. *Nature Reviews Cancer*. Nat Rev Cancer June 2012, pp 401–410. https://doi.org/10.1038/nrc3262.

[113] Galluzzi, L.; Pietrocola, F.; Bravo-San Pedro, J. M.; Amaravadi, R. K.; Baehrecke, E. H.; Cecconi, F.; Codogno, P.; Debnath, J.; Gewirtz, D. A.; Karantza, V.; et al. Autophagy in Malignant Transformation and Cancer Progression. *EMBO J.*, 2015, *34* (7), 856–880. https://doi.org/10.15252/embj.201490784.

[114] White, E.; Mehnert, J. M.; Chan, C. S. Autophagy, Metabolism, and Cancer. *Clinical Cancer Research*. American Association for Cancer Research Inc. November 15, 2015, pp 5037–5046. https://doi.org/10.1158/1078-0432.CCR-15-0490.

[115] Davidson, S. M.; Vander Heiden, M. G. Critical Functions of the Lysosome in Cancer Biology. *Annu. Rev. Pharmacol. Toxicol.*, 2017, *57*, 481–507. https://doi.org/10.1146/annurev-pharmtox-010715-103101.

[116] Sui, X.; Chen, R.; Wang, Z.; Huang, Z.; Kong, N.; Zhang, M.; Han, W.; Lou, F.; Yang, J.; Zhang, Q.; et al. Autophagy and Chemotherapy Resistance: A Promising Therapeutic Target for Cancer Treatment. *Cell Death and Disease*. Nature Publishing Group October 2013, p e838. https://doi.org/10.1038/cddis.2013.350.

[117] Li, X.; Zhou, Y.; Li, Y.; Yang, L.; Ma, Y.; Peng, X.; Yang, S.; Liu, J.; Li, H. Autophagy: A Novel Mechanism of Chemoresistance in Cancers. *Biomedicine and Pharmacotherapy*. Elsevier Masson SAS November 1, 2019, p 109415. https://doi.org/10.1016/j.biopha.2019.109415.

[118] Pérez-Hernández, M.; Arias, A.; Martínez-García, D.; Pérez-Tomás, R.; Quesada, R.; Soto-Cerrato, V. Targeting Autophagy for Cancer Treatment and Tumor Chemosensitization. *Cancers*. MDPI AG October 1, 2019. https://doi.org/10.3390/cancers11101599.

[119] Chude, C. I.; Amaravadi, R. K. Targeting Autophagy in Cancer: Update on Clinical Trials and Novel Inhibitors. *International Journal of Molecular Sciences*. MDPI AG June 16, 2017. https://doi.org/10.3390/ijms18061279.

[120] Mulcahy Levy, J. M.; Thorburn, A. Autophagy in Cancer: Moving from Understanding

Mechanism to Improving Therapy Responses in Patients. *Cell Death and Differentiation*. Springer Nature March 1, 2020, pp 843–857. https://doi.org/10.1038/s41418-019-0474-7.

[121] Martin, K. R.; Celano, S. L.; Solitro, A. R.; Gunaydin, H.; Scott, M.; O'Hagan, R. C.; Shumway, S. D.; Fuller, P.; MacKeigan, J. P. A Potent and Selective ULK1 Inhibitor Suppresses Autophagy and Sensitizes Cancer Cells to Nutrient Stress. *iScience*, 2018, *8*, 74–84. https://doi.org/10.1016/j.isci.2018.09.012.

[122] Wilks, S. T. Potential of Overcoming Resistance to HER2-Targeted Therapies through the PI3K/Akt/MTOR Pathway. *Breast*. Churchill Livingstone 2015, pp 548–555. https://doi.org/10.1016/j.breast.2015.06.002.

[123] Ní Bhaoighill, M.; Dunlop, E. A. Mechanistic Target of Rapamycin Inhibitors: Successes and Challenges as Cancer Therapeutics. *Cancer Drug Resist.*, 2019, *2* (4), 1069–1085. https://doi.org/10.20517/cdr.2019.87.

[124] Chen, Y.; Lee, C. H.; Tseng, B. Y.; Tsai, Y. H.; Tsai, H. W.; Yao, C. L.; Tseng, S. H. AZD8055 Exerts Antitumor Effects on Colon Cancer Cells by Inhibiting MTOR and Cell-Cycle Progression. *Anticancer Res.*, 2018, *38* (3), 1445–1454. https://doi.org/10.21873/anticanres.12369.

[125] Levy, J. M. M.; Thorburn, A. Targeting Autophagy during Cancer Therapy to Improve Clinical Outcomes. *Pharmacology and Therapeutics*. Elsevier Inc. 2011, pp 130–141. https://doi.org/10.1016/j.pharmthera.2011.03.009.

[126] Tang, T.; Yang, Z. yu; Wang, D.; Yang, X. yan; Wang, J.; Li, L.; Wen, Q.; Gao, L.; Bian, X. wu; Yu, S. cang. The Role of Lysosomes in Cancer Development and Progression. *Cell and Bioscience*. BioMed Central Ltd December 1, 2020, pp 1–18. https://doi.org/10.1186/s13578-020-00489-x.

[127] Geisslinger, F.; Müller, M.; Vollmar, A. M.; Bartel, K. Targeting Lysosomes in Cancer as Promising Strategy to Overcome Chemoresistance—A Mini Review. *Front. Oncol.*, 2020, *10*, 1156. https://doi.org/10.3389/fonc.2020.01156.

[128] Commisso, C.; Davidson, S. M.; Soydaner-Azeloglu, R. G.; Parker, S. J.; Kamphorst, J. J.; Hackett, S.; Grabocka, E.; Nofal, M.; Drebin, J. A.; Thompson, C. B.; et al. Macropinocytosis of Protein Is an Amino Acid Supply Route in Ras-Transformed Cells. *Nature*, 2013, *497* (7451), 633–637. https://doi.org/10.1038/nature12138.

[129] Carroll, B.; Dunlop, E. A. The Lysosome: A Crucial Hub for AMPK and MTORC1 Signalling. *Biochemical Journal*. Portland Press Ltd May 1, 2017, pp 1453–1466. https://doi.org/10.1042/BCJ20160780.

[130] Chourasia, A. H.; Boland, M. L.; Macleod, K. F. Mitophagy and Cancer. *Cancer and Metabolism*. BioMed Central Ltd. March 26, 2015, p 4. https://doi.org/10.1186/s40170-015-0130-8.

[131] Okamoto, K. Organellophagy: Eliminating Cellular Building Blocks via Selective Autophagy. *Journal of Cell Biology*. Rockefeller University Press 2014, pp 435–445. https://doi.org/10.1083/jcb.201402054.

[132] Machado, E.; White-Gilbertson, S.; Van De Vlekkert, D.; Janke, L.; Moshiach, S.; Campos, Y.; Finkelstein, D.; Gomero, E.; Mosca, R.; Qiu, X.; et al. Regulated Lysosomal Exocytosis Mediates Cancer Progression. *Sci. Adv.*, 2015, *1* (11), e1500603. https://doi.org/10.1126/sciadv.1500603.

[133] Serrano-Puebla, A.; Boya, P. Lysosomal Membrane Permeabilization as a Cell Death Mechanism in Cancer Cells. *Biochemical Society Transactions*. Portland Press Ltd April 17, 2018, pp 207–215. https://doi.org/10.1042/BST20170130.

[134] Wang, F.; Gómez-Sintes, R.; Boya, P. Lysosomal Membrane Permeabilization and Cell Death. *Traffic*. Blackwell Munksgaard December 1, 2018, pp 918–931. https://doi.org/10.1111/tra.12613.

[135] Aits, S.; Jäättelä, M. Lysosomal Cell Death at a Glance. *J. Cell Sci.*, 2013, *126* (9), 1905–1912. https://doi.org/10.1242/jcs.091181.

[136] Huai, J.; Vogtle, F. N.; Jocke, L.; Li, Y.; Kiefer, T.; Ricci, J. E.; Borner, C. TNFα-Induced Lysosomal Membrane Permeability Is Downstream of MOMP and Triggered by Caspasemediated NDUFS1 Cleavage and ROS Formation. *J. Cell Sci.*, 2013, *126* (17), 4015–4025. https://doi.org/10.1242/jcs.129999.

[137] Karch, J.; Schips, T. G.; Maliken, B. D.; Brody, M. J.; Sargent, M. A.; Kanisciak, O.; Molkentin, J. D. Autophagic Cell Death Is Dependent on Lysosomal Membrane Permeability through Bax and Bak. *Elife*, 2017, *6*. https://doi.org/10.7554/eLife.30543.

[138] Wang, F.; Salvati, A.; Boya, P. Lysosome-Dependent Cell Death and Deregulated Autophagy Induced by Amine-Modified Polystyrene Nanoparticles. *Open Biol.*, 2018, *4* (8). https://doi.org/10.1098/rsob.170271.

[139] Oberle, C.; Huai, J.; Reinheckel, T.; Tacke, M.; Rassner, M.; Ekert, P. G.; Buellesbach, J.; Borner, C. Lysosomal Membrane Permeabilization and Cathepsin Release Is a Bax/Bak-Dependent, Amplifying Event of Apoptosis in Fibroblasts and Monocytes. *Cell Death Differ.*, 2010, *17* (7), 1167–1178. https://doi.org/10.1038/cdd.2009.214.

[140] Boya, P.; Gonzalez-Polo, R. A.; Poncet, D.; Andreau, K.; Vieira, H. L. A.; Roumier, T.; Perfettini, J. L.; Kroemer, G. Mitochondrial Membrane Permeabilization Is a Critical Step of Lysosome-Initiated Apoptosis Induced by Hydroxychloroquine. *Oncogene*, 2003, *22* (25), 3927–3936. https://doi.org/10.1038/sj.onc.1206622.

[141] Kurz, T.; Terman, A.; Gustafsson, B.; Brunk, U. T. Lysosomes and Oxidative Stress in Aging and Apoptosis. *Biochimica et Biophysica Acta - General Subjects*. Biochim Biophys Acta November 2008, pp 1291–1303. https://doi.org/10.1016/j.bbagen.2008.01.009.

[142] Sumoza-Toledo, A.; Penner, R. TRPM2: A Multifunctional Ion Channel for Calcium Signalling. *Journal of Physiology*. J Physiol April 2011, pp 1515–1525. https://doi.org/10.1113/jphysiol.2010.201855.

[143] Gómez-Sintes, R.; Ledesma, M. D.; Boya, P. Lysosomal Cell Death Mechanisms in Aging. *Ageing Research Reviews*. Elsevier Ireland Ltd December 1, 2016, pp 150–168. https://doi.org/10.1016/j.arr.2016.02.009.

[144] Wang, F.; Gómez-Sintes, R.; Boya, P. Lysosomal Membrane Permeabilization and Cell Death. *Traffic*. Blackwell Munksgaard December 1, 2018, pp 918–931. https://doi.org/10.1111/tra.12613.

[145] Domagala, A.; Fidyt, K.; Bobrowicz, M.; Stachura, J.; Szczygiel, K.; Firczuk, M. Typical and Atypical Inducers of Lysosomal Cell Death: A Promising Anticancer Strategy. *International Journal of Molecular Sciences*. MDPI AG August 1, 2018. https://doi.org/10.3390/ijms19082256.

[146] Groth-Pedersen, L.; Jäättelä, M. Combating Apoptosis and Multidrug Resistant Cancers by

Targeting Lysosomes. *Cancer Letters*. Elsevier Ireland Ltd May 28, 2013, pp 265–274. https://doi.org/10.1016/j.canlet.2010.05.021.

[147] Gyparaki, M. T.; Papavassiliou, A. G. Lysosome: The Cell's "suicidal Bag" as a Promising Cancer Target. *Trends in Molecular Medicine*. Elsevier Ltd 2014, pp 239–241. https://doi.org/10.1016/j.molmed.2014.01.009.

[148] Bi, K.; Nishihara, K.; Machleidt, T.; Hermanson, S.; Wang, J.; Sakamuru, S.; Huang, R.; Xia, M. Identification of Known Drugs Targeting the Endoplasmic Reticulum Stress Response. *Anal. Bioanal. Chem.*, 2015, *407* (18), 5343–5351. https://doi.org/10.1007/s00216-015-8694-2.

[149] Hetz, C. The Unfolded Protein Response: Controlling Cell Fate Decisions under ER Stress and Beyond. *Nature Reviews Molecular Cell Biology*. Nature Publishing Group February 18, 2012, pp 89–102. https://doi.org/10.1038/nrm3270.

[150] Luo, B.; Lee, A. S. The Critical Roles of Endoplasmic Reticulum Chaperones and Unfolded Protein Response in Tumorigenesis and Anticancer Therapies. *Oncogene*. Oncogene February 14, 2013, pp 805–818. https://doi.org/10.1038/onc.2012.130.

[151] Wang, M.; Kaufman, R. J. The Impact of the Endoplasmic Reticulum Protein-Folding Environment on Cancer Development. *Nature Reviews Cancer*. Nature Publishing Group 2014, pp 581–597. https://doi.org/10.1038/nrc3800.

[152] Verfaillie, T.; Garg, A. D.; Agostinis, P. Targeting ER Stress Induced Apoptosis and Inflammation in Cancer. *Cancer Letters*. Elsevier Ireland Ltd May 28, 2013, pp 249–264. https://doi.org/10.1016/j.canlet.2010.07.016.

[153] Bhat, T. A.; Chaudhary, A. K.; Kumar, S.; O'Malley, J.; Inigo, J. R.; Kumar, R.; Yadav, N.; Chandra, D. Endoplasmic Reticulum-Mediated Unfolded Protein Response and Mitochondrial Apoptosis in Cancer. *Biochimica et Biophysica Acta - Reviews on Cancer*. Elsevier B.V. January 1, 2017, pp 58–66. https://doi.org/10.1016/j.bbcan.2016.12.002.

[154] Maas, N. L.; Diehl, J. A. Molecular Pathways: The Perks and Pitfalls of Targeting the Unfolded Protein Response in Cancer. *Clin. Cancer Res.*, 2015, *21* (4), 675–679. https://doi.org/10.1158/1078-0432.CCR-13-3239.

[155] Wang, Q.; Mora-Jensen, H.; Weniger, M. A.; Perez-Galan, P.; Wolford, C.; Hai, T.; Ron, D.; Chen, W.; Trenkle, W.; Wiestner, A.; et al. ERAD Inhibitors Integrate ER Stress with an Epigenetic Mechanism to Activate BH3-Only Protein NOXA in Cancer Cells. *Proc. Natl. Acad. Sci. U. S. A.*, 2009, *106* (7), 2200–2205. https://doi.org/10.1073/pnas.0807611106.

[156] Lee, A.-H.; Iwakoshi, N. N.; Glimcher, L. H. XBP-1 Regulates a Subset of Endoplasmic Reticulum Resident Chaperone Genes in the Unfolded Protein Response. *Mol. Cell. Biol.*, 2003, *23* (21), 7448–7459. https://doi.org/10.1128/mcb.23.21.7448-7459.2003.

[157] Liu, Y.; Adachi, M.; Zhao, S.; Hareyama, M.; Koong, A. C.; Luo, D.; Rando, T. A.; Imai, K.; Shinomura, Y. Preventing Oxidative Stress: A New Role for XBP1. *Cell Death Differ.*, 2009, *16* (6), 847–857. https://doi.org/10.1038/cdd.2009.14.

[158] Yamamoto, K.; Sato, T.; Matsui, T.; Sato, M.; Okada, T.; Yoshida, H.; Harada, A.; Mori, K. Transcriptional Induction of Mammalian ER Quality Control Proteins Is Mediated by Single or Combined Action of ATF6α and XBP1. *Dev. Cell*, 2007, *13* (3), 365–376. https://doi.org/10.1016/j.devcel.2007.07.018.

[159] Urra, H.; Dufey, E.; Avril, T.; Chevet, E.; Hetz, C. Endoplasmic Reticulum Stress and the

Hallmarks of Cancer. *Trends in Cancer*. Cell Press May 1, 2016, pp 252–262. https://doi.org/10.1016/j.trecan.2016.03.007.

[160] Ferri, K. F.; Kroemer, G. Organelle-Specific Initiation of Cell Death Pathways. *Nature Cell Biology*. Nat Cell Biol 2001. https://doi.org/10.1038/ncb1101-e255.

[161] Sano, R.; Reed, J. C. ER Stress-Induced Cell Death Mechanisms. *Biochimica et Biophysica Acta - Molecular Cell Research*. Elsevier December 1, 2013, pp 3460–3470. https://doi.org/10.1016/j.bbamcr.2013.06.028.

[162] Kara, M.; Oztas, E. Endoplasmic Reticulum Stress-Mediated Cell Death. In *Programmed Cell Death*; IntechOpen, 2020. https://doi.org/10.5772/intechopen.85401.

[163] Li, G.; Mongillo, M.; Chin, K. T.; Harding, H.; Ron, D.; Marks, A. R.; Tabas, I. Role of ERO1-α-Mediated Stimulation of Inositol 1,4,5-Triphosphate Receptor Activity in Endoplasmic Reticulum Stress-Induced Apoptosis. *J. Cell Biol.*, 2009, *186* (6), 783–792. https://doi.org/10.1083/jcb.200904060.

[164] Krebs, J.; Agellon, L. B.; Michalak, M. Ca2+ Homeostasis and Endoplasmic Reticulum (ER) Stress: An Integrated View of Calcium Signaling. *Biochemical and Biophysical Research Communications*. Academic Press Inc. May 19, 2015, pp 114–121. https://doi.org/10.1016/j.bbrc.2015.02.004.

[165] Bahar, E.; Kim, H.; Yoon, H. ER Stress-Mediated Signaling: Action Potential and Ca2+ as Key Players. *International Journal of Molecular Sciences*. MDPI AG September 15, 2016. https://doi.org/10.3390/ijms17091558.

[166] Rizzuto, R.; Pinton, P.; Carrington, W.; Fay, F. S.; Fogarty, K. E.; Lifshitz, L. M.; Tuft, R. A.; Pozzan, T. Close Contacts with the Endoplasmic Reticulum as Determinants of Mitochondrial Ca2+ Responses. *Science (80-.).*, 1998, *280* (5370), 1763–1766. https://doi.org/10.1126/science.280.5370.1763.

[167] Scorrano, L.; Oakes, S. A.; Opferman, J. T.; Cheng, E. H.; Sorcinelli, M. D.; Pozzan, T.; Korsmeyer, S. J. BAX and BAK Regulation of Endoplasmic Reticulum Ca2+: A Control Point for Apoptosis. *Science (80-.).*, 2003, *300* (5616), 135–139. https://doi.org/10.1126/science.1081208.

[168] Varadarajan, S.; Bampton, E. T. W.; Smalley, J. L.; Tanaka, K.; Caves, R. E.; Butterworth, M.; Wei, J.; Pellecchia, M.; Mitcheson, J.; Gant, T. W.; et al. A Novel Cellular Stress Response Characterised by a Rapid Reorganisation of Membranes of the Endoplasmic Reticulum. *Cell Death Differ.*, 2012, *19* (12), 1896–1907. https://doi.org/10.1038/cdd.2012.108.

[169] Patergnani, S.; Danese, A.; Bouhamida, E.; Aguiari, G.; Previati, M.; Pinton, P.; Giorgi, C. Various Aspects of Calcium Signaling in the Regulation of Apoptosis, Autophagy, Cell Proliferation, and Cancer. *International Journal of Molecular Sciences*. MDPI AG November 1, 2020, pp 1–27. https://doi.org/10.3390/ijms21218323.

[170] Stewart, T. A.; Yapa, K. T. D. S.; Monteith, G. R. Altered Calcium Signaling in Cancer Cells. *Biochimica et Biophysica Acta - Biomembranes*. Elsevier B.V. October 10, 2015, pp 2502–2511. https://doi.org/10.1016/j.bbamem.2014.08.016.

[171] Berridge, M. J.; Bootman, M. D.; Roderick, H. L. Calcium Signalling: Dynamics, Homeostasis and Remodelling. *Nature Reviews Molecular Cell Biology*. July 1, 2003, pp 517–529. https://doi.org/10.1038/nrm1155.

[172] Bong, A. H. L.; Monteith, G. R. Calcium Signaling and the Therapeutic Targeting of Cancer

Cells. *Biochimica et Biophysica Acta - Molecular Cell Research*. Elsevier B.V. November 1, 2018, pp 1786–1794. https://doi.org/10.1016/j.bbamcr.2018.05.015.

[173] Prevarskaya, N.; Ouadid-Ahidouch, H.; Skryma, R.; Shuba, Y. Remodelling of Ca2+ Transport in Cancer: How It Contributes to Cancer Hallmarks? *Philosophical Transactions of the Royal Society B: Biological Sciences*. Royal Society March 19, 2014. https://doi.org/10.1098/rstb.2013.0097.

[174] Roderick, H. L.; Cook, S. J. Ca2+ Signalling Checkpoints in Cancer: Remodelling Ca 2+ for Cancer Cell Proliferation and Survival. *Nature Reviews Cancer*. Nat Rev Cancer May 2008, pp 361–375. https://doi.org/10.1038/nrc2374.

[175] Varghese, E.; Samuel, S. M.; Sadiq, Z.; Kubatka, P.; Liskova, A.; Benacka, J.; Pazinka, P.; Kruzliak, P.; Büsselberg, D. Anti-Cancer Agents in Proliferation and Cell Death: The Calcium Connection. *Int. J. Mol. Sci.*, 2019, *20* (12), 3017. https://doi.org/10.3390/ijms20123017.

[176] Cui, C.; Merritt, R.; Fu, L.; Pan, Z. Targeting Calcium Signaling in Cancer Therapy. *Acta Pharmaceutica Sinica B*. Chinese Academy of Medical Sciences January 1, 2017, pp 3–17. https://doi.org/10.1016/j.apsb.2016.11.001.

[177] Paul, S. M.; Mytelka, D. S.; Dunwiddie, C. T.; Persinger, C. C.; Munos, B. H.; Lindborg, S. R.; Schacht, A. L. How to Improve RD Productivity: The Pharmaceutical Industry's Grand Challenge. *Nature Reviews Drug Discovery*. Nature Publishing Group March 19, 2010, pp 203–214. https://doi.org/10.1038/nrd3078.

[178] Adams, C. P.; Van Brantner, V. Market Watch : Estimating the Cost of New Drug Development: Is It Really $802 Million? *Health Affairs*. Health Aff (Millwood) March 2006, pp 420–428. https://doi.org/10.1377/hlthaff.25.2.420.

[179] Hay, M.; Thomas, D. W.; Craighead, J. L.; Economides, C.; Rosenthal, J. Clinical Development Success Rates for Investigational Drugs. *Nat. Biotechnol.*, 2014, *32* (1), 40–51. https://doi.org/10.1038/nbt.2786.

[180] Kola, I.; Landis, J. Can the Pharmaceutical Industry Reduce Attrition Rates? *Nat. Rev. Drug Discov.*, 2004, *3* (8), 711–715. https://doi.org/10.1038/nrd1470.

[181] Waring, M. J.; Arrowsmith, J.; Leach, A. R.; Leeson, P. D.; Mandrell, S.; Owen, R. M.; Pairaudeau, G.; Pennie, W. D.; Pickett, S. D.; Wang, J.; et al. An Analysis of the Attrition of Drug Candidates from Four Major Pharmaceutical Companies. *Nature Reviews Drug Discovery*. Nature Publishing Group July 2, 2015, pp 475–486. https://doi.org/10.1038/nrd4609.

[182] Mullard, A. Parsing Clinical Success Rates. *Nat. Rev. Drug Discov.*, 2016, *15* (7), 447. https://doi.org/10.1038/nrd.2016.136.

[183] Wilking, N.; Lopes, G.; Meier, K.; Simoens, S.; van Harten, W.; Vulto, A. Can We Continue to Afford Access to Cancer Treatment? *Eur. Oncol. Haematol.*, 2017, *13* (02), 114. https://doi.org/10.17925/eoh.2017.13.02.114.

[184] Sleire, L.; Førde-Tislevoll, H. E.; Netland, I. A.; Leiss, L.; Skeie, B. S.; Enger, P. Ø. Drug Repurposing in Cancer. *Pharmacological Research*. Academic Press October 1, 2017, pp 74–91. https://doi.org/10.1016/j.phrs.2017.07.013.

[185] Drew, D. A.; Chin, S. M.; Gilpin, K. K.; Parziale, M.; Pond, E.; Schuck, M. M.; Stewart, K.; Flagg, M.; Rawlings, C. A.; Backman, V.; et al. ASPirin Intervention for the REDuction of Colorectal Cancer Risk (ASPIRED): A Study Protocol for a Randomized Controlled Trial.

Trials, 2017, *18* (1). https://doi.org/10.1186/s13063-016-1744-z.

[186] Di Bello, E.; Zwergel, C.; Mai, A.; Valente, S. The Innovative Potential of Statins in Cancer: New Targets for New Therapies. *Front. Chem.*, 2020, *8*, 516. https://doi.org/10.3389/fchem.2020.00516.

[187] Miranda, V. C.; Braghiroli, M. I.; Faria, L. D.; Bariani, G.; Alex, A.; Bezerra Neto, J. E.; Capareli, F. C.; Sabbaga, J.; Lobo dos Santos, J. F.; Hoff, P. M.; et al. Phase 2 Trial of Metformin Combined With 5-Fluorouracil in Patients With Refractory Metastatic Colorectal Cancer. *Clin. Colorectal Cancer*, 2016, *15* (4), 321-328.e1. https://doi.org/10.1016/j.clcc.2016.04.011.

[188] Soria-Castro, R.; Schcolnik-Cabrera, A.; Rodríguez-López, G.; Campillo-Navarro, M.; Puebla-Osorio, N.; Estrada-Parra, S.; Estrada-García, I.; Chacón-Salinas, R.; Chávez-Blanco, A. D. Exploring the Drug Repurposing Versatility of Valproic Acid as a Multifunctional Regulator of Innate and Adaptive Immune Cells. *Journal of Immunology Research*. Hindawi Limited 2019. https://doi.org/10.1155/2019/9678098.

[189] Huang, J.; Zhao, D.; Liu, Z.; Liu, F. Repurposing Psychiatric Drugs as Anti-Cancer Agents. *Cancer Letters*. Elsevier Ireland Ltd April 10, 2018, pp 257–265. https://doi.org/10.1016/j.canlet.2018.01.058.

[190] Grinshpoon, A.; Barchana, M.; Ponizovsky, A.; Lipshitz, I.; Nahon, D.; Tal, O.; Weizman, A.; Levav, I. Cancer in Schizophrenia: Is the Risk Higher or Lower? *Schizophr. Res.*, 2005, *73* (2–3), 333–341. https://doi.org/10.1016/j.schres.2004.06.016.

[191] Li, H.; Li, J.; Yu, X.; Zheng, H.; Sun, X.; Lu, Y.; Zhang, Y.; Li, C.; Bi, X. The Incidence Rate of Cancer in Patients with Schizophrenia: A Meta-Analysis of Cohort Studies. *Schizophrenia Research*. Elsevier B.V. May 1, 2018, pp 519–528. https://doi.org/10.1016/j.schres.2017.08.065.

[192] Mortensen, P. B. The Incidence of Cancer in Schizophrenic Patients. *J. Epidemiol. Community Health*, 1989, *43* (1), 43–47. https://doi.org/10.1136/jech.43.1.43.

[193] Catts, V. S.; Catts, S. V. Apoptosis and Schizophrenia: Is the Tumour Suppressor Gene, P53, a Candidate Susceptibility Gene? *Schizophr. Res.*, 2000, *41* (3), 405–415. https://doi.org/10.1016/S0920-9964(99)00077-8.

[194] Dalton, S. O.; Mellemkjær, L.; Thomassen, L.; Mortensen, P. B.; Johansen, C. Risk for Cancer in a Cohort of Patients Hospitalized for Schizophrenia in Denmark, 1969-1993. *Schizophr. Res.*, 2005, *75* (2–3), 315–324. https://doi.org/10.1016/j.schres.2004.11.009.

[195] Raviv, G.; Laufer, M.; Baruch, Y.; Barak, Y. Risk of Prostate Cancer in Patients with Schizophrenia. *Compr. Psychiatry*, 2014, *55* (7), 1639–1642. https://doi.org/10.1016/j.comppsych.2014.05.007.

[196] Dalton, S. O.; Johansen, C.; Poulsen, A. H.; Nørgaard, M.; Sørensen, H. T.; McLaughlin, J. K.; Mortensen, P. B.; Friis, S. Cancer Risk among Users of Neuroleptic Medication: A Population-Based Cohort Study. *Br. J. Cancer*, 2006, *95* (7), 934–939. https://doi.org/10.1038/sj.bjc.6603259.

[197] Mortensen, P. B. Neuroleptic Medication and Reduced Risk of Prostate Cancer in Schizophrenic Patients. *Acta Psychiatr. Scand.*, 1992, *85* (5), 390–393. https://doi.org/10.1111/j.1600-0447.1992.tb10325.x.

[198] Shin, S. Y.; Lee, K. S.; Choi, Y. K.; Lim, H. J.; Lee, H. G.; Lim, Y.; Lee, Y. H. The

Antipsychotic Agent Chlorpromazine Induces Autophagic Cell Death by Inhibiting the Akt/Mtor Pathway in Human U-87MG Glioma Cells. *Carcinogenesis*, 2013, *34* (9), 2080–2089. https://doi.org/10.1093/carcin/bgt169.

[199] Shin, S. Y.; Kim, C. G.; Kim, S. H.; Kim, Y. S.; Lim, Y.; Lee, Y. H. Chlorpromazine Activates P2iWaf1/Cip1 Gene Transcription via Early Growth Response-1 (Egr-1) in C6 Glioma Cells. *Exp. Mol. Med.*, 2010, *42* (5), 395–405. https://doi.org/10.3858/emm.2010.42.5.041.

[200] Lee, W. Y.; Lee, W. T.; Cheng, C. H.; Chen, K. C.; Chou, C. M.; Chung, C. H.; Sun, M. S.; Cheng, H. W.; Ho, M. N.; Lin, C. W. Repositioning Antipsychotic Chlorpromazine for Treating Colorectal Cancer by Inhibiting Sirtuin 1. *Oncotarget*, 2015, *6* (29), 27580–27595. https://doi.org/10.18632/oncotarget.4768.

[201] Ranjan, A.; Srivastava, S. K. Penfluridol Suppresses Pancreatic Tumor Growth by Autophagy-Mediated Apoptosis. *Sci. Rep.*, 2016, *6*. https://doi.org/10.1038/srep26165.

[202] Gonçalves, J. M.; Silva, C. A. B.; Rivero, E. R. C.; Cordeiro, M. M. R. Inhibition of Cancer Stem Cells Promoted by Pimozide. *Clin. Exp. Pharmacol. Physiol.*, 2019, *46* (2), 116–125. https://doi.org/10.1111/1440-1681.13049.

[203] Takebe, N.; Harris, P. J.; Warren, R. Q.; Ivy, S. P. Targeting Cancer Stem Cells by Inhibiting Wnt, Notch, and Hedgehog Pathways. *Nature Reviews Clinical Oncology*. Nat Rev Clin Oncol February 2011, pp 97–106. https://doi.org/10.1038/nrclinonc.2010.196.

[204] Velnati, S.; Massarotti, A.; Antona, A.; Talmon, M.; Fresu, L. G.; Galetto, A. S.; Capello, D.; Bertoni, A.; Mercalli, V.; Graziani, A.; et al. Structure Activity Relationship Studies on Amb639752: Toward the Identification of a Common Pharmacophoric Structure for DGKalpha Inhibitors. *J. Enzyme Inhib. Med. Chem.*, 2020, *35* (1), 96–108. https://doi.org/10.1080/14756366.2019.1684911.

[205] Muehlbacher, M.; Tripal, P.; Roas, F.; Kornhuber, J. Identification of Drugs Inducing Phospholipidosis by Novel in Vitro Data. *ChemMedChem*, 2012, *7* (11), 1925–1934. https://doi.org/10.1002/cmdc.201200306.

[206] Livak, K. J.; Schmittgen, T. D. Analysis of Relative Gene Expression Data Using Real-Time Quantitative PCR and the 2-ΔΔCT Method. *Methods*, 2001, *25* (4), 402–408. https://doi.org/10.1006/meth.2001.1262.

[207] Ostad Haji, E.; Hiemke, C.; Pfuhlmann, B. Therapeutic Drug Monitoring for Antidepressant Drug Treatment. *Curr. Pharm. Des.*, 2012, *18* (36), 5818–5827. https://doi.org/10.2174/138161212803523699.

[208] Church, M. K.; Church, D. S. Pharmacology of Antihistamines. In *Indian Journal of Dermatology*; 2013; Vol. 58, pp 219–224. https://doi.org/10.4103/0019-5154.110832.

[209] Medina, V. A.; Rivera, E. S. Histamine Receptors and Cancer Pharmacology. *British Journal of Pharmacology*. October 2010, pp 755–767. https://doi.org/10.1111/j.1476-5381.2010.00961.x.

[210] Sarrouilhe, D.; Clarhaut, J.; Defamie, N.; Mesnil, M. Serotonin and Cancer: What Is the Link? *Curr. Mol. Med.*, 2015, *15* (1), 62–77. https://doi.org/10.2174/1566524015666150114113411.

[211] Sarrouilhe, D.; Mesnil, M. Serotonin and Human Cancer: A Critical View. *Biochimie*. Elsevier B.V. June 1, 2019, pp 46–50. https://doi.org/10.1016/j.biochi.2018.06.016.

[212] Reasor, M. J.; Hastings, K. L.; Ulrich, R. G. Drug-Induced Phospholipidosis: Issues and Future Directions. *Expert Opinion on Drug Safety*. July 2006, pp 567–583.

https://doi.org/10.1517/14740338.5.4.567.

[213] Halliwell, W. H. Cationic Amphiphilic Drug-Induced Phospholipidosis. In *Toxicologic Pathology*; SAGE Publications Inc., 1997; Vol. 25, pp 53–60. https://doi.org/10.1177/019262339702500111.

[214] Kornhuber, J.; Tripal, P.; Reichel, M.; Mühle, C.; Rhein, C.; Muehlbacher, M.; Groemer, T. W.; Gulbins, E. Functional Inhibitors of Acid Sphingomyelinase (FIASMAS): A Novel Pharmacological Group of Drugs with Broad Clinical Applications. *Cellular Physiology and Biochemistry*. Cell Physiol Biochem Press 2010, pp 9–20. https://doi.org/10.1159/000315101.

[215] Vater, M.; Möckl, L.; Gormanns, V.; Schultz Fademrecht, C.; Mallmann, A. M.; Ziegart-Sadowska, K.; Zaba, M.; Frevert, M. L.; Bräuchle, C.; Holsboer, F.; et al. New Insights into the Intracellular Distribution Pattern of Cationic Amphiphilic Drugs. *Sci. Rep.*, 2017, *7*. https://doi.org/10.1038/srep44277.

[216] Marceau, F.; Bawolak, M. T.; Lodge, R.; Bouthillier, J.; Gagné-Henley, A.; C.-Gaudreault, R.; Morissette, G. Cation Trapping by Cellular Acidic Compartments: Beyond the Concept of Lysosomotropic Drugs. *Toxicology and Applied Pharmacology*. February 15, 2012, pp 1–12. https://doi.org/10.1016/j.taap.2011.12.004.

[217] Lu, S.; Sung, T.; Lin, N.; Abraham, R. T.; Jessen, B. A. Lysosomal Adaptation: How Cells Respond to Lysosomotropic Compounds. *PLoS One*, 2017, *12* (3). https://doi.org/10.1371/journal.pone.0173771.

[218] Caccia, S.; Garattini, S. Formation of Active Metabolites of Psychotropic Drugs: An Updated Review of Their Significance. *Clin. Pharmacokinet.*, 1990, *18* (6), 434–459. https://doi.org/10.2165/00003088-199018060-00002.

[219] Sivandzade, F.; Bhalerao, A.; Cucullo, L. Analysis of the Mitochondrial Membrane Potential Using the Cationic JC-1 Dye as a Sensitive Fluorescent Probe. *BIO-PROTOCOL*, 2019, *9* (1). https://doi.org/10.21769/bioprotoc.3128.

[220] De Duve, C.; De Barsy, T.; Poole, B.; Trouet, A.; Tulkens, P.; Van Hoof, F. Lysosomotropic Agents. *Biochemical Pharmacology*. September 15, 1974. https://doi.org/10.1016/0006-2952(74)90174-9.

[221] Rodriguez-Enriquez, S.; Kim, I.; Currin, R. T.; Lemasters, J. J. Tracker Dyes to Probe Mitochondrial Autophagy (Mitophagy) in Rat Hepatocytes. *Autophagy*, 2006, *2* (1), 39–46. https://doi.org/10.4161/auto.2229.

[222] Biever, A.; Valjent, E.; Puighermanal, E. Ribosomal Protein S6 Phosphorylation in the Nervous System: From Regulation to Function. *Front. Mol. Neurosci.*, 2015, *8* (DEC). https://doi.org/10.3389/fnmol.2015.00075.

[223] Mizushima, N.; Yoshimori, T.; Levine, B. Methods in Mammalian Autophagy Research. *Cell*. February 5, 2010, pp 313–326. https://doi.org/10.1016/j.cell.2010.01.028.

[224] Goldman, S. D. B.; Funk, R. S.; Rajewski, R. A.; Krise, J. P. Mechanisms of Amine Accumulation in, and Egress from, Lysosomes. *Bioanalysis*. Future Science Ltd 2009, pp 1445–1459. https://doi.org/10.4155/BIO.09.128.

[225] Kornhuber, J.; Tripal, P.; Reichel, M.; Terfloth, L.; Bleich, S.; Wiltfang, J.; Gulbins, E. Identification of New Functional Inhibitors of Acid Sphingomyelinase Using a Structure-Property-Activity Relation Model. *J. Med. Chem.*, 2008, *51* (2), 219–237. https://doi.org/10.1021/jm070524a.

[226] Anderson, N.; Borlak, J. Drug-Induced Phospholipidosis. *FEBS Letters*. October 9, 2006, pp 5533–5540. https://doi.org/10.1016/j.febslet.2006.08.061.

[227] Aits, S.; Kricker, J.; Liu, B.; Ellegaard, A. M.; Hämälistö, S.; Tvingsholm, S.; Corcelle-Termeau, E.; Høgh, S.; Farkas, T.; Jonassen, A. H.; et al. Sensitive Detection of Lysosomal Membrane Permeabilization by Lysosomal Galectin Puncta Assay. *Autophagy*, 2015, *11* (8), 1408–1424. https://doi.org/10.1080/15548627.2015.1063871.

[228] Wu, Y. T.; Tan, H. L.; Shui, G.; Bauvy, C.; Huang, Q.; Wenk, M. R.; Ong, C. N.; Codogno, P.; Shen, H. M. Dual Role of 3-Methyladenine in Modulation of Autophagy via Different Temporal Patterns of Inhibition on Class I and III Phosphoinositide 3-Kinase. *J. Biol. Chem.*, 2010, *285* (14), 10850–10861. https://doi.org/10.1074/jbc.M109.080796.

[229] Montaser, M.; Lalmanach, G.; Mach, L. CA-074, but Not Its Methyl Ester CA-074Me, Is a Selective Inhibitor of Cathepsin B within Living Cells. *Biol. Chem.*, 2002, *383* (7–8), 1305–1308. https://doi.org/10.1515/BC.2002.147.

[230] Qadir, M.; O'Loughlin, K. L.; Fricke, S. M.; Williamson, N. A.; Greco, W. R.; Minderman, H.; Baer, M. R. Cyclosporin A Is a Broad-Spectrum Multidrug Resistance Modulator. *Clin. Cancer Res.*, 2005, *11* (6), 2320–2326. https://doi.org/10.1158/1078-0432.CCR-04-1725.

[231] Varalda, M.; Antona, A.; Bettio, V.; Roy, K.; Vachamaram, A.; Yellenki, V.; Massarotti, A.; Baldanzi, G.; Capello, D. Psychotropic Drugs Show Anticancer Activity by Disrupting Mitochondrial and Lysosomal Function. *Front. Oncol.*, 2020, *10*, 562196. https://doi.org/10.3389/fonc.2020.562196.

[232] Lu, D.; Carson, D. A. Spiperone Enhances Intracellular Calcium Level and Inhibits the Wnt Signaling Pathway. *BMC Pharmacol.*, 2009, *9*, 13. https://doi.org/10.1186/1471-2210-9-13.

[233] Newton, A. C. Protein Kinase C: Structure, Function, and Regulation Protein Kinase C: Structure, Function, and Regulation. *Artic. J. Biol. Chem.*, 1995, *270*, 28495–28498. https://doi.org/10.1074/jbc.270.48.28495.

[234] Foskett, J. K.; White, C.; Cheung, K. H.; Mak, D. O. D. Inositol Trisphosphate Receptor Ca2+ Release Channels. *Physiological Reviews*. Physiol Rev April 2007, pp 593–658. https://doi.org/10.1152/physrev.00035.2006.

[235] Mekahli, D.; Bultynck, G.; Parys, J. B.; de Smedt, H.; Missiaen, L. Endoplasmic-Reticulum Calcium Depletion and Disease. *Cold Spring Harbor Perspectives in Biology*. Cold Spring Harbor Laboratory Press June 2011, pp 1–30. https://doi.org/10.1101/cshperspect.a004317.

[236] Iurlaro, R.; Muñoz-Pinedo, C. Cell Death Induced by Endoplasmic Reticulum Stress. *FEBS J.*, 2016, *283* (14), 2640–2652. https://doi.org/10.1111/febs.13598.

[237] Malhotra, J. D.; Kaufman, R. J. ER Stress and Its Functional Link to Mitochondria: Role in Cell Survival and Death. *Cold Spring Harb. Perspect. Biol.*, 2011, *3* (9), 1–13. https://doi.org/10.1101/cshperspect.a004424.

[238] Wacquier, B.; Combettes, L.; Dupont, G. Cytoplasmic and Mitochondrial Calcium Signaling: A Two-Way Relationship. *Cold Spring Harb. Perspect. Biol.*, 2019, *11* (10). https://doi.org/10.1101/cshperspect.a035139.

[239] Zhuo, C.; Xun, Z.; Hou, W.; Ji, F.; Lin, X.; Tian, H.; Zheng, W.; Chen, M.; Liu, C.; Wang, W.; et al. Surprising Anticancer Activities of Psychiatric Medications: Old Drugs Offer New Hope for Patients with Brain Cancer. *Front. Pharmacol.*, 2019, *10*. https://doi.org/10.3389/fphar.2019.01262.

[240] Hendouei, N.; Saghafi, F.; Shadfar, F.; Hosseinimehr, S. J. Molecular Mechanisms of Anti-Psychotic Drugs for Improvement of Cancer Treatment. *European Journal of Pharmacology*. Elsevier B.V. August 5, 2019. https://doi.org/10.1016/j.ejphar.2019.05.031.

[241] Schulz, M.; Iwersen-Bergmann, S.; Andresen, H.; Schmoldt, A. Therapeutic and Toxic Blood Concentrations of Nearly 1,000 Drugs and Other Xenobiotics. *Crit. Care*, 2012, *16* (4). https://doi.org/10.1186/cc11441.

[242] Hollemans, M.; Elferink, R. O.; Philip, G.; Groot, D.; Strijland, A.; Tager, J. M. Accumulation of Weak Bases in Relation to Intralysosomal PH in Cultured Human Skin Fibroblasts. *BBA - Biomembr.*, 1981, *643* (1), 140–151. https://doi.org/10.1016/0005-2736(81)90226-1.

[243] Nadanaciva, S.; Lu, S.; Gebhard, D. F.; Jessen, B. A.; Pennie, W. D.; Will, Y. A High Content Screening Assay for Identifying Lysosomotropic Compounds. *Toxicol. Vitr.*, 2011, *25* (3), 715–723. https://doi.org/10.1016/j.tiv.2010.12.010.

[244] Lu, S.; Jessen, B.; Strock, C.; Will, Y. The Contribution of Physicochemical Properties to Multiple in Vitro Cytotoxicity Endpoints. *Toxicol. Vitr.*, 2012, *26* (4), 613–620. https://doi.org/10.1016/j.tiv.2012.01.025.

[245] Logan, R.; Kong, A. C.; Axcell, E.; Krise, J. P. Amine-Containing Molecules and the Induction of an Expanded Lysosomal Volume Phenotype: A Structure-Activity Relationship Study. *J. Pharm. Sci.*, 2014, *103* (5), 1572–1580. https://doi.org/10.1002/jps.23949.

[246] Gonzalez-Rothi, R. J.; Zander, D. S.; Ros, P. R. Fluoxetine Hydrochloride (Prozac)-Induced Pulmonary Disease. *Chest*, 1995, *107* (6), 1763–1765. https://doi.org/10.1378/chest.107.6.1763.

[247] Shahane, S. A.; Huang, R.; Gerhold, D.; Baxa, U.; Austin, C. P.; Xia, M. Detection of Phospholipidosis Induction: A Cell-Based Assay in High-Throughput and High-Content Format. *J. Biomol. Screen.*, 2014, *19* (1), 66–76. https://doi.org/10.1177/1087057113502851.

[248] Shaw, V.; Srivastava, S.; Srivastava, S. K. Repurposing Antipsychotics of the Diphenylbutylpiperidine Class for Cancer Therapy. *Seminars in Cancer Biology*. Academic Press 2019. https://doi.org/10.1016/j.semcancer.2019.10.007.

[249] Ranjan, A.; Srivastava, S. K. Penfluridol Suppresses Pancreatic Tumor Growth by Autophagy-Mediated Apoptosis. *Sci. Rep.*, 2016, *6*. https://doi.org/10.1038/srep26165.

[250] Vucicevic, L.; Misirkic-Marjanovic, M.; Harhaji-Trajkovic, L.; Maric, N.; Trajkovic, V. Mechanisms and Therapeutic Significance of Autophagy Modulation by Antipsychotic Drugs. *Cell Stress*. Shared Science Publishers OG November 1, 2018, pp 282–291. https://doi.org/10.15698/cst2018.11.161.

[251] Gassen, N. C.; Rein, T. Is There a Role of Autophagy in Depression and Antidepressant Action? *Frontiers in Psychiatry*. Frontiers Media S.A. 2019. https://doi.org/10.3389/fpsyt.2019.00337.

[252] Piao, S.; Amaravadi, R. K. Targeting the Lysosome in Cancer. *Annals of the New York Academy of Sciences*. Blackwell Publishing Inc. May 1, 2016, pp 45–54. https://doi.org/10.1111/nyas.12953.

[253] Petersen, N. H. T.; Olsen, O. D.; Groth-Pedersen, L.; Ellegaard, A. M.; Bilgin, M.; Redmer, S.; Ostenfeld, M. S.; Ulanet, D.; Dovmark, T. H.; Lønborg, A.; et al. Transformation-Associated Changes in Sphingolipid Metabolism Sensitize Cells to Lysosomal Cell Death Induced by Inhibitors of Acid Sphingomyelinase. *Cancer Cell*, 2013, *24* (3), 379–393.

https://doi.org/10.1016/j.ccr.2013.08.003.

[254] Breiden, B.; Sandhoff, K. Emerging Mechanisms of Drug-Induced Phospholipidosis. *Biological Chemistry*. De Gruyter 2019. https://doi.org/10.1515/hsz-2019-0270.

[255] Boya, P.; Kroemer, G. Lysosomal Membrane Permeabilization in Cell Death. *Oncogene*. October 27, 2008, pp 6434–6451. https://doi.org/10.1038/onc.2008.310.

[256] Ono, K.; Kim, S. O.; Han, J. Susceptibility of Lysosomes to Rupture Is a Determinant for Plasma Membrane Disruption in Tumor Necrosis Factor Alpha-Induced Cell Death. *Mol. Cell. Biol.*, 2003, *23* (2), 665–676. https://doi.org/10.1128/mcb.23.2.665-676.2003.

[257] Repnik, U.; Hafner Česen, M.; Turk, B. Lysosomal Membrane Permeabilization in Cell Death: Concepts and Challenges. *Mitochondrion*, 2014, *19* (Part A), 49–57. https://doi.org/10.1016/j.mito.2014.06.006.

[258] De Santi, M.; Baldelli, G.; Diotallevi, A.; Galluzzi, L.; Schiavano, G. F.; Brandi, G. Metformin Prevents Cell Tumorigenesis through Autophagy-Related Cell Death. *Sci. Rep.*, 2019, *9* (1). https://doi.org/10.1038/s41598-018-37247-6.

[259] Kucharewicz, K.; Dudkowska, M.; Zawadzka, A.; Ogrodnik, M.; Szczepankiewicz, A. A.; Czarnocki, Z.; Sikora, E. Simultaneous Induction and Blockade of Autophagy by a Single Agent. *Cell Death Dis.*, 2018, *9* (3). https://doi.org/10.1038/s41419-018-0383-6.

[260] Cirone, M.; Gilardini Montani, M. S.; Granato, M.; Garufi, A.; Faggioni, A.; D'Orazi, G. Autophagy Manipulation as a Strategy for Efficient Anticancer Therapies: Possible Consequences. *Journal of Experimental and Clinical Cancer Research*. BioMed Central Ltd. June 14, 2019. https://doi.org/10.1186/s13046-019-1275-z.

[261] Weinberg, S. E.; Chandel, N. S. Targeting Mitochondria Metabolism for Cancer Therapy. *Nature Chemical Biology*. Nature Publishing Group January 1, 2015, pp 9–15. https://doi.org/10.1038/nchembio.1712.

[262] Kroemer, G.; Galluzzi, L.; Brenner, C. Mitochondrial Membrane Permeabilization in Cell Death. *Physiological Reviews*. Physiol Rev January 2007, pp 99–163. https://doi.org/10.1152/physrev.00013.2006.

[263] Modica-Napolitano, J. S.; Aprille, J. R. Delocalized Lipophilic Cations Selectively Target the Mitochondria of Carcinoma Cells. *Adv. Drug Deliv. Rev.*, 2001, *49* (1–2), 63–70. https://doi.org/10.1016/S0169-409X(01)00125-9.

[264] Cuvillo, A. Del. Comparative Pharmacology of the H1 Antihistamines. *J. Investig. Allergol. & Clin. Immunol.*

[265] Mauri, M. C.; Paletta, S.; Di Pace, C.; Reggiori, A.; Cirnigliaro, G.; Valli, I.; Altamura, A. C. Clinical Pharmacokinetics of Atypical Antipsychotics: An Update. *Clinical Pharmacokinetics*. Springer International Publishing December 1, 2018, pp 1493–1528. https://doi.org/10.1007/s40262-018-0664-3.

[266] Walker, A. J.; Grainge, M.; Bates, T. E.; Card, T. R. Survival of Glioma and Colorectal Cancer Patients Using Tricyclic Antidepressants Post-Diagnosis. *Cancer Causes Control*, 2012, *23* (12), 1959–1964. https://doi.org/10.1007/s10552-012-0073-0.

[267] Coogan, P. F.; Strom, B. L.; Rosenberg, L. Antidepressant Use and Colorectal Cancer Risk. *Pharmacoepidemiol. Drug Saf.*, 2009, *18* (11), 1111–1114. https://doi.org/10.1002/pds.1808.

[268] Chubak, J.; Boudreau, D. M.; Rulyak, S. J.; Mandelson, M. T. Colorectal Cancer Risk in

Relation to Antidepressant Medication Use. *Int. J. Cancer*, 2011, *128* (1), 227–232. https://doi.org/10.1002/ijc.25322.

[269] Ellegaard, A. M.; Dehlendorff, C.; Vind, A. C.; Anand, A.; Cederkvist, L.; Petersen, N. H. T.; Nylandsted, J.; Stenvang, J.; Mellemgaard, A.; Østerlind, K.; et al. Repurposing Cationic Amphiphilic Antihistamines for Cancer Treatment. *EBioMedicine*, 2016, *9*, 130–139. https://doi.org/10.1016/j.ebiom.2016.06.013.

[270] Bray, F.; Ferlay, J.; Soerjomataram, I.; Siegel, R. L.; Torre, L. A.; Jemal, A. Global Cancer Statistics 2018: GLOBOCAN Estimates of Incidence and Mortality Worldwide for 36 Cancers in 185 Countries. *CA. Cancer J. Clin.*, 2018, *68* (6), 394–424. https://doi.org/10.3322/caac.21492.

[271] Testa, U.; Pelosi, E.; Castelli, G. Colorectal Cancer: Genetic Abnormalities, Tumor Progression, Tumor Heterogeneity, Clonal Evolution and Tumor-Initiating Cells. *Med. Sci.*, 2018, *6* (2), 31. https://doi.org/10.3390/medsci6020031.

[272] Van Der Jeught, K.; Xu, H. C.; Li, Y. J.; Lu, X. Bin; Ji, G. Drug Resistance and New Therapies in Colorectal Cancer. *World Journal of Gastroenterology*. Baishideng Publishing Group Co., Limited September 14, 2018, pp 3834–3848. https://doi.org/10.3748/wjg.v24.i34.3834.

[273] Dalton, S. O.; Mellemkjær, L.; Thomassen, L.; Mortensen, P. B.; Johansen, C. Risk for Cancer in a Cohort of Patients Hospitalized for Schizophrenia in Denmark, 1969-1993. *Schizophr. Res.*, 2005, *75* (2–3), 315–324. https://doi.org/10.1016/j.schres.2004.11.009.

[274] Dalton, S. O.; Johansen, C.; Poulsen, A. H.; Nørgaard, M.; Sørensen, H. T.; McLaughlin, J. K.; Mortensen, P. B.; Friis, S. Cancer Risk among Users of Neuroleptic Medication: A Population-Based Cohort Study. *Br. J. Cancer*, 2006, *95* (7), 934–939. https://doi.org/10.1038/sj.bjc.6603259.

[275] Wisher, D. Martindale: The Complete Drug Reference. 37th Ed. *J. Med. Libr. Assoc.*, 2012, *100* (1), 75–76. https://doi.org/10.3163/1536-5050.100.1.018.

[276] Correll, C. U. From Receptor Pharmacology to Improved Outcomes: Individualising the Selection, Dosing, and Switching of Antipsychotics. *Eur. Psychiatry*, 2010, *25* (SUPPL. 2), S12–S21. https://doi.org/10.1016/S0924-9338(10)71701-6.

[277] Cherciu, I.; Bărbălan, A.; Pirici, D.; Mărgăritescu, C.; Săftoiu, A. Stem Cells, Colorectal Cancer and Cancer Stem Cell Markers Correlations. *Curr. Heal. Sci. J.*, 2014, *40* (3), 153–15361. https://doi.org/10.12865/CHSJ.40.03.01.

[278] Liang, L.; MacDonald, K.; Schwiebert, E. M.; Zeitlin, P. L.; Guggino, W. B. Spiperone, Identified through Compound Screening, Activates Calcium-Dependent Chloride Secretion in the Airway. *Am. J. Physiol. Physiol.*, 2009, *296* (1), C131–C141. https://doi.org/10.1152/ajpcell.00346.2008.

[279] Gundlach, A. L.; Largent, B. L.; Snyder, S. H. 125I-Spiperone: A Novel Ligand for D2 Dopamine Receptors. *Life Sci.*, 1984, *35* (19), 1981–1988. https://doi.org/10.1016/0024-3205(84)90479-X.

[280] Im, D.; Inoue, A.; Fujiwara, T.; Nakane, T.; Yamanaka, Y.; Uemura, T.; Mori, C.; Shiimura, Y.; Kimura, K. T.; Asada, H.; et al. Structure of the Dopamine D2 Receptor in Complex with the Antipsychotic Drug Spiperone. *Nat. Commun.*, 2020, *11* (1). https://doi.org/10.1038/s41467-020-20221-0.

[281] Kondej, M.; Stępnicki, P.; Kaczor, A. A. Multi-Target Approach for Drug Discovery against

Schizophrenia. *International Journal of Molecular Sciences*. MDPI AG October 10, 2018. https://doi.org/10.3390/ijms19103105.

[282] Putney, J. W.; Tomita, T. Phospholipase C Signaling and Calcium Influx. *Advances in Biological Regulation*. Elsevier Ltd 2012, pp 152–164. https://doi.org/10.1016/j.advenzreg.2011.09.005.

[283] Carreras-Sureda, A.; Pihán, P.; Hetz, C. Calcium Signaling at the Endoplasmic Reticulum: Fine-Tuning Stress Responses. *Cell Calcium*. Elsevier Ltd March 1, 2018, pp 24–31. https://doi.org/10.1016/j.ceca.2017.08.004.

[284] Szegezdi, E.; Logue, S. E.; Gorman, A. M.; Samali, A. Mediators of Endoplasmic Reticulum Stress-Induced Apoptosis. *EMBO Reports*. European Molecular Biology Organization September 2006, pp 880–885. https://doi.org/10.1038/sj.embor.7400779.

[285] Marciniak, S. J.; Yun, C. Y.; Oyadomari, S.; Novoa, I.; Zhang, Y.; Jungreis, R.; Nagata, K.; Harding, H. P.; Ron, D. CHOP Induces Death by Promoting Protein Synthesis and Oxidation in the Stressed Endoplasmic Reticulum. *Genes Dev.*, 2004, *18* (24), 3066–3077. https://doi.org/10.1101/gad.1250704.

[286] Zito, E.; Melo, E. P.; Yang, Y.; Wahlander, Å.; Neubert, T. A.; Ron, D. Oxidative Protein Folding by an Endoplasmic Reticulum-Localized Peroxiredoxin. *Mol. Cell*, 2010, *40* (5), 787–797. https://doi.org/10.1016/j.molcel.2010.11.010.

[287] Hu, H.; Tian, M.; Ding, C.; Yu, S. The C/EBP Homologous Protein (CHOP) Transcription Factor Functions in Endoplasmic Reticulum Stress-Induced Apoptosis and Microbial Infection. *Frontiers in Immunology*. Frontiers Media S.A. January 4, 2019, p 3083. https://doi.org/10.3389/fimmu.2018.03083.

[288] Lee, S.; Min, K. T. The Interface between ER and Mitochondria: Molecular Compositions and Functions. *Molecules and Cells*. Korean Society for Molecular and Cellular Biology 2018, pp 1000–1007. https://doi.org/10.14348/molcells.2018.0438.

[289] Doghman-Bouguerra, M.; Lalli, E. ER-Mitochondria Interactions: Both Strength and Weakness within Cancer Cells. *Biochimica et Biophysica Acta - Molecular Cell Research*. Elsevier B.V. April 1, 2019, pp 650–662. https://doi.org/10.1016/j.bbamcr.2019.01.009.

[290] Jung, Y. S.; Park, J. Il. Wnt Signaling in Cancer: Therapeutic Targeting of Wnt Signaling beyond β-Catenin and the Destruction Complex. *Experimental and Molecular Medicine*. Springer Nature February 1, 2020, pp 183–191. https://doi.org/10.1038/s12276-020-0380-6.

7. Supplementary material

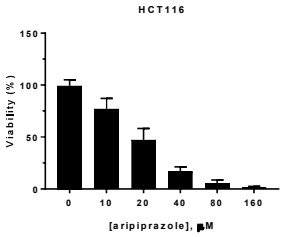
HCT116
Viability (%)
150
100
50
0
0 10 20 40 80 160
[aripiprazole], μM

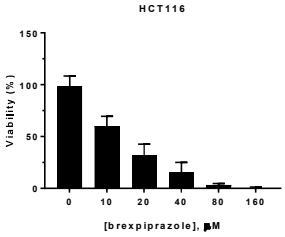
HCT116
Viability (%)
150
100
50
0
0 10 20 40 80 160
[brexpiprazole], μM

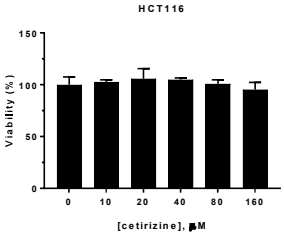
HCT116
Viability (%)
150
100
50
0
0 10 20 40 80 160
[cetirizine], μM

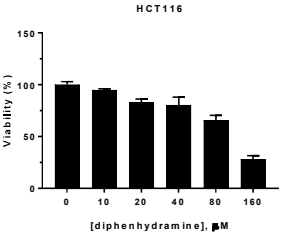
HCT116
Viability (%)
150
100
50
0
0 10 20 40 80 160
[diphenhydramine], μM

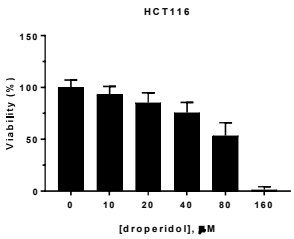
HCT116
Viability (%)
150
100
50
0
0 10 20 40 80 160
[droperidol], μM

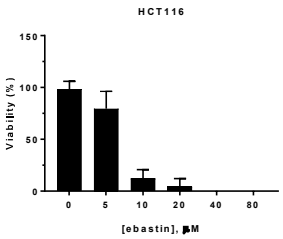
HCT116
Viability (%)
150
100
50
0
0 5 10 20 40 80
[ebastin], μM

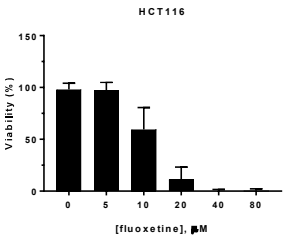
HCT116
Viability (%)
150
100
50
0
0 5 10 20 40 80
[fluoxetine], μM

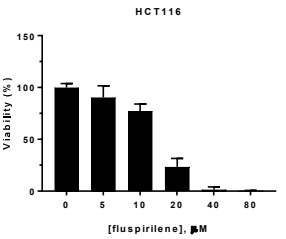
HCT116
Viability (%)
150
100
50
0
0 5 10 20 40 80
[fluspirilene], μM

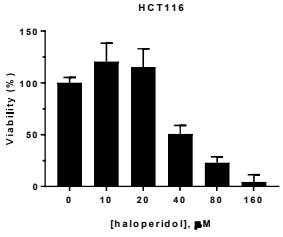
HCT116
Viability (%)
150
100
50
0
0 10 20 40 80 160
[haloperidol], μM

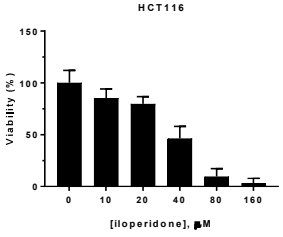
HCT116
Viability (%)
150
100
50
0
0 10 20 40 80 160
[iloperidone], μM

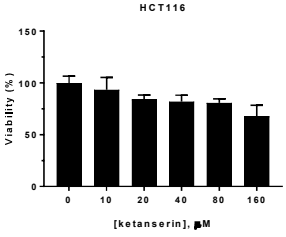
HCT116
Viability (%)
150
100
50
0
0 10 20 40 80 160
[ketanserin], μM

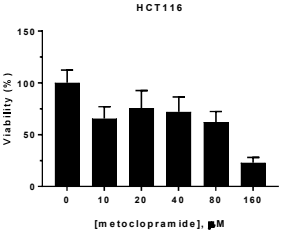
HCT116
Viability (%)
150
100
50
0
0 10 20 40 80 160
[metoclopramide], μM

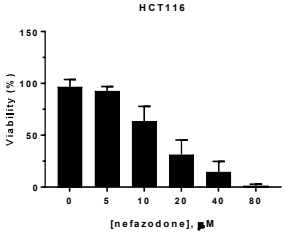
HCT116
Viability (%)
150
100
50
0
0 5 10 20 40 80
[nefazodone], μM

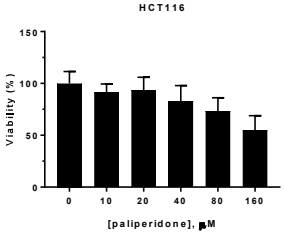
HCT116
Viability (%)
150
100
50
0
0 10 20 40 80 160
[paliperidone], μM

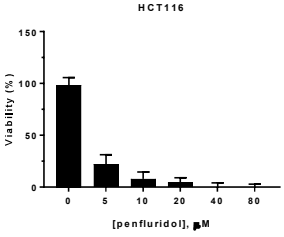
HCT116
Viability (%)
150
100
50
0
0 5 10 20 40 80
[penfluridol], μM

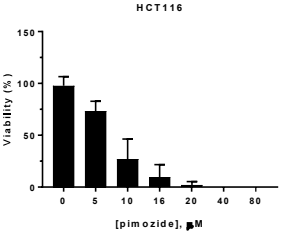
HCT116
Viability (%)
150
100
50
0
0 5 10 16 20 40 80
[pimozide], μM

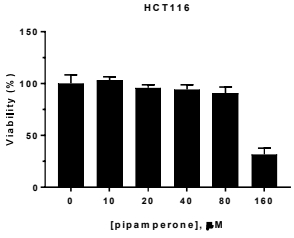
HCT116
Viability (%)
150
100
50
0
0 10 20 40 80 160
[pipamperone], μM

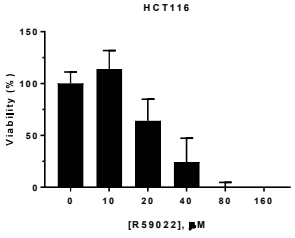
HCT116
Viability (%)
150
100
50
0
0 10 20 40 80 160
[R59022], μM

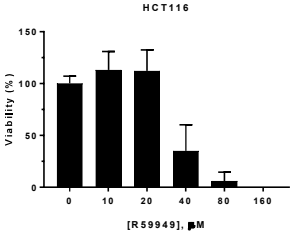
HCT116
Viability (%)
150
100
50
0
0 10 20 40 80 160
[R59949], μM

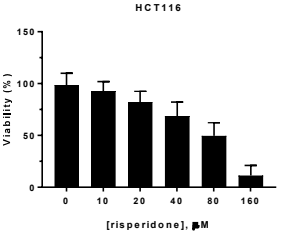
HCT116
Viability (%)
150
100
50
0
0 10 20 40 80 160
[risperidone], μM

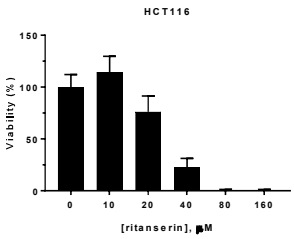
HCT116
Viability (%)
150
100
50
0
0 10 20 40 80 160
[ritanserin], μM

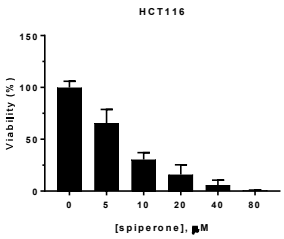
HCT116
Viability (%)
150
100
50
0
0 5 10 20 40 80
[spiperone], μM

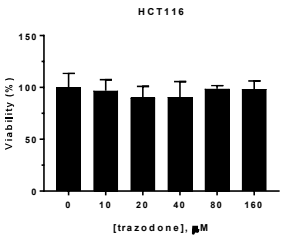
HCT116
Viability (%)
150
100
50
0
0 10 20 40 80 160
[trazodone], μM

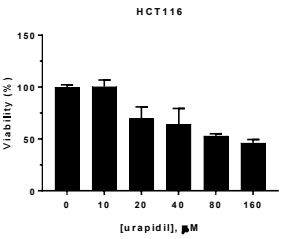
HCT116
Viability (%)
150
100
50
0
0 10 20 40 80 160
[urapidil], μM

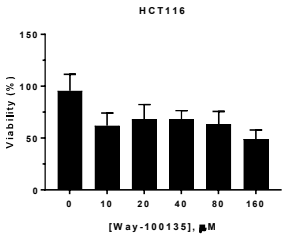
HCT116
Viability (%)
150
100
50
0
0 10 20 40 80 160
[Way-100135], μM

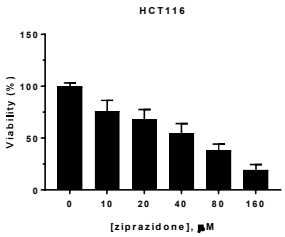
HCT116
Viability (%)
150
100
50
0
0 10 20 40 80 160
[ziprazidone], μM

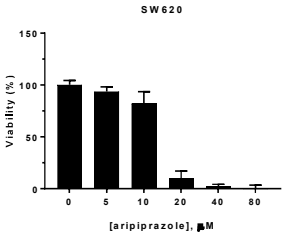
SW620
Viability (%)
150
100
50
0
0 5 10 20 40 80
[aripiprazole], μM

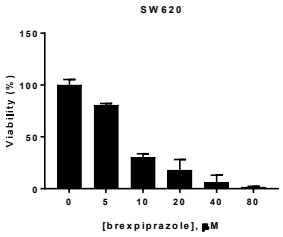
SW620
Viability (%)
150
100
50
0
0 5 10 20 40 80
[brexpiprazole], μM

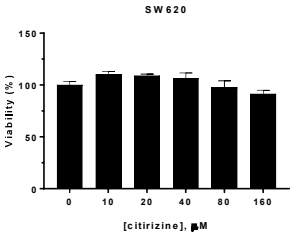
SW620
Viability (%)
150
100
50
0
0 10 20 40 80 160
[citirizine], μM

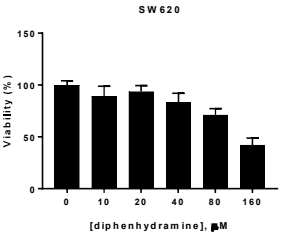
SW620
Viability (%)
150
100
50
0
0 10 20 40 80 160
[diphenhydramine], μM

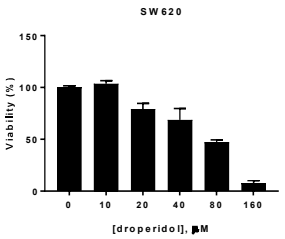
SW620
Viability (%)
150
100
50
0
0 10 20 40 80 160
[droperidol], μM

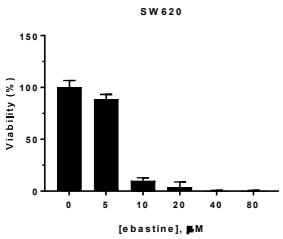
SW620
Viability (%)
150
100
50
0
0 5 10 20 40 80
[ebastine], μM

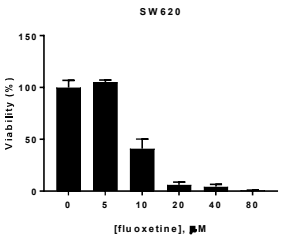
SW620
Viability (%)
150
100
50
0
0 5 10 20 40 80
[fluoxetine], μM

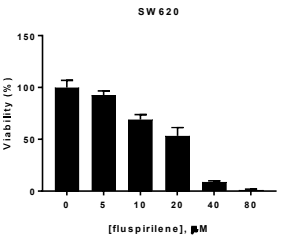
SW620
Viability (%)
150
100
50
0
0 5 10 20 40 80
[fluspirilene], μM

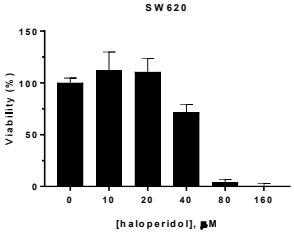
SW620
Viability (%)
150
100
50
0
0 10 20 40 80 160
[haloperidol], μM

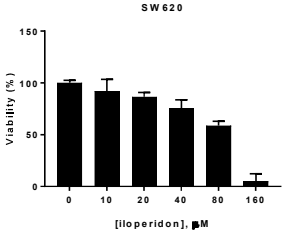
SW620
Viability (%)
150
100
50
0
0 10 20 40 80 160
[iloperidon], μM

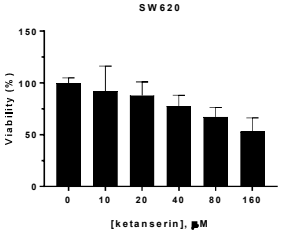
SW620
Viability (%)
150
100
50
0
0 10 20 40 80 160
[ketanserin], μM

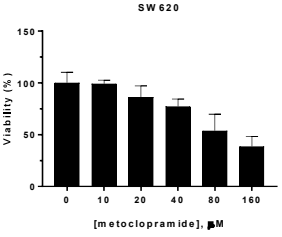
SW620
Viability (%)
150
100
50
0
0 10 20 40 80 160
[metoclopramide], μM

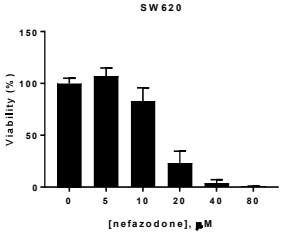
SW620
Viability (%)
150
100
50
0
0 5 10 20 40 80
[nefazodone], μM

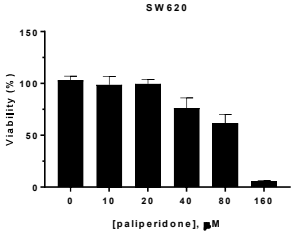
SW620
Viability (%)
150
100
50
0
0 10 20 40 80 160
[paliperidone], μM

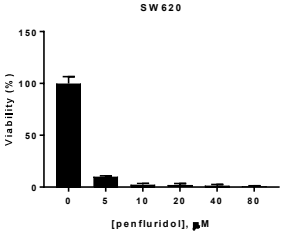
SW620
Viability (%)
150
100
50
0
0 5 10 20 40 80
[penfluridol], μM

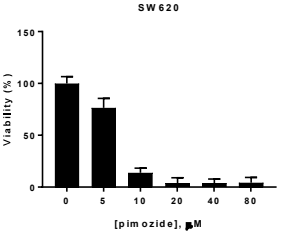
SW620
Viability (%)
150
100
50
0
0 5 10 20 40 80
[pimozide], μM

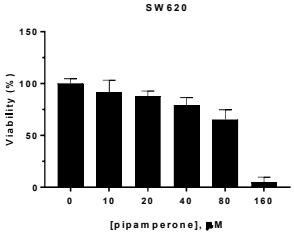
SW620
Viability (%)
150
100
50
0
0 10 20 40 80 160
[pipamperone], μM

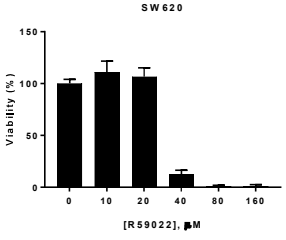
SW620
Viability (%)
150
100
50
0
0 10 20 40 80 160
[R59022], μM

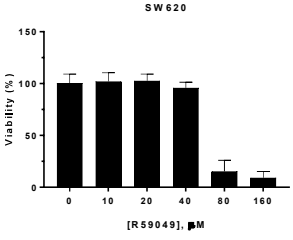
SW620
Viability (%)
150
100
50
0
0 10 20 40 80 160
[R59049], μM

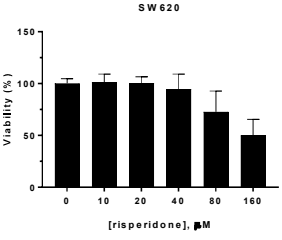
SW620
Viability (%)
150
100
50
0
0 10 20 40 80 160
[risperidone], μM

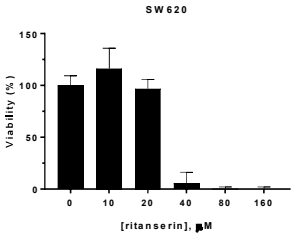
SW620
Viability (%)
150
100
50
0
0 10 20 40 80 160
[ritanserin], μM

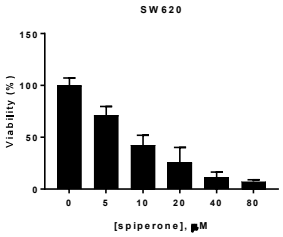
SW620
Viability (%)
150
100
50
0
0 5 10 20 40 80
[spiperone], μM

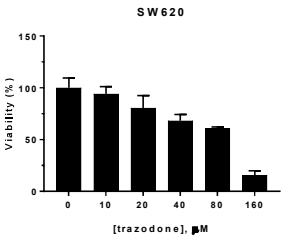
SW620
Viability (%)
150
100
50
0
0 10 20 40 80 160
[trazodone], μM

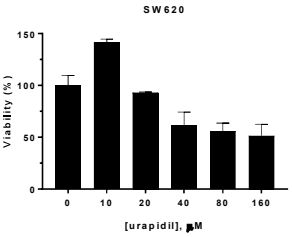
SW620
Viability (%)
150
100
50
0
0 10 20 40 80 160
[urapidil], μM

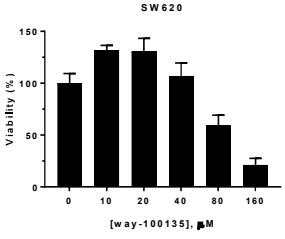
SW620
Viability (%)
150
100
50
0
0 10 20 40 80 160
[way-100135], μM

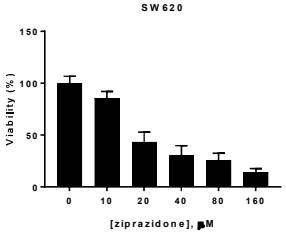
SW620
Viability (%)
150
100
50
0
0 10 20 40 80 160
[ziprazidone], μM

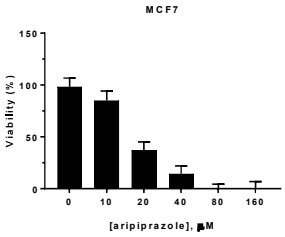
MCF7
Viability (%)
150
100
50
0
0 10 20 40 80 160
[aripiprazole], μM

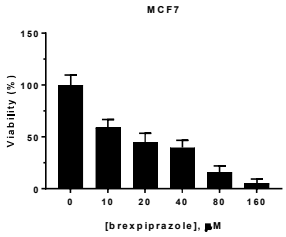
MCF7
Viability (%)
150
100
50
0
0 10 20 40 80 160
[brexpiprazole], μM

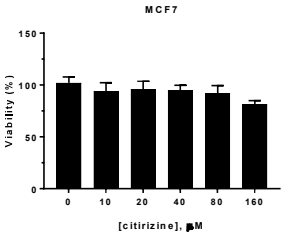
MCF7
Viability (%)
150
100
50
0
0 10 20 40 80 160
[citirizine], μM

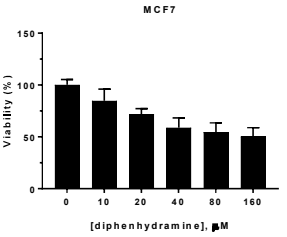
MCF7
Viability (%)
150
100
50
0
0 10 20 40 80 160
[diphenhydramine], μM

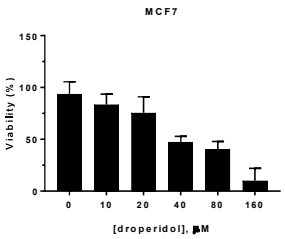
MCF7
Viability (%)
150
100
50
0
0 10 20 40 80 160
[droperidol], μM

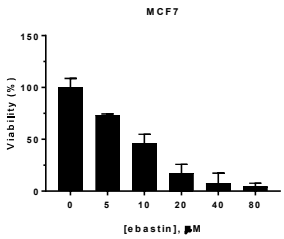
MCF7
Viability (%)
150
100
50
0
0 5 10 20 40 80
[ebastin], μM

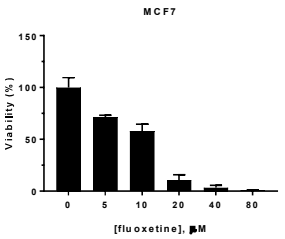
MCF7
Viability (%)
150
100
50
0
0 5 10 20 40 80
[fluoxetine], μM

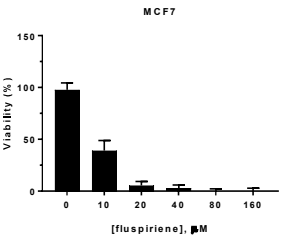
MCF7
Viability (%)
150
100
50
0
0 10 20 40 80 160
[fluspiriene], μM

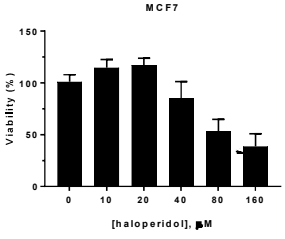
MCF7
Viability (%)
150
100
50
0
0 10 20 40 80 160
[haloperidol], μM

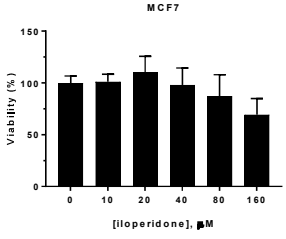
MCF7
Viability (%)
150
100
50
0
0 10 20 40 80 160
[iloperidone], μM

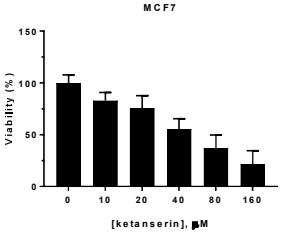
MCF7
Viability (%)
150
100
50
0
0 10 20 40 80 160
[ketanserin], μM

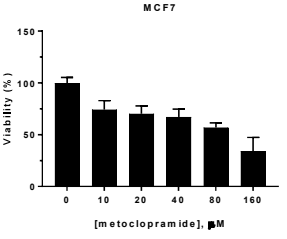
MCF7
Viability (%)
150
100
50
0
0 10 20 40 80 160
[metoclopramide], μM

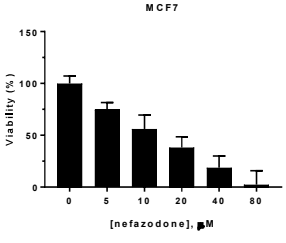
MCF7
Viability (%)
150
100
50
0
0 5 10 20 40 80
[nefazodone], μM

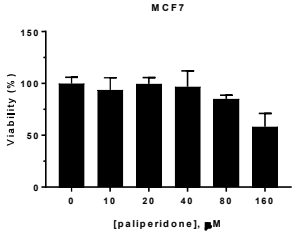
MCF7
Viability (%)
150
100
50
0
0 10 20 40 80 160
[paliperidone], μM

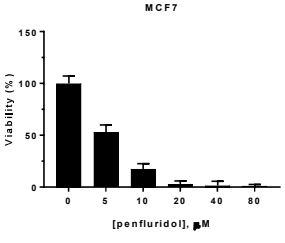
MCF7
Viability (%)
150
100
50
0
0 5 10 20 40 80
[penfluridol], μM

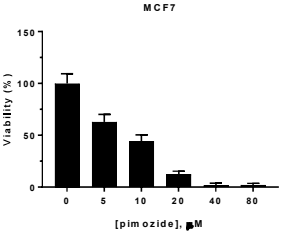
MCF7
Viability (%)
150
100
50
0
0 5 10 20 40 80
[pimozide], μM

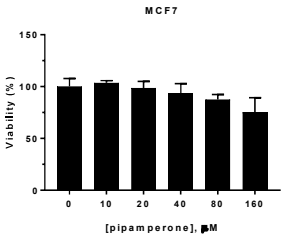
MCF7
Viability (%)
150
100
50
0
0 10 20 40 80 160
[pipamperone], μM

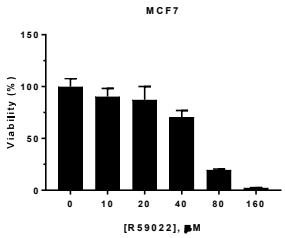
MCF7
Viability (%)
150
100
50
0
0 10 20 40 80 160
[R59022], μM

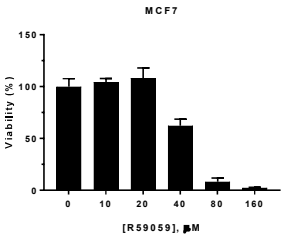
MCF7
Viability (%)
150
100
50
0
0 10 20 40 80 160
[R59059], μM

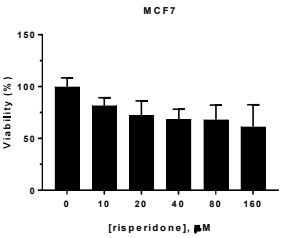
MCF7
Viability (%)
150
100
50
0
0 10 20 40 80 160
[risperidone], μM

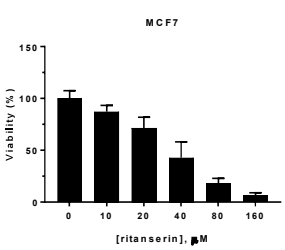
MCF7
Viability (%)
150
100
50
0
0 10 20 40 80 160
[ritanserin], μM

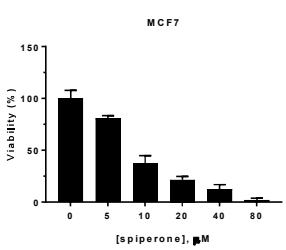
MCF7
Viability (%)
150
100
50
0
0 5 10 20 40 80
[spiperone], μM

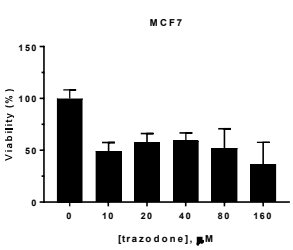
MCF7
Viability (%)
150
100
50
0
0 10 20 40 80 160
[trazodone], μM

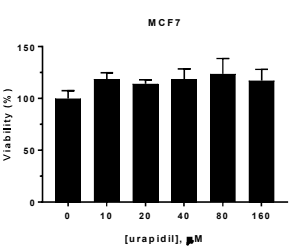
MCF7
Viability (%)
150
100
50
0
0 10 20 40 80 160
[urapidil], μM

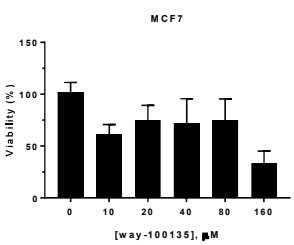
MCF7
Viability (%)
150
100
50
0
0 10 20 40 80 160
[way-100135], μM

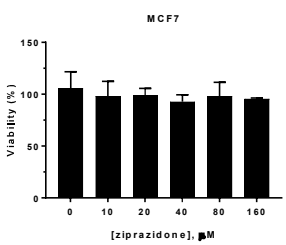
MCF7
Viability (%)
150
100
50
0
0 10 20 40 80 160
[ziprazidone], μM

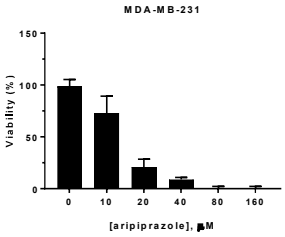
MDA-MB-231
Viability (%)
150
100
50
0
0 10 20 40 80 160
[aripiprazole], μM

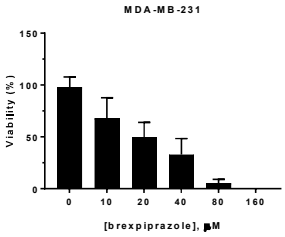
MDA-MB-231
Viability (%)
150
100
50
0
0 10 20 40 80 160
[brexpiprazole], μM

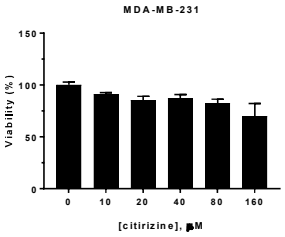
MDA-MB-231
Viability (%)
150
100
50
0
0 10 20 40 80 160
[citirizine], μM

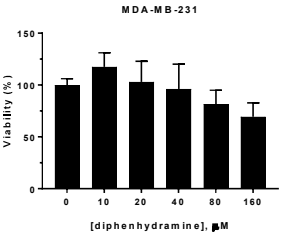
MDA-MB-231
Viability (%)
150
100
50
0
0 10 20 40 80 160
[diphenhydramine], μM

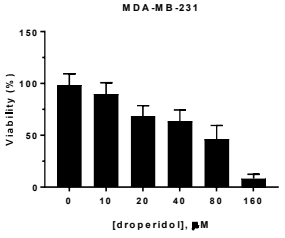
MDA-MB-231
Viability (%)
150
100
50
0
0 10 20 40 80 160
[droperidol], μM

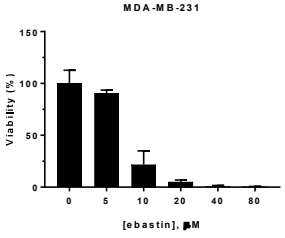
MDA-MB-231
Viability (%)
150
100
50
0
0 5 10 20 40 80
[ebastin], μM

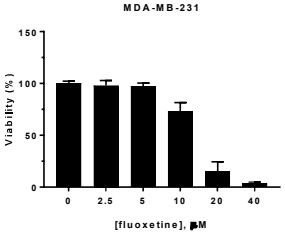
MDA-MB-231
Viability (%)
150
100
50
0
0 2.5 5 10 20 40
[fluoxetine], μM

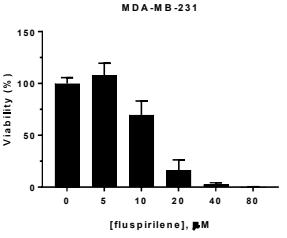
MDA-MB-231
Viability (%)
150
100
50
0
0 5 10 20 40 80
[fluspirilene], μM

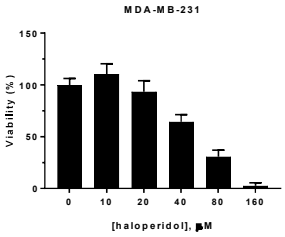
MDA-MB-231
Viability (%)
150
100
50
0
0 10 20 40 80 160
[haloperidol], μM

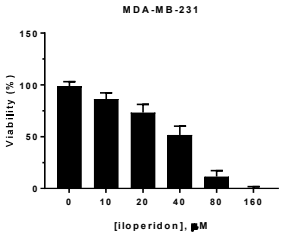
MDA-MB-231
Viability (%)
150
100
50
0
0 10 20 40 80 160
[iloperidon], μM

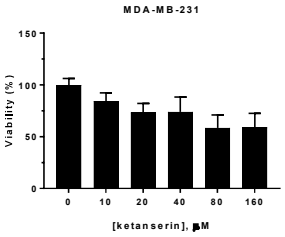
MDA-MB-231
Viability (%)
150
100
50
0
0 10 20 40 80 160
[ketanserin], μM

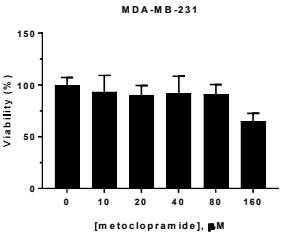
MDA-MB-231
Viability (%)
150
100
50
0
0 10 20 40 80 160
[metoclopramide], μM

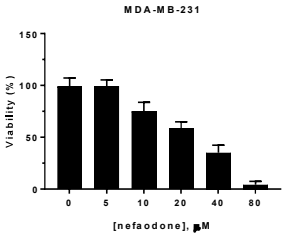
MDA-MB-231
Viability (%)
150
100
50
0
0 5 10 20 40 80
[nefaodone], μM

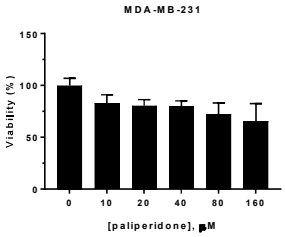
MDA-MB-231
Viability (%)
150
100
50
0
0 10 20 40 80 160
[paliperidone], μM

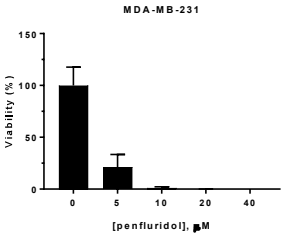
MDA-MB-231
Viability (%)
150
100
50
0
0 5 10 20 40
[penfluridol], μM

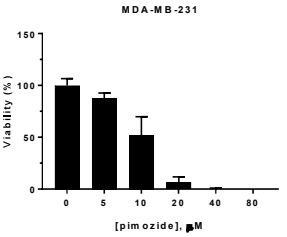
MDA-MB-231
Viability (%)
150
100
50
0
0 5 10 20 40 80
[pimozide], μM

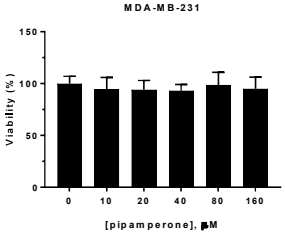
MDA-MB-231
Viability (%)
150
100
50
0
0 10 20 40 80 160
[pipamperone], μM

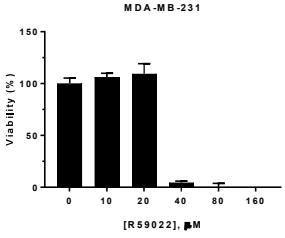
MDA-MB-231
Viability (%)
150
100
50
0
0 10 20 40 80 160
[R59022], μM

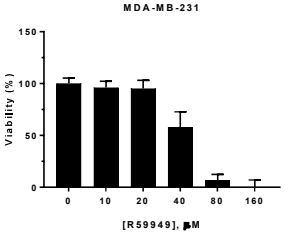
MDA-MB-231
Viability (%)
150
100
50
0
0 10 20 40 80 160
[R59949], μM

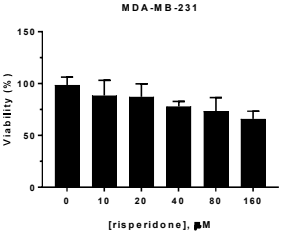
MDA-MB-231
Viability (%)
150
100
50
0
0 10 20 40 80 160
[risperidone], μM

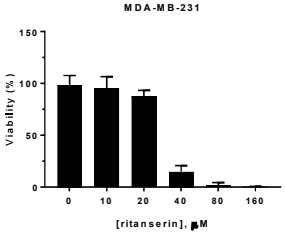
MDA-MB-231
Viability (%)
150
100
50
0
0 10 20 40 80 160
[ritanserin], μM

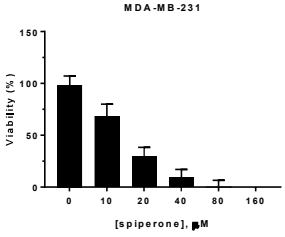
MDA-MB-231
Viability (%)
150
100
50
0
0 10 20 40 80 160
[spiperone], μM

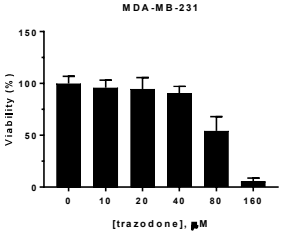
MDA-MB-231
Viability (%)
150
100
50
0
0 10 20 40 80 160
[trazodone], μM

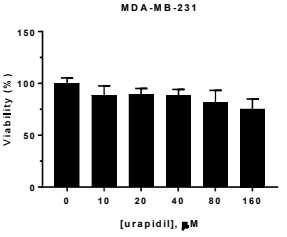
MDA-MB-231
Viability (%)
150
100
50
0
0 10 20 40 80 160
[urapidil], μM

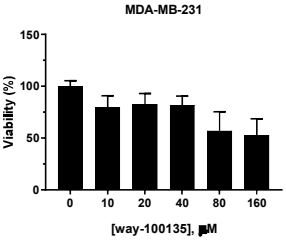
MDA-MB-231
Viability (%)
150
100
50
0
0 10 20 40 80 160
[way-100135], μM

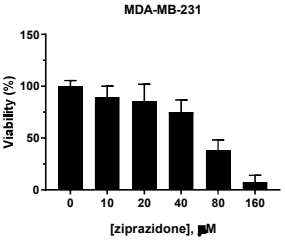
MDA-MB-231
Viability (%)
150
100
50
0
0 10 20 40 80 160
[ziprazidone], μM

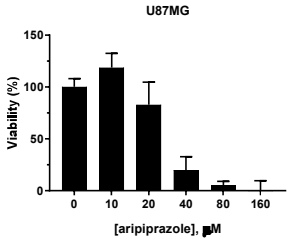
U87MG
Viability (%)
150
100
50
0
0 10 20 40 80 160
[aripiprazole], μM

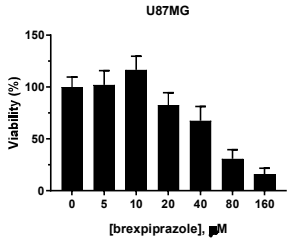
U87MG
Viability (%)
150
100
50
0
0 5 10 20 40 80 160
[brexpiprazole], μM

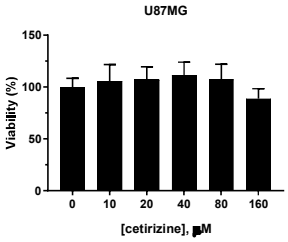
U87MG
Viability (%)
150
100
50
0
0 10 20 40 80 160
[cetirizine], μM

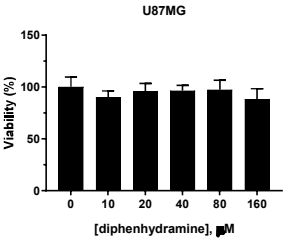
U87MG
Viability (%)
150
100
50
0
0 10 20 40 80 160
[diphenhydramine], μM

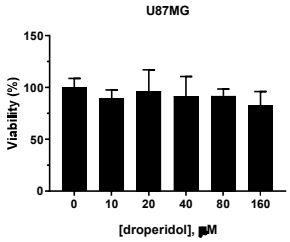
U87MG
Viability (%)
150
100
50
0
0 10 20 40 80 160
[droperidol], μM

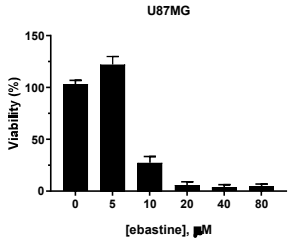
U87MG
Viability (%)
150
100
50
0
0 5 10 20 40 80
[ebastine], μM

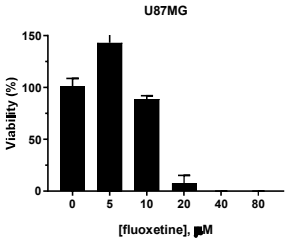
U87MG
Viability (%)
150
100
50
0
0 5 10 20 40 80
[fluoxetine], μM

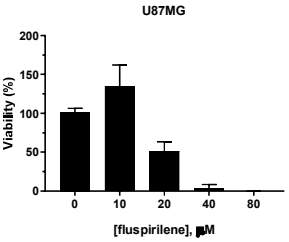
U87MG
Viability (%)
200
150
100
50
0
0 10 20 40 80
[fluspirilene], μM

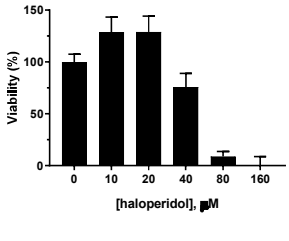
U87MG
Viability (%)
150
100
50
0
0 10 20 40 80 160
[haloperidol], μM

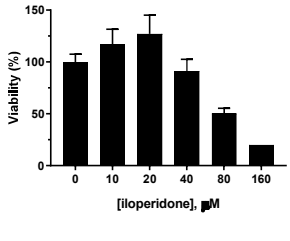
U87MG
Viability (%)
150
100
50
0
0 10 20 40 80 160
[iloperidone], μM

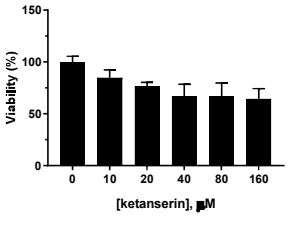
U87MG
Viability (%)
150
100
50
0
0 10 20 40 80 160
[ketanserin], μM

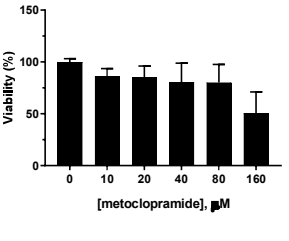
U87MG
Viability (%)
150
100
50
0
0 10 20 40 80 160
[metoclopramide], μM

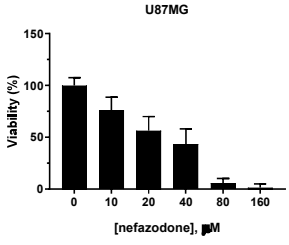
U87MG
Viability (%)
150
100
50
0
0 10 20 40 80 160
[nefazodone], μM

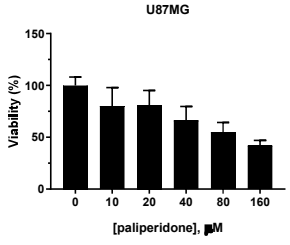
U87MG
Viability (%)
150
100
50
0
0 10 20 40 80 160
[paliperidone], μM

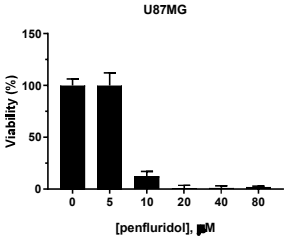
U87MG
Viability (%)
150
100
50
0
0 5 10 20 40 80
[penfluridol], μM

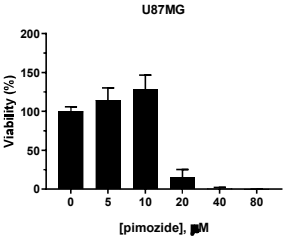
U87MG
Viability (%)
200
150
100
50
0
0 5 10 20 40 80
[pimozide], μM

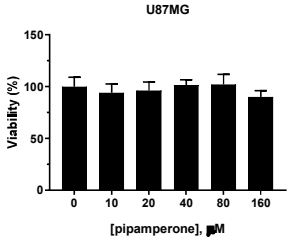
U87MG
Viability (%)
150
100
50
0
0 10 20 40 80 160
[pipamperone], μM

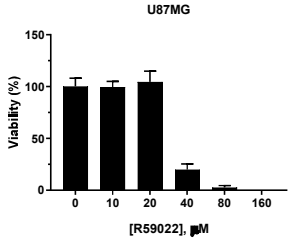
U87MG
Viability (%)
150
100
50
0
0 10 20 40 80 160
[R59022], μM

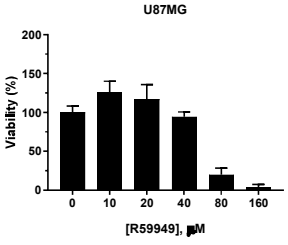
U87MG
Viability (%)
200
150
100
50
0
0 10 20 40 80 160
[R59949], μM

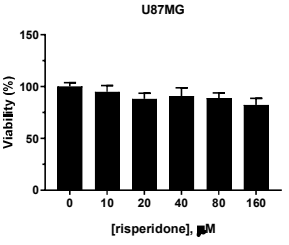
U87MG
Viability (%)
150
100
50
0
0 10 20 40 80 160
[risperidone], μM

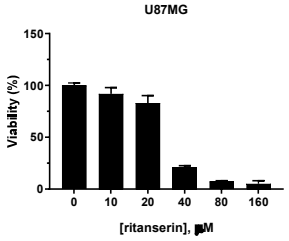
U87MG
Viability (%)
150
100
50
0
0 10 20 40 80 160
[ritanserin], μM

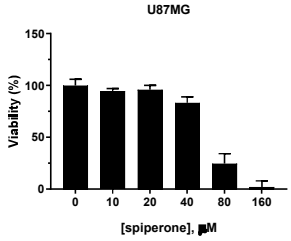
U87MG
Viability (%)
150
100
50
0
0 10 20 40 80 160
[spiperone], μM

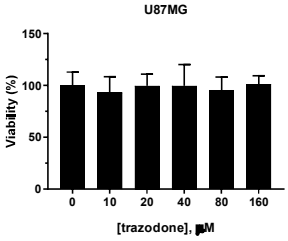
U87MG
Viability (%)
150
100
50
0
0 10 20 40 80 160
[trazodone], μM

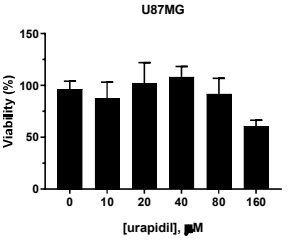
U87MG
Viability (%)
150
100
50
0
0 10 20 40 80 160
[urapidil], μM

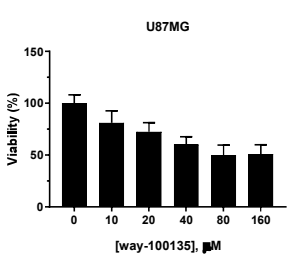
U87MG
Viability (%)
150
100
50
0
0 10 20 40 80 160
[way-100135], μM

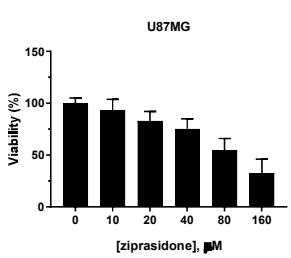
U87MG
Viability (%)
150
100
50
0
0 10 20 40 80 160
[ziprasidone], μM

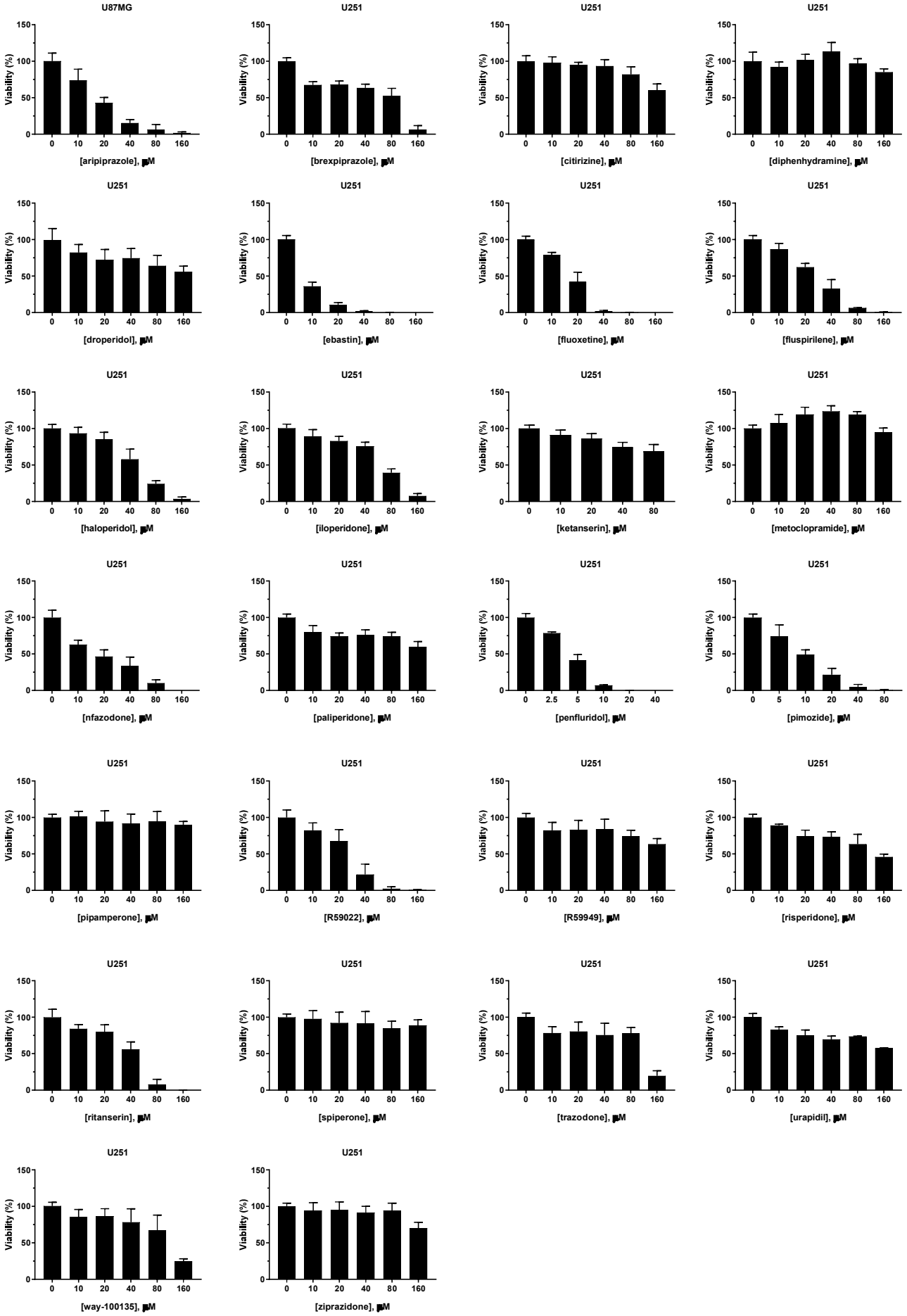

Supplementary figure 1. Effect of psychotropic drugs on cancer cell lines viability. Six cancer cell lines were treated for 72 h with scalar doses of drugs ranging from 10 to 160 µmol/L. The screened drugs included antipsychotics, antidepressant, antihistamines and three compounds used in scientific research with reported serotonin receptors antagonistic activity (R59949, R59022; WAY-100135). Cell viability is shown as percentage of viable cells versus control. Data are presented as mean ± standard deviation (SD) from three independent experiments, each performed in quadruplicate

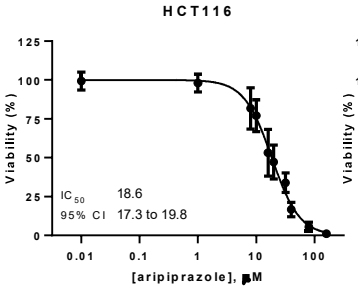
HCT116
Viability (%)
IC50 18.6
95% CI 17.3 to 19.8
[aripiprazole], μM

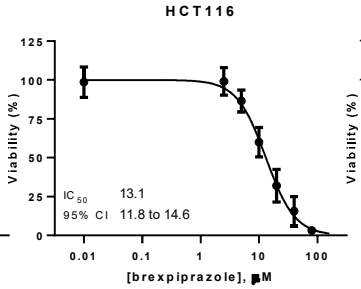
HCT116
Viability (%)
IC50 13.1
95% CI 11.8 to 14.6
[brexpiprazole], μM

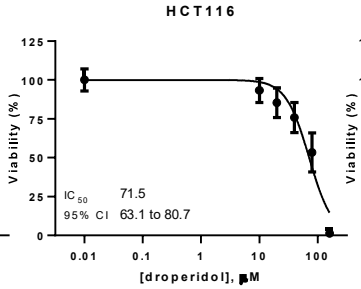
HCT116
Viability (%)
IC50 71.5
95% CI 63.1 to 80.7
[droperidol], μM

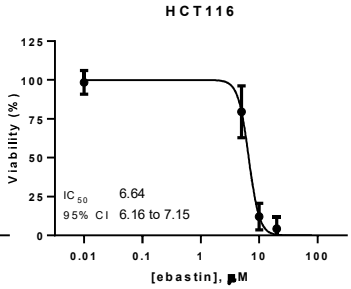
HCT116
Viability (%)
IC50 6.64
95% CI 6.16 to 7.15
[ebastin], μM

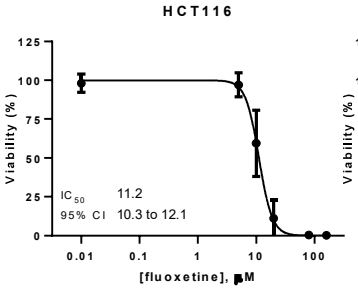
HCT116
Viability (%)
IC50 11.2
95% CI 10.3 to 12.1
[fluoxetine], μM

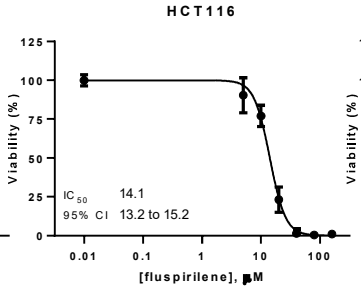
HCT116
Viability (%)
IC50 14.1
95% CI 13.2 to 15.2
[fluspirilene], μM

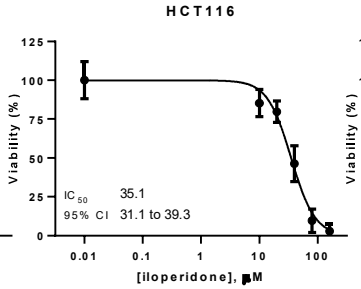
HCT116
Viability (%)
IC50 35.1
95% CI 31.1 to 39.3
[iloperidone], μM

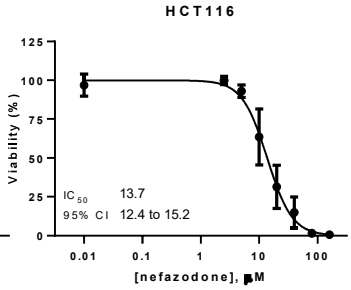
HCT116
Viability (%)
IC50 13.7
95% CI 12.4 to 15.2
[nefazodone], μM

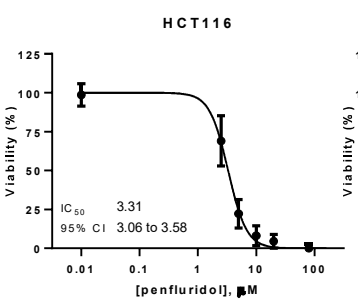
HCT116
Viability (%)
IC50 3.31
95% CI 3.06 to 3.58
[penfluridol], μM

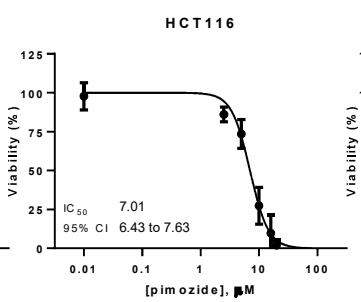
HCT116
Viability (%)
IC50 7.01
95% CI 6.43 to 7.63
[pimozide], μM

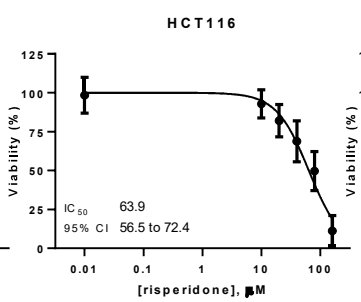
HCT116
Viability (%)
IC50 63.9
95% CI 56.5 to 72.4
[risperidone], μM

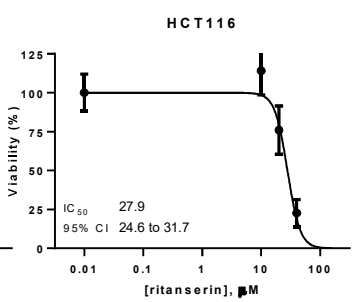
HCT116
Viability (%)
IC50 27.9
95% CI 24.6 to 31.7
[ritanserin], μM

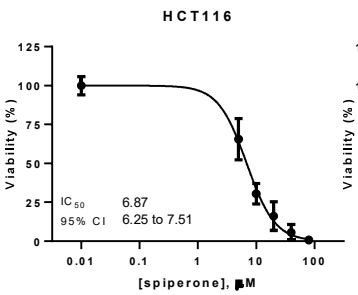
HCT116
Viability (%)
IC50 6.87
95% CI 6.25 to 7.51
[spiperone], μM

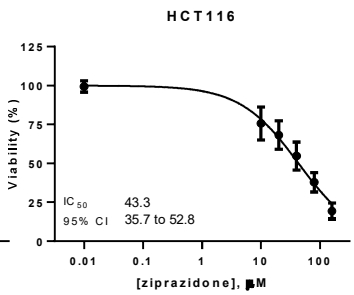
HCT116
Viability (%)
IC50 43.3
95% CI 35.7 to 52.8
[ziprazidone], μM

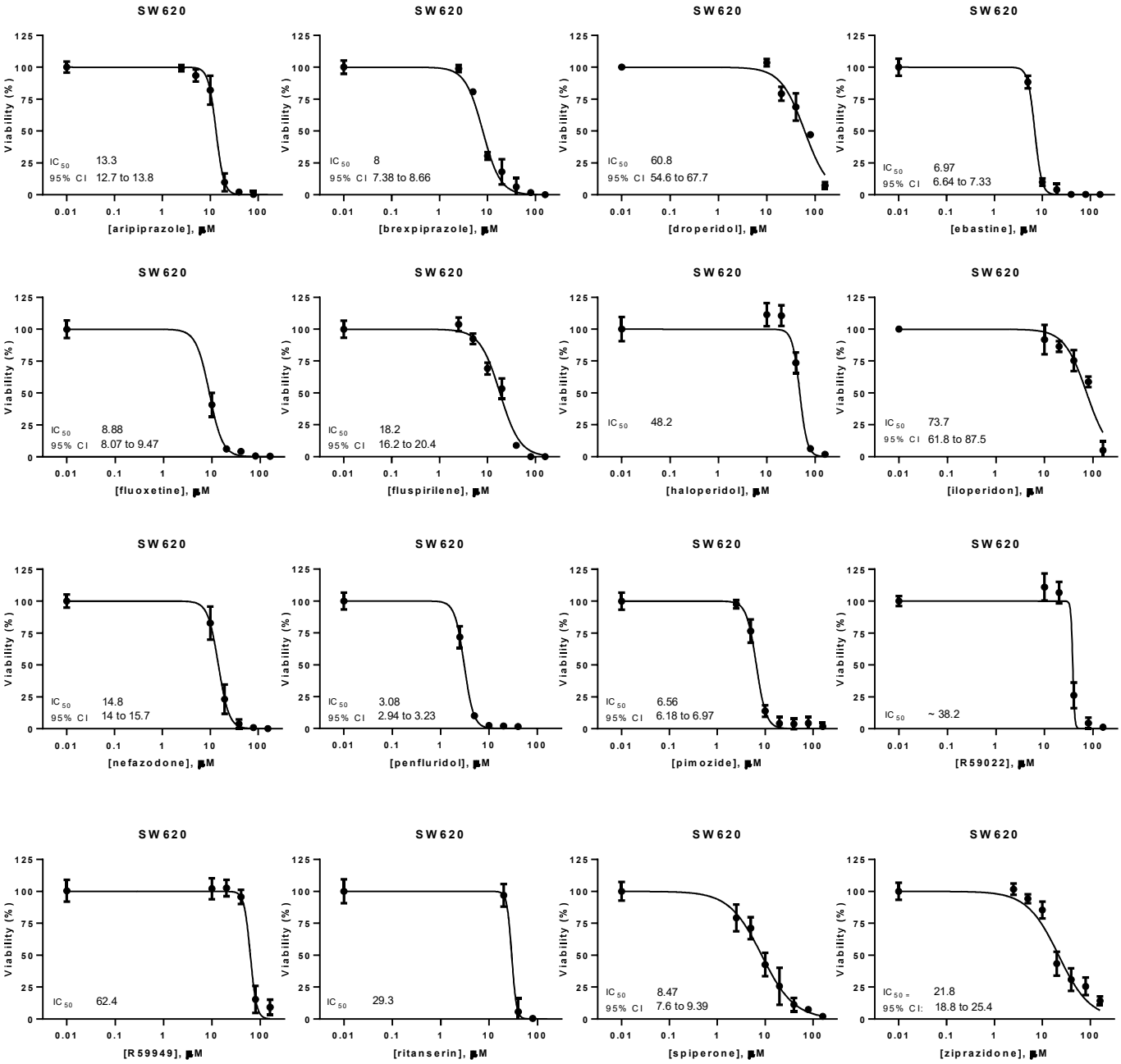
SW620
Viability (%)
IC50 13.3
95% CI 12.7 to 13.8
[aripiprazole], μM
SW620
IC50 8
95% CI 7.38 to 8.66
[brexpiprazole], μM
SW620
IC50 60.8
95% CI 54.6 to 67.7
[droperidol], μM
SW620
IC50 6.97
95% CI 6.64 to 7.33
[ebastine], μM
SW620
IC50 8.88
95% CI 8.07 to 9.47
[fluoxetine], μM
SW620
IC50 18.2
95% CI 16.2 to 20.4
[fluspirilene], μM
SW620
IC50 48.2
[haloperidol], μM
SW620
IC50 73.7
95% CI 61.8 to 87.5
[iloperidon], μM
SW620
IC50 14.8
95% CI 14 to 15.7
[nefazodone], μM
SW620
IC50 3.08
95% CI 2.94 to 3.23
[penfluridol], μM
SW620
IC50 6.56
95% CI 6.18 to 6.97
[pimozide], μM
SW620
IC50 ~ 38.2
[R59022], μM
SW620
IC50 62.4
[R59949], μM
SW620
IC50 29.3
[ritanserin], μM
SW620
IC50 8.47
95% CI 7.6 to 9.39
[spiperone], μM
SW620
IC50 = 21.8
95% CI: 18.8 to 25.4
[ziprazidone], μM

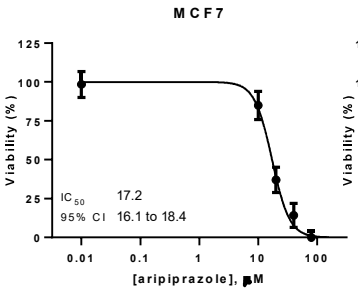
MCF7
Viability (%)
IC50 17.2
95% CI 16.1 to 18.4
[aripiprazole], μM

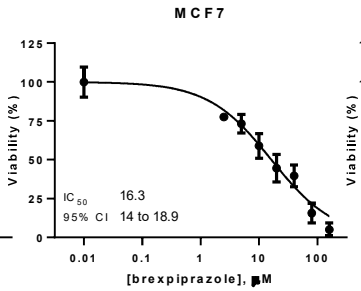
MCF7
Viability (%)
IC50 16.3
95% CI 14 to 18.9
[brexpiprazole], μM

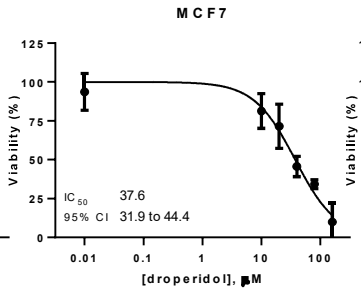
MCF7
Viability (%)
IC50 37.6
95% CI 31.9 to 44.4
[droperidol], μM

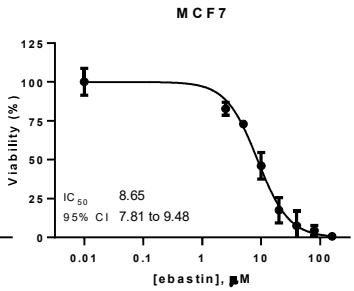
MCF7
Viability (%)
IC50 8.65
95% CI 7.81 to 9.48
[ebastin], μM

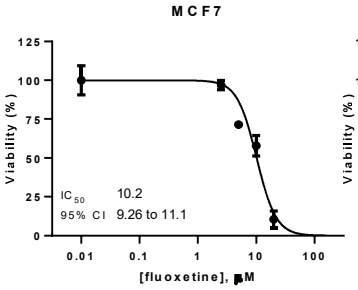
MCF7
Viability (%)
IC50 10.2
95% CI 9.26 to 11.1
[fluoxetine], μM

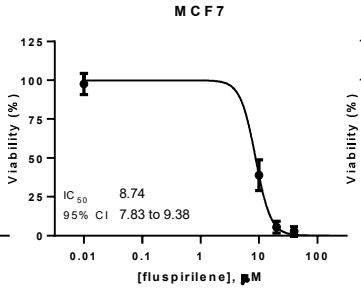
MCF7
Viability (%)
IC50 8.74
95% CI 7.83 to 9.38
[fluspirilene], μM

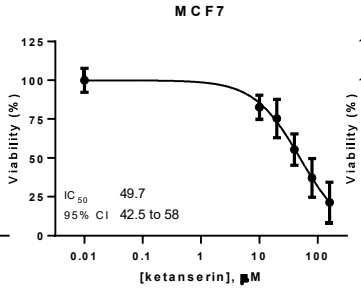
MCF7
Viability (%)
IC50 49.7
95% CI 42.5 to 58
[ketanserin], μM

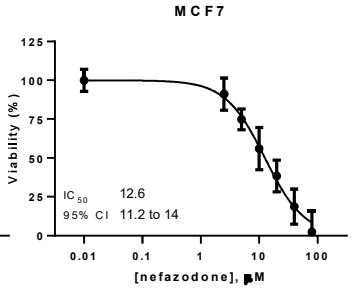
MCF7
Viability (%)
IC50 12.6
95% CI 11.2 to 14
[nefazodone], μM

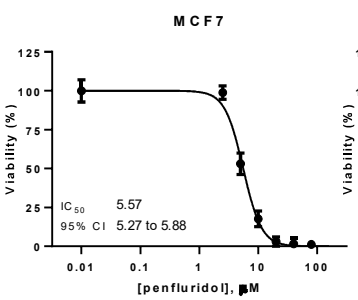
MCF7
Viability (%)
IC50 5.57
95% CI 5.27 to 5.88
[penfluridol], μM

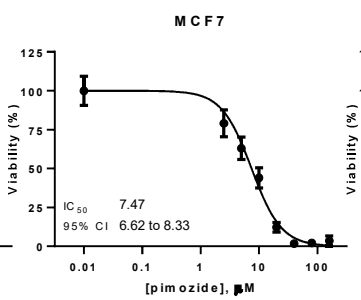
MCF7
Viability (%)
IC50 7.47
95% CI 6.62 to 8.33
[pimozide], μM

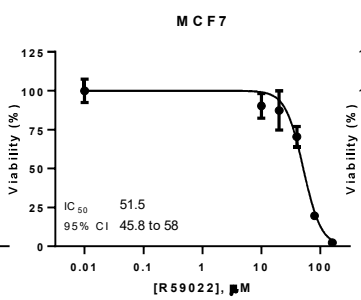
MCF7
Viability (%)
IC50 51.5
95% CI 45.8 to 58
[R59022], μM

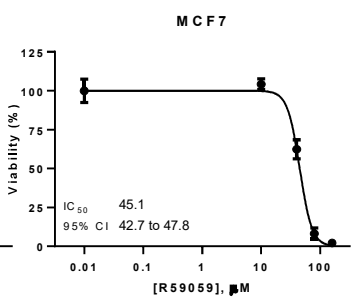
MCF7
Viability (%)
IC50 45.1
95% CI 42.7 to 47.8
[R59059], μM

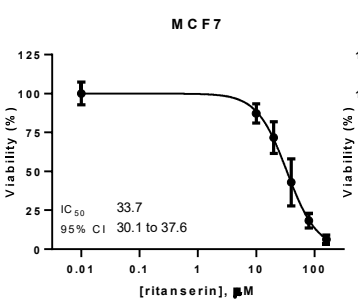
MCF7
Viability (%)
IC50 33.7
95% CI 30.1 to 37.6
[ritanserin], μM

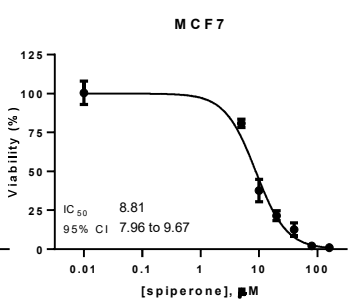
MCF7
Viability (%)
IC50 8.81
95% CI 7.96 to 9.67
[spiperone], μM

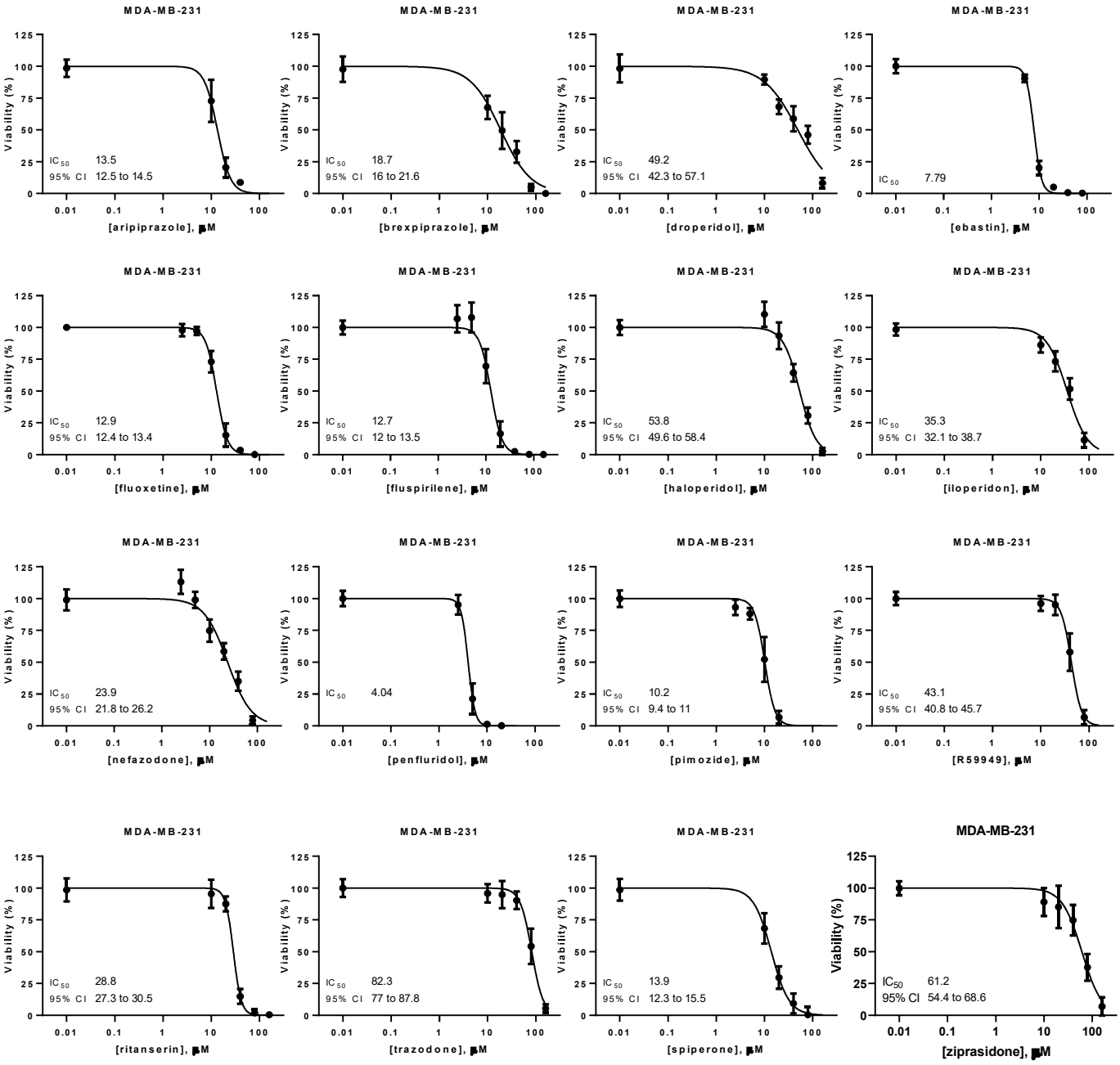
MDA-MB-231
Viability (%)
IC50 13.5
95% CI 12.5 to 14.5
[aripiprazole], μM
MDA-MB-231
IC50 18.7
95% CI 16 to 21.6
[brexpiprazole], μM
MDA-MB-231
IC50 49.2
95% CI 42.3 to 57.1
[droperidol], μM
MDA-MB-231
IC50 7.79
[ebastin], μM
MDA-MB-231
IC50 12.9
95% CI 12.4 to 13.4
[fluoxetine], μM
MDA-MB-231
IC50 12.7
95% CI 12 to 13.5
[fluspirilene], μM
MDA-MB-231
IC50 53.8
95% CI 49.6 to 58.4
[haloperidol], μM
MDA-MB-231
IC50 35.3
95% CI 32.1 to 38.7
[iloperidon], μM
MDA-MB-231
IC50 23.9
95% CI 21.8 to 26.2
[nefazodone], μM
MDA-MB-231
IC50 4.04
[penfluridol], μM
MDA-MB-231
IC50 10.2
95% CI 9.4 to 11
[pimozide], μM
MDA-MB-231
IC50 43.1
95% CI 40.8 to 45.7
[R59949], μM
MDA-MB-231
IC50 28.8
95% CI 27.3 to 30.5
[ritanserin], μM
MDA-MB-231
IC50 82.3
95% CI 77 to 87.8
[trazodone], μM
MDA-MB-231
IC50 13.9
95% CI 12.3 to 15.5
[spiperone], μM
MDA-MB-231
Viability (%)
IC50 61.2
95% CI 54.4 to 68.6
[ziprasidone], μM

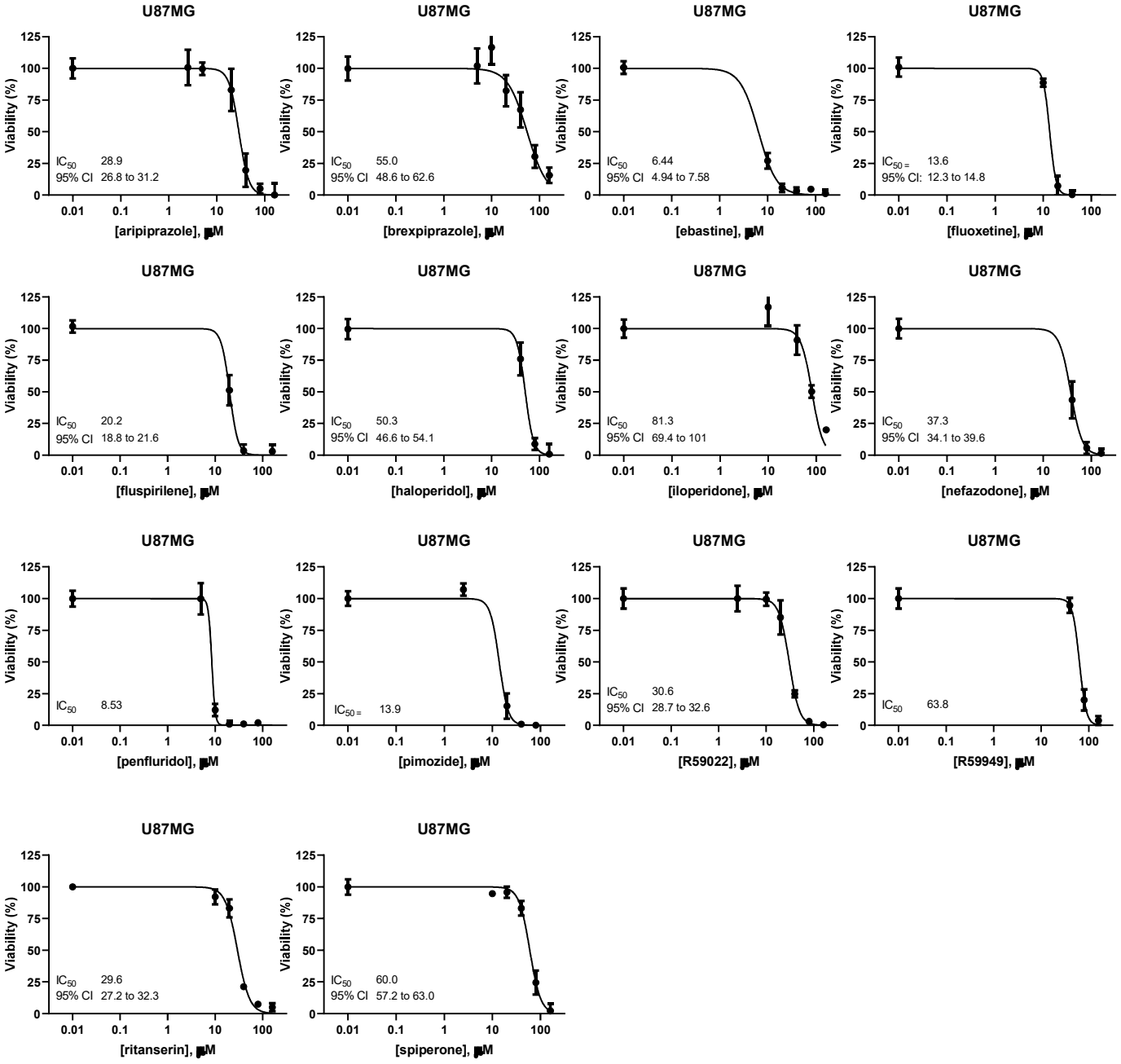
U87MG
Viability (%)
IC50 28.9
95% CI 26.8 to 31.2
[aripiprazole], μM
U87MG
IC50 55.0
95% CI 48.6 to 62.6
[brexpiprazole], μM
U87MG
IC50 6.44
95% CI 4.94 to 7.58
[ebastine], μM
U87MG
IC50 = 13.6
95% CI: 12.3 to 14.8
[fluoxetine], μM
U87MG
IC50 20.2
95% CI 18.8 to 21.6
[fluspirilene], μM
U87MG
IC50 50.3
95% CI 46.6 to 54.1
[haloperidol], μM
U87MG
IC50 81.3
95% CI 69.4 to 101
[iloperidone], μM
U87MG
IC50 37.3
95% CI 34.1 to 39.6
[nefazodone], μM
U87MG
IC50 8.53
[penfluridol], μM
U87MG
IC50 = 13.9
[pimozide], μM
U87MG
IC50 30.6
95% CI 28.7 to 32.6
[R59022], μM
U87MG
IC50 63.8
[R59949], μM
U87MG
IC50 29.6
95% CI 27.2 to 32.3
[ritanserin], μM
U87MG
IC50 60.0
95% CI 57.2 to 63.0
[spiperone], μM

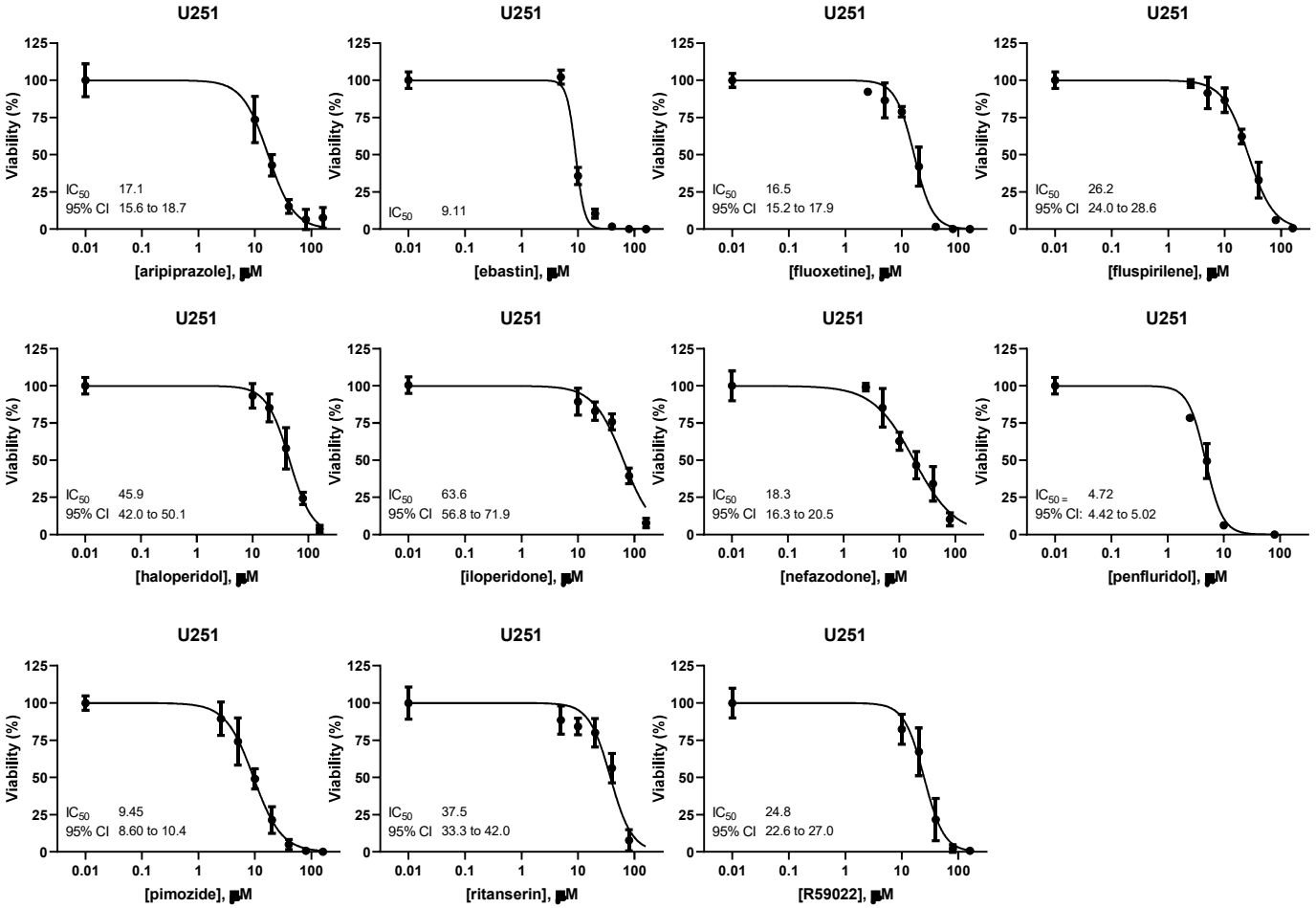

Supplementary figure 2. Dose response curves showing the cytotoxic effect of psychotropic drugs on neoplastic cells. Cells were treated for 72 h with scalar doses of drugs ranging from 10 to 160 µmol/L. Viabilities were assessed by MTT assay, normalized for cells treated with vehicle only and expressed as percentage. The best fit values of IC_{50} values were calculated the by using a variable slope model (GraphPad Prism 7). Each data point represents the mean of at least three independent experiments. IC_{50}, drug concentration reducing by 50% viability compared to control; 95% CI, 95% confidence interval.

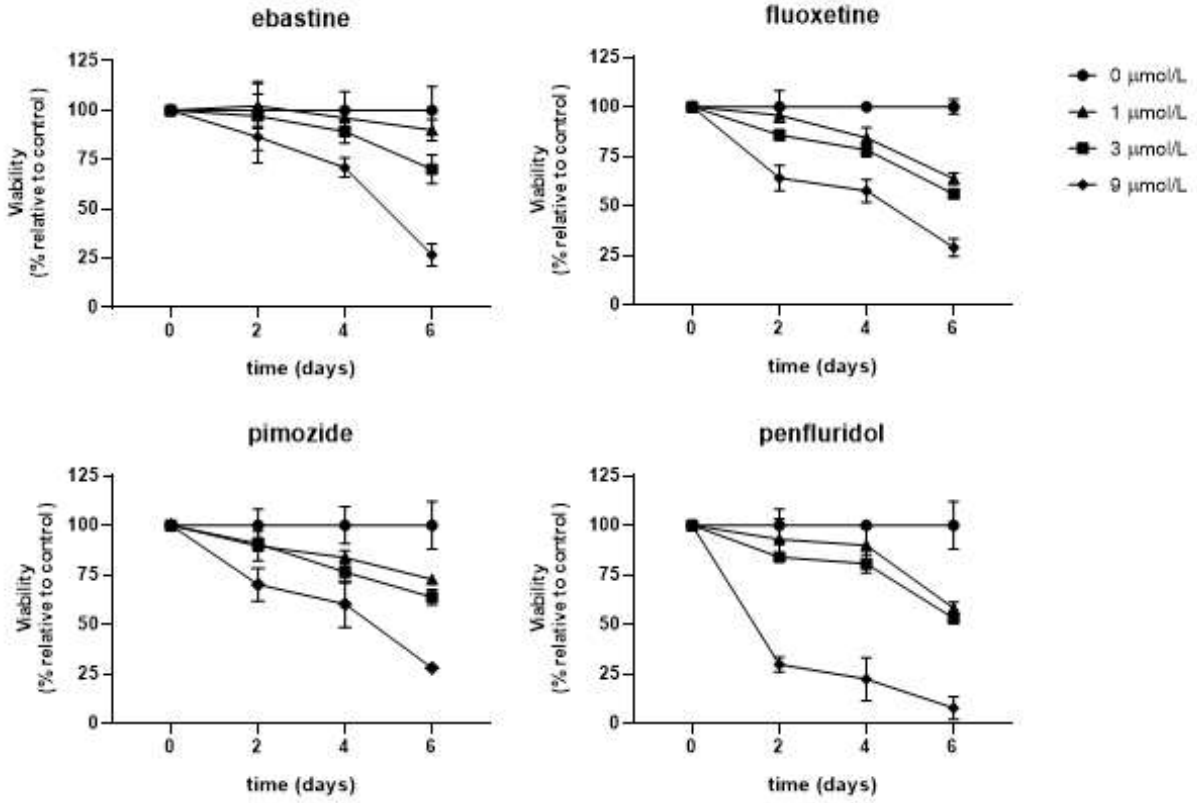

Supplementary Figure 3. Dose and time response curves showing the cytotoxic effect of ebastine, fluoxetine, pimozide and penfluridol on MCF7 cells. Cell were treated for 6 days with increasing doses of drugs. Viabilities were assessed by MTT assay and normalized relative to controls treated with vehicle only. Data are expressed as the mean ± SD of one representative out of three independent experiments performed in quintuplicate.3

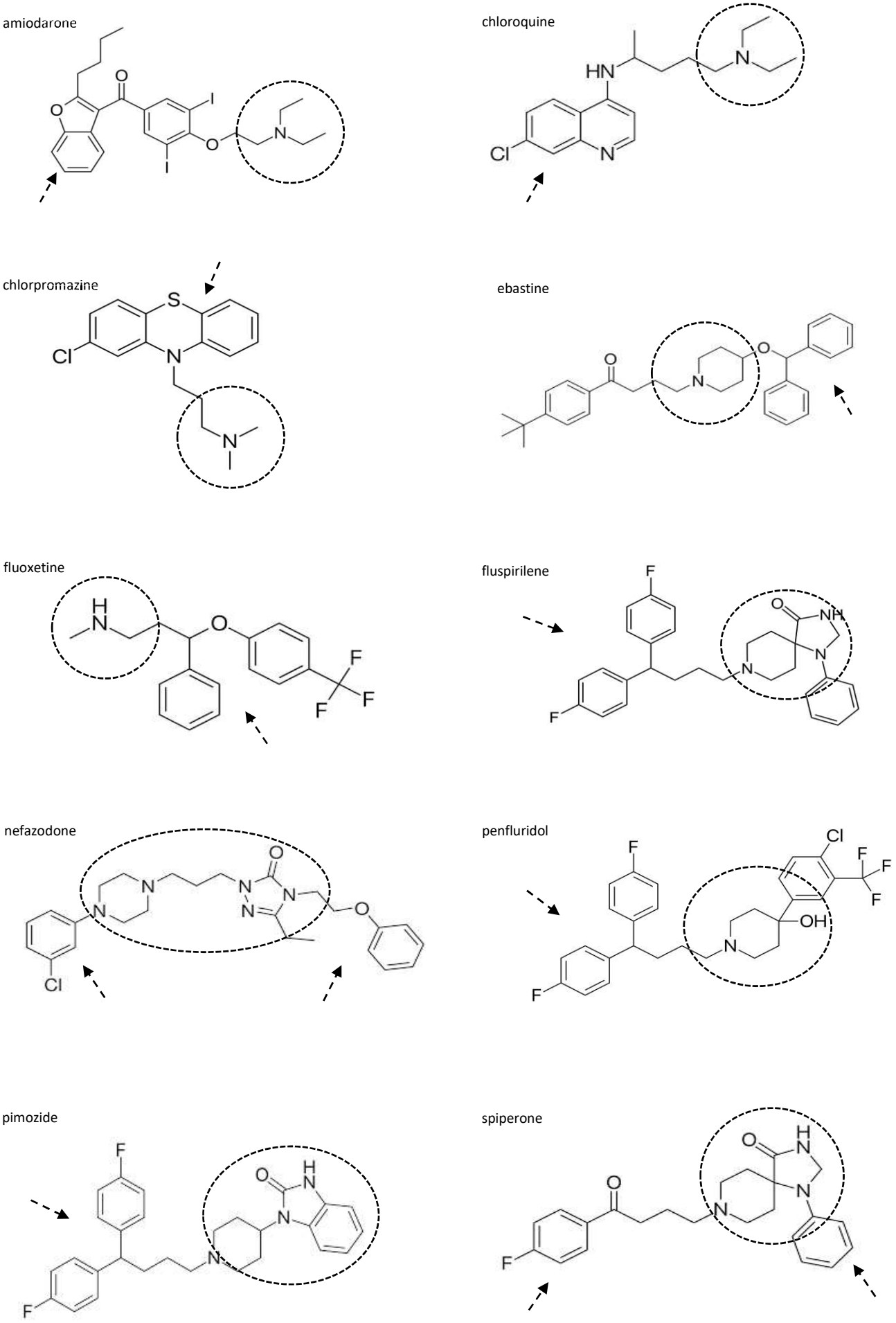

Supplementary Figure 4. CADs features of psychotropic drugs with antitumoral activity. Structure of cationic amphiphilic drugs and psychotropic drugs are shown. Circles indicate the hydrophilic region containing an amine group protonated at physiological pH, arrows indicate the hydrophobic region containing aromatic groups.

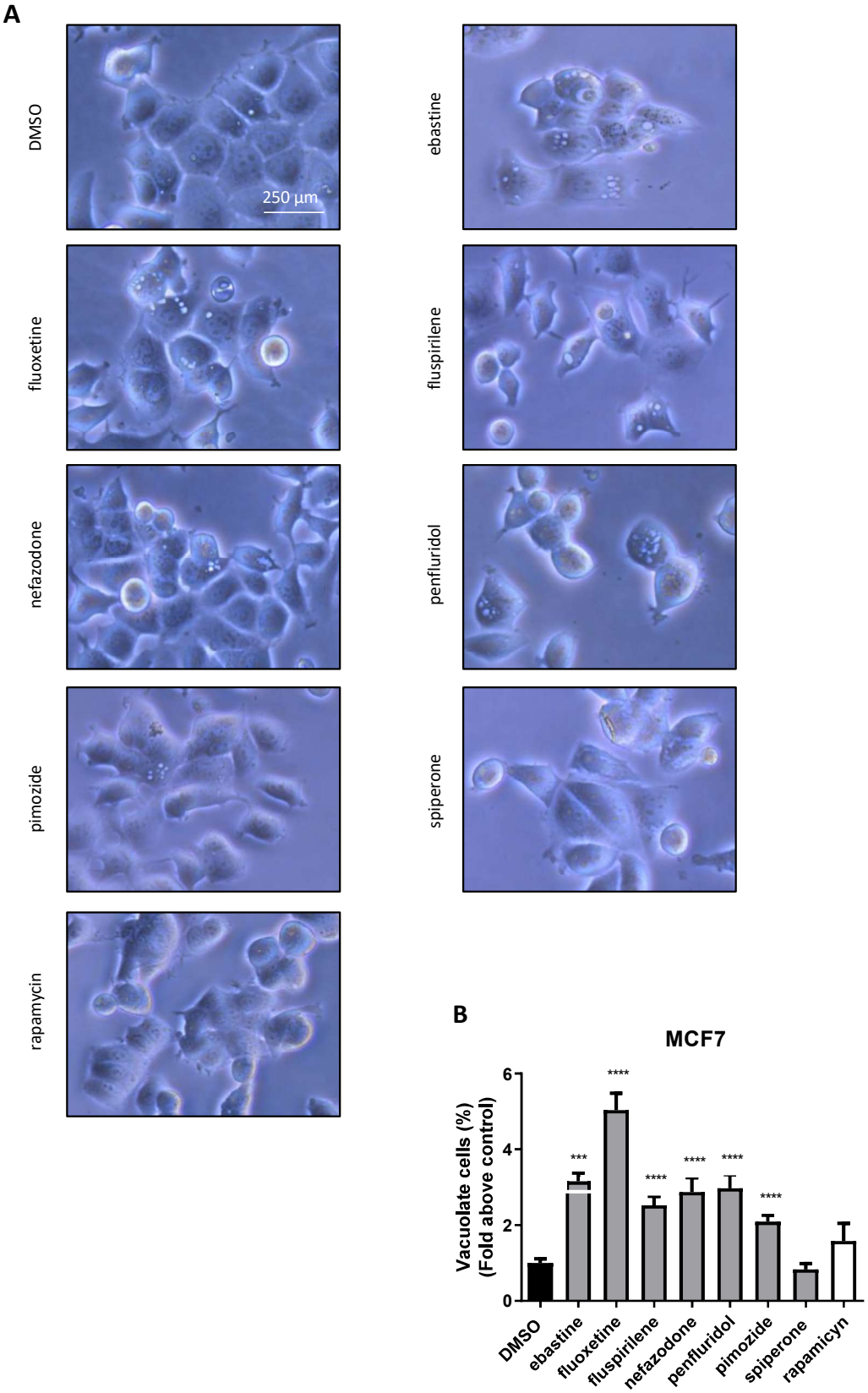

Supplementary Figure 5. Vacuolar structures formation after treatment of MCF7 cells with psychotropic drugs. Morphological alterations associated with the treatment of MCF7 cells with psychotropic drugs (5 µmol/L) were investigated after 6 h of exposure by phase contrast microscopy (original magnification 20x). Representative images of cells treated with DMSO, positive control, ebastine, fluoxetine, fluspirilene, nefazodone, penfluridol, pimozide, spiperone and rapamycin, positive control (A). Histogram showing quantification of vacuoles as fold change relative to control (B). Data are expressed as the mean ± SD of a representative experiment out of three independent experiments performed in triplicate. **, Student's T-test $p < 0.01$; ***, Student's T-test $p < 0.001$.

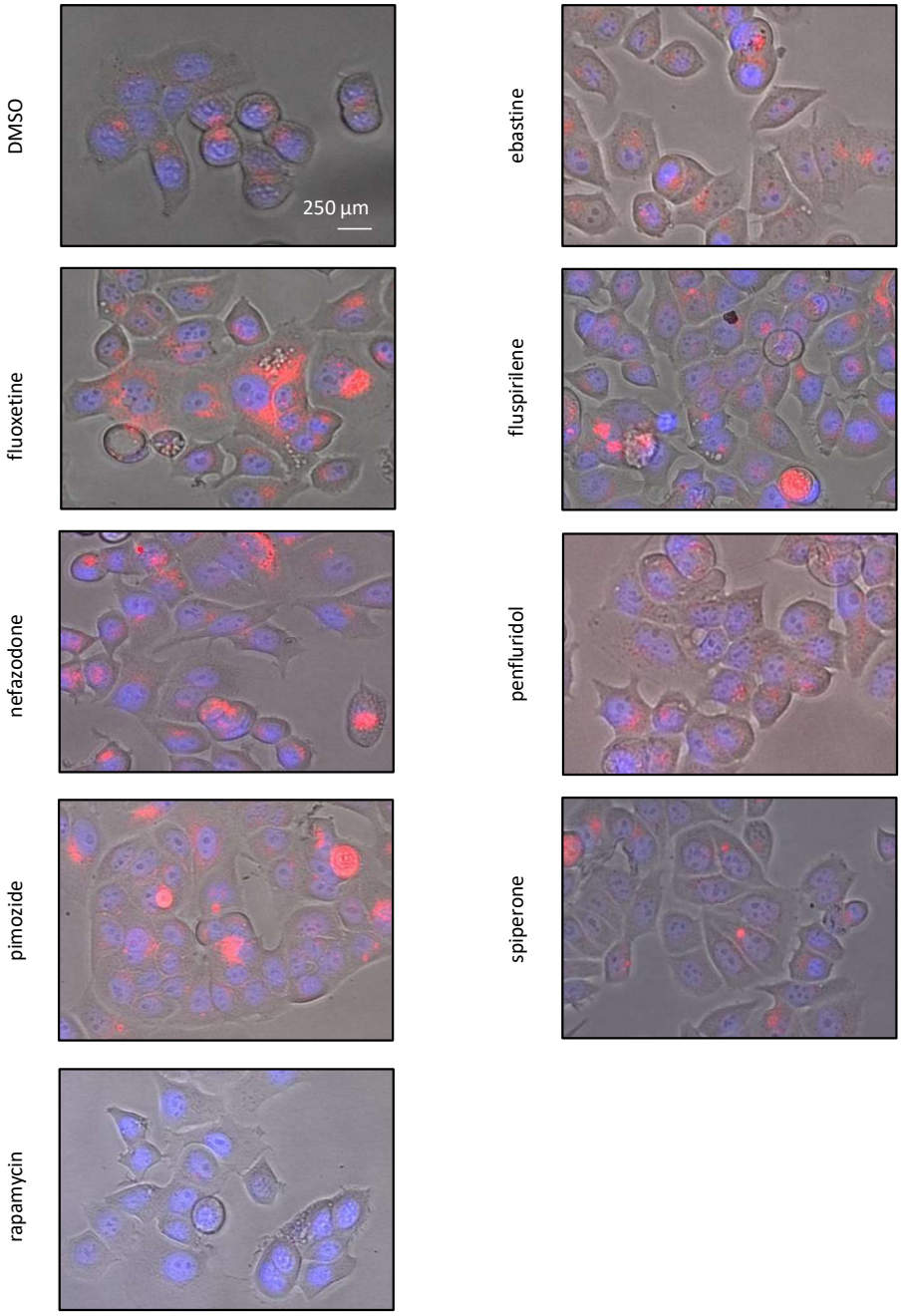

Supplementary Figure 6. Psychotropic drugs induce acidic compartment formation perturbing lysosomal and autophagic functioning. Vacuolar structures associated to treatment with psychotropic drugs in MCF7 were analyzed, after 6h exposure, staining cells with Lysotracker Deep Red. Pictures were acquired at fluorescence microscopy (magnification: 20x). representative images of cells treated with DMSO, negative control, ebastine, fluoxetine, fluspirilene, nefazodone, penfluridol, pimozide, spiperone and rapamycin

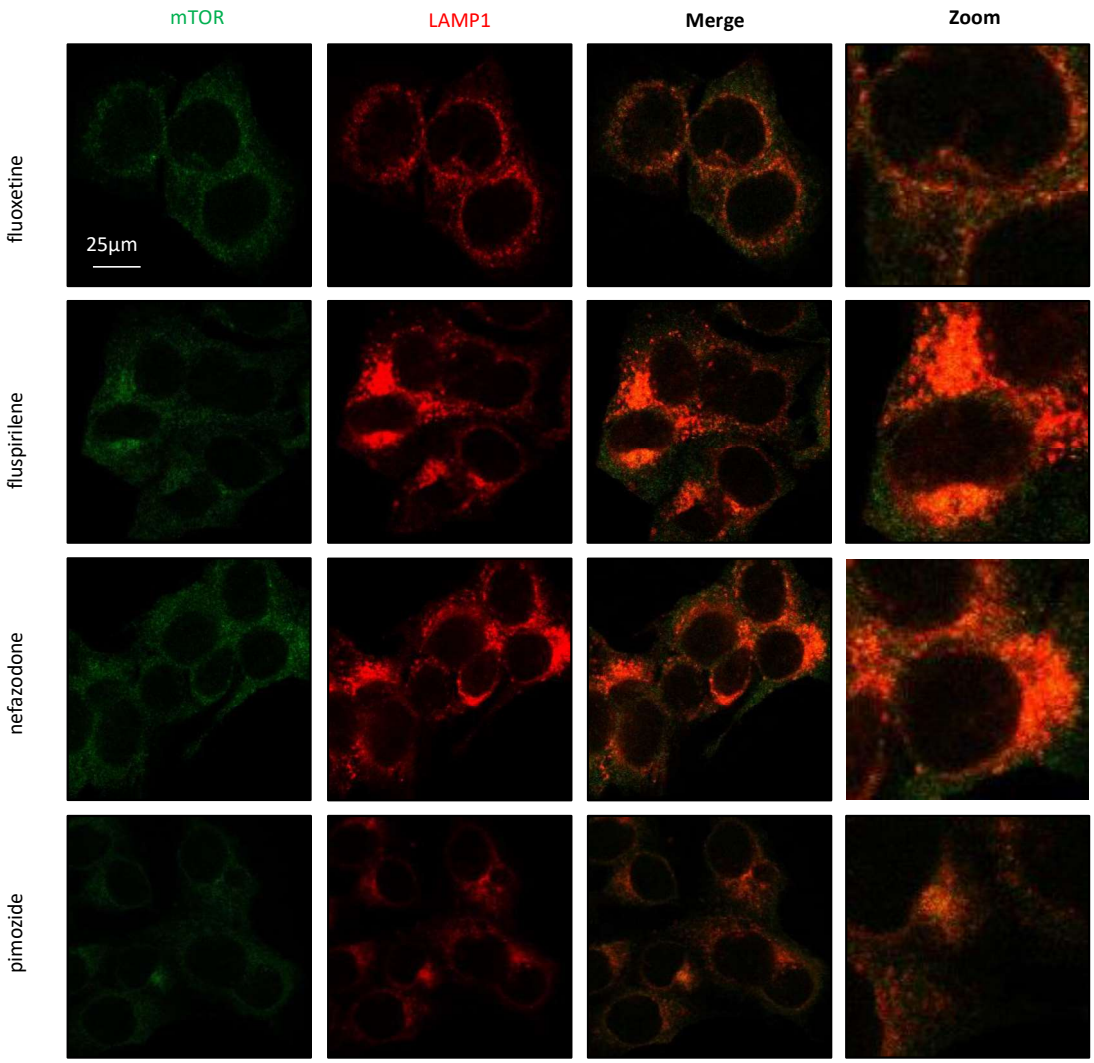

Supplementary Figure 7. Psychotropic drugs alter autophagy flux through mTOR pathway inhibition. Delocalization of mTOR from lysosomal membrane was evaluated in MCF7 after 16h treatment with psychoactive drugs. mTOR was stained using mTOR primary antibody and Alexa Fluor 488 secondary antibody (green). Lysosomes were stained using LAMP1 primary antibody and Alexa Fluor 536 secondary antibody (red). Representative images of fluoxetine, fluspirilene, nefazodone, pimozide

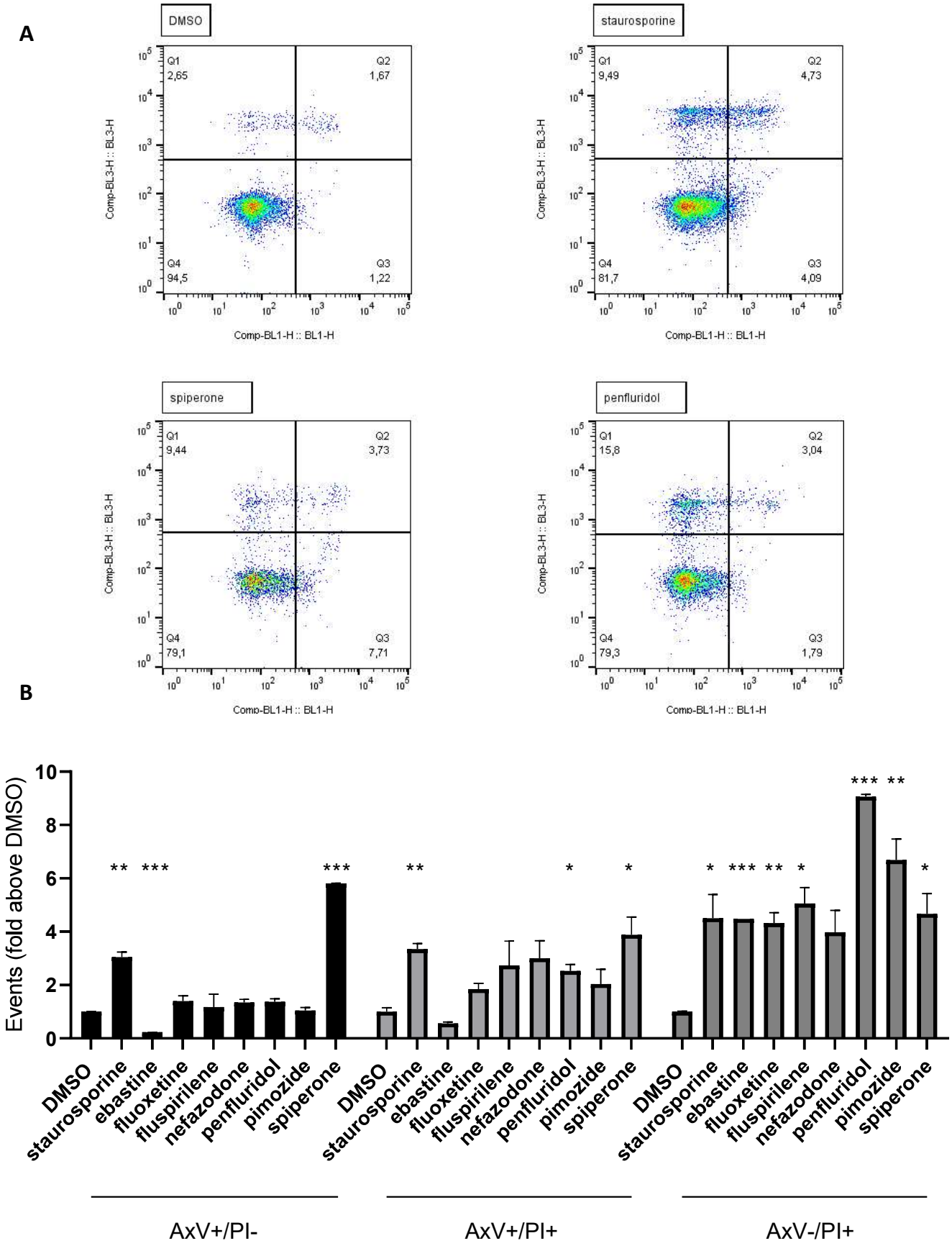

Supplementary Figure 8. Spiperone induces apoptosis in MCF7 cells. MCF7 cells treated for 48 hours with vehicle and psychotropic drugs at a concentration of 10 µmol/L for all the drugs except for penfluridol, 5 µmol/L. Staurosporine 0.5 µmol/L was used as apoptosis positive control. (A) representative populations observed by FACS analysis. (B) Graph showing Annexin V and Propidium Iodide positive/negative events as fold change relative to vehicle (DMSO). Data show mean ± SD of one representative experiment out of three independent experiments performed in duplicate. *, Student's T-test $p < 0.05$; **, Student's T-test $p < 0.01$; ***, Student's T-test $p < 0.001$

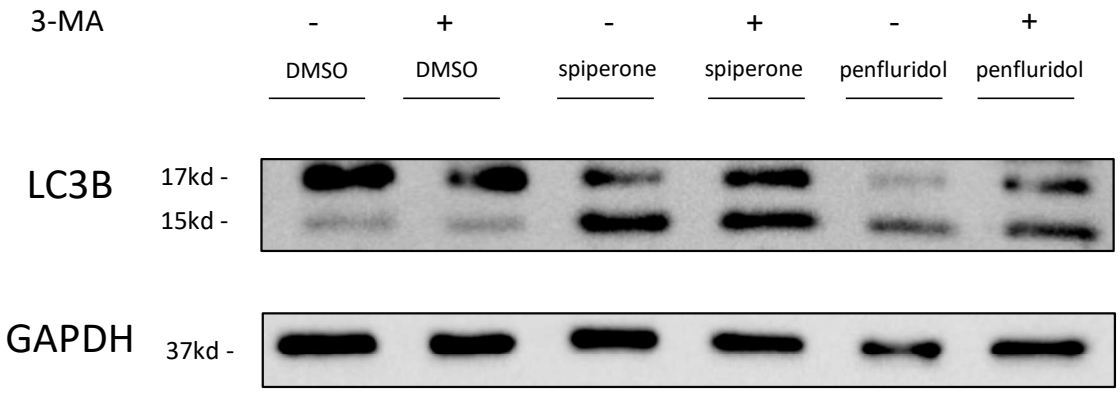

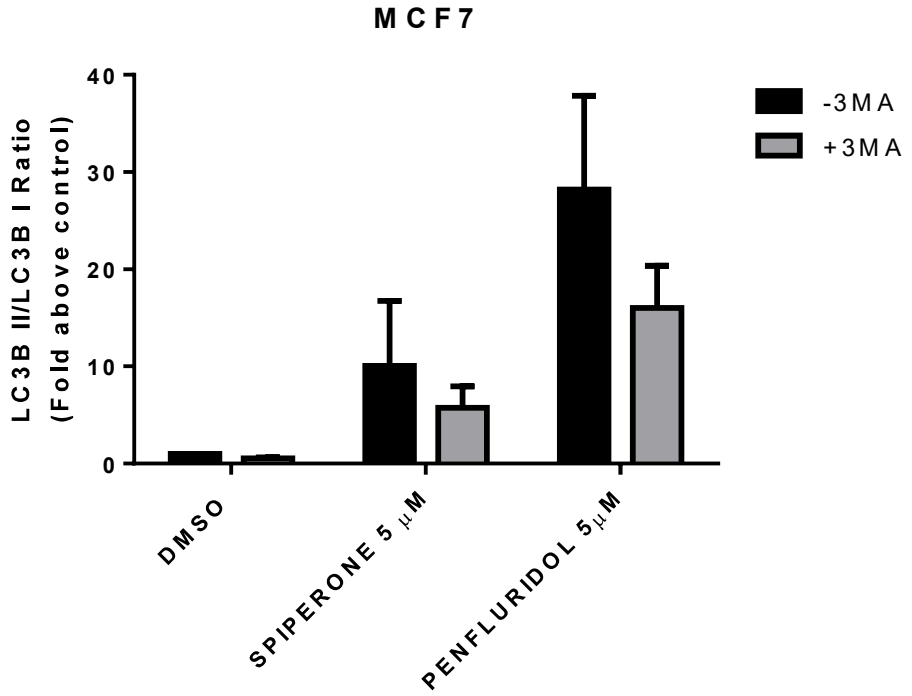

Supplementary Figure 9. 3-MA does not induce LC3B expression upon psychotropic drugs stimulation. Western blot analysis showing effects on autophagic pathway after 16 hours treatment with spiperone and penfluridol plus 3-MA on MCF7. Lysates analyzed LC3B and GAPDH (A). Histogram showing quantification of the relative expression of LC3B II/I. Densitometry are expressed as the mean ± SD of three independent experiments.

8. Publications

frontiers in Oncology

ORIGINAL RESEARCH
published: 19 October 2020
doi: 10.3389/fonc.2020.562196

Psychotropic Drugs Show Anticancer Activity by Disrupting Mitochondrial and Lysosomal Function

Marco Varalda[1,2†], Annamaria Antona[1†], Valentina Bettio[1,2], Konkonika Roy[3], Ajay Vachamaram[1,3], Vaibhav Yellenki[1], Alberto Massarotti[4], Gianluca Baldanzi[1,3] and Daniela Capello[1,2]*

[1] Department of Translational Medicine, Centre of Excellence in Aging Sciences, University of Piemonte Orientale, Novara, Italy, [2] UPO Biobank, University of Piemonte Orientale, Novara, Italy, [3] Center for Translational Research on Allergic and Autoimmune Diseases (CAAD), University of Piemonte Orientale, Novara, Italy, [4] Department Pharmaceutical Sciences, University of Piemonte Orientale, Novara, Italy

Background and Purpose: Drug repositioning is a promising strategy for discovering new therapeutic strategies for cancer therapy. We investigated psychotropic drugs for their antitumor activity because of several epidemiological studies reporting lower cancer incidence in individuals receiving long term drug treatment.

Experimental Approach: We investigated 27 psychotropic drugs for their cytotoxic activity in colorectal carcinoma, glioblastoma and breast cancer cell lines. Consistent with the cationic amphiphilic structure of the most cytotoxic compounds, we investigated their effect on mitochondrial and lysosomal compartments.

Results: Penfluridol, ebastine, pimozide and fluoxetine, fluspirilene and nefazodone showed significant cytotoxicity, in the low micromolar range, in all cell lines tested. In MCF7 cells these drugs caused mitochondrial membrane depolarization, increased the acidic vesicular compartments and induced phospholipidosis. Both penfluridol and spiperone induced AMPK activation and autophagy. Neither caspase nor autophagy inhibitors rescued cells from death induced by ebastine, fluoxetine, fluspirilene and nefazodone. Treatment with 3-methyladenine partially rescued cell death induced by pimozide and spiperone, whereas enhanced the cytotoxic activity of penfluridol. Conversely, inhibition of lysosomal cathepsins significantly reduced cell death induced by ebastin, penfluridol, pimozide, spiperone and mildly in fluoxetine treated cells. Lastly, Spiperone cytotoxicity was restricted to colorectal cancer and breast cancer and caused apoptotic cell death in MCF7 cells.

Conclusions: The cytotoxicity of psychotropic drugs with cationic amphiphilic structures relied on simultaneous mitochondrial and lysosomal disruption and induction of cell death that not necessarily requires apoptosis. Since dual targeting of lysosomes and mitochondria constitutes a new promising therapeutic approach for cancer, particularly those in which the apoptotic machinery is defective, these data further support their clinical development for cancer therapy.

Keywords: lysosomotropism, cationic amphiphilic drugs (CADs), autophagy, psychotropic drug, cancer, repositioning

OPEN ACCESS

Edited by:
Brian Gabrielli, The University of Queensland, Australia

Reviewed by:
Vladimir Trajkovic, University of Belgrade, Serbia
Xiuli Dan, National Institute on Aging, National Institutes of Health (NIH), United States

***Correspondence:**
Daniela Capello
daniela.capello@med.uniupo.it

† These authors share first authorship

Specialty section:
This article was submitted to Pharmacology of Anti-Cancer Drugs, a section of the journal Frontiers in Oncology

Received: *14 May 2020*
Accepted: *15 September 2020*
Published: *19 October 2020*

Citation:
Varalda M, Antona A, Bettio V, Roy K, Vachamaram A, Yellenki V, Massarotti A, Baldanzi G and Capello D (2020) Psychotropic Drugs Show Anticancer Activity by Disrupting Mitochondrial and Lysosomal Function. Front. Oncol. 10:562196. doi: 10.3389/fonc.2020.562196

INTRODUCTION

Cancer represents a major public health problem, with total cure remaining elusive for most cancer types (1, 2). Chemotherapy resistance in patients with recurrent and advanced disease (3) and strong systemic toxicity, especially in elderly (4), have raised concerns over the progress of cancer therapy, making it necessary to change the paradigm in the search for new treatments, more effective and with milder adverse effects. Thus, alternative cell death pathways capable of killing apoptosis- and therapy resistant cancer cells, have gained vast interest among cancer researchers, leading to the identification of autophagy and lysosomal cell death programs as attractive means to circumvent therapy resistance (5–8). Lysosomal activation is common in aggressive cancers, where lysosomes promote disease progression and treatment resistance (9–13). In cancer, cell transformation increases the requirement for new biomass production, and the core function of the lysosomes is to recycle endogenous or exogenous macromolecules to provide energy and metabolic precursors for the synthesis of new cell mass. In response to typical challenges encountered by cancer cells, such as nutrient starvation, growth factor withdrawal, energy depletion, organelle damage, or accumulation of abnormal proteins, autophagy is further enhanced to meet the cellular needs (10, 13). In certain circumstances, however, the prolonged over activation of the autophagosomal/lysosomal pathway can lead to autophagic-dependent cell death a caspase-independent form of programmed cell death (14), that can be evaluated as an alternative cancer treatment modality (15). On the other hand, since many tumors are highly dependent on autophagy for survival and treatment resistance, pharmacological inhibition of lysosomal activity can limit the growth of advanced diseases and improve response to therapy (5, 16). Moreover, the cancer-associated changes in lysosomal composition result in reduced lysosomal membrane stability, thereby sensitizing tumor cells to lysosome-dependent cell death (LDCD) (17). The main feature LDCD is lysosomal membrane permeabilization (LMP) (17, 18) with translocation to the cytoplasm of the lysosomal contents, including cathepsins, which act as the main executors of this cell death modality (19). Mitochondria have a well-recognized role in the production of ATP, metabolic intermediates and also participate in several signaling pathways; accumulating evidence now suggests that mitochondrial bioenergetics, biosynthesis and signaling are required for tumorigenesis. Thus, emerging studies have begun to demonstrate that mitochondrial functions are a potentially fruitful field for cancer therapy (20, 21). Drug repositioning is a strategy for identifying new uses for approved drugs that are outside the scope of the original medical indication (22, 23) and psychotropic medications are promising compounds for cancer treatment. Epidemiological studies have repeatedly reported that individuals who are receiving long term drug treatment with antipsychotics (24, 25), anti-depressant (26–28) or anti-allergic drugs (29) have a lower cancer incidence than the general population, suggesting that these medications might have a direct effect on neoplastic cells. Pre-clinical studies confirmed the direct anti-tumoral activity of these compounds in a wide range of malignancies (30–34). However, despite the large body of experimental evidence, the mechanisms of actions of these compounds in cancer cells remain poorly defined.

In this study we screened a panel of psychotropic compounds for their cytotoxicity in different tumor cell lines to clarify the pharmacological properties underpinning their clinical application for cancer therapy. We identified a group of drugs characterized by cationic amphiphilic properties impairing both mitochondrial and lysosomal function and reducing cancer cells viability at clinically relevant concentrations.

METHODS

Cell Culture

HCT116, SW620, MCF7, MDA-MB-231, U87 and U251 cell lines were purchased from the American Type Culture Collection (ATCC). HCT116, MCF7, and U251 cells were cultured in Dulbecco's Modified Eagle Medium (DMEM, Gibco; Life Technologies) supplemented with 10% fetal bovine serum (FBS, Euroclone) and 1% antibiotics and antimycotics (Penicillin, Streptomycin, Amphotericin, Sigma). SW620 and MDA-MB-213 cells were cultured in RPMI-1640 (Gibco, Life Technologies) with 10% fetal bovine serum (FBS, Euroclone) and 1% antibiotics and antimycotics (Penicillin, Streptomycin, Amphotericin, Sigma). U87 cells were cultured in Minimum Essential Medium (MEM, Gibco; Life Technologies) with 10% FBS and 1% antibiotics and antimycotics. All the cell lines were maintained in incubator at 37°C with 5% CO_2.

Drugs

Psychotropic drugs used in the screening were purchased from Cayman Chemicals, Sigma, TCI Chemicals and Selleck Chemicals. List of drug used: aripiprazole, brexpiprazole, cetirizine, diphenhydramine, droperidol, ebastine, fluoxetine, fluspirilene, haloperidol, iloperidone, ketanserin, metoclopramide, nefazodone, paliperidone, penfluridol, pimozide, pipamperone, R59022, R59949, risperidone, ritanserin, spiperone, trazodone, urapidil, way-100135, and ziprasidone. All drugs were dissolved in DMSO at a 10 mmol/L concentration and stored, in small aliquots at −20°C.

MTT Viability Assay

For each cell line, 1000 cells/well were plated in a volume of 100 μL in 96 wells plate. Cells were treated with different concentrations of drug (160, 80, 40, 20, and 10 μmol/L) and incubated for 72 h. For each concentration of drug, the same concentration of vehicle (DMSO) was used as control. MTT (thiazolyl blue tetrazolium bromide, Sigma) 0.5 mg/ml was, then, added to each well and incubated for 4 h at 37°C and 5% CO_2. Crystals were dissolved using 100 μl of acidic isopropanol (4 mmol/L HCl) and the absorbance (570 and 650 nm) was read at the spectrophotometer (Victor, PerkinElmer).

To perform viability assay with biogenic amines 4,000 cells/well from MCF7 and HCT116 were plated in 96 wells plate. Cells were treated with different doses of serotonin, dopamine and histamine (Cayman Chemicals) in DMEM 0% FBS and viability was evaluated after 24- and 48-h treatment by MTT assay.

Viability Rescue Assay

To perform viability rescue experiments, 1,500 MCF7 cells were plated in 96 wells plate and treated with 10 μmol/L spiperone, nefazodone, fluoxetine, fluspirilene, ebastine, pimozide or 5 μmol/L penfluridol in combination with vehicle alone (DMSO), or with 5 μmol/L carbobenzoxy-valyl-alanyl-aspartyl-[O-methyl]fluoromethylketone (zVAD-fmk, AdipoGen), 2.5 mmol/L 3-methyladenine (3-MA, AdipoGen), 5 mmol/L N-[[(2S,3S)-3-[(propylamino) arbonyl]-2-oxiranyl]carbonyl]-L-isoleucyl-L-proline, methyl ester (CA-074 me, Cayman Chemical), 5 μmol/L cyclosporin A (Cayman Chemical) and 5 μmol/L N-Acetyl-L-cysteine (NAC, Sigma Aldrich). MTT viability assay was performed after 72 h as previously described, except for NAC where, prior to MTT adding, medium was removed and each well was washed with 100 μL of phosphate buffered saline. For biogenic amines viability rescue, 1,500 MCF7 cells were seeded in 96 wells plate and treated with IC_{50} concentration of the following drugs: spiperone, nefazodone, fluoxetine, fluspirilene, ebastine, pimozide, penfluridol in combination with vehicle (DMSO) or 5 μmol/L dopamine, serotonin or histamine. MTT viability assay was performed as described before after 24, 48, and 72 h.

Apoptosis Assay

Fifty thousand MCF7 cells were plated in 24 wells plate and treated for 48 h with 10 μmol/L fluoxetine, ebastine, pimozide, fluspirilene, spiperone, nefazodone, or 5 μmol/L penfluridol.

Cells were then stained following the manufacturer's instruction (AdipoGen). Briefly, cells were incubated for 10 min at room temperature with annexin binding buffer 1X (10 mmol/L HEPES/NaOH, pH 7.4, 140 mmol/L NaCl, 2.5 mmol/L CaCl2) containing Annexin V-FITC. Lastly, cells were washed and resuspended in annexin binding buffer 1X. Propidium iodide was added to all the samples 5 min before FACS analysis (Attune Nxt, Flow Cytometer, Thermo Fisher Scientific). Data were analyzed with FlowJo™ software (Becton, Dickinson and Company).

Migration Assay

Migration assay was performed using culture-insert 2 well in μ-dish (ibidi GmbH, Martinsried, Germany) as previously described (35). Briefly 30,000 HCT116 cells and 25,000 MCF7 cells were plated in each side of the insert in 24 wells plate. After 24 h, inserts were removed, and cells were treated with respective psychotropic drugs (5 μmol/L) or DMSO (0.05%) in complete medium. Images were acquired at 0 and 24 h after treatment, with phase contrast microscope and analyzed through ImageJ software (NIH, USA). Data were shown as % of closure rate relative to time 0.

Vacuolization Assay

MCF7 cells were plated at the concentration of 25,000 cells/well in 48 wells plate and then treated with fluoxetine, ebastine, penfluridol, pimozide, fluspirilene, spiperone, nefazodone at the concentration of 5 μmol/L or rapamycin (10 μmol/L). After 2 h treatment one well from each treatment was treated with bafilomycin A1 (50 nmol/L) or 3-MA (1 mmol/L). Pictures were acquired with a phase contrast microscope 4 and 6 h after treatment, images were analyzed by ImageJ software. Analysis shows the percentage of vacuolization rate for each treatment.

Mitochondrial Membrane Potential Analysis

Mcf7 cells were plated at the concentration of 20,000 cells/well in 48 wells plate and treated with 5 μmol/L fluoxetine, ebastine, fluspirilene, nefazodone penfluridol, pimozide, spiperone. DMSO 0.05% was used as negative control. After treatment, cells were stained with 10 μg/ml JC-1 dye (Adipogen) in PBS for 30 min in the dark at 37°C. FCCP (Cayman chemicals) was added for 15 min after the staining as positive control. Signals were acquired with a fluorescence microscope (FLoid Cell Imaging Station, Life Technology) and images were analyzed by ImageJ software calculating red/green fluorescence ratio.

Lysotracker Assay

MCF7 cells were plated at the concentration of 20,000 cells/well in 48 wells plate and treated with 5 μmol/L fluoxetine, ebastine, fluspirilene, nefazodone penfluridol, pimozide, spiperone or 10 μmol/L rapamycin for 16 h. After the treatment, medium was removed and cells were stained with Lysotracker Deep Red (Invitrogen, 50 nmol/L) and Hoechst 33342 (5 μg/ml) for nuclei staining, in the dark at 37°C for 30 min. Signals were acquired with a fluorescence microscope (FLoid Cell Imaging Station, Life Technology). Lysotracker red signal/blue nuclei signal was analyzed by ImageJ software.

Phospholipidosis Assay

MCF7 cells were plated at the concentration of 20,000 cells/well in 48 wells plate and treated with 5 μmol/L ebastine, fluoxetine, fluspirilene, nefazodone penfluridol, pimozide, spiperone or 10 μmol/L rapamycin and stained with 1X LipidTox green (Thermo Fisher Scientific) for 16 h.

Subsequently, nuclei were stained using Hoechst 33342 (5 μg/ml) and plate was incubated for 30 min in the dark at 37°C. Afterwards, cells were washed with PBS and fixed with paraformaldehyde 4% for 15 min in the dark. Signals were acquired with a fluorescence microscope (FLoid Cell Imaging Station, Life Technology) and images were analyzed by ImageJ software.

Western Blotting

MCF7 cells were plated at the concentration of 150,000 cells/well in 6 wells plate and treated with 5 μmol/L ebastine, fluoxetine, fluspirilene, nefazodone penfluridol, pimozide, spiperone for 16 h. For experiment of autophagic flux two conditions were carried out for each drug: drug alone and co-treatment of drug and chloroquine 50 μmol/L. For experiment to evaluate LC3B expression upon 3-MA treatment, cells were pre-treated with 3-MA 1 mmol/L for 2 h and then cotreated with spiperone and penfluridol 5 μmol/L for 16 h. After treatments, whole cell lysates were prepared using RIPA lysis buffer (25 mmol/L Hepes pH 8, 135 mmol/L NaCl, 5 mmol/L EDTA, 1 mmol/L EGTA, 1 mmol/L ZnCl2, 50 mmol/L NaF, 1% Nonidet P40, 10% glycerol) with protease inhibitors (AEBSF, aprotinin, bestatin,

E-64, EDTA, leupeptin, Sigma-Aldrich) and orthovanadate. Lysates were then kept on a wheel for 20 min at 4°C and after centrifuged at 12,500 g for 15 min. Proteins contained in the samples were collected and quantified using Pierce BCA protein assay kit (Thermo Fisher Scientific). Successively, proteins were denatured at 95°C for 5 min in presence of 2% Sodium Dodecyl Sulfate (SDS), 150 mmol/L dithiothreitol (DTT) and 0.01% bromophenol blue. Electrophoresis of the samples was performed using 6, 8, 10, or 15% polyacrylamide gels and proteins were transferred from the gel to a PolyVinylidene DiFluoride membrane (PVDF, Amersham). Lastly, the membrane was saturated using 3% Bovine Serum Albumin (BSA, Sigma) in TBS/Tween-20 0.1% [Tris Buffered Saline 1X containing Trizma base 50 mmol/L, NaCl 120 mmol/L, 0.1% Polyethylene glycol sorbitan monolaurate (Tween-20)] for 1 h and incubated with primary antibody dissolved in the same buffer with sodium azide 0.01%. Primary antibodies were anti-LC3B (Thermo Scientific), anti-P-P70S6K T389 (Cell Signaling Technology), anti-P70S6K (Cell Signaling Technology), anti-P-S6 S235/236 (Cell Signaling Technology), anti-S6 (Cell Signaling Technology) anti-P-AMPKα T172 (Cell Signaling Technology), anti-AMPK (Cell Signaling Technology), anti-GAPDH (Cell Signaling Technology). The day after, primary antibody was removed and the membrane was washed with TBS-Tween-20 0.1% for 15 min three times and then incubated with horseradish peroxidase conjugated secondary anti-mouse or anti-rabbit antibody (Perkin Elmer Life Science) diluted 1:3000 in TBS-Tween-20 0.1% for 45 min. After washing, reading of the membrane was performed using ECL Western Lightning Chemiluminescence Reagent Plus (Perkin Elmer Life Science) and images acquired with the Chemidoc Touch (Bio-Rad).

Immunofluorescence Microscopy Analysis

MCF7 cells at the concentration of 50,000 cells/well were seeded onto glass coverslips and treated with 5 μmol/L fluoxetine, ebastine, penfluridol, pimozide, fluspirilene, spiperone, nefazodone for 16 h. After the treatment, cells were washed with PBS and fixed with PFA 4% for 10 min at room temperature and washed with PBS. Then cells were permeabilized incubating with cold HEPES-Triton X-100 (20 mM HEPES pH 7.4, 300 mM sucrose, 50 mM NaCl, 3 mM $MgCl_2$, 0.5% Triton X-100) for 5 min at 4°C. Cells were washed with 0.2% PBS-BSA and saturated using 2% PBS-BSA for 15 min before placing primary antibodies.

Antibodies used in these experiments were anti-mTOR (Cell Signaling Technology), anti-Galectin-1 (Santa Cruz Biotechnology), anti-LAMP1 (Santa Cruz Biotechnology). Cells were incubated with primary antibodies for 30 min, then washed, saturated with 2% PBS-BSA and incubated with secondary antibodies conjugated with Alexa Fluor-488, −536 (Invitrogen) and DAPI for 30 min.

After the incubation, glasses were mounted on glass slides using Mowiol (20% Mowiol 4–88, 2.5% DABCO in PBS, pH 7.4). Images were acquired at confocal microscope Leica TCS SP8 or fluorescence microscope DM5500B (Leica) and analyzed using ImageJ software.

Compounds Chemical Analysis

The properties of the compounds (LogP and basic pKa) were investigated using ACD/ LAB software. As reported in the publication of Muehlbacher (36) there is not a clear CADs classification based on chemical properties. We decided to apply the same parameters based on LogP and pKa applied in the Muehlbacher's manuscript. In particular, compounds were considered CADs when LogP $>$ 3, for the amphiphilic characteristics, and a PKa $>$ 7.4 for the cationic characteristics.

Statistical Analysis

Prism 8.0 software was used for statistical analysis (GraphPad software Inc., San Diego, CA). In viability assays, IC_{50} was determined using a variable slope model referring to the values obtained during the assay; a semi-logarithmic dose-response curve was created.

Statistical significance was analyzed using Student's *t*-test with $p < 0.05$ as the criterion of significance when two groups were compared. Analysis of contingency tables were performed using Prism 8.0 software (GraphPad software Inc., San Diego, CA) and statistical significance was evaluated using Fisher exact test with $p < 0.05$.

RESULTS

The Antitumoral Activity of Psychotropic Drugs Transcends the Conventional Therapeutic Classes and Tumor Type

To identify compounds with potential, clinically relevant, anticancer activity we first assessed their effect on six different tumor types represented by two colorectal cancer (CRC; HCT116 and SW620), two breast cancer (BC, MCF7, and MDA-MB-231) and two glioblastoma (GB; U87MG and U251MG) cell lines. Cells were treated for 72 h with scalar doses of drugs ranging from 10 to 160 μmol/L. The screened drugs ($N = 26$) were represented by antipsychotics ($n = 14$), antidepressant ($n = 2$), antihistamines ($n = 3$) and three compounds used in scientific research with reported serotonin receptors antagonistic activity (**Figure 1**, **Supplementary Figure 1**, **Supplementary Table 1**). For drugs that induced more than 50% cell viability reduction at a concentration lower than 100 μmol/L, in a dose-dependent manner, the IC_{50} values were calculated (**Supplementary Figure 2**, **Supplementary Table 1**).

The most effective drugs in all cell lines tested belonged to all three pharmacological classes investigated (antipsychotics, antidepressants, and antihistamines) (**Figure 1**, **Supplementary Figures 1**, **2**, **Supplementary Table 1**). The six most potent drugs induced more than 50% cell viability reduction at a concentration lower that 10 μmol/L (penfluridol, ebastine), 15 μmol/L (pimozide and fluoxetine) or 25 μmol/L (fluspirilene and nefazodone) in all cell lines tested; spiperone and brexpiprazole proved to be highly effective in both CRC and BC (with $IC_{50} < 10$ μmol/L and $10 < IC_{50} < 20$ μmol/L, respectively) whereas their cytotoxicity was negligible in GB. A tendency for the diphenylbutylpiperidines pimozide, fluspirilene and penfluridol to be more effective in BC and CRC than in

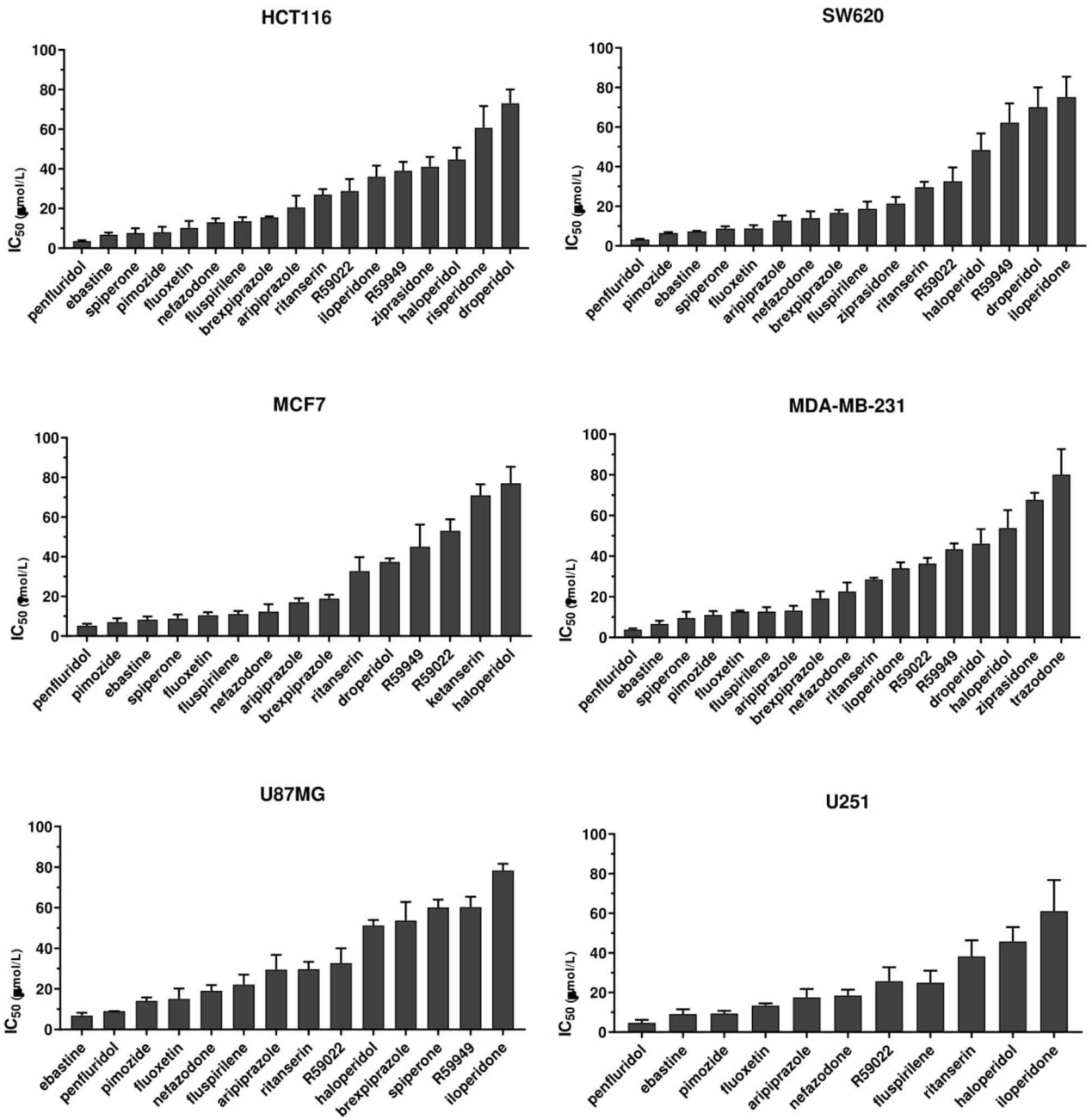

FIGURE 1 | Anticancer activity of psychotropic drugs. Two CRC (HCT116 and SW620), 2 BC (MCF7 and MDA-MB-231) and 2 GB (U87MG and U251) cell lines were treated for 72 h with scalar doses of drugs ranging from 10 to 160 μmol/L. The screened drugs included antipsychotics, antidepressant, antihistamines, and three compounds used in scientific research with reported serotonin receptors antagonistic activity (R59949, R59022; WAY-100135). Viabilities were assessed by MTT assay. Data are presented as mean IC_{50} ± standard error of the mean (SEM) from three-five independent experiments, each performed in quadruplicate. IC_{50}, drug concentration reducing by 50% viability compared to control. Histograms show drugs with $IC_{50} < 100$ μmol/L.

GB was also observed (**Supplementary Table 1**). Aripiprazole and ritanserin demonstrated a moderate cytotoxicity, whereas droperidol, haloperidol and iloperidone showed a weak effect only in a fraction of cell lines. Notably, in the lower range of concentrations, some compounds induced a moderate increase in cell viability reflecting cell proliferation: haloperidol in all cell lines tested; ritanserin and the two structurally related compounds R59022 and R5949 in CRC cell lines only, whereas iloperidone in MCF7 and U87MG cell lines (**Supplementary Figure 1**).

Eight compounds, represented by the antihistamines cetirizine and diphenhydramine, the antipsychotics paliperidone,

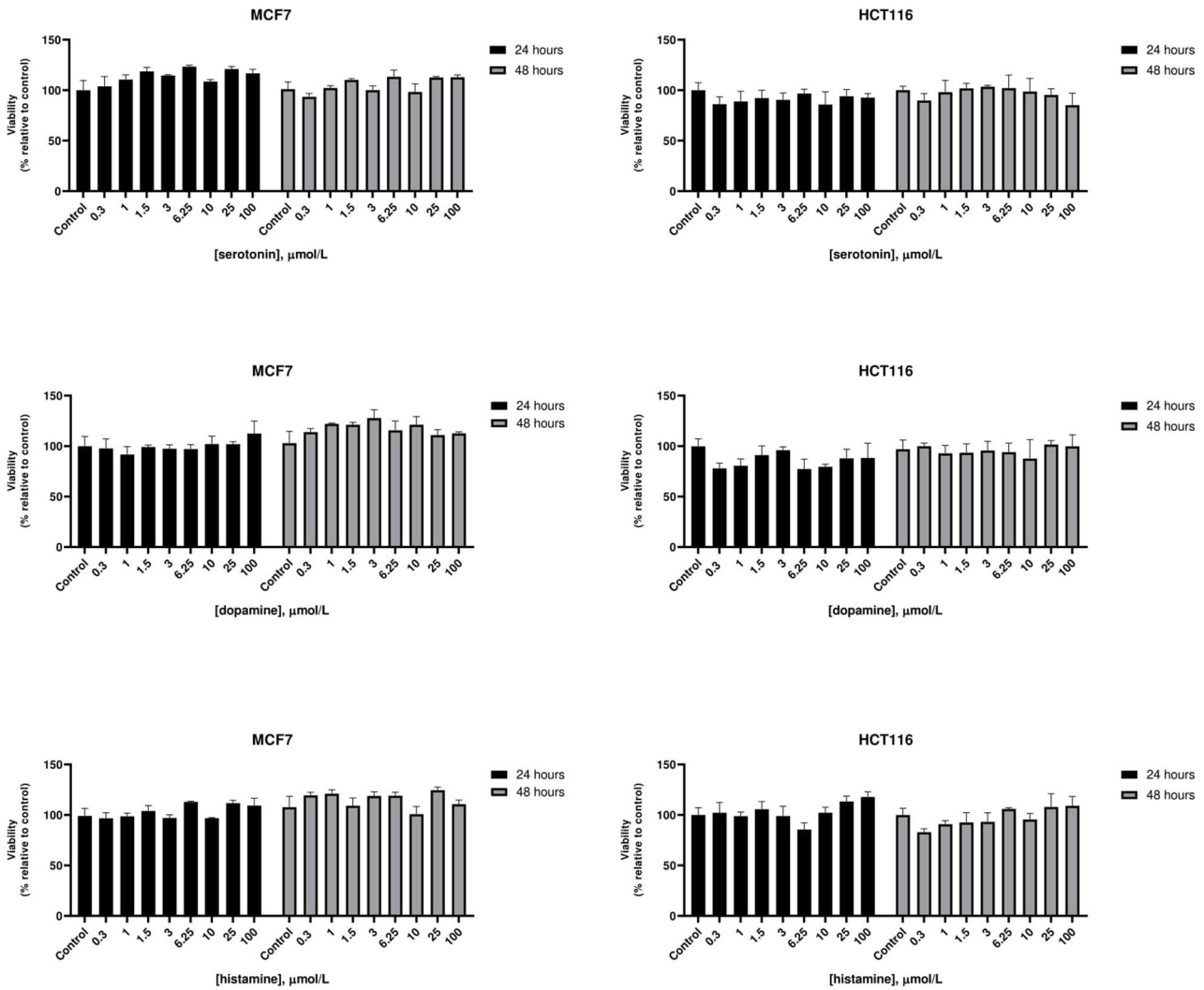

FIGURE 2 | Effect of biogenic amines on HCT116 and MCF7 cell viability. MCF7 and HCT116 cells were grown for 24 or 48 h in serum-free medium in presence of scalar doses of biogenic amines serotonin, dopamine, or histamine. Viabilities were assessed by MTT assay and presented as the percentage of viable cells vs. control. Data show mean ± SD of one representative experiment out of three independent experiments performed in quadruplicate.

pipamperone and risperidone, the antihypertensives ketanserin and urapidil, and the antiemetic metoclopramide showed no cytotoxicity, or caused a reduction of at least 50% of cell viability only at very high concentrations (>60 µmol/L) (**Supplementary Figure 1**, **Supplementary Table 1**). A few of these drugs i.e., urapidil, cetirizine, diphenhydramine and metoclopramide even induced cell growth in one or more cell lines tested (**Supplementary Figure 1**). These results clearly suggest that the cytotoxic effect of these compounds in the micromolar range is not associated with their conventional pharmacological properties and clinical use.

Cytotoxicity of Psychotropic Drugs Is Not Mediated by Biogenic Amine Receptors

At therapeutic concentrations, the main pharmacological targets of these compounds are biogenic amines receptors (37, 38). The precise role of biogenic amines such as histamine, dopamine, and serotonin in cancer is still debated (39–41). To test biogenic amines in our cell lines modes, we treated HCT116 and MCF7 cells with a wide range of concentrations of serotonin, dopamine and histamine and evaluated viabilities after 24 and 48 h. In our assay conditions we observed no significant effect on cell proliferation even at very high doses (**Figure 2**). Long term treatment of MCF7 cells with the strongest cytotoxic compounds penfluridol, ebastine, pimozide or fluoxetine at clinically significant concentrations determined only a modest increase of drugs efficacy, with IC_{50} values that remained above 3 µmol/L even after 6 days of treatment (**Supplementary Figure 3**).

Notably, neither dopamine, nor serotonin and histamine, added to the culture media, were able to rescue the cytotoxic effect of these drugs (**Figure 3**).

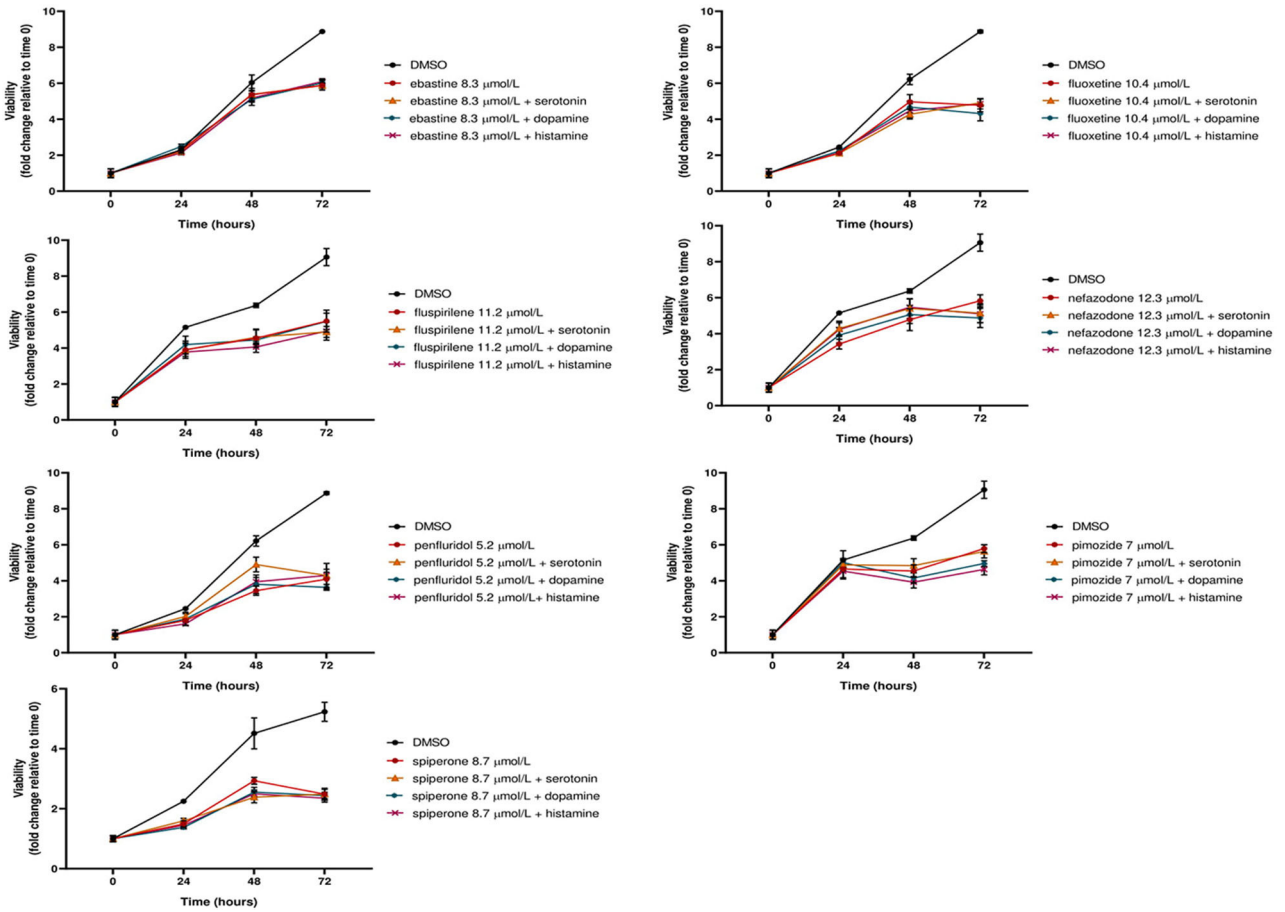

FIGURE 3 | The cytotoxic effect of psychotropic drugs is not reduced by co-treatment with biogenic amines. MCF7 cells were treated with psychotropic drugs alone (at a concentration equivalent to IC_{50}) or in presence of 5 μmol/L biogenic amines serotonin, dopamine or histamine. Viabilities were assessed by MTT assay at different time points and presented as fold change relative to control cells treated with vehicle only. Data show mean ± SD of one representative experiment out of three independent experiments performed in quadruplicate.

These data further support the hypothesis that these compounds affect tumor cell viability through a mechanism that is not mediated by the major neuroreceptor systems implicated in their psychotropic effects.

Psychotropic Drugs Affect Tumor Cell Migration

To determine the effect of psychotropic drugs on the motility of cancer cells, we assessed MCF7 and HCT116 cells migration by the wound-healing assay (**Figure 4**). All active drugs caused a reduction in the motility of MCF7 cells with the strongest effects observed with penfluridol, spiperone, urapidil and brexpiprazole (**Figure 4A**). On the contrary, the migration rate of HCT116 cells was unexpectedly increased by the cytotoxic compounds ebastine and penfluridol, as well as by different other compounds such as urapidil, diphenhydramine, ritanserin, R59022 and R59949; spiperone, and to a lesser extent, ketanserin and trazodone, reduced HCT116 cells motility (**Figure 4B**). Overall, these results show that: (i) the impact of the different compounds on the migration rate is not strictly associated with their cytotoxic effect or their conventional pharmacological properties and clinical use; (ii) the effect of the compounds on cell motility is cell line specific.

Psychotropic Drugs With Significant Antitumoral Activity Display a Cationic Amphiphilic Structure

Cationic amphiphilic drugs (CADs) are defined as chemical compounds with the ability to passively diffuse through lipid bilayers stacking in acid organelles such as lysosomes (42). These compounds contain both a hydrophobic and a hydrophilic domain; the hydrophobic domain contains one or more aromatic rings whereas the hydrophilic part contains a functional amine group that can be ionized (43). CADs family comprises a broad spectrum of compound classes, including dozens of approved drugs that are used to treat a wide range of diseases including allergies, heart diseases, and psychiatric disorders (44, 45). Since the antitumoral activity of compounds investigated in this study is not apparently related to their conventional pharmacological

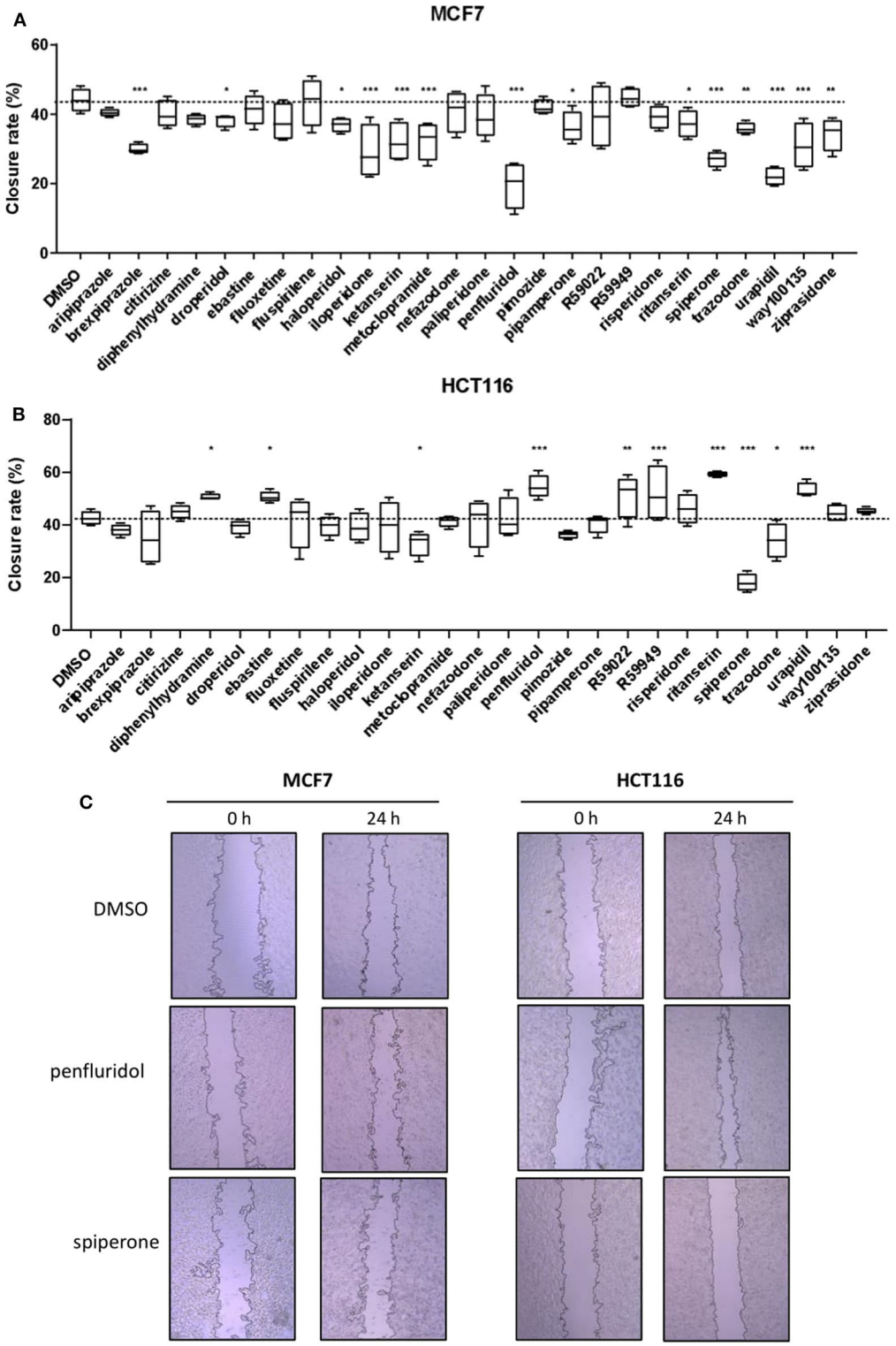

FIGURE 4 | Effect of psychotropic drugs on cancer cells migration. Cell motility was evaluated by wound healing assay. MCF7 **(A)** and HCT116 **(B)** cells were plated in 2 wells IBIDI chambers. After removing the insert, cells were treated with drugs (5 μmol/L) in DMEM 10% FBS. The widths of wounds were measured at 0 and 24 h. Graphs show the closure rate. Data are presented as mean ± SD from three independent experiments, each performed in triplicate. *, Student's *T*-test $p < 0.05$; **, Student's *T*-test $p < 0.01$; ***, Student's *T*-test $p < 0.001$. Representative images of MCF7 and HCT116 wounds after treatment with penfluridol, spiperone, and DMSO **(C)**.

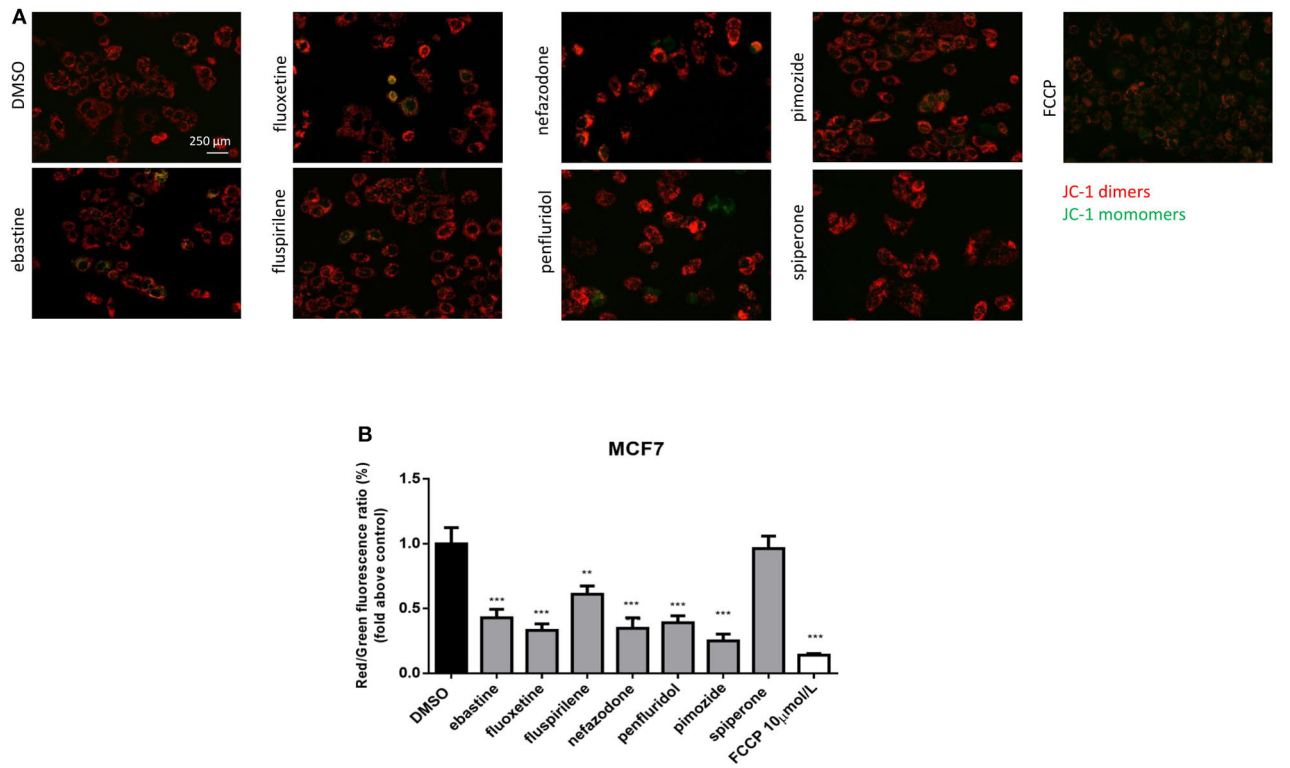

FIGURE 5 | Psychotropic drugs induce mitochondrial membrane depolarization. Mitochondrial membrane potential depolarization was evaluated by JC-1 staining after overnight treatment with psychotropic compounds (5 µmol/L) in MCF7 cells. Pictures were acquired by fluorescence microscopy. Representative images of cell treated with the negative control DMSO, carbonyl cyanide 4-[trifluoromethoxy]phenylhydrazone (FCCP), positive control, ebastine, fluoxetine, fluspirilene, nefazodone, penfluridol, pimozide, and spiperone **(A)**. Histogram showing quantification of red/green fluorescent ratio as fold change relative to control **(B)**. Data are presented as mean ± SD from three independent experiments, each performed in triplicate. **, Student's *T*-test $p < 0.01$; ***, Student's *T*-test $p < 0.001$.

properties and clinical use, we investigated the CADs properties of psychotropic drugs used in our screening evaluating their chemical structure, logP and pKa in comparison to the well-known CADs compounds amiodarone, chlorpromazine and chloroquine (**Supplementary Table 2**) (46, 47). Since there is not a clear CADs classification based on chemical properties, we set LogP and pKa cut off as suggested by Muehlbacher (36). Overall, 14 psychotropic drugs out of 26 were classified as CADs. Five out of seven most cytotoxic drugs in MCF7 (IC_{50} < 15 µmol/L) were CADs, whereas spiperone and nefazodone, were excluded from CAD classification just because of a LogP or pKa value below the selected cut off (**Supplementary Figure 4**, **Supplementary Table 2**). Since CADs were represented also among drugs without cytotoxic activity (e.g., haloperidol, iloperidone, or ritanserin), cationic amphiphilic characteristics contribute strongly, but are not sufficient to confer significant antitumoral activity to psychotropic compounds.

Psychotropic Drugs Cause Mitochondrial Membrane Depolarization

CADs can readily pass through phospholipids bilayers, particularly through membranes with a large transmembrane potential such as the mitochondrial inner membrane. They readily accumulate in the mitochondrial matrix, causing mitochondrial membrane depolarization (45, 48, 49). Therefore, we evaluated the alteration in mitochondrial membrane potential ($\Delta\psi m$) as a function of drug treatment, using the lipophilic cationic dye JC-1 (50). MCF7 cells were treated, for 16 h, with 5 µmol/L of each drug or with FCCP, used as positive control. A significant reduction in $\Delta\psi m$ was observed after treatment with ebastine, fluoxetine, penfluridol, pimozide, nefazodone and fluspirilene, but not with spiperone (**Figure 5**).

Psychotropics Drugs Induce Vacuolization and Increase Acidic Compartments

CADs are known to concentrate in acidic cell compartments because the retro-diffusion of the protonated form is inefficient (mechanism known as ion-trapping or pH partitioning). If sufficiently intense, this sequestration results in the osmotic formation of numerous large, fluid-filled vacuoles already after short term exposure to drugs (46). These molecules are collectively referred to as lysosomotropic agents, for their propensity to concentrate into lysosomes (51). To test the hypothesis that cytotoxic psychotropic drugs concentrate in MCF7 cells by this mechanism, MCF7 were cultured in the presence of 10% FBS and treated with

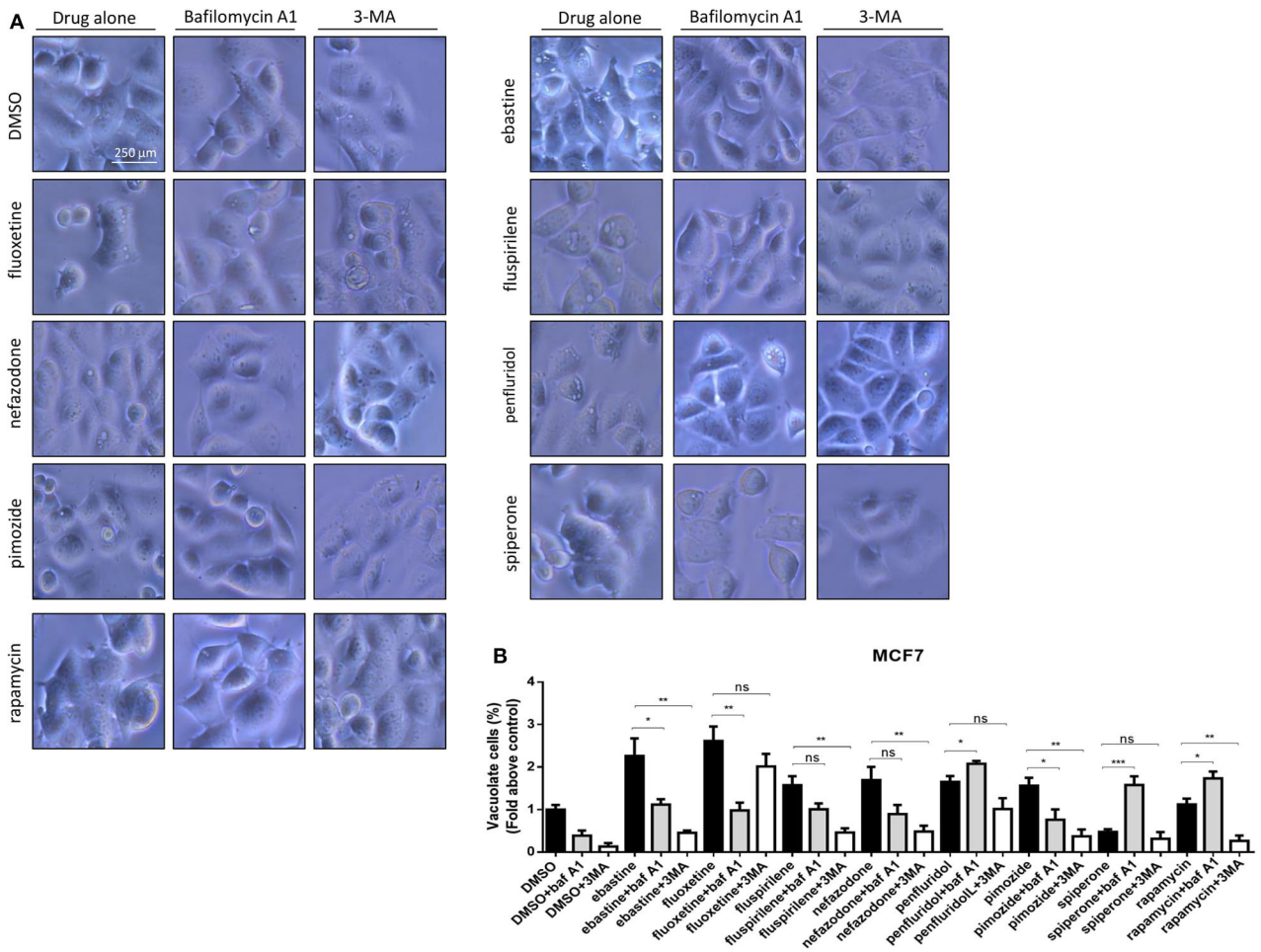

FIGURE 6 | Vacuolar structures formation after treatment of MCF7 cells with psychotropic drugs. Morphological alterations associated with psychotropic drugs treatment in MCF7 were investigated after 4 h exposure by phase contrast microscopy. Representative images of cells treated with the negative control DMSO, ebastine, fluoxetine, fluspirilene, nefazodone, penfluridol, pimozide and spiperone and rapamycin alone or with bafilomycin A1 and 3-MA **(A)**. Histogram showing quantification of vacuoles as fold change relative to control **(B)**. Data are expressed as the mean ± SD of a representative experiment out of three independent experiments performed in triplicate. *$p < 0.05$; **, Student's *T*-test $p < 0.01$; ***, Student's *T*-test $p < 0.001$.

drugs alone or in the presence of the V-ATPase inhibitor bafilomycin A1 or class III PI3K inhibitor 3-MA (**Figure 6**, **Supplementary Figure 5**). Fluoxetine induced a strong vacuolar morphology already 6 h after treatment as previously reported (46) (**Supplementary Figure 5A**); a less prominent, but still significant increase of vacuolar structures was also observed after treatment with fluspirilene, ebastine, pimozide, penfluridol and nefazodone, whereas increase of vacuoles was not observed with spiperone (**Supplementary Figure 5**). The mTOR inhibitor rapamycin used as a positive control of autophagy induced a mild vacuolar morphology.

In the presence of bafilomycin A1, a significant reduction of vacuoles formation was observed with fluoxetine, ebastine, fluspirilene, pimozide, and nefazodone, suggesting that these drugs require an acidic environment to accumulate and induce vesicles formation; on the contrary, a higher number of vesicles was observed after treatment with penfluridol and spiperone, suggesting that these drugs do not require pre-existing acidic compartments to induce vacuolization although they can cause the formation of autophagosome structures that accumulate after inhibition of autophagosome-lysosome fusion and autolysosome acidification by bafilomycin A1 (**Figure 6**). The autophagosome nature of vacuoles induced by all these compounds was supported by the reduction of the number of vesicles in the presence of the class III PI3K inhibitor 3-MA (**Figure 6**).

The nature of the vacuoles induced by psychotropic drugs was further investigated by staining MCF7 cells with the LysoTracker dye, which is a highly soluble small molecule that is retained in acidic subcellular compartments, such as late endosomes and lysosomes, whose presence is an indirect indication for autophagic activity (52). Although a transient increase of pH in autophagosome-lysosome structures was observed after short term treatment with penfluridol (**Figure 6B**), LysoTracker dye staining clearly shows a strong increase of acidic compartments

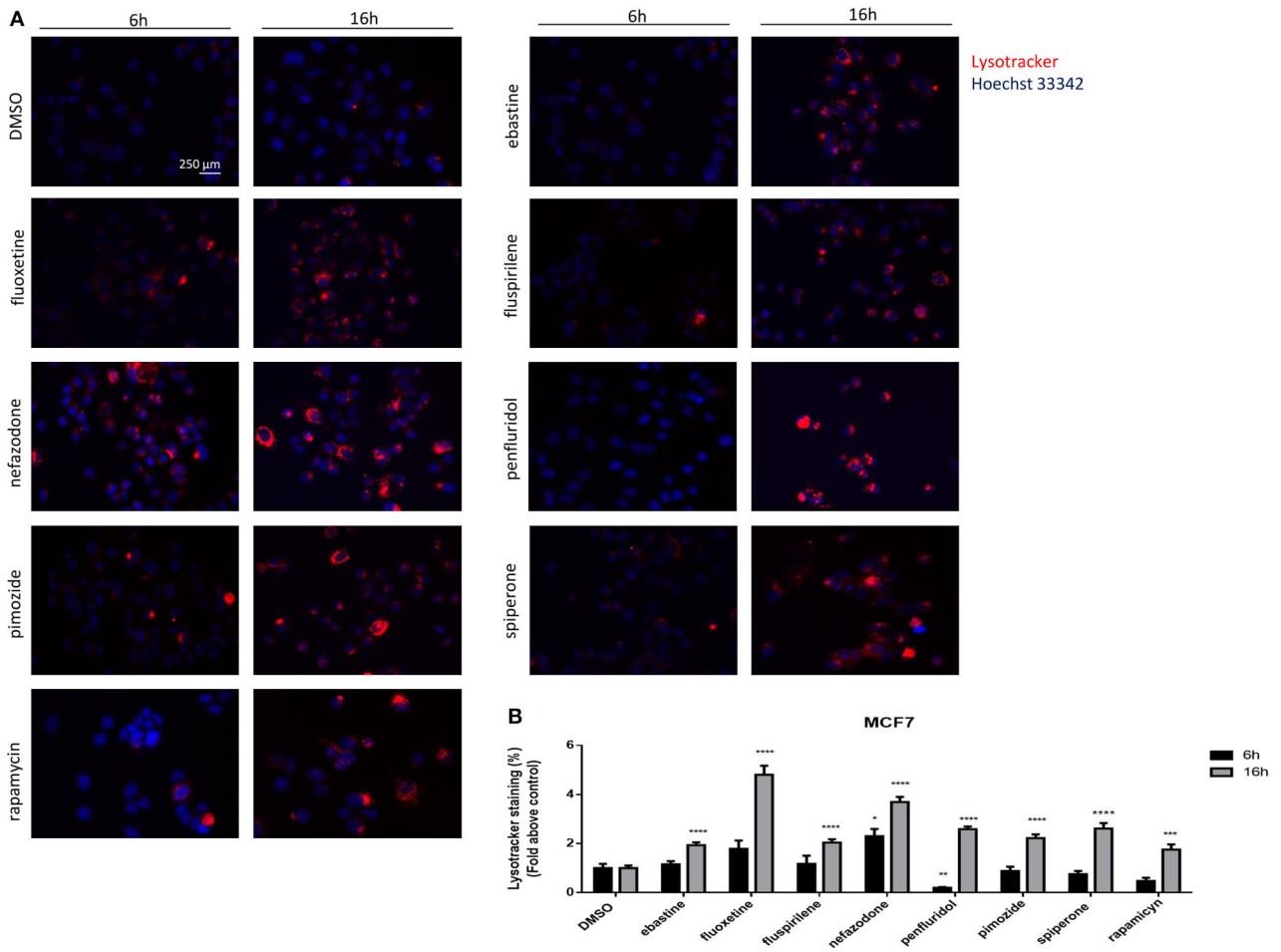

FIGURE 7 | Psychotropic drugs induce acidic compartment formation perturbing lysosomal and autophagic functioning. Effects of psychotropic drugs on intracellular acidic compartments were evaluated by Lysotracker Deep Red staining after 6 and 16 h of treatment. Nuclei were stained using Hoechst 33342. Pictures were acquired by fluorescence microscopy (magnification: 20×). Representative images of cells treated with DMSO, negative control, rapamycin, positive control, ebastine, fluoxetine, fluspirilene, nefazodone, penfluridol, pimozide, and spiperone **(A)**. Graphs showing quantification of red lysotracker staining/blue nuclei staining ratio as fold change relative to negative control **(B)**. Data are expressed as the mean ± SD of a representative experiment out of three independent experiments performed in triplicate. *$p < 0.05$; **, Student's T-test $p < 0.01$; ***, Student's T-test $p < 0.001$; ****$p < 0.0001$.

after overnight treatment with all drugs tested, consistent with increased autophagosome-lysosome acidic structures (**Figure 7**, **Supplementary Figure 6**).

Spiperone and Penfluridol Induce Autophagy by Modulating mTOR and AMPK Pathways

The increase of acidic structures can be a consequence of both autophagy induction and reduced turnover in the autophagosomal compartment caused by impaired autophagosome-lysosome fusion and/or lysosomal function. In order to clarify this issue, we investigated the main regulators of autophagy: mTOR pathway (represented by phosphorylations in 70S6K T389 and ribosomal protein S6 S235/236) and AMPK activation (**Figure 8**). Starvation, a strong inducer of autophagy, was used as positive control. A strong inhibition of mTOR pathway, comparable to that obtained with starvation, was observed after treatment with penfluridol, whereas a milder but significant downregulation of the pathway was detected with spiperone and, to a lesser extent, with the other compounds (**Figures 8A–C**), since S6 Ser 235/236 phosphorylation might also be modulated by kinases different from P70S6K (53). Notably, a partial delocalization of mTOR from the lysosomal membrane, further supporting mTOR inhibition, was observed after treatment with both penfluridol and spiperone (**Figure 8G**, **Supplementary Figure 7**).

In agreement with mTOR dislocation, a significant increase of AMPK phosphorylation in the activation site T172, comparable to that induced by starvation, was observed after treatment with penfluridol and spiperone. On the contrary, AMPK phosphorylation was unaffected or slightly reduced after treatment with all other compounds (**Figures 8A,D**).

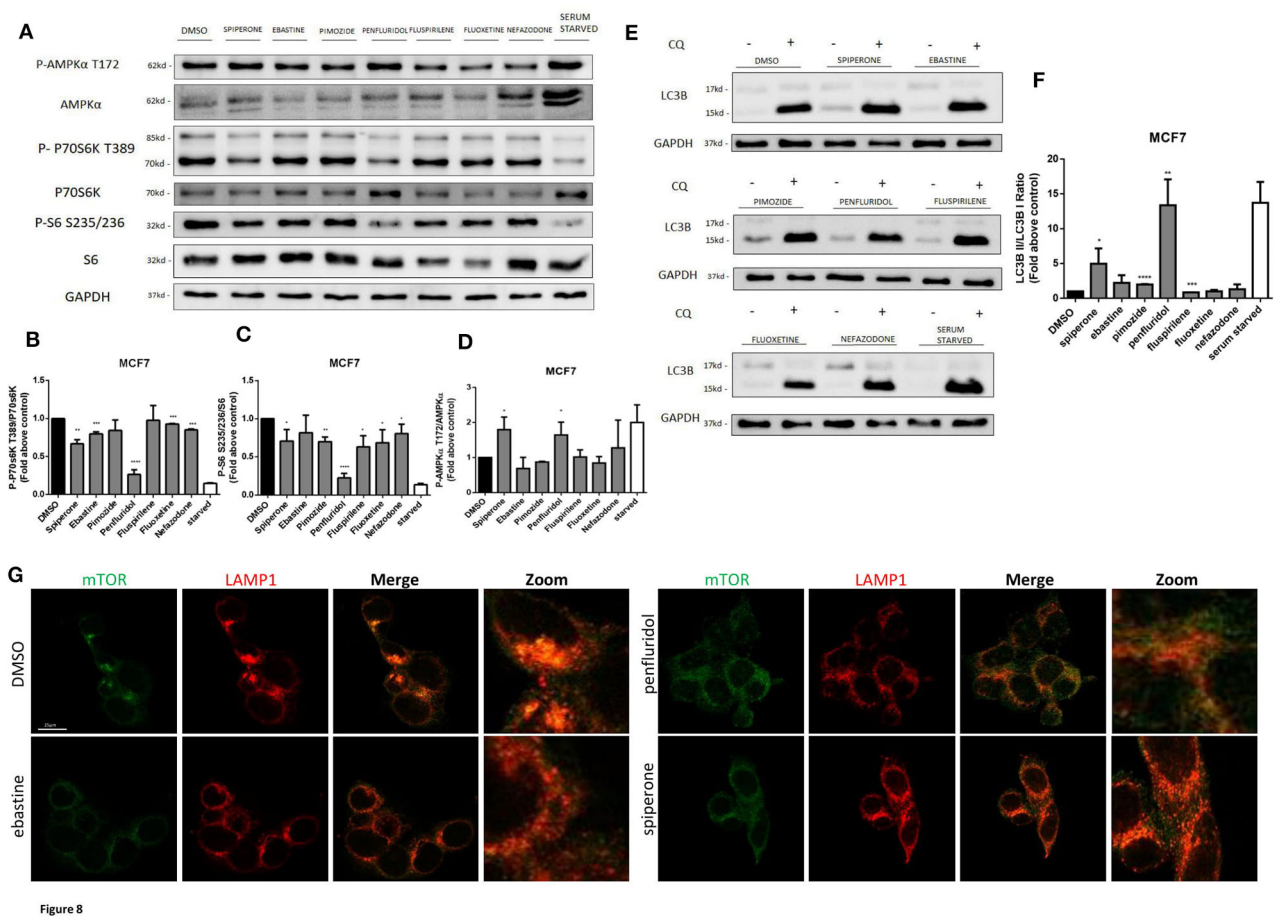

FIGURE 8 | Effect of psychotropic drugs on mTOR and AMPK pathways and autophagic flux. Western blot analysis of MCF7 cells after 16 h treatment with psychotropic drugs. Lysates were analyzed for p-AMPKα T172, AMPKα, p-P70S6K T389, P70S6K, P-S6 S235/236, S6, LC3B, and GAPDH **(A)**. Histogram showing quantification of P70S6K **(B)**, S6 **(C)** and AMPK **(D)** phosphorylation normalized on total protein P70S6K, S6 and AMPKα, respectively. WB **(E)** and histogram **(F)** showing the relative expression of LC3B II/I upon chloroquine treatment. Densitometric analyses are expressed as the mean ± SD of three independent experiments performed in triplicate. * Student's *T*-test $p < 0.05$ **, Student's *T*-test $p < 0.01$; ***, Student's *T*-test $p < 0.001$, ****$p < 0.0001$. Delocalization of mTOR from the lysosomal membrane was evaluated in MCF7 after 16 h treatment with psychotropic drugs. mTOR was stained using mTOR primary antibody and Alexa Fluor 488 secondary antibody (green). Lysosomes were stained using LAMP1 primary antibody and Alexa Fluor 536 secondary antibody (red). Representative images of DMSO, negative control, ebastine, penfluridol, and spiperone **(G)**.

The conversion of the cytosolic LC3B form, LC3B-I, into the faster migrating, phosphatidylethanolamine-conjugated, LC3B-II form, a marker of autophagy induction (54) was significantly enhanced in cells treated with penfluridol, spiperone and pimozide (**Figures 8E,F**).

Psychotropic Drugs With Cationic Amphiphilic Properties Cause Lysosomal Disruption

CADs can accumulate into lysosomes and impair lysosomal enzymatic activities (44, 55). It has also been shown that several antipsychotic and antidepressant drugs extensively accumulate in lysosomes and inhibit acid sphingomyelinase and phospholipases (36, 56). Lysosomes are a major site of cellular membranes degradation and complex lipids metabolism, therefore the hallmark of drug-induced lysosomal impairment is accumulation of phospholipids (42, 57). Therefore, we investigated whether the antitumoral activity of psychotropic drugs was associated with lysosomal impairment by incubating cells in the presence of phospholipids conjugated to fluorescent dye. After incubation for 24 h with LipidTOX, MCF7 cells treated with ebastine, fluspirilene, fluoxetine, pimozide and penfluridol showed a strong increase of phospholipids aggregates; on the contrary, this phenotype was not observed after treatment with non-CADs spiperone and nefazodone and with the inducer of autophagy rapamycin (**Figures 9A,B**).

Drugs with cationic amphiphilic properties accumulating into lysosomes can also induce LMP. This phenomenon can lead to the release of lysosomal enzymes inside the cytoplasm and possibly cell death (17). Galectin-1 is a small protein normally located in the cytoplasm and in the nucleus, that

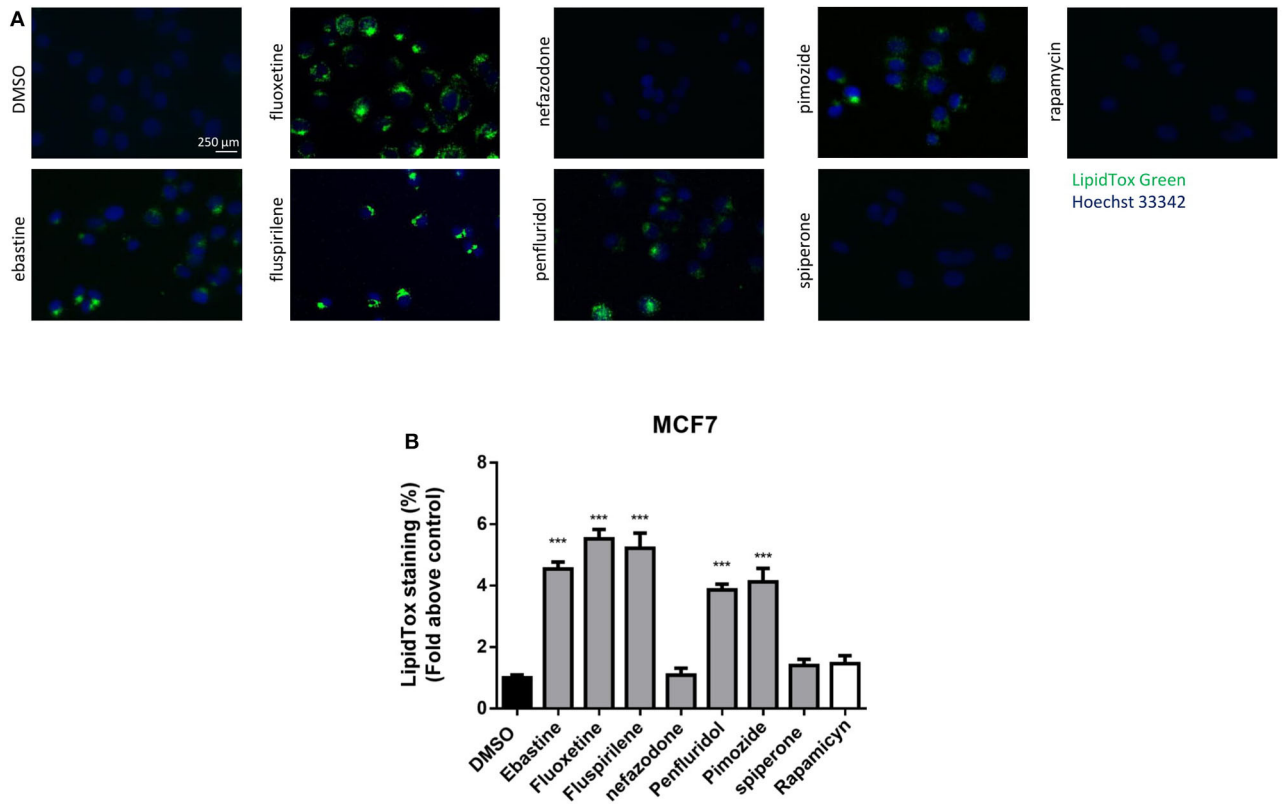

FIGURE 9 | Treatment with psychotropic drugs induces phospholipidosis in MCF7 cells. Accumulation of phospholipids in MCF7 cell line was evaluated after 16 h treatment with drugs using LipidTox green staining. Nuclei were stained using Hoechst 33342. Pictures were acquired by fluorescence microscopy (magnification: 20×). Representative images of cells treated with DMSO, negative control, ebastine, fluoxetine, fluspirilene, nefazodone, penfluridol, pimozide, spiperone, and rapamycin **(A)**. Histogram showing quantification of Green LipidTox staining/blue nuclei staining ratio as fold change relative to control **(B)**. Data are presented as mean ± standard deviation from three independent experiments, each performed in triplicate. ***, Student's *T*-test $p < 0.001$.

accumulates and forms complexes to the lysosomal membrane in case of lysosomal membrane damage and LMP (58). To evaluate lysosomal membrane damage in response to psychotropic drug treatment we investigated galectin-1 complex formation by immunofluorescence. The formation of galectin-1 complexes was observed with all the drugs tested, apart from nefazodone, indicating that cytotoxic psychotropic drugs can induce lysosomal membrane damage (**Figures 10A,B**).

Psychotropic Drugs Induce Different Types of Cell Death

To assess if apoptosis is involved in psychotropic drugs-induced cell death we performed PI/Annexin V staining in MCF7 cells. FACS analysis at different time points showed an increase in necrosis cells with all the drugs but a significant induction of apoptosis after 48 h of treatment with the sole spiperone (**Supplementary Figure 8**). These data were further confirmed by viability rescue experiments with a pan caspase inhibitor zVAD-fmk. As shown in **Figure 11A**, zVAD-fmk significantly rescued cell death only in cells treated with spiperone and staurosporine, whereas it was ineffective with the other drugs.

Since apoptosis is not the primary mechanism of death elicited by cytotoxic psychotropic drugs, except for spiperone, we investigated the role of autophagy by treating cells with the autophagy inhibitor 3-MA (59). As shown in **Figure 11B**, 3-MA co-treatment significantly rescued cell viability in cells treated with rapamycin and in cells treated with spiperone and pimozide. Conversely, 3-MA enhanced penfluridol cytotoxicity, whereas it did not show any effect in combination with ebastine, fluoxetine, nefazodone and fluspirilene. However, since it was reported that in particular conditions 3-MA could induce autophagy (59) we performed western blot analysis to investigate the conversion of the cytosolic LC3 I to II form in MCF7 cells treated with spiperone and penfluridol alone or in combination with 3-MA (**Supplementary Figure 9**). Our data indicate that in our experimental set-up 3-MA does not induce autophagy, on the contrary it is effective in suppressing LC3 II conversion.

To further investigate the mechanism of the observed cytotoxicity we assessed whether inhibition of lysosomal cathepsins B and L rescued cell viability in MCF7 cells, for this purpose we performed experiments with the inhibitor CA-074 me (60). As displayed in **Figure 11C** CA-074 me significantly

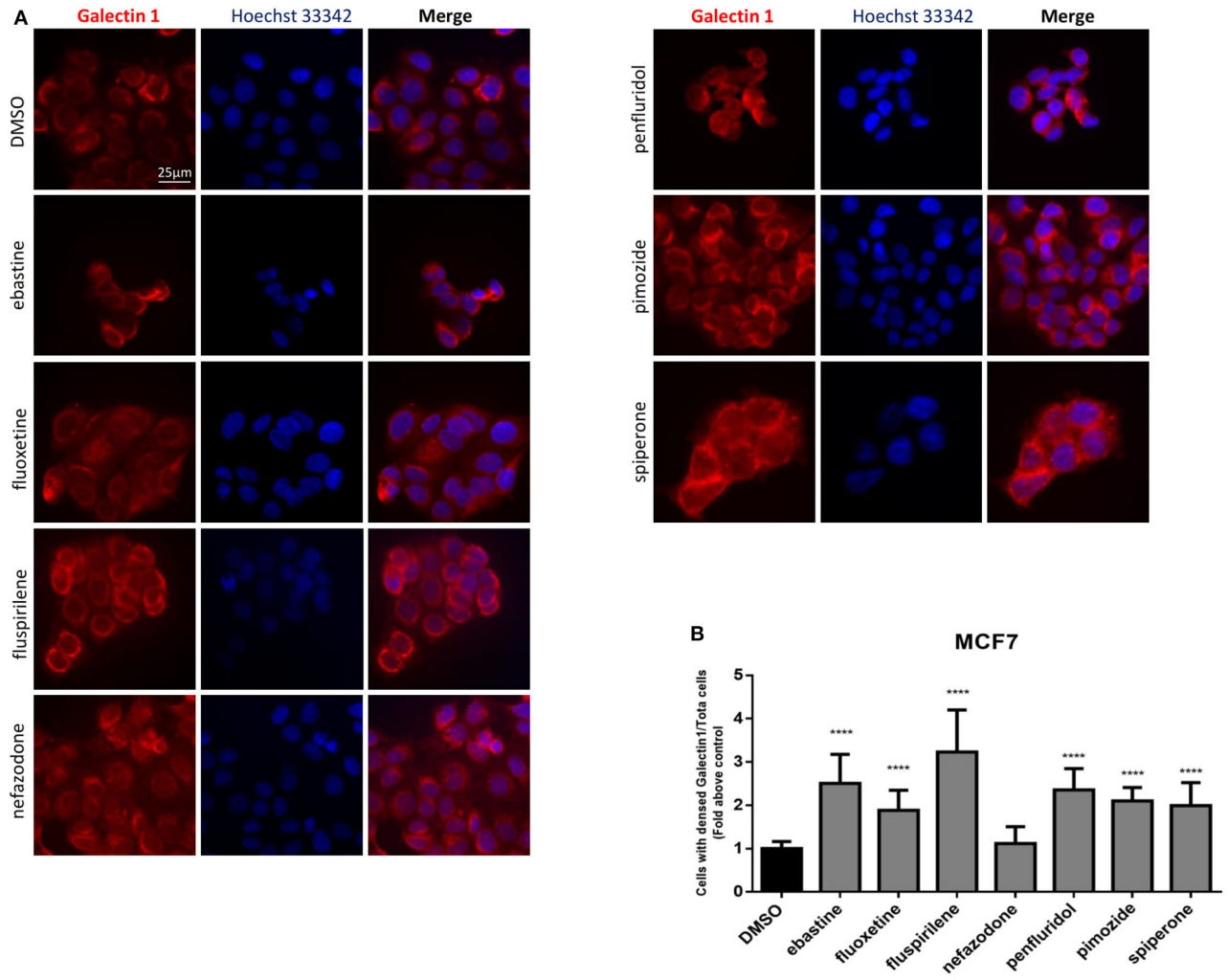

FIGURE 10 | Treatment with psychotropic drugs induced formation of galectin-1 complexes. Formation of galectin-1 complexes in MCF7 after 16 h treatment with psychotropic drugs was observed by fluorescence microscopy (magnification: 63X). Galectin-1 was stained with anti galectin-1 primary antibody and Alexa Fluor 563 secondary antibody. Nuclei were stained using DAPI. Representative images showing cells treated with psychotropic drugs: DMSO, ebastine, fluoxetine, fluspirilene, nefazodone, penfluridol, pimozide, and spiperone **(A)**. Histogram showing the number of cells presenting galectin-1 complexes/total number of cells ratio as fold change relative to control **(B)** Data are presented as mean ± standard deviation from three independent experiments, each performed in triplicate. ****$p < 0.0001$.

rescued cell death induced by ebastine, penfluridol, pimozide and spiperone, while a mild but not significant effect was observed in cells co-treated with fluoxetine.

Additionally, in order to clarify if oxidative stress was involved in psychotropic drugs-induced cell death, we co-treated MCF7 cells with the antioxidant NAC, however no significant effect was observed in terms of viability rescue (**Figure 11D**). With cyclosporin A, an inhibitor of the mitochondrial permeability transition pore (mPTP), an additive cytotoxic effect was observed with all drugs tested (**Figure 11E**). Cyclosporin A has been reported to be a broad-spectrum multidrug resistance modulator (61) and this activity possibly induces psychotropic drugs retention resulting in a boost of cytotoxicity.

DISCUSSION

Although cancer treatment has witnessed remarkable progress over the past few decades, cancer remains a major threat to humans, with total cure remaining elusive. Repurposing of well-characterized and well-tolerated drugs for cancer therapy has emerged as an attractive alternative for a long and costly process of drug development (23). Psychotropic drugs are revealing promising candidates for drug repositioning in cancer. Although several *in vitro* and *in vivo* models reported the efficacy of this family of drugs in reducing cancer cell viability and tumor growth (30, 32, 62), the pharmacological properties underpinning the possible clinical application of psychotropic drugs for cancer therapy remain poorly understood. In this study we investigated

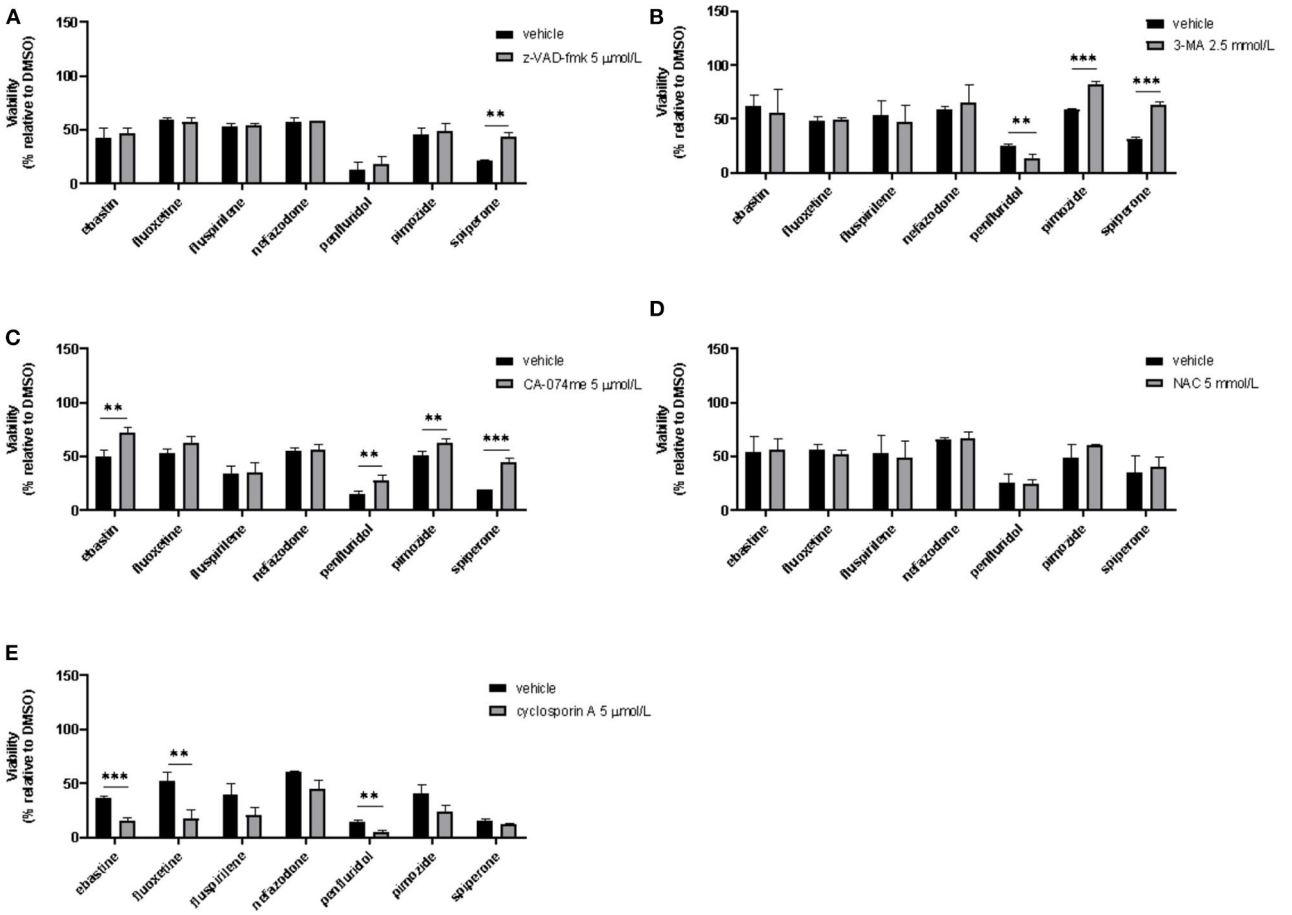

FIGURE 11 | Effect of co-treatment of psychotropic drugs and the pan-caspase inhibitor zVAD-fmk, the autophagy inhibitor 3-MA, the cathepsin inhibitor CA-074 me, the antioxidant NAC or the inhibitor of mitochondrial membrane depolarization cyclosporin A. MCF7 cells were treated for 72 h with vehicle or psychotropic drugs (all 10 μmol/L except penfluridol, 5 μmol/L) alone, or in combination with zVAD-fmk, 5 μmol/L **(A)**, 3-MA, 2.5 mmol/L **(B)**, CA-075 me, 5 μmol/L **(C)**, NAC, 5 mmol/L **(D)**, cyclosporin A, 5 μmol/L **(E)** Data show mean ± SD of at least three independent experiments performed in triplicate. The graphs show cell viability as the percentage of viable cells vs. control. **, Student's *T*-test $p < 0.01$; ***, Student's T-test $p < 0.001$.

a large panel of psychotropic drugs for their potential anti-tumoral activity evaluating their cytotoxic effect in six cell lines derived from three different tumor types. By using stringent screening conditions, we identified only a few compounds that significantly reduced cell viability at clinically relevant concentrations. These were represented by the antipsychotics penfluridol, pimozide, fluspirilene, nefazodone, and spiperone, the antidepressant fluoxetine and the antihistamine ebastine. Except for spiperone, whose cytotoxicity was negligible in GB, all the other compounds showed cytotoxic activity in all cell lines tested.

The comparable efficacy, in three different tumor types, of compounds with clinically different indications allows us to speculate a common mechanism of action independent from the phenotypic and molecular profile of the tumor and not associated with the conventional pharmacological properties and clinical use of these compounds. This hypothesis is corroborated by the negligible cytotoxicity observed with other drugs with superimposable biogenic amine receptors targeting, by the lack of rescue of cell viability after co-treatment with biogenic amines and by the drug concentration necessary to observe a biologic effect, that it is at least one order of magnitude higher than that needed for their conventional pharmacological targets (63).

Based on the analysis of structure and chemical-physical properties, most psychotropic compounds with a significant cytotoxic activity can be classified as CADs (36, 43). It is well-demonstrated the formation of cytoplasmic vesicles in cells exposed to CADs results from extensive ion-trapping-based accumulation of lysosomotropic weak bases in acidic compartments (36, 55). Vacuoles formation, inhibited by the disruption of the lysosomal V-ATPase, was observed after short term exposure of MCF7 cells to CADs fluoxetine, ebastine, fluspirilene, pimozide but also to nefazodone, that is not formally a CADs but might display some of their features. Accumulation of vacuoles in the presence of bafilomycin A1 was instead observed after treatment with penfluridol and spiperone, suggesting that the formation of vesicles by these drugs does not necessarily depend on ion-trapping in acidic compartments,

but is favored by the block of lysosomal activity. The acidic autophagosome nature of these vesicles was confirmed by the requirement of class III PI3K for their formation and by the positive staining with the lysosomotropic dye LysoTracker. Notably, both spiperone and penfluridol, that induced the formation of autophagosome structures independently from the ion-trapping mechanism are likely true activator of autophagy, as demonstrated by stimulation of AMPK and LC3B conversion and downregulation of mTOR pathway observed in MCF7 cells.

Although lysosomotropic CADs can increase lysosomal pH after compound sequestration which could lead to suboptimal conditions for lysosomal digestion (64, 65), lysosomal pH increase may be a transient change and pH could be restored after extended exposure to lysosomotropic compounds (47, 66, 67). The increased LysoTracker dye staining we observed after overnight treatment with drugs indicates a pH recovery after compound sequestration and reflects the increased lysosomal volume, suggestive of the occurrence of lysosome biogenesis induced by lysosomotropic drugs (47, 68). Moreover, drug interactions with the lysosomal lipid bilayer and membrane proteins could influence the dynamics of membrane fusion and/or fission, thereby affecting trafficking steps and lysosomal egress (67), causing a reduction in autophagic flux and lysosomal enlargement.

Due to their chemical structure, CADs can accumulate in acidic lysosomes (46) and incorporate to luminal membranes where they function as effective inhibitors of acid sphingomyelinase and other lysosomal lipases (36, 44). At therapeutically relevant concentrations, CADs have been shown to cause the lysosomal accumulation of various lipid species, including sphingomyelin, phosphatidylethanolamine, phosphatidylserine, phosphatidylcholine, lysophosphatidic acid, and cholesterol, with induction of phospholipidosis (42, 57). In our experimental model, CADs ebastine, fluspirilene, fluoxetine and pimozide, that very rapidly accumulated in cells by ion-trapping, caused a strong increase of phospholipids aggregates. Our observations are supported by papers reporting the capacity of these compounds to induce phospholipidosis. Gonzalez-Rothi in 1995 first described the complication of pulmonary phospholipidosis in a patient with manic-depressive illness after treatment with fluoxetine (69); penfluridol, pimozide, and fluspirilene have been reported in a screening of drugs capable to inhibit sphingomyelinase and were found to induce phospholipidosis in neuroglioma H4 cells (36, 44), whereas ebastine was identified by electron microscope screening to evaluate chemicals for drug-induced phospholipidosis (70). Our results demonstrate that, also in cancer cells, ebastine, fluspirilene, fluoxetine and pimozide act as typical CADs, impairing lysosomal activity.

Some compounds investigated in this study, including the antipsychotics diphenylbutylpiperidines fluspirilene, penfluridol, and pimozide and antidepressants such as fluoxetine have been previously reported as autophagy inducers in neurons and in different cancer cell types such as BC and GB by affecting a variety of targets (31, 71–73). Our study shows that the cytotoxic activity of most of these compounds is essentially based on their common cationic amphiphilic properties and their capacity to perturb acidic intracellular compartments. Moreover, although all investigated drugs caused the formation of acidic structures, apparently inducing the autophagic flux, only spiperone, penfluridol and, potentially, pimozide can be considered true autophagy activators. Overall, these data raise a critical issue related to clinical use of these compounds as autophagy enhancers, but they also reveal interesting therapeutic implications for compounds that transiently increase upstream autophagic flow while compromising downstream lysosomal function.

The lysosome is emerging as a driving force in the progression of numerous human cancers, in which enhanced function of the autophagy–lysosome system enables efficient nutrient scavenging and growth in nutrient-poor microenvironments, promote the metastatic potential and treatment resistance (11). But lysosomal activation in aggressive cancers can lead to alterations in lysosomal structure and function, which, paradoxically, renders cancer cells more sensitive to lysosomal destabilization (5, 74). This frailty can be targeted by lysosomotropic compound that may have an antitumor effect preferentially killing the more sensitive cancer cells by inducing dysregulation of lysosomal lipid metabolism and LMP with release into the cytosol of cathepsins, potent inducers of cell death (17, 75, 76). In our study, we observed increased Lysotracker staining, suggestive of lysosomal swelling that is considered a typical condition preceding LMP (17, 77–79) and galectin-1 complexes, a surrogate marker of lysosomal membrane damage (58), suggesting a possible role of lysosomes in cancer cell death. This was confirmed for ebastine, penfluridol, pimozide, and fluoxetine, whose cytotoxic activity was partially rescued by inhibitor of cathepsins B and L but not by treatment with both apoptosis or autophagy inhibitors.

Inhibition of apoptosis and autophagy were also ineffective in reducing cell death induced by nefazodone and fluspirilene and further experiments are required to clarify the mechanisms of cell death induced by these drugs.

Notably, while inhibition of autophagy significantly rescued pimozide and spiperone cytotoxicity, it further increased cell death induced by penfluridol, the compound that demonstrated the highest cytotoxicity in all cell lines tested. The strong antitumoral activity of penfluridol may be due to its ability to induce both ADCD and LMP. Most of the known compounds that affect autophagy in neoplastic cells are either inducers or inhibitors of this process (80, 81). However, molecules that can modulate autophagy in a dual mode, by both inducing and inhibiting the process, seem to represent a novel and effective strategy for anticancer therapy (82, 83).

Finally, all psychotropic compounds with cationic amphiphilic properties caused a significant reduction in $\Delta\psi m$. Since oncogenic activation leads to increased mitochondrial metabolism and higher $\Delta\psi m$ compared to that of non-cancer cells (20) and experimental evidence demonstrates that irreversible mitochondrial membrane depolarization can induce cell death also in apoptotic resistant cells (84), CADs appear excellent candidates for mitochondrial targeting in cancer, as they can easily diffuse in tumor tissues and interact with negatively charged mitochondrial membranes

(20, 45, 49). Since in our cell line model cytotoxicity of psychotropic drugs was not mediated by ROS and thiols oxidation whereas apoptosis has been demonstrated only in cells treated with spiperone, studies are underway to explore the molecular mechanisms underlying CADs induced mitochondrial membrane depolarization and its role in inducing cancer cell death.

In addition to acute cytotoxicity, observed, *in vitro*, at lower micromolar concentrations, *in vivo* psychotropic drugs with cationic amphiphilic properties can also impair cancer cell metabolism and sensitize tumors to chemotherapy at plasma concentrations achieved with standard therapeutic regimens (85, 86). Suggestive of their efficacy in human clinical setting, epidemiologic studies have reported a reduced incidence of glioma and CRC among users of tricyclic antidepressants (27), a lower CRC risk under therapy with fluoxetine (26, 87) and an association between post-diagnostic use of cationic amphiphilic antihistamines and reduced cancer mortality as compared with similar use of antihistamines that do not classify as CADs (88).

In conclusion, the data presented above identify a subset of psychotropic drugs as putative anticancer agents and open a feasible, safe, and economically sound possibility to test the clinical anticancer efficacy of this therapeutic class of compounds. In particular, the cytotoxicity of psychotropic drugs with cationic amphiphilic structures relied on simultaneous mitochondrial and lysosomal disruption and induction of cell death that not necessarily requires apoptosis. Since dual targeting of lysosomes and mitochondria constitutes a new promising therapeutic approach for cancer, particularly those in which the apoptotic machinery is defective, these data further support their clinical development.

DATA AVAILABILITY STATEMENT

The raw data supporting the conclusions of this article will be made available by the authors, without undue reservation.

AUTHOR CONTRIBUTIONS

MV and AA equally contributed in study design, conducting experiments, acquiring data, analyzing data, and writing the manuscript. VB contributed in data analysis and revising the manuscript. KR, VY, and AV contributed in conducting experiments. AM and GB contributed in data interpretation and manuscript editing. DC contributed in study design, data interpretation, manuscript writing, and the final approval of the manuscript. All authors critically reviewed and agreed on the final version of the manuscript.

FUNDING

This study was (partially) funded by the Università del Piemonte Orientale–FAR 2016 e FAR 2017 (DC), by the Italian Ministry of Education, University and Research (MIUR) program Departments of Excellence 2018–2022, AGING Project—Department of Translational Medicine, Università del Piemonte Orientale (DC), by Consorzio Interuniversitario di Biotecnologie (CIB) call Network-CIB: Catalisi dell'Innovazione nelle Biotecnologie (PRIN 201799WCRH, GB).

SUPPLEMENTARY MATERIAL

The Supplementary Material for this article can be found online at: https://www.frontiersin.org/articles/10.3389/fonc.2020.562196/full#supplementary-material

REFERENCES

1. Ferlay J, Colombet M, Soerjomataram I, Mathers C, Parkin DM, Pineros M, et al. Estimating the global cancer incidence and mortality in 2018: GLOBOCAN sources and methods. *Int J Cancer*. (2019) 144:1941–53. doi: 10.1002/ijc.31937
2. Bray F, Ferlay J, Soerjomataram I, Siegel RL, Torre LA, Jemal A. Global cancer statistics 2018: GLOBOCAN estimates of incidence and mortality worldwide for 36 cancers in 185 countries. *CA Cancer J Clin*. (2018) 68:394–424. doi: 10.3322/caac.21492
3. Robey RW, Pluchino KM, Hall MD, Fojo AT, Bates SE, Gottesman MM. Revisiting the role of ABC transporters in multidrug-resistant cancer. *Nat Rev Cancer*. (2018) 18:452–64. doi: 10.1038/s41568-018-0005-8
4. Dale W, Chow S, Sajid S. Socioeconomic considerations and shared-care models of cancer care for older adults. *Clin Geriatr Med*. (2016) 32:35–44. doi: 10.1016/j.cger.2015.08.007
5. Piao S, Amaravadi RK. Targeting the lysosome in cancer. *Ann N Y Acad Sci*. (2016) 1371:45–54. doi: 10.1111/nyas.12953
6. Mulcahy Levy JM, Thorburn A. Autophagy in cancer: moving from understanding mechanism to improving therapy responses in patients. *Cell Death Differ*. (2020) 27:843–57. doi: 10.1038/s41418-019-0474-7
7. Chang A. Chemotherapy, chemoresistance and the changing treatment landscape for NSCLC. *Lung Cancer*. (2011) 71:3–10. doi: 10.1016/j.lungcan.2010.08.022
8. Domagala A, Fidyt K, Bobrowicz M, Stachura J, Szczygiel K, Firczuk M. Typical and atypical inducers of lysosomal cell death: a promising anticancer strategy. *Int J Mol Sci*. (2018) 19:2256. doi: 10.3390/ijms19082256
9. Mosesson Y, Mills GB, Yarden Y. Derailed endocytosis: an emerging feature of cancer. *Nat Rev Cancer*. (2008) 8:835–50. doi: 10.1038/nrc2521
10. Galluzzi L, Pietrocola F, Bravo-San Pedro JM, Amaravadi RK, Baehrecke EH, Cecconi F, et al. Autophagy in malignant transformation and cancer progression. *EMBO J*. (2015) 34:856–80. doi: 10.15252/embj.201490784
11. Davidson SM, Vander Heiden MG. Critical functions of the lysosome in cancer biology. *Annu Rev Pharmacol Toxicol*. (2017) 57:481–507. doi: 10.1146/annurev-pharmtox-010715-103101
12. Lawrence RE, Zoncu R. The lysosome as a cellular centre for signalling, metabolism and quality control. *Nat Cell Biol*. (2019) 21:133–42. doi: 10.1038/s41556-018-0244-7
13. Russell RC, Yuan HX, Guan KL. Autophagy regulation by nutrient signaling. *Cell Res*. (2014) 24:42–57. doi: 10.1038/cr.2013.166
14. Liu Y, Levine B. Autosis and autophagic cell death: the dark side of autophagy. *Cell Death Differ*. (2015) 22:367–76. doi: 10.1038/cdd.2014.143
15. Denton D, Kumar S. Autophagy-dependent cell death. *Cell Death Differ*. (2019) 26:605–16. doi: 10.1038/s41418-018-0252-y
16. Ho CJ, Gorski SM. Molecular mechanisms underlying autophagy-mediated treatment resistance in cancer. *Cancers*. (2019) 11:1775. doi: 10.3390/cancers11111775
17. Wang F, Gomez-Sintes R, Boya P. Lysosomal membrane permeabilization and cell death. *Traffic*. (2018) 19:918–31. doi: 10.1111/tra.12613

18. Serrano-Puebla A, Boya P. Lysosomal membrane permeabilization as a cell death mechanism in cancer cells. *Biochem Soc Trans*. (2018) 46:207–15. doi: 10.1042/BST20170130
19. Repnik U, Borg Distefano M, Speth MT, Ng MYW, Progida C, Hoflack B, et al. L-leucyl-L-leucine methyl ester does not release cysteine cathepsins to the cytosol but inactivates them in transiently permeabilized lysosomes. *J Cell Sci*. (2017) 130:3124–40. doi: 10.1242/jcs.204529
20. Weinberg SE, Chandel NS. Targeting mitochondria metabolism for cancer therapy. *Nat Chem Biol*. (2015) 11:9–15. doi: 10.1038/nchembio.1712
21. Zong WX, Rabinowitz JD, White E. Mitochondria and cancer. *Mol Cell*. (2016) 61:667–76. doi: 10.1016/j.molcel.2016.02.011
22. Ashburn TT, Thor KB. Drug repositioning: identifying and developing new uses for existing drugs. *Nat Rev Drug Discov*. (2004) 3:673–83. doi: 10.1038/nrd1468
23. Sleire L, Forde HE, Netland IA, Leiss L, Skeie BS, Enger PO. Drug repurposing in cancer. *Pharmacol Res*. (2017) 124:74–91. doi: 10.1016/j.phrs.2017.07.013
24. Chou FH, Tsai KY, Su CY, Lee CC. The incidence and relative risk factors for developing cancer among patients with schizophrenia: a nine-year follow-up study. *Schizophr Res*. (2011) 129:97–103. doi: 10.1016/j.schres.2011.02.018
25. Li H, Li J, Yu X, Zheng H, Sun X, Lu Y, et al. The incidence rate of cancer in patients with schizophrenia: a meta-analysis of cohort studies. *Schizophr Res*. (2018) 195:519–28. doi: 10.1016/j.schres.2017.08.065
26. Coogan PF, Strom BL, Rosenberg L. Antidepressant use and colorectal cancer risk. *Pharmacoepidemiol Drug Saf*. (2009) 18:1111–4. doi: 10.1002/pds.1808
27. Walker AJ, Grainge M, Bates TE, Card TR. Survival of glioma and colorectal cancer patients using tricyclic antidepressants post-diagnosis. *Cancer Causes Control*. (2012) 23:1959–64. doi: 10.1007/s10552-012-0073-0
28. Chan HL, Chiu WC, Chen VC, Huang KY, Wang TN, Lee Y, et al. SSRIs associated with decreased risk of hepatocellular carcinoma: a population-based case-control study. *Psychooncology*. (2018) 27:187–92. doi: 10.1002/pon.4493
29. Faustino-Rocha AI, Ferreira R, Gama A, Oliveira PA, Ginja M. Antihistamines as promising drugs in cancer therapy. *Life Sci*. (2017) 172:27–41. doi: 10.1016/j.lfs.2016.12.008
30. Huang J, Zhao D, Liu Z, Liu F. Repurposing psychiatric drugs as anti-cancer agents. *Cancer Lett*. (2018) 419:257–65. doi: 10.1016/j.canlet.2018.01.058
31. Shaw V, Srivastava S, Srivastava SK. Repurposing antipsychotics of the diphenylbutylpiperidine class for cancer therapy. *Semin Cancer Biol*. (2019). doi: 10.1016/j.semcancer.2019.10.007. [Epub ahead of print].
32. Zhuo C, Xun Z, Hou W, Ji F, Lin X, Tian H, et al. Surprising anticancer activities of psychiatric medications: old drugs offer new hope for patients with brain cancer. *Front Pharmacol*. (2019) 10:1262. doi: 10.3389/fphar.2019.01262
33. Garcia-Quiroz J, Camacho J. Astemizole: an old anti-histamine as a new promising anti-cancer drug. *Anticancer Agents Med Chem*. (2011) 11:307–14. doi: 10.2174/187152011795347513
34. Frick LR, Rapanelli M. Antidepressants: influence on cancer and immunity? *Life Sci*. (2013) 92:525–32. doi: 10.1016/j.lfs.2013.01.020
35. Velnati S, Massarotti A, Antona A, Talmon M, Fresu LG, Galetto AS, et al. Structure activity relationship studies on Amb639752: toward the identification of a common pharmacophoric structure for DGKalpha inhibitors. *J Enzyme Inhib Med Chem*. (2020) 35:96–108. doi: 10.1080/14756366.2019.1684911
36. Muehlbacher M, Tripal P, Roas F, Kornhuber J. Identification of drugs inducing phospholipidosis by novel *in vitro* data. *ChemMedChem*. (2012) 7:1925–34. doi: 10.1002/cmdc.201200306
37. Ostad Haji E, Hiemke C, Pfuhlmann B. Therapeutic drug monitoring for antidepressant drug treatment. *Curr Pharm Des*. (2012) 18:5818–27. doi: 10.2174/138161212803523699
38. Church MK, Church DS. Pharmacology of antihistamines. *Indian J Dermatol*. (2013) 58:219–24. doi: 10.4103/0019-5154.110832
39. Medina VA, Rivera ES. Histamine receptors and cancer pharmacology. *Br J Pharmacol*. (2010) 161:755–67. doi: 10.1111/j.1476-5381.2010.00961.x
40. Sarrouilhe D, Clarhaut J, Defamie N, Mesnil M. Serotonin and cancer: what is the link? *Curr Mol Med*. (2015) 15:62–77. doi: 10.2174/1566524015666150114113411
41. Sarrouilhe D, Mesnil M. Serotonin and human cancer: a critical view. *Biochimie*. (2019) 161:46–50. doi: 10.1016/j.biochi.2018.06.016
42. Reasor MJ, Hastings KL, Ulrich RG. Drug-induced phospholipidosis: issues and future directions. *Expert Opin Drug Saf*. (2006) 5:567–83. doi: 10.1517/14740338.5.4.567
43. Halliwell WH. Cationic amphiphilic drug-induced phospholipidosis. *Toxicol Pathol*. (1997) 25:53–60. doi: 10.1177/019262339702500111
44. Kornhuber J, Tripal P, Reichel M, Muhle C, Rhein C, Muehlbacher M, et al. Functional inhibitors of acid sphingomyelinase (FIASMAs): a novel pharmacological group of drugs with broad clinical applications. *Cell Physiol Biochem*. (2010) 26:9–20. doi: 10.1159/000315101
45. Vater M, Mockl L, Gormanns V, Schultz Fademrecht C, Mallmann AM, Ziegart-Sadowska K, et al. New insights into the intracellular distribution pattern of cationic amphiphilic drugs. *Sci Rep*. (2017) 7:44277. doi: 10.1038/srep44277
46. Marceau F, Bawolak MT, Lodge R, Bouthillier J, Gagne-Henley A, Gaudreault RC, et al. Cation trapping by cellular acidic compartments: beyond the concept of lysosomotropic drugs. *Toxicol Appl Pharmacol*. (2012) 259:1–12. doi: 10.1016/j.taap.2011.12.004
47. Lu S, Sung T, Lin N, Abraham RT, Jessen BA. Lysosomal adaptation: how cells respond to lysosomotropic compounds. *PLoS ONE*. (2017) 12:e0173771. doi: 10.1371/journal.pone.0173771
48. Caccia S, Garattini S. Formation of active metabolites of psychotropic drugs. An updated review of their significance. *Clin Pharmacokinet*. (1990) 18:434–59. doi: 10.2165/00003088-199018060-00002
49. Modica-Napolitano JS, Aprille JR. Delocalized lipophilic cations selectively target the mitochondria of carcinoma cells. *Adv Drug Deliv Rev*. (2001) 49:63–70. doi: 10.1016/S0169-409X(01)00125-9
50. Sivandzade F, Bhalerao A, Cucullo L. Analysis of the mitochondrial membrane potential using the cationic JC-1 dye as a sensitive fluorescent probe. *Bio Protoc*. (2019) 9:e3128. doi: 10.21769/BioProtoc.3128
51. de Duve C, de Barsy T, Poole B, Trouet A, Tulkens P, Van Hoof F. Commentary. Lysosomotropic agents. *Biochem Pharmacol*. (1974) 23:2495–531. doi: 10.1016/0006-2952(74)90174-9
52. Rodriguez-Enriquez S, Kim I, Currin RT, Lemasters JJ. Tracker dyes to probe mitochondrial autophagy (mitophagy) in rat hepatocytes. *Autophagy*. (2006) 2:39–46. doi: 10.4161/auto.2229
53. Biever A, Valjent E, Puighermanal E. Ribosomal protein S6 phosphorylation in the nervous system: from regulation to function. *Front Mol Neurosci*. (2015) 8:75. doi: 10.3389/fnmol.2015.00075
54. Mizushima N, Yoshimori T, Levine B. Methods in mammalian autophagy research. *Cell*. (2010) 140:313–26. doi: 10.1016/j.cell.2010.01.028
55. Goldman SD, Funk RS, Rajewski RA, Krise JP. Mechanisms of amine accumulation in, and egress from, lysosomes. *Bioanalysis*. (2009) 1:1445–59. doi: 10.4155/bio.09.128
56. Kornhuber J, Tripal P, Reichel M, Terfloth L, Bleich S, Wiltfang J, et al. Identification of new functional inhibitors of acid sphingomyelinase using a structure-property-activity relation model. *J Med Chem*. (2008) 51:219–37. doi: 10.1021/jm070524a
57. Anderson N, Borlak J. Drug-induced phospholipidosis. *FEBS Lett*. (2006) 580:5533–40. doi: 10.1016/j.febslet.2006.08.061
58. Aits S, Kricker J, Liu B, Ellegaard AM, Hamalisto S, Tvingsholm S, et al. Sensitive detection of lysosomal membrane permeabilization by lysosomal galectin puncta assay. *Autophagy*. (2015) 11:1408–24. doi: 10.1080/15548627.2015.1063871
59. Wu YT, Tan HL, Shui G, Bauvy C, Huang Q, Wenk MR, et al. Dual role of 3-methyladenine in modulation of autophagy via different temporal patterns of inhibition on class I and III phosphoinositide 3-kinase. *J Biol Chem*. (2010) 285:10850–61. doi: 10.1074/jbc.M109.080796
60. Montaser M, Lalmanach G, Mach L. CA-074, but not its methyl ester CA-074Me, is a selective inhibitor of cathepsin B within living cells. *Biol Chem*. (2002) 383:1305–1308. doi: 10.1515/BC.2002.147
61. Qadir M, O'Loughlin KL, Fricke SM, Williamson NA, Greco WR, Minderman H. Cyclosporin A is a broad-spectrum multidrug resistance modulator. *Clin Cancer Res*. (2005) 11:2320–6. doi: 10.1158/1078-0432.CCR-04-1725
62. Hendouei N, Saghafi F, Shadfar F, Hosseinimehr SJ. Molecular mechanisms of anti-psychotic drugs for improvement of cancer treatment. *Eur J Pharmacol*. (2019) 856:172402. doi: 10.1016/j.ejphar.2019.05.031
63. Schulz M, Schmoldt A. Therapeutic and toxic blood concentrations of more than 800 drugs and other xenobiotics. *Pharmazie*. (2003) 58:447–74.

64. Hollemans M, Elferink RO, De Groot PG, Strijland A, Tager JM. Accumulation of weak bases in relation to intralysosomal pH in cultured human skin fibroblasts. *Biochim Biophys Acta*. (1981) 643:140–51. doi: 10.1016/0005-2736(81)90226-1
65. Nadanaciva S, Lu S, Gebhard DF, Jessen BA, Pennie WD, Will Y. A high content screening assay for identifying lysosomotropic compounds. *Toxicol In Vitro*. (2011) 25:715–23. doi: 10.1016/j.tiv.2010.12.010
66. Lu S, Jessen B, Strock C, Will Y. The contribution of physicochemical properties to multiple *in vitro* cytotoxicity endpoints. *Toxicol In Vitro*. (2012) 26:613–20. doi: 10.1016/j.tiv.2012.01.025
67. Logan R, Kong AC, Axcell E, Krise JP. Amine-containing molecules and the induction of an expanded lysosomal volume phenotype: a structure-activity relationship study. *J Pharm Sci*. (2014) 103:1572–80. doi: 10.1002/jps.23949
68. Zhitomirsky B, Yunaev A, Kreiserman R, Kaplan A, Stark M, Assaraf YG. Lysosomotropic drugs activate TFEB via lysosomal membrane fluidization and consequent inhibition of mTORC1 activity. *Cell Death Dis*. (2018) 9:1191. doi: 10.1038/s41419-018-1227-0
69. Gonzalez-Rothi RJ, Zander DS, Ros PR. Fluoxetine hydrochloride (Prozac)-induced pulmonary disease. *Chest*. (1995) 107:1763–5. doi: 10.1378/chest.107.6.1763
70. Shahane SA, Huang R, Gerhold D, Baxa U, Austin CP, Xia M. Detection of phospholipidosis induction: a cell-based assay in high-throughput and high-content format. *J Biomol Screen*. (2014) 19:66–76. doi: 10.1177/1087057113502851
71. Ranjan A, Srivastava SK. Penfluridol suppresses pancreatic tumor growth by autophagy-mediated apoptosis. *Sci Rep*. (2016) 6:26165. doi: 10.1038/srep26165
72. Vucicevic L, Misirkic-Marjanovic M, Harhaji-Trajkovic L, Maric N, Trajkovic V. Mechanisms and therapeutic significance of autophagy modulation by antipsychotic drugs. *Cell Stress*. (2018) 2:282–291. doi: 10.15698/cst2018.11.161
73. Gassen NC, Rein T. Is there a role of autophagy in depression and antidepressant action? *Front Psychiatry*. (2019) 10:337. doi: 10.3389/fpsyt.2019.00337
74. Petersen NH, Olsen OD, Groth-Pedersen L, Ellegaard AM, Bilgin M, Redmer S, et al. Transformation-associated changes in sphingolipid metabolism sensitize cells to lysosomal cell death induced by inhibitors of acid sphingomyelinase. *Cancer Cell*. (2013) 24:379–93. doi: 10.1016/j.ccr.2013.08.003
75. Breiden B, Sandhoff K. Emerging mechanisms of drug-induced phospholipidosis. *Biol Chem*. (2019) 401:31–46. doi: 10.1515/hsz-2019-0270
76. Boya P, Kroemer G. Lysosomal membrane permeabilization in cell death. *Oncogene*. (2008) 27:6434–51. doi: 10.1038/onc.2008.310
77. Ono K, Kim SO, Han J. Susceptibility of lysosomes to rupture is a determinant for plasma membrane disruption in tumor necrosis factor alpha-induced cell death. *Mol Cell Biol*. (2003) 23:665–76. doi: 10.1128/MCB.23.2.665-676.2003
78. Wang F, Salvati A, Boya P. Lysosome-dependent cell death and deregulated autophagy induced by amine-modified polystyrene nanoparticles. *Open Biol*. (2018) 8:170271. doi: 10.1098/rsob.170271
79. Repnik U, Hafner Cesen M, Turk B. Lysosomal membrane permeabilization in cell death: concepts and challenges. *Mitochondrion*. (2014) 19(Pt A):49–57. doi: 10.1016/j.mito.2014.06.006
80. Santi M, Baldelli G, Diotallevi A, Galluzzi L, Schiavano GF, Brandi G. Metformin prevents cell tumorigenesis through autophagy-related cell death. *Sci Rep*. (2019) 9:66. doi: 10.1038/s41598-018-37247-6
81. Chude CI, Amaravadi RK. Targeting autophagy in cancer: update on clinical trials and novel inhibitors. *Int J Mol Sci*. (2017) 18:1279. doi: 10.3390/ijms18061279
82. Kucharewicz K, Dudkowska M, Zawadzka A, Ogrodnik M, Szczepankiewicz AA, Czarnocki Z, et al. Simultaneous induction and blockade of autophagy by a single agent. *Cell Death Dis*. (2018) 9:353. doi: 10.1038/s41419-018-0383-6
83. Cirone M, Gilardini Montani MS, Granato M, Garufi A, Faggioni A, D'Orazi G. Autophagy manipulation as a strategy for efficient anticancer therapies: possible consequences. *J Exp Clin Cancer Res*. (2019) 38:262. doi: 10.1186/s13046-019-1275-z
84. Kroemer G, Galluzzi L, Brenner C. Mitochondrial membrane permeabilization in cell death. *Physiol Rev*. (2007) 87:99–163. doi: 10.1152/physrev.00013.2006
85. del Cuvillo A, Mullol J, Bartra J, Davila I, Jauregui I, Montoro J, et al. Comparative pharmacology of the H1 antihistamines. *J Investig Allergol Clin Immunol*. (2006) 16(Suppl. 1):3–12.
86. Mauri MC, Paletta S, Maffini M, Colasanti A, Dragogna F, Di Pace C, et al. Clinical pharmacology of atypical antipsychotics: an update. *EXCLI J*. (2014) 13:1163–91.
87. Chubak J, Boudreau DM, Rulyak SJ, Mandelson MT. Colorectal cancer risk in relation to antidepressant medication use. *Int J Cancer*. (2011) 128:227–32. doi: 10.1002/ijc.25322
88. Ellegaard AM, Dehlendorff C, Vind AC, Anand A, Cederkvist L, Petersen NHT, et al. Repurposing cationic amphiphilic antihistamines for cancer treatment. *EBioMedicine*. (2016) 9:130–9. doi: 10.1016/j.ebiom.2016.06.013

Conflict of Interest: The authors declare that the research was conducted in the absence of any commercial or financial relationships that could be construed as a potential conflict of interest.

Journal of Enzyme Inhibition and Medicinal Chemistry

ISSN: (Print) (Online) Journal homepage: https://www.tandfonline.com/loi/ienz20

Structure activity relationship studies on Amb639752: toward the identification of a common pharmacophoric structure for DGKα inhibitors

Suresh Velnati , Alberto Massarotti , Annamaria Antona , Maria Talmon , Luigia Grazia Fresu , Alessandra Silvia Galetto , Daniela Capello , Alessandra Bertoni , Valentina Mercalli , Andrea Graziani , Gian Cesare Tron & Gianluca Baldanzi

To cite this article: Suresh Velnati , Alberto Massarotti , Annamaria Antona , Maria Talmon , Luigia Grazia Fresu , Alessandra Silvia Galetto , Daniela Capello , Alessandra Bertoni , Valentina Mercalli , Andrea Graziani , Gian Cesare Tron & Gianluca Baldanzi (2020) Structure activity relationship studies on Amb639752: toward the identification of a common pharmacophoric structure for DGKα inhibitors, Journal of Enzyme Inhibition and Medicinal Chemistry, 35:1, 96-108, DOI: 10.1080/14756366.2019.1684911

To link to this article: https://doi.org/10.1080/14756366.2019.1684911

JOURNAL OF ENZYME INHIBITION AND MEDICINAL CHEMISTRY
2020, VOL. 35, NO. 1, 96–108
https://doi.org/10.1080/14756366.2019.1684911

Taylor & Francis
Taylor & Francis Group

RESEARCH PAPER

OPEN ACCESS Check for updates

Structure activity relationship studies on Amb639752: toward the identification of a common pharmacophoric structure for DGKα inhibitors

Suresh Velnati[a,b]*, Alberto Massarotti[c]*, Annamaria Antona[a], Maria Talmon[d], Luigia Grazia Fresu[d], Alessandra Silvia Galetto[a,e], Daniela Capello[a], Alessandra Bertoni[a], Valentina Mercalli[c], Andrea Graziani[f,g], Gian Cesare Tron[c]† and Gianluca Baldanzi[a,b]†

[a]Department of Translational Medicine, University of Piemonte Orientale, Novara, Italy; [b]Institute for Research and Cure of Autoimmune Diseases, CAAD, University of Piemonte Orientale, Novara, Italy; [c]Department of Pharmaceutical Sciences, University of Piemonte Orientale, Novara, Italy; [d]Department of Health Sciences, School of Medicine, University of Piemonte Orientale, Novara, Italy; [e]Palliative Care Division, A.S.L., Vercelli, Italy; [f]Università Vita-Salute San Raffaele, Milan, Italy; [g]Department of Molecular Biotechnology and Health Sciences, Molecular Biotechnology Center, University of Torino, Turin, Italy

ABSTRACT

A series of analogues of Amb639752, a novel diacylglycerol kinase (DGK) inhibitor recently discovered by us via virtual screening, have been tested. The compounds were evaluated as DGK inhibitors on α, θ, and ζ isoforms, and as antagonists on serotonin receptors. From these assays emerged two novel compounds, namely **11** and **20**, which with an IC_{50} respectively of 1.6 and 1.8 μM are the most potent inhibitors of DGKα discovered to date. Both compounds demonstrated the ability to restore apoptosis in a cellular model of X-linked lymphoproliferative disease as well as the capacity to reduce the migration of cancer cells, suggesting their potential utility in preventing metastasis. Finally, relying on experimental biological data, molecular modelling studies allow us to set a three-point pharmacophore model for DGK inhibitors.

ARTICLE HISTORY
Received 8 August 2019
Revised 21 October 2019
Accepted 21 October 2019

KEYWORDS
Diacylglycerol kinase; kinase inhibitors; structure–activity relationship; enzyme assays; molecular modelling

1. Introduction

Diacylglycerol kinases (DGKs) are a large family of enzymes that share a common catalytic activity: the phosphorylation of diacylglycerol (DAG) to phosphatidic acid (PA). Remarkably, both the substrate (DAG) and the product (PA) of the DGK-catalysed reaction, are bioactive lipids that can act as second messengers[1]. DGK activity consequently serves as a switch to simultaneously dampen DAG-mediated signals and boost PA-mediated signals[2]. Ten mammalian DGK isoforms (α, β, γ, δ, ε, ζ, η, θ, ι, and κ) have been identified and divided into five groups (type I–V) according to their structural features[3,4]. The expression of these isoforms varies depending on the cell type. Among the 10 isoforms, the α isoform is among the most studied and characterised. This kinase is highly expressed in the brain, spleen, and thymus and, along with θ isoform, in the bone marrow. This enzyme is also highly expressed in T-lymphocytes, where it acts together with DGKζ as negative regulator of the T-cell receptor (TCR) response, and a mediator of IL-2 mediated proliferation[3,5]. The biological relevance of DGKα is best demonstrated in patients with X-linked lymphoproliferative disease (XLP-1), who experience life-threatening, uncontrolled accumulation of $CD8^+$ T cells in response to the Epstein–Barr virus (EBV) infection[6]. In those patients, germline mutations of the adaptor protein SAP (SH2D1A) perturb TCR signalling and render DGKα constitutively active[7]. Deregulated DGKα activity renders patient-derived lymphocytes resistant to reactivation-induced cell death (RICD). Thus, antigen-activated lymphocytes accumulate in lymphonodes and liver, resulting in severe immunopathology[8]. Importantly, DGKα inhibitors restore RICD sensitivity *in vitro* and *in vivo*, thus avoiding immunopathology and suggesting a putative therapeutic use of those molecules in XLP-1[9].

Apart from T-cell regulation, DGKα also plays a role in cancer, mediating numerous aspects of cancer cell progression including survival[10,11], migration and invasion of cancer cells[12–14]. In particular, it has been reported that DGKα is over expressed in hepatocellular carcinoma[15], and melanoma cells[11] while other reports suggested that the growth of colon and breast cancer cell lines was significantly inhibited by DGKα-siRNA[16] and DGKα/atypical PKC/β1 integrin signalling pathway was crucial for matrix invasion of breast carcinoma cells[17]. In addition, expression is also higher in lymphonodal metastasis than in breast and gastric original tumour[18,19]. Finally, knock down of DGKα impairs glioblastoma tumorigenesis[20,21].

For all these reasons, the identification of strong and selective DGKα inhibitors, it is an important field of research. To date, only a handful of two-digit micromolar inhibitors of DGKα have been identified, but only three were the most characterised, namely, R59949, R59022, and ritanserin (Figure 1).

In our assay system, R59949 and R59022 have an IC_{50} of 11 and 20 μM, respectively[9]. Their efficacy has been evaluated *in vivo*

CONTACT Andrea Graziani andrea.graziani@hsr.it Università Vita-Salute San Raffaele, Milan 20132, Italy; Gian Cesare Tron giancesare.tron@uniupo.it Department of Pharmaceutical Science, University of Piemonte Orientale, Novara 28100, Italy
*These authors contributed equally to this work.
†These authors shared senior authorship.

Supplemental data for this article can be accessed here.

studies on mice, and is limited by their rapid clearance ($t_{1/2}$=~2 h)[22]. Furthermore, these two inhibitors are also able to target different isoforms of DGK, in particular R59022 acts on type III and V (ε e θ), while R59949 on type I and II (γ, δ e κ)[23,24] and a study conducted by Boroda et al. recently demonstrated their strong antagonistic activity on 5-HT_2 receptors (R59022 IC_{50} $5HT_{2A}$=2.2 nM; R5994 IC_{50} $5HT_{2A}$=9.2 nM)[25].

A search on ChEMBL database[26] (https://www.ebi.ac.uk/chembl/) show how these two molecules have activity at the same range of concentration with other biological targets, behaving like a sort of promiscuous ligands. Ritanserin, a well-known serotoninergic antagonist, is structurally similar to R59022, differing for an H-F isosteric substitution on a phenyl ring. Despite this small modification, Boroda et al. showed that ritanserin was a DGKα inhibitor (IC_{50}=15 μM) more potent than R59022 and R59949 and with a better pharmacokinetic profile ($t_{1/2}$=40 h in human)[25]. However, the comparison of ritanserin IC_{50} as serotonin antagonist and as DGKα inhibitor, 0.9 nM and 15,000 nM, respectively, reveal that ritanserin is much a powerful serotonin antagonist than a DGK inhibitor. In addition, ritanserin is also a potent inhibitor on dopaminergic receptors with an IC_{50} of 69 nM[27].

Due to these drawbacks, at the beginning, in order to eliminate the strong serotoninergic activity of R59949, we reasoned to replace its protonable nitrogen atom, which at physiologically pH mimics the amino group of serotonin, with a carbon atom. We decided therefore to synthesise compound **1** (Figure 2) (see supporting information for its synthesis and a complete characterisation) and to test it as DGKα inhibitor.

Interestingly, the compound was totally devoid of inhibitory activity on the enzyme, showing the importance of the basic nitrogen atom not only for the anti-serotoninergic activity, but also for the interaction with the kinase. With this in mind, we recently used an in-silico approach based on chemical homology with the two commercially available DGKα inhibitors R59022 and R59949 using the programmes ROCS[28] and EON[29]. From this study, we identified a compound, Amb639752 (Figure 2), featuring a lower IC_{50} for DGKα than ritanserin (IC_{50}=17 μM), a better selectivity for the α-isoform and devoid of anti-serotoninergic activity. Along with CU-3, which features an IC_{50} of 0.6 μM on DGKα[30] but contains a reactive Michael acceptor[31], Amb639752 is the most effective pharmacological tool available to study DGKα[9]. In this manuscript, we report the structure–activity studies on Amb639752 and, in combination with data on ritanserin, the generation of a pharmacophore model for this class of compounds, which could be useful for the identification of other potential DGKα inhibitors.

2. Methods

2.1. Chemistry procedures

Commercially available reagents and solvents were used without further purification. Toluene were distilled immediately before use from Na/benzophenone under a slight positive atmosphere of dry nitrogen. Dichloromethane was dried by distillation from P_2O_5 and stored on activated molecular sieves (4 Å). When needed the reactions were performed in flame- or oven-dried glassware under a positive pressure of dry nitrogen. Melting points were determined in open glass capillary with a Stuart scientific SMP3 apparatus and are uncorrected. All compounds were checked by IR (FT-IR THERMO-NICOLET AVATAR), ^{1}H and 13C APT (JEOL ECP 300 MHz spectrometer), and mass spectrometry (Thermo Finningan LCQ-deca XP-plus, San Jose, CA) equipped with an ESI source and an ion trap detector. Chemical shifts are reported in parts per million (ppm). Flash column chromatography was performed on silica gel (Merck Kieselgel 60, 230–400 mesh ASTM, Kenilworth, NJ). Thin layer chromatography (TLC) was carried out on 5 × 20 cm plates with a layer thickness of 0.25 mm (Merck Silica gel 60 F_{254}, Kenilworth, NJ). When necessary they were developed with $KMnO_4$ reagent. Purity of tested compounds was established by elemental analysis. Elemental analysis (C, H, N) of the target compounds is within ±0.4% of the calculated values, confirming ≥95% purity.

2.1.1. Preparation of 2-chloro-1-(2,6-dimethyl-1H-indol-3-yl)ethan-1-one (5)

In a Schlenk tube, under nitrogen, 2,6-dimethyl-1*H*-indole (**3**) (0.20 g, 1.38 mmol, 1 eq) was dissolved in 4 mL of dichloroethane dry and 0.25 mL of DBU (1.66 mmol, 1.2 eq) were added. The resulting solution was heated at 90 °C. When reached this temperature, chloroacetyl chloride (**4**) (0.12 mL, 1.52 mmol, 1.1 eq) was added. The reaction was stirred for 30 min, then solvent was evaporated and the crude purified by column chromatography using PE/EtOAc 7:3 and PE/EtOAc 5:5 as eluants to give 270 mg of product as violet solid: yield 90%; m.p. 243.7–244.2 °C; ^{1}H NMR (300 MHz, DMSO-d_6) δ 11.88 (br s, NH), 7.85 (d, J = 7.9 Hz, 1H), 7.18 (s, 1H), 6.99 (d, J = 8.0 Hz, 1H), 4.89 (s, 2H), 2.68 (s, 3H), 2.39 (s, 3H). MS (ESI) *m/z*: 222 $[M+H]^+$.

2.1.2. Preparation of tert-butyl 4-(2-(2,6-dimethyl-1H-indol-3-yl)-2-oxoethyl)piperazine-1-carboxylate (6)

Under nitrogen, 200 mg of **5** (0.90 mmol, 1 eq) was dissolved in toluene dry, then *N*-Boc-piperazine (0.17 g, 0.90 mmol, 1 eq), K_2CO_3 (0.32 g, 2.25 mmol, 2.5 eq), and KI (0.015 g, 0.09 mmol,

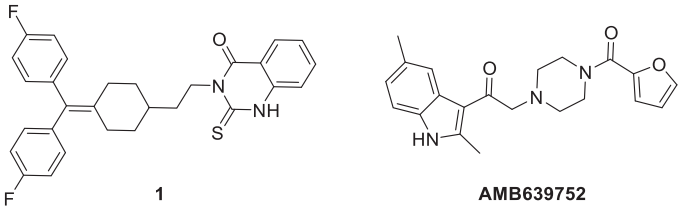

Figure 2. Structures of the deaza analogue of R59949 and Amb639752.

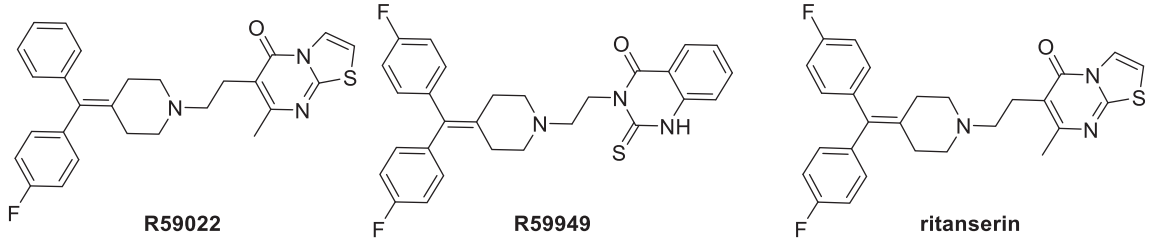

Figure 1. Three of the most studied DGKα inhibitors.

0.1 eq) were added. The reaction was heated at 80 °C overnight. Solvent was evaporated and the crude was purified by column chromatography using PE/EtOAc 4:6 and PE/EtOAc 2:8 as eluants to give 215 mg of product as yellow amorphous solid: yield 63%; ^{1}H NMR (300 MHz, $CDCl_3$) δ 8.52 (br s, NH), 7.77 (d, $J = 8.2$ Hz, 1H), 7.12 (s, 1H), 7.08 (d, $J = 8.0$ Hz, 1H), 3.79 (s, 2H), 3.47–3.43 (m, 6H), 2.75 (s, 3H), 2.64 (br s, 2H), 2.44 (s, 3H), 1.47 (s, 9H). IR (KBr): 3190, 2964, 1698, 1413, 1417, 1364, 1126, 806 ν_{max}/cm^{-1}. MS (ESI) *m/z*: 372 $[M + H]^+$.

2.1.3. Preparation of 1-(2,6-dimethyl-1H-indol-3-yl)-2-(piperazin-1-yl)ethan-1-one (7)

Two hundred and fifteen milligrams of **6** (0.58 mmol, 1 eq) were dissolved in dichloromethane dry. The resulting solution was cooled at 0 °C and 0.69 mL of trifluoroacetic acid (9.28 mmol, 16 eq) was added. After 3 h, the reaction was worked up adding NaOH 2 M solution until pH = 12. Then, NaCl solid was added and the solution was extracted with THF (x2). The combined organic phases were dried on sodium sulphate. After evaporation of the solvent, the crude was purified by column chromatography using EtOAc/MeOH 9:1 and MeCN/NH_3 9:1 as eluants to give 103 mg of the product as yellowish solid: yield: 65%; m.p.: 232.9–233.6 °C; ^{1}H NMR (300 MHz, DMSO-d_6) δ 11.79 (br s, NH), 7.85 (d, $J = 7.9$ Hz, 1H), 7.15 (s, 1H), 6.95 (d, $J = 8.2$ Hz, 1H), 3.83(br s, 4H), 3.62 (s, 2H), 2.86 (br s, 4H), 2.67 (s, 3H), 2.38 (s, 3H); IR (KBr): 3446, 3181, 2813, 1634, 1455, 1330, 821 ν_{max}/cm^{-1}; MS (ESI) *m/z*: 272 $[M + H]^+$.

2.1.4. General procedure for the synthesis of final compounds 8, 11–22

1-(2,6-Dimethyl-1*H*-indol-3-yl)-2-(piperazin-1-yl)ethan-1-one (**7**) (1 eq) was dissolved in dichloromethane dry. To the resulting solution EDCI (1 eq), TEA (2 eq), DMAP (0.1 eq) and the appropriate carboxylic acid (1 eq) were sequentially added. The reaction was stirred under nitrogen at room temperature overnight. Evaporation of the solvent gave a crude which was directly purified by column chromatography.

2.1.5. 2-(4-Benzoylpiperazin-1-yl)-1-(2,6-dimethyl-1H-indol-3-yl)ethan-1-one (8)

Yellow solid; yield 29%; column eluants: EtOAc, EtOAc/MeOH 9:1; m.p.: 213.8–214.3 °C. ^{1}H NMR (300 MHz, DMSO-d_6) δ 11.72 (br s, NH), 7.85 (d, $J = 8.2$ Hz, 1H), 7.46–7.40 (m, 5H), 7.15 (s, 1H), 6.96 (d, $J = 7.9$ Hz, 1H), 3.67 (br s, 4H), 3.18 (br s, 2H) 2.67 (s, 3H), 2.61–2.56 (m, 4H), 2.38 (s, 3H); ^{13}C NMR (75 MHz, DMSO-d_6) δ 192.8, 169.5, 144.7, 136.5, 135.7, 131.5, 130.0, 129.0, 127.5, 125.1, 123.4, 121.2, 112.9, 111.6, 66.9, 53.2, 53.1, 21.7, 15.7; IR (KBr) 3189, 2990, 2828, 1609, 1446, 1282, 807 ν_{max}/cm^{-1}. MS (ESI) *m/z*: 374 $[M–H]^+$. Anal. Calcd. for $C_{23}H_{25}N_3O_2$: C, 73.57; H, 6.71; N, 11.19; found C, 73.76; H, 6.94; N, 10.85.

2.1.6. 2-(4-(4-Chlorobenzoyl)piperazin-1-yl)-1-(2,6-dimethyl-1H-indol-3-yl)ethan-1-one (11)

Yellow solid; yield 33%; column eluants: EtOAc, EtOAc/MeOH 9:1; m.p.: 240.7–241.3 °C; ^{1}H NMR (300 MHz, DMSO-d_6) δ 11.70 (br s, NH), 7.85 (d, $J = 7.9$ Hz, 1H), 7.50 (br d, AA'XX', 2H), 7.42 (br d, AA'XX', 2H), 7.14 (s, 1H), 6.95 (d, $J = 8.2$ Hz, 1H), 3.67 (br s, 4H), 3.33 (br s), 2.67 (s, 3H), 2.61–2.56 (m, 4H), 2.38 (s, 3H); ^{13}C NMR (75 MHz, DMSO-d_6) δ 193.17, 168.4, 144.8, 135.7, 135.2, 134.8, 131.5, 129.5, 129.1, 125.1, 123.5, 121.2, 112.7, 111.6, 53.14, 53.14, 52.9, 21.7, 15.7. IR (KBr): 3225, 2793, 2358, 1609, 1442, 1261, 864 ν_{max}/cm^{-1}. MS (ESI) *m/z*: 410 $[M + H]^+$. Anal. Calcd. for $C_{23}H_{24}ClN_3O_2$: C, 67.39; H, 5.90; N, 10.25; found C, 67.11; H, 6.12; N, 10.54.

2.1.7. 1-(2,6-Dimethyl-1H-indol-3-yl)-2-(4-(4-methoxybenzoyl)piperazin-1-yl)ethan-1-one (12)

Yellow solid; yield 53%; column eluants: EtOAc, EtOAc/MeOH 9:1; m.p.: 219.9–220.8 °C.; ^{1}H NMR (300 MHz, DMSO-d_6) δ 11.70 (br s, NH), 7.85 (d, $J = 8.2$ Hz, 1H), 7.38 (br d, AA'XX', 2H), 7.14 (s, 1H), 6.99–6.94 (m, 3H), 3.79 (br d, 3H), 3.67 (br s, 2H), 3.51 (br s, 4H) 2.67 (s, 3H), 2.58 (br s, 4H), 2.38 (s, 3H); ^{13}C NMR (75 MHz, DMSO-d_6) δ 192.8, 169.5, 144.6, 136.5, 135.7, 131.5, 130.0, 129.0, 127.5, 125.1, 123.4, 121.2, 112.8, 111.6, 66.9, 55.8, 53.2, 53.1, 21.7, 15.7; IR (KBr): 3235, 3003, 2807, 1613, 1463, 1253, 977 ν_{max}/cm^{-1}; MS (ESI) *m/z*: 406 $[M + H]^+$. Anal. Calcd. for $C_{24}H_{27}N_3O_3$: C, 71.09; H, 6.71; N, 10.36; found C, 71.10; H, 6.75; N, 10.32.

2.1.8. 4-(4-(2-(2,6-Dimethyl-1H-indol-3-yl)-2-oxoethyl)piperazine-1-carbonyl)benzonitrile (13)

Yellow solid; yield 23%; column eluants: EtOAc, EtOAc/MeOH 9:1; m.p.: 243.9–244.8 °C. ^{1}H NMR (300 MHz, DMSO-d_6) δ 11.70 (br s, NH), 7.92–7.84 (m, 3H), 7.58 (br d, AA'XX', 2H), 7.15 (s, 1H), 6.96 (br d, 1H), 3.68 (br s, 4H), 3.29 (br s, 2H), 2.67 (s, 3H), 2.51 (br s, 4H), 2.38 (s, 3H); ^{13}C NMR (75 MHz, DMSO-d_6) δ 192.5, 166.3, 143.2, 139.4, 134.1, 131.6, 129.9, 126.8, 123.5, 121.9, 119.6, 117.4, 111.2, 111.1, 110.1, 65.1, 51.7, 51.2, 20.1, 14.1; IR (KBr): 3410, 3254, 2816, 2790, 2233, 1609, 1454, 1291, 979 ν_{max}/cm^{-1}; MS (ESI) *m/z*: 401$[M + H]^+$. Anal. Calcd. for $C_{24}H_{24}N_4O_2$: C, 71.98; H, 6.04; N, 13.99; found C, 72.13; H, 6.23; N, 14.08.

2.1.9. 1-(2,6-Dimethyl-1H-indol-3-yl)-2-(4-(thiophene-2-carbonyl)piperazin-1-yl)ethan-1-one (14)

Yellow solid; yield 29%; column eluants: EtOAc, EtOAc/MeOH 9:1; m.p.: 200.3–201.2 °C; ^{1}H NMR (300 MHz, DMSO-d_6) δ 11.74 (br s, NH), 7.86 (d, $J = 8.2$ Hz, 1H), 7.76 (br d, 1H), 7.41–7.40 (m, 1H), 7.15–7.10 (m, 2H), 6.96 (d, $J = 8.2$ Hz, 1H), 3.75–3.67 (m, 4H), 3.37 (br s, 2H) 2.68 (s, 3H), 2.62 (s, 4H), 2.38 (s, 3H); ^{13}C NMR (75 MHz, DMSO-d_6) δ 192.8, 167.8, 144.7, 137.8, 135.7, 131.5, 130.0, 129.6, 127.7, 125.1, 124.1, 123.4, 121.2, 112.8, 111.6, 66.7, 53.3, 21.7, 15.7; IR (KBr): 3270, 2927, 2793, 1642, 1454, 1261, 809 ν_{max}/cm^{-1}; MS (ESI) *m/z*: 382$[M + H]^+$; Anal. Calcd. for $C_{21}H_{23}N_3O_2S$: C, 66.12; H, 6.08; N, 11.01; found C, 66.23; H, 6.26; N, 10.93.

2.1.10. 1-(2,6-Dimethyl-1H-indol-3-yl)-2-(4-nicotinoylpiperazin-1-yl)ethan-1-one (15)

Yellow solid; yield 39%; column eluants: EtOAc, EtOAc/MeOH 9:1; m.p.: 216.2–216.8 °C; ^{1}H NMR (300 MHz, DMSO-d_6) δ 11.70 (br s, NH), 8.65–8.61 (m, 2H), 7.87–7.82 (m, 2H), 7.50–7.45 (m, 1H), 7.15 (s, 1H), 6.95 (br d, 1H), 3.68 (br s, 4H), 3.37 (br s, 2H), 2.67 (s, 3H), 2.56 (br s, 4H), 2.37 (s, 3H); ^{13}C NMR (75 MHz, DMSO-d_6) δ 192.6, 167.2, 151.0, 148.1, 144.7, 135.7, 135.4, 132.3, 131.5, 125.1, 124.1, 123.5, 121.2, 116.2, 111.6, 66.7, 53.4, 52.9, 21.7, 15.7; IR (KBr): 3414, 3213, 2828, 1621, 1454, 1267, 1301, 817 ν_{max}/cm^{-1}; MS (ESI) *m/z*: 377 $[M + H]^+$; Anal. Calcd. for $C_{22}H_{24}N_4O_2$: C, 70.19; H, 6.43; N, 14.88; found C, 70.21; H, 6.44; N, 14.73.

2.1.11. 1-(2,6-Dimethyl-1H-indol-3-yl)-2-(4-(2-methylbenzoyl)piperazin-1-yl)ethan-1-one (16)

Yellow solid; yield 41%; column eluants: EtOAc, EtOAc/MeOH 9:1; m.p.: 200.5–201.6 °C; ^{1}H NMR (300 MHz, DMSO-d$_6$) δ 11.70 (br s, NH), 7.85 (d, J = 8.2 Hz, 1H), 7.31–7.27 (m, 3H), 7.26–7.24 (m, 2H), 7.15 (d, 1H), 3.69 (br s, 2H), 3.34 (br s, 2H), 3.15 (br s, 2H), 2.67 (s, 3H), 2.51 (br s, 4H), 2.44 (s, 3H), 2.38 (s, 3H); ^{13}C NMR (75 MHz, DMSO-d$_6$) δ 192.6, 169.0, 144.7, 135.7, 134.2, 131.8, 131.5, 130.7, 129.2, 126.4, 126.2, 123.4, 121.2, 112.8, 66.8, 53.5, 53.0, 46.8, 41.4, 21.7, 19.2, 15.7; IR (KBr): 3431, 3221, 2919, 2797, 1615, 1454, 1257, 748 ν_{max}/cm^{-1}; MS (ESI) *m/z*: 390 [M + H]$^+$. Anal. Calcd. for $C_{24}H_{27}N_3O_2$: C, 74.01; H, 6.99; N, 10.79; found C, 74.01; H, 7.01; N, 10.63.

2.1.12. 1-(2,6-Dimethyl-1H-indol-3-yl)-2-(4-(3-methoxybenzoyl)piperazin-1-yl)ethan-1-one (17)

Yellow solid; yield 32%; column eluants: EtOAc, EtOAc/MeOH 9:1; m.p.: 209.8–210.4 °C; ^{1}H NMR (300 MHz, DMSO-d$_6$) δ 11.71 (br s, NH), 7.85 (d, J = 7.9 Hz, 1H), 7.34 (t, 1H), 7.15 (br s, 1H), 7.02–6.92 (m, 4H), 3.78 (s, 3H), 3.68 (br s, 3H), 3.35 (br s, 3H), 2.67 (br s, 7H), 2.38 (s, 3H); ^{13}C NMR (75 MHz, DMSO-d$_6$) δ 192.7, 169.1, 159.7, 144.7, 137.9, 135.7, 131.5, 130.2, 125.1, 123.4, 121.2, 119.4, 115.7, 112.7, 111.6, 66.8, 55.8, 53.3, 53.11, 47.4, 21.7, 15.7; IR (KBr): 3131, 3049, 2944, 1651, 1455, 1292, 1130, 968 ν_{max}/cm^{-1}; MS (ESI) *m/z*: 406 [M + H]$^+$. Anal. Calcd. for $C_{24}H_{27}N_3O_3$: C, 71.09; H, 6.71; N, 10.36; found C, 70.85; H, 6.45; N, 10.76.

2.1.13. 2-(4-(3,4-Difluorobenzoyl)piperazin-1-yl)-1-(2,6-dimethyl-1H-indol-3-yl)ethan-1-one (18)

Yellow solid; yield 27%; column eluants: EtOAc, EtOAc/MeOH 9:1; m.p.: 233.8–235.0 °C; ^{1}H NMR (300 MHz, DMSO-d$_6$) δ 11.71 (br s, NH), 7.85 (d, J = 7.9 Hz, 1H), 7.56–7.47 (m, 2H), 7.28 (br s, 1H), 7.15 (s, 1H), 6.96 (d, J = 7.9 Hz, 1H), 3.68 (br s, 2H), 3.33 (br s, 2H), 2.67 (s, 3H), 2.51 (br s, 6H), 2.38 (s, 3H); MS (ESI) *m/z*: 412 [M + H]$^+$; IR (KBr): 3252, 2919, 2795, 1618, 1469, 1286, 1046, 980 ν_{max}/cm^{-1}; MS (ESI) 412 [M + H]$^+$. Anal. Calcd. for $C_{23}H_{23}F_2N_3O_2$: C, 67.14; H, 5.63; N, 10.21; found C, 67.43; H, 5.79; N, 10.59.

2.1.14. 2-(4-(3-Chlorobenzoyl)piperazin-1-yl)-1-(2,6-dimethyl-1H-indol-3-yl)ethan-1-one (19)

Yellow solid; yield 32%; column eluants: EtOAc, EtOAc/MeOH 9:1; m.p.: 222.3–223.5 °C; ^{1}H NMR (300 MHz, CDCl$_3$) δ 9.42 (br s, NH), 7.71 (d, J = 7.9 Hz, 1H), 7.40–7.25 (m, 4H), 7.04 (d, J = 8.2 Hz, 2H), 3.85 (br s, 4H), 3.47 (br s, 2H), 2.80 (br s, 1H), 2.68 (br s, 6H), 2.40 (s, 3H); ^{13}C NMR (75 MHz CDCl$_3$,) δ 192.5, 169.0, 144.7, 137.5, 135.3, 134.7, 132.3, 130.0, 127.3, 125.2, 124.0, 123.7, 120.6, 112.8, 111.4, 67.0, 53.7, 53.7, 29.6, 21.5, 15.7; IR (KBr): 3264, 2916, 2795, 1646, 1454, 1256, 978, 809 ν_{max}/cm^{-1}; MS (ESI) *m/z*: 410 [M + H]$^+$. Anal. Calcd. for $C_{23}H_{24}ClN_3O_2$: C, 67.39; H, 5.90; N, 10.25; found C, 67.38; H, 5.90; N, 10.24.

2.1.15. 1-(2,6-Dimethyl-1H-indol-3-yl)-2-(4-(4-methylbenzoyl)piperazin-1-yl)ethan-1-one (20)

Yellow solid; yield 48%; column eluants: EtOAc, EtOAc/MeOH 9:1; m.p.: 230.9–231.2 °C; ^{1}H NMR (300 MHz, DMSO-d$_6$) δ 11.71 (br s, NH), 7.86–7.82 (m, 1H), 7.31–7.23 (m, 4H), 7.15 (s, 1H), 6.96 (d, J = 7.9 Hz, 1H), 3.69 (br s, 2H), 3.35 (br s, 4H), 2.67 (s, 3H), 2.51. IR (KBr): 3228, 2915, 2792, 1607, 1454, 1260, 979 ν_{max}/cm^{-1}; MS (ESI) *m/z*: 390 [M + H]$^+$; Anal. Calcd. for $C_{24}H_{27}N_3O_2$: C, 74.01; H, 6.99; N, 10.79; found C, 74.12; H, 7.02; N, 10.79.

2.1.16. 2-(4-(Cyclopentanecarbonyl)piperazin-1-yl)-1-(2,6-dimethyl-1H-indol-3-yl)ethan-1-one (21)

Brown oil; yield 61%; column eluants: EtOAc, EtOAc/MeOH 9:1; ^{1}H NMR (300 MHz, CDCl$_3$) δ 9.00 (br s, NH), 7.73 (d, J = 8.2 Hz, 1H), 7.26 (br d, 1H), 7.12 (s, 1H), 7.05 (d, J = 8.2 Hz, 1H), 3.83 (s, 2H), 3.75 (br s, 2H), 3.63 (br s, 2H), 2.80–2.71 (m, 7H), 2.45 (s, 3H), 1.92–1.46 (m, 7H); IR (KBr): 3253, 2944, 2862, 1650, 1620, 1455, 1234, 957 ν_{max}/cm^{-1}; MS (ESI) *m/z*: 368 [M + H]$^+$; Anal. Calcd. for $C_{22}H_{29}N_3O_2$: C, 71.90; H, 7.95; N, 11.43; found C, 72.23; H, 8.31; N, 11.32.

2.1.17. 1-(4-(2-(2,6-Dimethyl-1H-indol-3-yl)-2-oxoethyl)piperazin-1-yl)heptan-1-one (22)

Brown oil; yield 76%; column eluants: EtOAc, EtOAc/MeOH 9:1; ^{1}H NMR (300 MHz, CDCl$_3$) δ 10.25 (br s, NH), 7.68 (d, J = 8.2 Hz, 1H), 7.08 (s, 1H), 7.00 (d, J = 7.9 Hz, 1H), 3.83 (s, 2H), 3.73 (br s, 2H), 3.56 (br s, 2H), 2.77–2.71 (m, 3H), 2.62 (s, 3H), 2.38 (s, 3H), 2.32–2.27 (m, 5H), 1.59–1.54 (m, 2H), 1.26 (br s, 4H), 0.85 (br t, 3H); ^{13}C NMR (75 MHz, CDCl$_3$) δ 191.7, 172.4, 145.4, 135.5, 132.1, 124.0, 123.6, 120.4, 112.4, 111.6, 66.2, 53.3, 53.1, 45.3, 41.2, 34.5, 31.6, 28.9, 25.0, 22.5, 21.5, 15.6, 14.1; IR (KBr): 2927, 2857, 1731, 1645, 1455, 1434, 1234, 668 ν_{max}/cm^{-1}; MS (ESI) *m/z*: 384 [M + H]$^+$; Anal. Calcd. for $C_{23}H_{33}N_3O_2$: C, 72.03; H, 8.67; N, 10.96; found C, 72.03; H, 8.73; N, 11.21.

2.2. Cell lines

Madin-Darby canine kidney (MDCK) cells stably expressing One Strep Tag DGKα (OST-DGKα) were prepared by infecting MDCK cells with a vector expressing an inducible OST tagged DGKα constructs[17]. MDCK cells infected with empty vector were used as controls. MDCK cells were cultured in MEM (minimal essential medium) with 5% FBS (foetal bovine serum) and 1% antibiotic–antimycotic solution. Routinely, cells were splitted every 3–4 days with trypsin–EDTA 0.25% in standard 100 mm dishes.

Human embryonic kidney 293T cells (10 cm^2 plates) were cultured in RPMI with 10% FBS and 1% penicillin/streptomycin and cultures were maintained by splitting them for every 2–3 days using trypsin–EDTA 0.25%.

Michigan Cancer Foundation 7 (MCF7) cells were cultured in DMEM with 10% FBS + 1% penicillin/streptomycin and cultures were maintained by splitting them for every 2–3 days using trypsin–EDTA 0.25%.

2.3. Primary cells

PBL were isolated from healthy anonymous human donors by Ficoll-Paque PLUS (GE Healthcare, Chicago, IL) density gradient centrifugation, washed, and resuspended at 2×10^6 cell/mL in RPMI-GlutaMAX containing 10% heat inactivated FCS, 2 mM glutamine, and 100 U/mL of penicillin and streptomycin. T cells were activated with 1 μg/mL anti-CD3 (UCHT1) and anti-CD28 (clone CD28.2) antibodies. After three days, activated T cells were washed and cultured in medium additionated of 100 IU/mL rhIL-2 (Peprotech, Rocky Hill, NJ) at 1.2×10^6 cells/mL for $\geq$7 days by changing media for every 2–3 days.

Human monocytes were isolated from healthy anonymous human buffy coats (provided by the Transfusion Service of

Ospedale Maggiore della Carità, Novara, Italy) by the standard technique of dextran sedimentation and Histopaque (density = 1.077 g cm^3, Sigma-Aldrich, Milano, Italy) gradient centrifugation (400×*g*, 30 min, room temperature) and recovered by fine suction at the interface, as described previously[32]. Purified monocytes populations were obtained by adhesion (90 min, 37 °C, 5% CO_2) in serum-free RPMI 1640 medium (Sigma-Aldrich, Milano, Italy) supplemented with 2 mM glutamine and antibiotics. Cell viability (trypan blue dye exclusion) was usually >98%.

2.4. Preparation of DGKα enriched homogenates

Large cultures of MDCK cells for enzyme preparation were done by plating 5×10^6 cells in 245 mm^2 dishes. Once they reached nearly 70% confluence, cells were treated with doxycycline (1 μg/mL, two days). After two days of treatment, each plate was washed in cold PBS and cells homogenised in 5 mL of homogenate buffer (25 mM Hepes (pH 8), 20% glycerol, 135 mM NaCl, 5 mM ethylenediaminetetraacetic acid (EDTA), 1 mM ethylene glycol-bis(-beta-aminoethyl ether)-N,N,N′,N′-tetraacetic acid (EGTA), 1 mM sodium orthovanadate, and protease inhibitor cocktail) for each dish. Cells were collected with a rubber scraper, homogenised by passing them through a 29 G-needle syringe 20 times and stored in aliquots at −80 °C. Presence of OST-DGKα was confirmed by western blotting and enzyme assay, transduced DGKα has an activity >100 folds the endogenous DGK.

2.5. Preparation of DGKζ and DGKθ enriched homogenates

293T cells were transiently transfected with indicated DGK isoform plasmid DNA using Lipofectamine 3000, Invitrogen (Carlsbad, CA). Forty eight hours after transfection, cells were harvested and homogenised with a 29 G-needle using 500 μL of homogenate buffer for each dish and immediately stored in aliquots at −80 °C. Cells transfected with empty vector were used as controls, overexpressed DGK has an activity >50 folds the endogenous.

2.6. DGK assay

Essentionally, the same procedure was followed as reported previously in Velnati et al.[9] In brief, DGK activity was assayed by measuring initial velocities (5 min at 27 °C) in presence of saturating substrate concentrations. Reaction conditions: 0.9 μg/μL 1,2-dioleoyl-sn-glycerol, 5 mM ATP, 0.01 μCi/μL [γ^{32}P]-ATP, 1 mM sodium orthovanadate, 10 mM $MgCl_2$, 1.2 mM EGTA in 7.5 mM Hepes pH 8[12]. Reaction mixture is assembled mixing enzyme (24.5 μL of homogenate), 100× inhibitor or DMSO (0.5 μL), 5× ATP solution (10 μL of 25 mM ATP, 0.05 μCi/μL [γ^{32}P]-ATP (Perkin-Elmer, Milan, Italy), 5 mM sodium orthovanadate, 50 mM $MgCl_2$), and 3.3× DAG solution (15 μL of 3 μg/μL 1,2-dioleoyl-sn-glycerol resuspended by sonication in 4 mM EGTA in 25 mM Hepes pH 8). The reaction was stopped after 5 min by adding 200 μL of freshly prepared 1 M HCl and lipid was extracted by adding 200 μL of CH_3OH:$CHCl_3$ 1:1 solution and vortexing for 1 min. The two phases were separated by centrifugation (12,000 RCF for 2 min). Twenty-five microlitres of the lower organic phase was spotted in small drops on silica TLC plates. TLC was run 10 cm and dried before radioactive signals were detected by GS-250 molecular imager and was quantified by quantity one (Bio-Rad, Hercules, CA) software assuring the absence of saturated spots.

Percentage residual activity was calculated as follows: (OST-DGKα homogenate with inhibitor − vector homogenate)/(OST-DGKα homogenate with DMSO − vector homogenate)×100.

2.7. Superoxide anion (O^{2-}) production

All the experiments were performed in triplicate using cells isolated from each single donor.

Monocytes (250,000 cells/well) were treated for 1 h with the indicated drugs (10 μM) with or without serotonin (1 μM). Then, cells were stimulated with phorbol 12-myristate 13-acetate (PMA; Sigma-Aldrich, Milano, Italy) 1 μM for 30 min. PMA is a well-known stimulus that induces a strong and significant respiratory burst via PKC activation[33]. Superoxide anion production was then evaluated by the superoxide dismutase (SOD)-sensitive cytochrome C (CytC) reduction assay and expressed as nmoles CytC reduced/10^6 cells/30 min, using an extinction coefficient of 21.1 mM. To avoid interference with spectrophotometrical recordings, cells were incubated with RPMI 1640 without phenol red, antibiotics, and FBS.

2.8. RICD assay in SAP silenced T cells

Activated human PBLs were transfected with 200 pmol of siRNA oligonucleotides specific for the target protein (Stealth Select siRNA; Life Technologies, Carlsbad, CA) or a non-specific control oligo (Life Technologies, Carlsbad, CA). Transient transfections were performed using Amaxa nucleofector kits for human T cells (Lonza, Basel, Switzerland) and the Amaxa Nucleofector II or 4D systems (programmes T-20 or EI-115). Cells were cultured in IL-2 (100 IU/mL) for four days to allow target gene knockdown. Knockdown efficiency was periodically evaluated by Western blotting.

Non-specific Stealth RNAi Negative Control Duplexes (12935-300, Life Technologies, Carlsbad, CA) were used as a negative control.

siRNA SAP: sense strand UGUACUGCCUAUGUGUGCUGUAUCA, antisense strand UGAUACAGCAGACAUAGGCAGUACA.

To test restimulation induced cell death, activated T cells (10^5 cells/well) were plated in triplicate in 96-well round-bottom plate and treated with anti-CD3 (clone OKT3) (10 ng/mL) in RPMI-GlutaMAX supplemented with 100 IU/mL rhIL-2 for 24 h. In these assays, inhibitors (10 μM) were added 30 min before the restimulation with OKT3. 24 h after treatment, cells were stained with 20 ng/mL propidium iodide and collected for a constant time of 30 s per sample on Attune Nxt Flow Cytometer (Thermo Fisher Scientific, Waltham, MA). Cell death is expressed as % cell loss and calculated as:

$$\%\ \text{cell loss} = \left(1 - \left(\frac{\text{number of viable cells in sample}}{\text{number of viable cells in control}}\right) \times 100\right)$$

Results were expressed as mean ± standard error of the mean (SEM). We always compared controls and SAP silenced lymphocytes from the same donors as there is a large individual variability in RICD sensitivity.

2.9. Migration assays

Cell migration assays were performed using the Culture-Insert 2 well in μ-Dish (ibidi GmbH, Martinsried, Germany).

Briefly, 25,000 MCF7 cells were plated in each well and cultured for 24 h. The day after, the culture insert was removed and the cells were washed with PBS before treating them with respective DGKα inhibitors (10 μM) or DMSO for 15 h in complete medium (DMEM 10% FBS + 1% penicillin/streptomycin), while medium without FBS was used as a negative control for migration.

Phase-contrast pictures were taken immediately after treatment (0 h) and after 15 h under 5× magnification.

Finally, wound areas were determined using ImageJ software (NIH, , Bethesda, MD). Wound reduction was calculated by using the following formula: (wound area at 15 h/wound at 0 h)×100, the values obtained were expressed as the percentage of wound area compared to the initial area.

2.10. Quantification and statistical analysis

Data for the screen on OST-DGKα homogenates are the mean of duplicates. The compounds showing inhibitory activity in this assay were tested >4 times and the mean ± SEM is reported.

To calculate IC_{50} values of active inhibitors, the inhibitor activity was measured at least three times at 0.1, 1.0, 10.0, and 100.0 μM concentration. Data were analysed using [inhibitor] vs. normalised response parameters with least square [ordinary] curve fitting method in GraphPad PRISM 8.0 software (GraphPad Software, La Jolla, CA) mentioning 95% confidence interval and IC_{50} values always greater than 0.0. Graph shows the mean ± SEM of inhibitor activity at the indicated concentration. In all the experiments, the data were normalised with the controls.

Evaluation of *in vitro* assays across multiple treatments (RICD), SOD-sensitive CytC reduction assay, migration assays were analysed by using one-way ANOVA with multiple comparisons correction using GraphPad PRISM 8.0 software (GraphPad Software, La Jolla, CA). Error bars are described in figure legends as ± SEM or ± SD where appropriate. A single, double, triple and four asterisk denotes significance of a p value ≤0.05, ≤0.01, ≤0.001, and ≤0.0001 respectively in all experiments.

2.11. Pharmacophoric model

A representative 3D structure of each compound was generated using OMEGA2 software[34–36]. The generated file was used to generate a pharmacophore model with the Pharmagist web server (bioinfo3d.cs.tau.ac.il/PharmaGist/)[37].

3. Results

3.1. Chemistry

At the beginning, we purchased 14 analogues of Amb639752 by vendors (Figure 3), while one analogue (**2**), being not commercially available, was synthesised (see Supplementary material). All the compounds were evaluated for their inhibitory activity on DGKα at a concentration of 100 μM (Table 1).

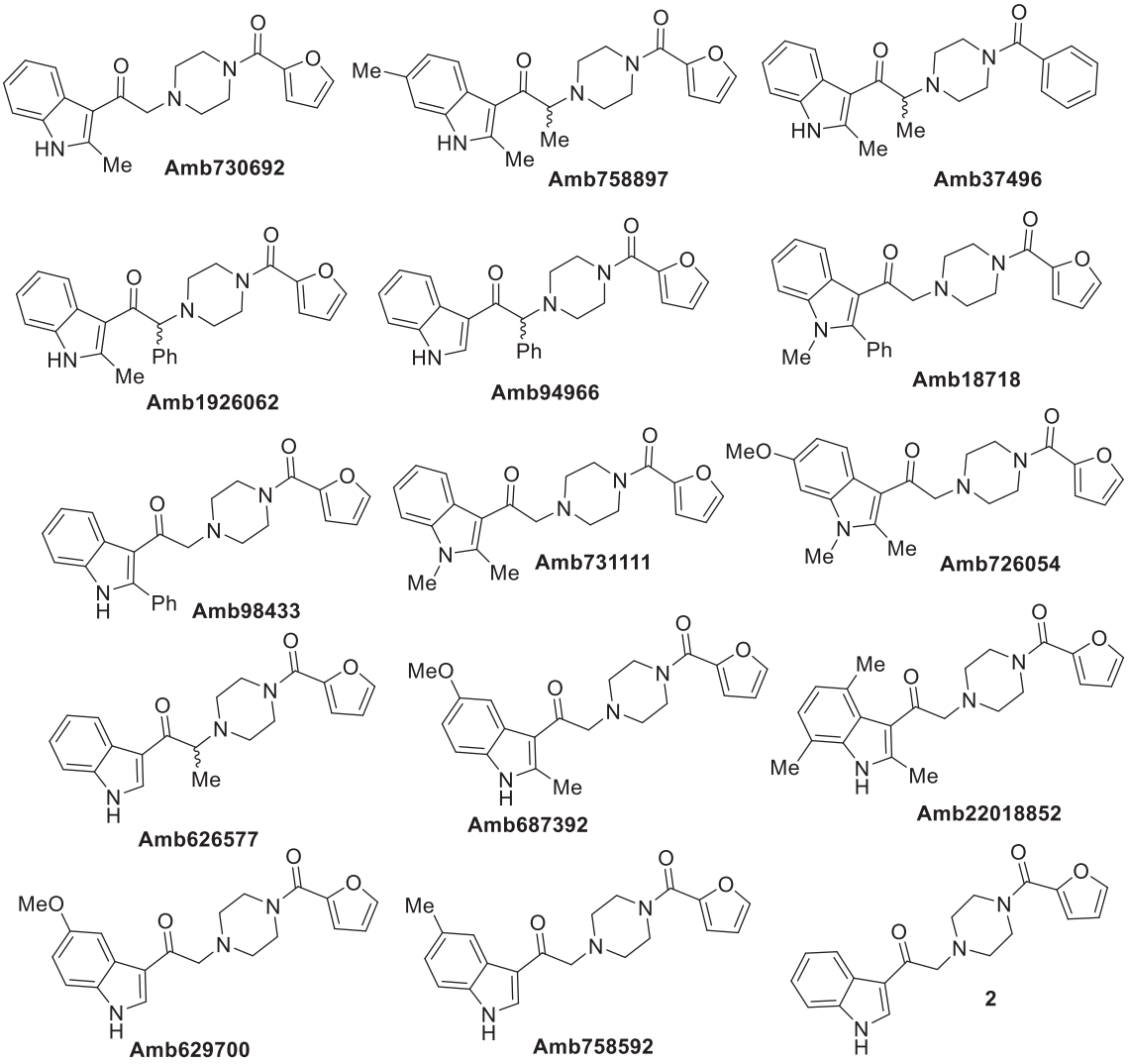

Figure 3. First set of compounds tested for their inhibitory activity on DGKα.

Each inhibitor was tested in duplicate at least once, and DGKα activity was expressed as percentage of residual DGKα activity compared to DMSO control in the same assay. Assay uses OST-DGKα overexpressing cell lysates in presence of saturating exogenous DAG and ATP. We considered R59022 (commercially available) and the lead compound Amb63975230 as our reference molecules. As expected, our reference inhibitors R59022 and Amb639752 featured 73% and 96% inhibition respectively, confirming the quality of data obtained.

This first screening showed us how Amb639752 exhibits a rigid structure activity relationship. Indeed, both the methyl groups on the 2,6 position of indole are mandatory, the NH indole cannot be alkylated as well as ramifications on the alkyl chain are detrimental. We then focussed our attention on furan ring knowing its intrinsic toxicity via metabolic activation[38]. Unfortunately, there were no analogues available by vendors. Our first goal was to replace the furan moiety with the phenyl ring, investigating two different synthetic pathways.

Table 1. Inhibitory activity on DGKα (I).

Compound	Residue activity at 100 μM
R59022	27
R59949	28
Amb639752	4
Amb758897	67
Amb37496	114
Amb626577	127
Amb1926062	88
Amb94966	196
Amb730692	45
Amb98433	81
Amb18718	135
Amb726054	126
Amb731111	130
Amb22018852	160
Amb687392	115
Amb758592	150
Amb629700	101
2	135

In the first one, the commercially available 2,6-dimethyl-1*H*-indole **3** was acylated with 2-chloroacetyl chloride **4**, in the presence of DBU in dichloroethane[39] to give the derivative **5** 90% yield. Then, the acylated compound **5** was reacted with *N*-Boc piperazine in the presence of potassium carbonate and potassium iodide to afford the piperazinic derivative **6** in 63% yield. Boc deprotection with trifluoroacetic acid, followed by coupling with benzoic acid using the condensing agent EDCI afforded the final compound **8** (Scheme 1).

In the second synthetic strategy, we initially coupled the benzoic acid with *N*-Boc piperazine in the presence of EDCI to give piperazinic derivative **9** in 49% yield. Boc deprotection gave in quantitative yield the compound **10**. Due to its high aqueous solubility, solvent was evaporated and the crude as trifluoroacetate salt was directly used for the next step, where it was reacted with the acylated indole **5** to give the final compound **8** in 25% yield (Scheme 2) (see Supplementary material for full synthetic details).

Overall yield calculation was 11% for both strategies, but with the first route it was possible to use a common synthetic intermediate **7** which can be coupled with different carboxylic acids. Furthermore, the second route requires more purification steps. For this reason, we applied the first route and coupled the advanced intermediate **7** with 12 different carboxylic acids (Figure 4) to afford compounds **11**–**22** (Figure 5).

All those molecules were dissolved in DMSO and tested at a concentration of 100 μM for the ability to inhibit DGKα using equal amounts of DMSO as control. We identified eight compounds capable of reducing OST-DGKα activity similar or superior to R59022 (Table 2).

3.2. Potency and isoform specificity of active molecules

To measure the inhibitor potency, we determined the IC_{50} values for the compounds that resulted active when tested at 100 μM by measuring the residual OST-DGKα activity over a dose range of inhibitor concentrations (0.1 μM, 1.0 μM, 10.0 μM, and 100.0 μM).

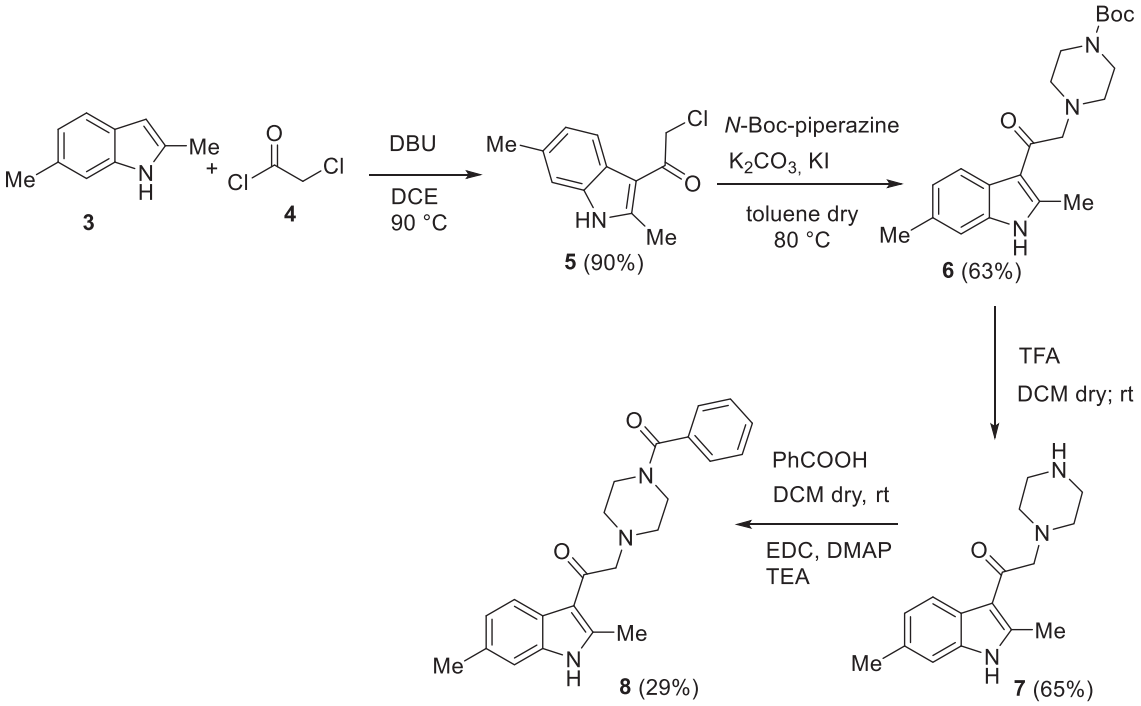

Scheme 1. The first synthetic route for the compound **8**.

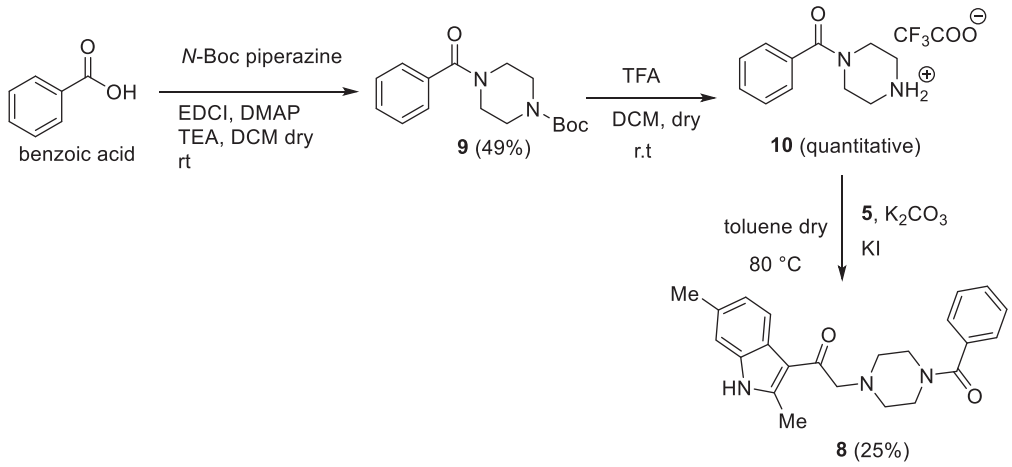

Scheme 2. The second synthetic route for the compound **8**.

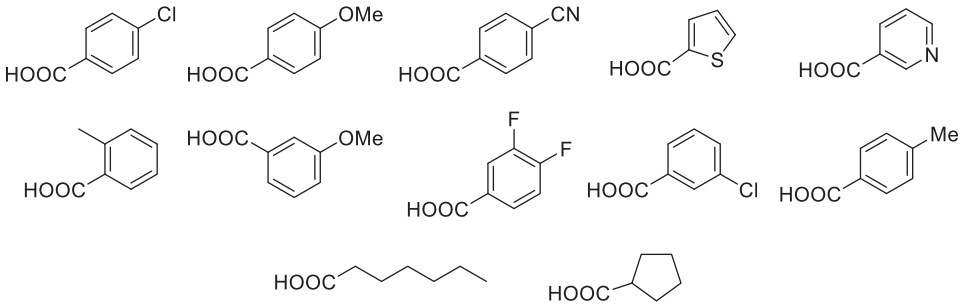

Figure 4. Carboxylic acids used.

For R59022 and Amb639752, we measured IC_{50} values of $15.2 \pm 5.8\,\mu M$ and $6.9 \pm 3.0\,\mu M$ respectively which were comparable to previous reports using similar assay conditions[9]. Considering those two as reference/template compounds, we measured the IC_{50} values of **8**, **11**, **12**, **13**, **14**, **16**, **19**, and **20** as 3.2 ± 1.0, 1.6 ± 0.4, 3.6 ± 1.2, 6.9 ± 2.3, 3.0 ± 1.0, 32.8 ± 11.5, 49.7 ± 31.7, and $1.8 \pm 0.4\,\mu M$, respectively, signifying that their activity is equal or superior to the template compounds (Figure 6).

Due to their higher IC_{50} values, we thus decided to exclude **16** and **19** for further experiments. In summary, we recognised six compounds with equal or superior inhibitory activity compared to commercially available DGKα inhibitors.

To check the isoform specificity of those active molecules, we tested them, along with Amb639752, for their ability to inhibit DGKα, DGKζ (the other major DGK isoform expressed in lymphocytes), and the more distantly related and widely expressed DGKθ. At the highest concentration of 100 μM, all those molecules resulted in highly specific against DGKα as like their parent molecule, Amb639752 by completely inhibit DGKα whereas they do not have significant effects on DGKζ and DGKθ apart from **20** which, at the contrary, acts as an activator of DGKθ (Figure 7).

3.3. Activity of compounds on serotonin receptors

R59022, R59949, and ritanserin feature a dual activity as DGKα inhibitors and serotonin receptor antagonists[25]. Conversely, Amb639752 was reported as a selective DGKα inhibitor which has no effects on serotonin activity[9]. Thus, we investigated whether the active molecules identified affect serotonin signalling.

To this purpose, we measured the effect of serotonin on PMA-induced oxidative burst in human monocytes. As previously shown, 1 μM serotonin reverses the oxidative burst to control values[33]. Known serotonin receptor antagonists ritanserin and ketanserin (10 μM) impaired serotonin action, while pure DGKα inhibitors such as Amb639752 had no effect (Figure 8). These data indicate that this assay is sensitive to perturbations in serotonin signalling independently of activity against DGKα. Interestingly, as like Amb639752, all the newly synthesised active molecules did not affect serotonin action (Figure 8), indicating that all those molecules are not serotonin receptor antagonists.

3.4. DGKα inhibitors restore RICD in SAP deficient T cells

Ruffo et al. demonstrated that the defective RICD observed in T cells from XLP-1 patients was rescued by silencing DGKα expression or by pre-treatment with DGKα inhibitors R59949 or R59022[8]. Interestingly, R59022 also showed beneficial effects in an *in vivo* model of XLP-1, but due to its poor pharmacological proprieties, its use in human patients results unlikely. We therefore tested the effect all those active molecules along with Amb639752 on RICD sensitivity of SAP-deficient T cells. As additional controls, we also included ritanserin and ketanserin to evaluate the contribution of serotonin antagonism to the effects observed.

To evaluate inhibitor efficacy in physiological context, we modelled XLP-1 by silencing SAP in primary peripheral blood T lymphocytes (PBLs) and restimulating them with anti-CD3 antibody (OKT3 10 ng/mL, 24 h). We pre-treated the cells with the indicated

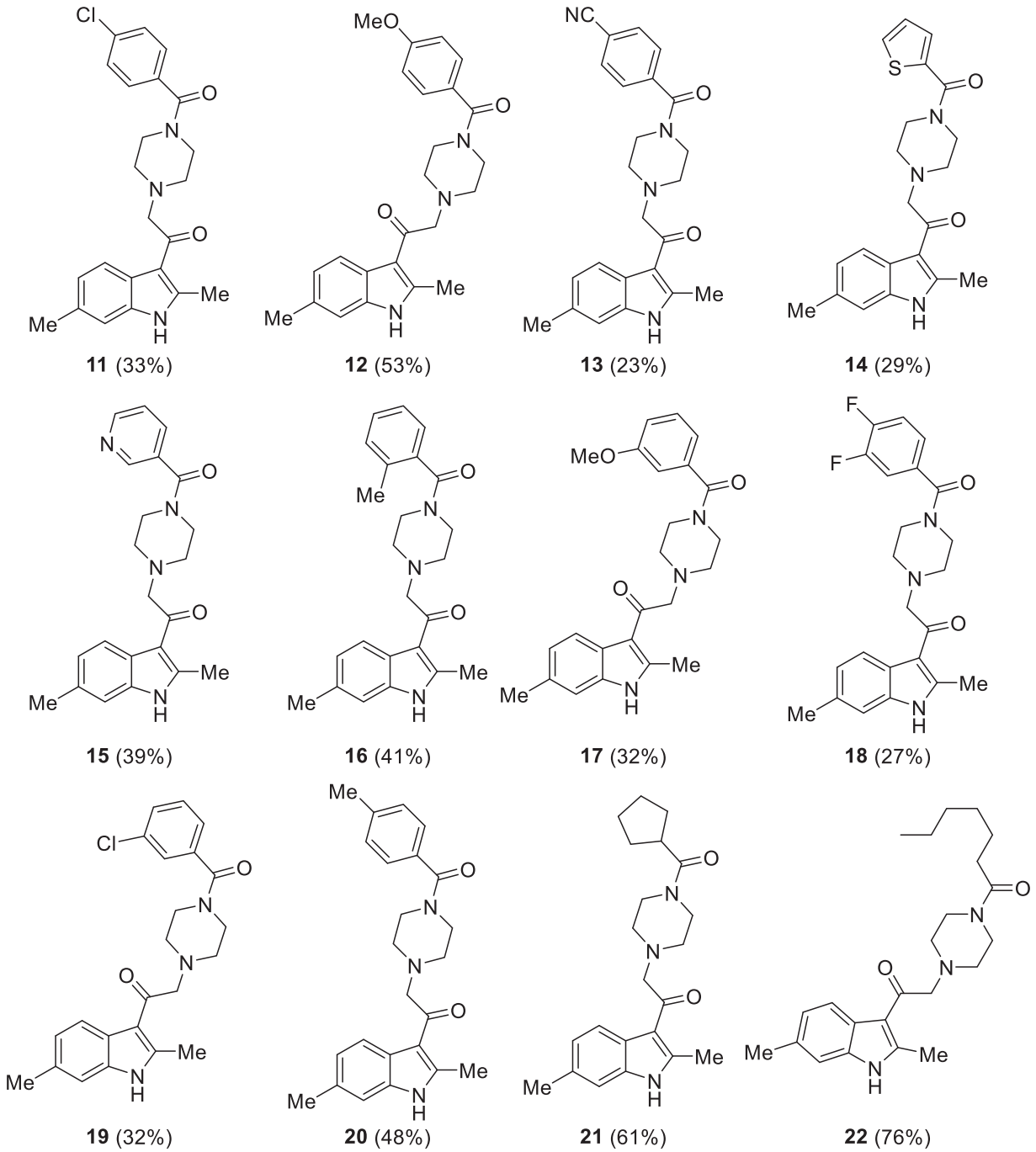

Figure 5. Putative DGKα inhibitors synthesised. In brackets the yield of the coupling reaction with the common intermediate **7**.

inhibitors for 30 min at a concentration of 10 μM[8]. In control siRNA-transfected cells, DGKα inhibitors poorly affect RICD, with Amb639752, **11** and **14** slightly reducing it (Figure 9). Conversely, DGKα inhibitors significantly rescued the apoptotic defect of SAP-deficient T cells although not reaching control levels. At 10 μM, all the new molecules showed an efficacy comparable to Amb637952 and ritanserin used as positive reference molecules. Conversely, the serotonin antagonist ketanserin is inactive, excluding the involvement of serotonin receptors in rescuing the RICD in SAP-deficient T cells (Figure 9).

In summary, these data confirm that the newly identified DGKα inhibitors can rescue RICD susceptibility in T cell models of XLP-1 suggesting a putative use for XLP-1 therapy.

Table 2. Inhibitory activity on DGKα (II).

Compound	Residue activity at 100 μM	IC_{50} (μM)
8	5	3.2
11	6	1.6
12	6	3.6
13	14	6.9
14	6	3.0
15	89	–
16	27	32.8
17	41	–
18	47	–
19	26	49.7
20	3	1.8
21	39	–
22	48	–

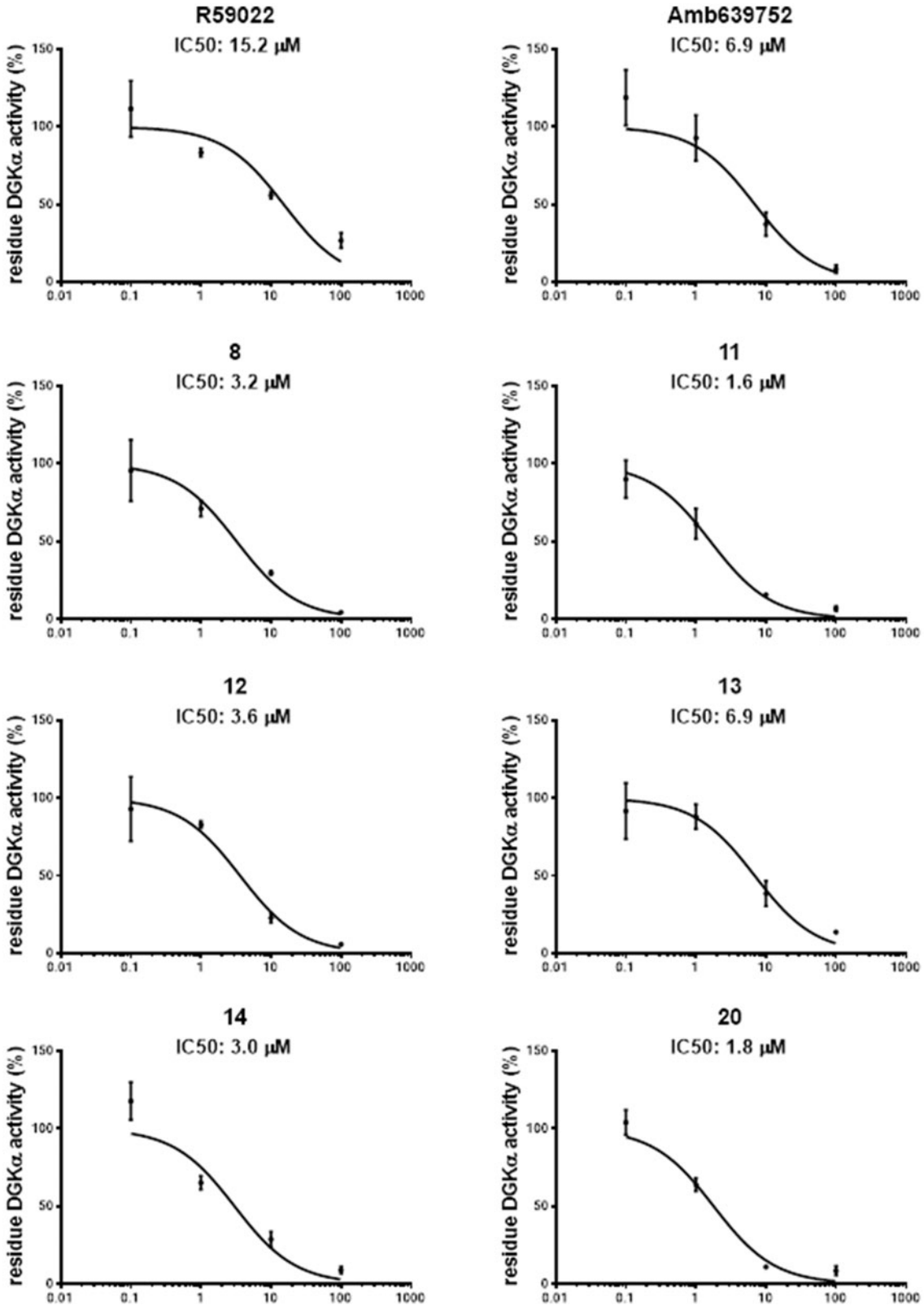

Figure 6. Dose–response curves for novel DGKα inhibitors. Dose–response of the most active compounds along with their IC_{50} values. Data from at least three independent experiments performed in triplicate.

3.5. DGKα inhibitors reduce migration of the cancer cells (MCF7)

Previous studies conducted in our laboratory demonstrated that the inhibition of DGK activity decreases chemotaxis, proliferation, migration, and invasion of many cancer cell lines[12–14]. To evaluate if our newly synthetised DGKα inhibitors were effective in impairing cancer cell migration, we measured serum induced wound healing in MCF7 breast cancer cells in presence of 10 μM inhibitor. In presence of serum, none of the inhibitors is toxic for MCF7 cells even after prolonged treatment (data not shown). After 15 h of treatment, all the newly synthesised active molecules

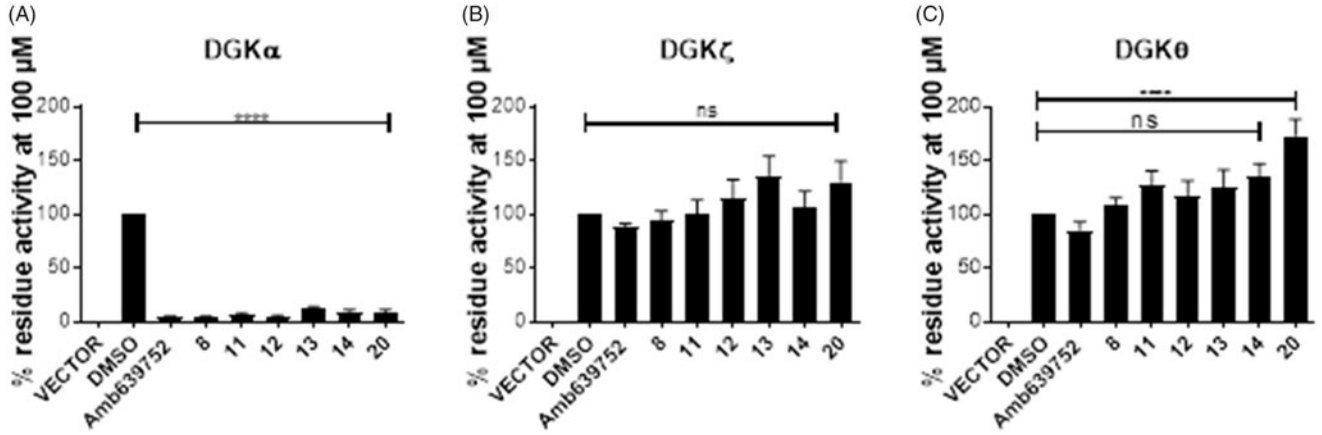

Figure 7. Isoform specificity of novel DGKα inhibitors. 293T cells were transfected with different DGK isoforms (A – DGKα, B – DGKζ, C – DGKθ, respectively) or empty vectors and homogenised. All the molecules were tested at 100 μM for their capacity to inhibit the DGK activity of the different isoform homogenates. Data are means ± SEM of at least three independent experiments performed in triplicate.

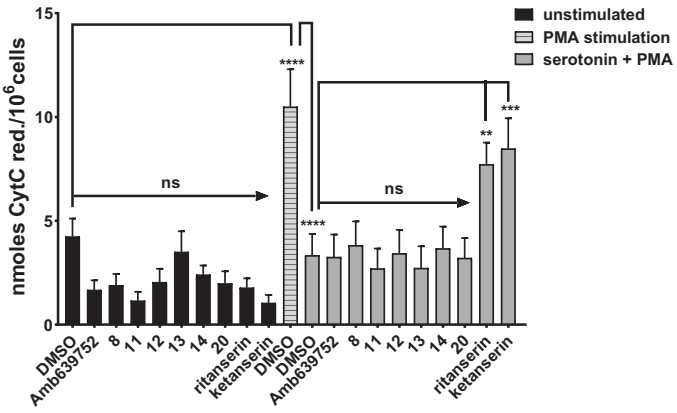

Figure 8. Novel DGKα inhibitors do not affect serotonin signalling. Human monocytes were pre-incubated for 1 h with the indicated drugs in absence or presence of serotonin and then stimulated with PMA 1 μM for 30 min (■ control unstimulated cells, ▭ PMA stimulated cells, ■ PMA and serotonin stimulated cells). Results are expressed as n moles of reduced cytochrome C/10^6 cells. Data are means ± SEM of 10 independent experiments performed in triplicate.

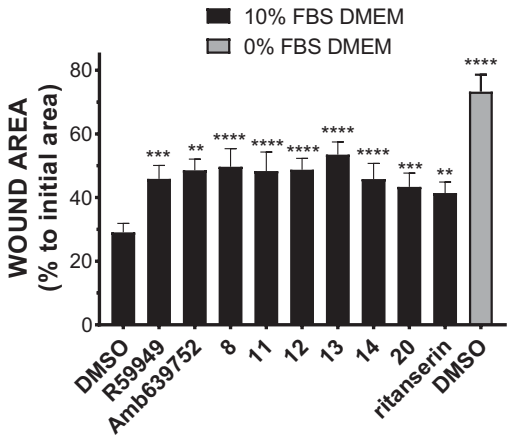

Figure 10. Novel DGKα inhibitors slow tumour cell migration. MCF7 monolayer was wounded and treated for 15 h with serum in presence of our new DGKα inhibitors (10 μM) or vehicle (DMSO). Results are expressed as the percentage of wound area compared to the initial area. Data are the mean ± SEM of nine independent experiments.

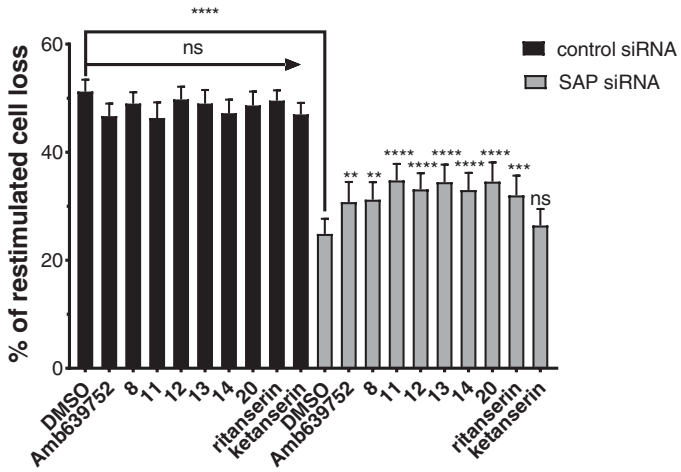

Figure 9. DGKα inhibitors partially restores apoptosis in SAP deficient lymphocytes. Lymphocytes from normal subjects were transfected with control or SAP specific siRNA (■ control siRNA, ■ SAP siRNA). After 4 days, the cells were restimulated with CD3 agonist OKT3 (10 ng/mL) in presence of respective inhibitor. Vehicle (DMSO) was used as control. Twenty-four hours later, the % of cell loss was evaluated by PI staining. Data are the mean ± SEM of nine independent experiments performed in triplicate.

equally reduced cell migration when compared to the vehicle (DMSO) delaying wound closure (Figure 10).

Besides being in good agreement with the notion that DGKα is required for cancer cells migration, this observation indicates that our new DGKα inhibitors reduce cancer cell motility, suggesting a potential utility in a metastasis setting.

3.6. Generation of a pharmacophore hypothesis

From the data obtained, it is possible to identify some key pharmacophoric points crucial for the biological activity of the Amb compounds on DGKs namely: (i) a basic nitrogen; (ii) the methyl groups at the 2 and 6 position of the indole nucleus, and (iii) a (hetero)aromatic ring. This information allows us to build a four-point pharmacophoric model represented in Figure 11 superimposed with the minimised structure of compound **11**. Although, we are not able to evaluate the importance of the two carbonyl groups, it represents the first attempts in order to identify the minimum structural request to interact with DGK catalytic site considering the molecular structure of the four most active inhibitors discovered to date (Amb639752, ritanserin, R59022, and R59949). We feel that this model might be useful to identify novel

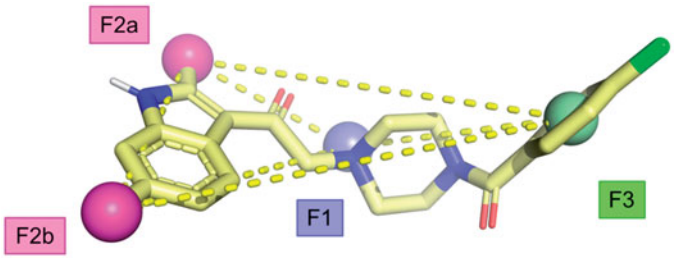

Figure 11. Proposed pharmacophoric model.

compounds active on DGKα through more targeted virtual screening campaigns, overcoming the current scaffolds.

4. Discussion

As a key component of several signal transduction pathways, DGKα represent an emerging pharmacological target. We have demonstrated the efficacy of DGKα inhibitors for XLP-1 treatment[8], while others have proposed them for cancer treatment[22] and to remove immune-checkpoints promoting immune vigilance against cancer[40]. Commercially available DGKα inhibitors are limited by poor specificity[25,41] and pharmacokinetic[20]. The CU-3 molecule described by other features a noteworthy activity and specificity but its reactive chemical structure make unlikely an *in vivo* use[30]. With intent of developing molecules suitable for therapeutic use we selected Amb639752 as a novel inhibitor with remarkable DGKα activity. Amb639752 also features improved selectivity for DGKα as it does not affect serotonin signalling[9]. Despite numerous efforts a structure of mammalian DGKs is still missing, thus we decided to explore the structure–activity relationship of this molecule to improve its activity and pave the way for further developments. Our efforts allowed us to build a pharmacophoric model for DGKα inhibitors characterised by three required features. We also characterised a set of novel compounds with improved IC_{50} in the low μM range and identified the most profitable synthetic route for them. The mode of DGKα inhibition by those molecules is still unknown apart for ritanserin, which binds at the same time the DGKα catalytic accessory domain and the C1 domain putatively promoting a close inactive conformation[41].

The second-generation inhibitors we described in this work maintain the specificity of Amb639752 as they not affect DGKζ, the predominant isoform of lymphocytes[42] and the broadly expressed DGKθ[43]. Those DGKα inhibitors are active in a lymphocyte based XLP-1 assay and in a cancer cell migration assay, holding the promise for a potential therapeutic application. However, their efficacy is still to be determined in *in vivo* models of disease where some of the parental compounds showed efficacy but poor pharmacokinetic[8,20].

Disclosure statement

The authors declare no competing financial interest.

Funding

This work was supported by Università del Piemonte Orientale, Telethon Foundation [Grant GGP16252 to AG and GB], National Ministry of University and Research PRIN 2017 [Grant 201799WCRH to GB], Consorzio Interuniversitario di Biotecnologie (CIB) bando "Network-CIB: Catalisi dell'Innovazione nelle biotecnologie" to GB.

References

1. Cai J, Abramovici H, Gee SH, Topham MK. Diacylglycerol kinases as sources of phosphatidic acid. Biochim Biophys Acta 2009;1791:942–8.
2. Krishna S, Zhong X. Role of diacylglycerol kinases in T cell development and function. Crit Rev Immunol 2013;33:97–118.
3. Merida I, Avila-Flores A, Merino E. Diacylglycerol kinases: at the hub of cell signalling. Biochem J 2008;409:1–18.
4. Sakane F, Imai S, Kai M, et al. Diacylglycerol kinases: why so many of them? Biochim Biophys Acta 2007;1771:793–806.
5. Baldanzi G, Bettio V, Malacarne V, Graziani A. Diacylglycerol kinases: shaping diacylglycerol and phosphatidic acid gradients to control cell polarity. Front Cell Dev Biol 2016;4:140.
6. Tangye SG. XLP: clinical features and molecular etiology due to mutations in sh2d1a encoding sap. J Clin Immunol 2014;34:772–9.
7. Baldanzi G, Pighini A, Bettio V, et al. Sap-mediated inhibition of diacylglycerol kinase alpha regulates TCR-induced diacylglycerol signaling. J Immunol 2011;187:5941–51.
8. Ruffo E, Malacarne V, Larsen SE, et al. Inhibition of diacylglycerol kinase α restores restimulation-induced cell death and reduces immunopathology in XLP-1. Sci Transl Med 2016;8:321–327.
9. Velnati S, Ruffo E, Massarotti A, et al. Identification of a novel DGKalpha inhibitor for XLP-1 therapy by virtual screening. Eur J Med Chem 2019;164:378–90.
10. Bacchiocchi R, Baldanzi G, Carbonari D, et al. Activation of alpha-diacylglycerol kinase is critical for the mitogenic properties of anaplastic lymphoma kinase. Blood 2005;106:2175–82.
11. Yanagisawa K, Yasuda S, Kai M, et al. Diacylglycerol kinase alpha suppresses tumor necrosis factor-alpha-induced apoptosis of human melanoma cells through NF-kappaB activation. Biochim Biophys Acta 2007;1771:462–74.
12. Baldanzi G, Cutrupi S, Chianale F, et al. Diacylglycerol kinase-alpha phosphorylation by Src on Y335 is required for activation, membrane recruitment and Hgf-induced cell motility. Oncogene 2008;27:942–56.
13. Filigheddu N, Cutrupi S, Porporato PE, et al. Diacylglycerol kinase is required for Hgf-induced invasiveness and anchorage-independent growth of mda-mb-231 breast cancer cells. Anticancer Res 2007;27:1489–92.
14. Rainero E, Caswell PT, Muller PA, et al. Diacylglycerol kinase alpha controls RCP-dependent integrin trafficking to promote invasive migration. J Cell Biol 2012;196:277–95.
15. Takeishi K, Taketomi A, Shirabe K, et al. Diacylglycerol kinase alpha enhances hepatocellular carcinoma progression by activation of Ras–Raf–MEK–ERK pathway. J Hepatol 2012;57:77–83.
16. Torres-Ayuso P, Daza-Martin M, Martin-Perez J, et al. Diacylglycerol kinase alpha promotes 3D cancer cell growth and limits drug sensitivity through functional interaction with Src. Oncotarget 2014;5:9710–26.
17. Rainero E, Cianflone C, Porporato PE, et al. The diacylglycerol kinase alpha/atypical PKC/beta1 integrin pathway in SDF-1alpha mammary carcinoma invasiveness. PLoS One 2014;9:e97144.

18. Hao X, Sun B, Hu L, et al. Differential gene and protein expression in primary breast malignancies and their lymph node metastases as revealed by combined cDNA microarray and tissue microarray analysis. Cancer 2004;100:1110–22.
19. Marchet A, Mocellin S, Belluco C, et al. Gene expression profile of primary gastric cancer: towards the prediction of lymph node status. Ann Surg Oncol 2007;14:1058–64.
20. Dominguez CL, Floyd DH, Xiao A, et al. Diacylglycerol kinase α is a critical signaling node and novel therapeutic target in glioblastoma and other cancers. Cancer Discov 2013;3: 782–97.
21. Kefas B, Floyd DH, Comeau L, et al. A miR-297/hypoxia/DGK-α axis regulating glioblastoma survival. Neuro Oncol 2013; 15:1652–63.
22. Purow B. Molecular pathways: targeting diacylglycerol kinase alpha in cancer. Clin Cancer Res 2015;21:5008–12.
23. Jiang Y, Sakane F, Kanoh H, Walsh JP. Selectivity of the diacylglycerol kinase inhibitor 3-[2-(4-[bis-(4-fluorophenyl)methylene]-1-piperidinyl)ethyl]-2, 3-dihydro-2-thioxo-4(1h)quinazolinone (r59949) among diacylglycerol kinase subtypes. Biochem Pharmacol 2000;59:763–72.
24. Sato M, Liu K, Sasaki S, et al. Evaluations of the selectivities of the diacylglycerol kinase inhibitors r59022 and r59949 among diacylglycerol kinase isozymes using a new non-radioactive assay method. Pharmacology 2013;92:99–107.
25. Boroda S, Niccum M, Raje V, et al. Dual activities of ritanserin and r59022 as DGKα inhibitors and serotonin receptor antagonists. Biochem Pharmacol 2017;123:29–39.
26. Gaulton A, Hersey A, Nowotka M, et al. The ChEMBL database in 2017. Nucleic Acids Res 2017;45:D945–D954.
27. Leysen JE, Gommeren W, Van Gompel P, et al. Receptor-binding properties in vitro and in vivo of ritanserin: a very potent and long acting serotonin-S2 antagonist. Mol Pharmacol 1985;27:600–11.
28. Hawkins PC, Skillman AG, Nicholls A. Comparison of shape-matching and docking as virtual screening tools. J Med Chem 2007;50:74–82.
29. Muchmore SW, Souers AJ, Akritopoulou-Zanze I. The use of three-dimensional shape and electrostatic similarity searching in the identification of a melanin-concentrating hormone receptor 1 antagonist. Chem Biol Drug Des 2006;67: 174–6.
30. Liu K, Kunii N, Sakuma M, et al. A novel diacylglycerol kinase α-selective inhibitor, CU-3, induces cancer cell apoptosis and enhances immune response. J Lipid Res 2016;57:368–79.
31. Baell JB, Holloway GA. New substructure filters for removal of pan assay interference compounds (pains) from screening libraries and for their exclusion in bioassays. J Med Chem 2010;53:2719–40.
32. Lavagno L, Gunella G, Bardelli C, et al. Anti-inflammatory drugs and tumor necrosis factor-alpha production from monocytes: role of transcription factor NF-kappa B and implication for rheumatoid arthritis therapy. Eur J Pharmacol 2004;501:199–208.
33. Talmon M, Rossi S, Pastore A, et al. Vortioxetine exerts anti-inflammatory and immunomodulatory effects on human monocytes/macrophages. Br J Pharmacol 2018;175:113–24.
34. Omega, version 2.4.6; OpenEye Scientific Software: Santa Fe, NM. Available from: http://www.eyesopen.com
35. Hawkins PCD, Skillman AG, Warren GL, et al. Conformer generation with omega: algorithm and validation using high quality structures from the Protein Databank and Cambridge Structural Database. J Chem Inf Model 2010;50:572–84.
36. Hawkins PCD, Nicholls A. Conformer generation with omega: learning from the data set and the analysis of failures. J Chem Inf Model 2012;52:2919–36.
37. Schneidman-Duhovny D, Dror O, Inbar Y, et al. Pharmagist: a webserver for ligand-based pharmacophore detection. Nucleic Acids Res 2008;36:W223–228.
38. Wermuth C, Aldous D, Raboisson P, Rognan D. The practice of medicinal chemistry. 4th ed. London, UK: Academic Press; 2015.
39. Johansson H, Urruticoechea A, Larsen I, Sejer Pedersen D. A scalable method for regioselective 3-acylation of 2-substituted indoles under basic conditions. J Org Chem 2015;80: 471–81.
40. Sakane F, Mizuno S, Komenoi S. Diacylglycerol kinases as emerging potential drug targets for a variety of diseases: an update. Front Cell Dev Biol 2016;4:82.
41. Franks CE, Campbell ST, Purow BW, et al. The ligand binding landscape of diacylglycerol kinases. Cell Chem Biol 2017;24: 870–80.e5.
42. Joshi RP, Schmidt AM, Das J, et al. The ζ isoform of diacylglycerol kinase plays a predominant role in regulatory T cell development and TCR-mediated ras signaling. Sci Signal 2013;6:ra102.
43. Tu-Sekine B, Goldschmidt HL, Raben DM. DGK-θ: structure, enzymology, and physiological roles. Front Cell Dev Biol 2016;4:101.